

# Global Carbon Budget 2024

Pierre Friedlingstein [1,2], Michael O'Sullivan [1], Matthew W. Jones [3], Robbie M. Andrew [4], Judith Hauck [5,6], Peter Landschützer [7], Corinne Le Quéré [3], Hongmei Li [8,9], Ingrid T. Lujckx [10], Are Olsen [11,12], Glen P. Peters [4], Wouter Peters [10,13], Julia Pongratz [14,9], Clemens Schwingshackl [14], Stephen Sitch [1], Josep G. Canadell [15], Philippe Ciais [16], Robert B. Jackson [17], Simone R. Alin [18], Almut Armeth [19], Vivek Arora [20], Nicholas R. Bates [21], Meike Becker [11,12], Nicolas Bellouin [22], Carla F. Berghoff [23], Henry C. Bittig [24], Laurent Bopp [2], Patricia Cadule [2], Katie Campbell [25], Matthew A. Chamberlain [26], Naveen Chandra [27], Frédéric Chevallier [16], Louise P. Chini [28], Thomas Colligan [29], Jeanne Decayeux [30], Laique M. Djeutchouang [31,32], Xinyu Dou [33], Carolina Duran Rojas [1], Kazutaka Enyo [34], Wiley Evans [25], Amanda R. Fay [35], Richard A. Feely [18], Daniel J. Ford [1], Adrianna Foster [36], Thomas Gasser [37], Marion Gehlen [16], Thanos Gkritzalis [7], Giacomo Grassi [38], Luke Gregor [39], Nicolas Gruber [39], Özgür Gürses [5], Ian Harris [40], Matthew Hefner [41,42], Jens Heinke [43], George C. Hurtt [28], Yosuke Iida [34], Tatiana Ilyina [44,8,9], Andrew R. Jacobson [45], Atul K. Jain [46], Tereza Jarníková [47], Annika Jersild [29], Fei Jiang [48], Zhe Jin [49,50], Etsushi Kato [51], Ralph F. Keeling [52], Kees Klein Goldewijk [53], Jürgen Knauer [54,15], Jan Ivar Korsbakken [4], Xin Lan [55,56], Siv K. Lauvset [57,12], Nathalie Lefèvre [58], Zhu Liu [33], Junjie Liu [59,60], Lei Ma [28], Shamil Maksyutov [61], Gregg Marland [41,42], Nicolas Mayot [62], Patrick C. McGuire [63], Nicolas Metzler [58], Natalie M. Monacci [64], Eric J. Morgan [52], Shin-Ichiro Nakaoka [61], Craig Neill [26], Yosuke Niwa [61], Tobias Nützel [14], Lea Olivier [5,14], Tsuneo Ono [65], Paul I. Palmer [66,67], Denis Pierrot [68], Zhangcai Qin [69], Laure Resplandy [70], Alizée Roobaert [7], Thais M. Rosan [1], Christian Rödenbeck [71], Jörg Schwinger [57,12], T. Luke Smallman [66,67], Stephen M. Smith [72], Reinel Sospedra-Alfonso [73], Tobias Steinhoff [74,57], Qing Sun [75], Adrienne J. Sutton [18], Roland Sférian [30], Shintaro Takao [61], Hiroaki Tatebe [76,77], Hanqin Tian [78], Bronte Tilbrook [26,79], Olivier Torres [2], Etienne Tourigny [80], Hiroyuki Tsujino [81], Francesco Tubiello [82], Guido van der Werf [10], Rik Wanninkhof [68], Xuhui Wang [50], Dongxu Yang [83], Xiaojuan Yang [84], Zhen Yu [85], Wenping Yuan [86], Xu Yue [87], Sönke Zaehle [71], Ning Zeng [88, 29], Jiye Zeng [61].

1. Faculty of Environment, Science and Economy, University of Exeter, Exeter EX4 4QF, UK

2. Laboratoire de Météorologie Dynamique, Institut Pierre-Simon Laplace, CNRS, Ecole Normale Supérieure, Université PSL, Sorbonne Université, Ecole Polytechnique, Paris, France

3. Tyndall Centre for Climate Change Research, School of Environmental Sciences, University of East Anglia, Norwich Research Park, Norwich NR4 7TJ, UK

4. CICERO Center for International Climate Research, Oslo 0349, Norway

5. Alfred-Wegener-Institut, Helmholtz-Zentrum für Polar- und Meeresforschung, Am Handelshafen 12, 27570 Bremerhaven, Germany

6. Universität Bremen, Bremen, Germany

7. Flanders Marine Institute (VLIZ), Jacobsenstraat 1, 8400, Ostend, Belgium

- 38 8. Helmholtz-Zentrum Hereon, Max-Planck-Straße 1, 21502 Geesthacht, Germany
- 39 9. Max Planck Institute for Meteorology, Bundesstraße 53, 20146 Hamburg, Germany
- 40 10. Wageningen University, Environmental Sciences Group, P.O. Box 47, 6700AA, Wageningen, The
- 41 Netherlands
- 42 11. Geophysical Institute, University of Bergen, Allégaten 70, 5007 Bergen, Norway
- 43 12. Bjerknes Centre for Climate Research, Bergen, Norway
- 44 13. University of Groningen, Centre for Isotope Research, Groningen, The Netherlands
- 45 14. Ludwig-Maximilians-Universität München, Luisenstr. 37, 80333 München, Germany
- 46 15. CSIRO Environment, Canberra, ACT 2101, Australia
- 47 16. Laboratoire des Sciences du Climat et de l'Environnement, LSCE/IPSL, CEA-CNRS-UVSQ, Université
- 48 Paris-Saclay, F-91198 Gif-sur-Yvette, France
- 49 17. Department of Earth System Science, Woods Institute for the Environment, and Precourt Institute for
- 50 Energy, Stanford University, Stanford, CA 94305–2210, United States of America
- 51 18. National Oceanic and Atmospheric Administration, Pacific Marine Environmental Laboratory
- 52 (NOAA/PMEL), 7600 Sand Point Way NE, Seattle, WA 98115, USA
- 53 19. Karlsruhe Institute of Technology, Institute of Meteorology and Climate Research/Atmospheric
- 54 Environmental Research, 82467 Garmisch-Partenkirchen, Germany
- 55 20. Canadian Centre for Climate Modelling and Analysis, Environment and Climate Change Canada, Victoria,
- 56 BC, Canada
- 57 21. ASU-BIOS, Bermuda Institute of Ocean Sciences, 31 Biological Lane, Ferry Reach, St. Georges., GE01,
- 58 Bermuda
- 59 22. Department of Meteorology, University of Reading, Reading, RG6 6BB, UK
- 60 23. Instituto Nacional de Investigación y Desarrollo Pesquero, Paseo Victoria Ocampo N°1, Escollera Norte,
- 61 B7602HSA, Mar del Plata, Argentina
- 62 24. Leibniz Institute for Baltic Sea Research Warnemuende (IOW), Seestrasse 15, 18119 Rostock, Germany
- 63 25. Hakai Institute, British Columbia, V0P 1H0, Canada
- 64 26. CSIRO Environment, Castray Esplanade, Hobart, Tasmania 7004, Australia
- 65 27. Research Institute for Global Change, JAMSTEC, 3173-25 Showa-machi, Kanazawa, Yokohama, 236-0001,
- 66 Japan
- 67 28. Department of Geographical Sciences, University of Maryland, College Park, Maryland 20742, USA
- 68 29. Earth System Science Interdisciplinary Center, University of Maryland, College Park, MD 20740, USA
- 69 30. Centre National de Recherches Météorologiques, Université de Toulouse, Météo-France, CNRS UMR 3589,
- 70 Toulouse, France
- 71 31. School for Climate Studies, Stellenbosch University, Private Bag X1, Matieland, Stellenbosch, 7602, South
- 72 Africa
- 73 32. Southern Ocean Carbon – Climate Observatory, CSIR, Rosebank, Cape Town, 7700, South Africa
- 74 33. Department of Earth System Science, Tsinghua University, Beijing, China
- 75 34. Japan Meteorological Agency, 3-6-9 Toranomon, Minato City, Tokyo 105-8431, Japan
- 76 35. Columbia University and Lamont-Doherty Earth Observatory, New York, NY, USA

- 77 36. Climate and Global Dynamics Laboratory, National Center for Atmospheric Research, Boulder, CO 80305,  
78 USA
- 79 37. International Institute for Applied Systems Analysis (IIASA), Schlossplatz 1, A-2361 Laxenburg, Austria
- 80 38. European Commission, Joint Research Centre (JRC), Ispra, Italy
- 81 39. Environmental Physics Group, ETH Zürich, Institute of Biogeochemistry and Pollutant Dynamics and  
82 Center for Climate Systems Modeling (C2SM), Zürich, Switzerland
- 83 40. NCAS-Climate, Climatic Research Unit, School of Environmental Sciences, University of East Anglia,  
84 Norwich Research Park, Norwich, NR4 7TJ, UK
- 85 41. Research Institute for Environment, Energy, and Economics, Appalachian State University, Boone, North  
86 Carolina, USA
- 87 42. Department of Geological and Environmental Sciences, Appalachian State University, Boone, North  
88 Carolina, USA
- 89 43. Potsdam Institute for Climate Impact Research (PIK), member of the Leibniz Association, P.O. Box 60 12  
90 03, 14412 Potsdam, Germany
- 91 44. Universität Hamburg, Bundesstraße 55, 20146 Hamburg, Germany
- 92 45. Cooperative Institute for Research in Environmental Sciences, CU Boulder and NOAA Global Monitoring  
93 Laboratory, Boulder, USA
- 94 46. Department of Climate, Meteorology and Atmospheric Sciences, University of Illinois, Urbana, IL 61821,  
95 USA
- 96 47. University of East Anglia, Norwich, UK
- 97 48. Jiangsu Provincial Key Laboratory of Geographic Information Science and Technology, International  
98 Institute for Earth System Science, Nanjing University, Nanjing, 210023, China
- 99 49. State Key Laboratory of Tibetan Plateau Earth System and Resource Environment, Institute of Tibetan  
100 Plateau Research, Chinese Academy of Sciences, Beijing 100101, China
- 101 50. Institute of Carbon Neutrality, Sino-French Institute for Earth System Science, College of Urban and  
102 Environmental Sciences, Peking University, Beijing 100871, China
- 103 51. Institute of Applied Energy (IAE), Minato-ku, Tokyo 105-0003, Japan
- 104 52. University of California, San Diego, Scripps Institution of Oceanography, La Jolla, CA 92093-0244, USA
- 105 53. Utrecht University, Faculty of Geosciences, Department IMEW, Copernicus Institute of Sustainable  
106 Development, Heidelberglaan 2, P.O. Box 80115, 3508 TC, Utrecht, the Netherlands
- 107 54. Hawkesbury Institute for the Environment, Western Sydney University, Penrith, New South Wales,  
108 Australia
- 109 55. Cooperative Institute for Research in Environmental Sciences (CIRES), University of Colorado Boulder,  
110 Boulder, CO 80309, USA
- 111 56. National Oceanic and Atmospheric Administration Global Monitoring Laboratory (NOAA/GML), 325  
112 Broadway R/GML, Boulder, CO 80305, USA
- 113 57. NORCE Norwegian Research Centre, Jahnebakken 5, 5007 Bergen, Norway
- 114 58. LOCEAN/IPSL laboratory, Sorbonne Université, CNRS/IRD/MNHN, Paris, 75252, France
- 115 59. Jet Propulsion Laboratory, California Institute of Technology, Pasadena, CA, USA

116 60. California Institute of Technology, Pasadena, CA, USA  
117 61. Earth System Division, National Institute for Environmental Studies, 16-2 Onogawa, Tsukuba, Ibaraki, 305-  
118 8506 Japan  
119 62. Sorbonne Université, Laboratoire d'Océanographie de Villefranche, Villefranche-sur-Mer, France  
120 63. Department of Meteorology & National Centre for Atmospheric Science (NCAS), University of Reading,  
121 Reading, UK  
122 64. University of Alaska Fairbanks, College of Fisheries and Ocean Sciences, Fairbanks, AK, 99709, USA  
123 65. Fisheries Research and Education Agency, 2-12-4 Fukuura, Kanazawa-Ku, Yokohama 236-8648, Japan  
124 66. National Centre for Earth Observation, University of Edinburgh, EH9 3FF, UK  
125 67. School of GeoSciences, University of Edinburgh, EH9 3FF, UK  
126 68. NOAA Atlantic Oceanographic and Meteorological Laboratory (NOAA/AOML), 4301 Rickenbacker  
127 Causeway, Miami, Florida 33149, USA  
128 69. School of Atmospheric Sciences, Sun Yat-sen University, Zhuhai 519000, China  
129 70. Princeton University, Department of Geosciences and Princeton Environmental Institute, Princeton, NJ,  
130 USA  
131 71. Max Planck Institute for Biogeochemistry, P.O. Box 600164, Hans-Knöll-Str. 10, 07745 Jena, Germany  
132 72. Smith School of Enterprise and the Environment, University of Oxford, Oxford, UK  
133 73. Canadian Centre for Climate Modelling and Analysis, Environment and Climate Change Canada, Victoria,  
134 British Columbia, Canada  
135 74. GEOMAR Helmholtz Centre for Ocean Research Kiel, Wischhofstr. 1-3, 24148 Kiel, Germany  
136 75. Institute for Climate and Environmental Physics, Bern, Switzerland  
137 76. Research Center for Environmental Modeling and Application, Japan Agency for Marine-Earth Science and  
138 Technology, Yokohama, Japan  
139 77. Advanced Institute for Marine Ecosystem Change, Japan Agency for Marine-Earth Science and Technology,  
140 Yokohama, Japan  
141 78. Schiller Institute of Integrated Science and Society, Department of Earth and Environmental Sciences,  
142 Boston College, Chestnut Hill, MA 02467, USA  
143 79. Australian Antarctic Partnership Program, University of Tasmania, Hobart, Australia  
144 80. Barcelona Supercomputing Center, Barcelona, Spain  
145 81. JMA Meteorological Research Institute, Tsukuba, Ibaraki, Japan  
146 82. Statistics Division, Food and Agriculture Organization of the United Nations, Via Terme di Caracalla, Rome  
147 00153, Italy  
148 83. Institute of Atmospheric Physics, Chinese Academy of Sciences, Beijing, China  
149 84. Climate Change Science Institute and Environmental Sciences Division, Oak Ridge National Lab, Oak  
150 Ridge, TN 37831, USA.  
151 85. School of Ecology and Applied Meteorology, Nanjing University of Information Science and Technology,  
152 Nanjing 210044, PR. China  
153 86. Institute of Carbon Neutrality, College of Urban and Environmental Sciences, Peking University, Beijing  
154 100091, China



155 87. School of Environmental Science and Engineering, Nanjing University of Information Science and  
156 Technology (NUIST), Nanjing, 210044, China

157 88. Department of Atmospheric and Oceanic Science, University of Maryland, Maryland, USA

158

159 *Correspondence to:* Pierre Friedlingstein (p.friedlingstein@exeter.ac.uk)

## 160 **Abstract**

161 Accurate assessment of anthropogenic carbon dioxide (CO<sub>2</sub>) emissions and their redistribution among the  
162 atmosphere, ocean, and terrestrial biosphere in a changing climate is critical to better understand the global  
163 carbon cycle, support the development of climate policies, and project future climate change. Here we describe  
164 and synthesise datasets and methodologies to quantify the five major components of the global carbon budget  
165 and their uncertainties. Fossil CO<sub>2</sub> emissions (E<sub>FOS</sub>) are based on energy statistics and cement production data,  
166 while emissions from land-use change (E<sub>LUC</sub>) are based on land-use and land-use change data and bookkeeping  
167 models. Atmospheric CO<sub>2</sub> concentration is measured directly, and its growth rate (G<sub>ATM</sub>) is computed from the  
168 annual changes in concentration. The global net uptake of CO<sub>2</sub> by the ocean (S<sub>OCEAN</sub>, called the ocean sink) is  
169 estimated with global ocean biogeochemistry models and observation-based fCO<sub>2</sub>-products. The global net  
170 uptake of CO<sub>2</sub> by the land (S<sub>LAND</sub>, called the land sink) is estimated with dynamic global vegetation models.  
171 Additional lines of evidence on land and ocean sinks are provided by atmospheric inversions, atmospheric  
172 oxygen measurements and Earth System Models. The sum of all sources and sinks results in the carbon budget  
173 imbalance (B<sub>IM</sub>), a measure of imperfect data and incomplete understanding of the contemporary carbon cycle.  
174 All uncertainties are reported as  $\pm 1\sigma$ .

175 For the year 2023, E<sub>FOS</sub> increased by 1.3% relative to 2022, with fossil emissions at  $10.1 \pm 0.5$  GtC yr<sup>-1</sup> ( $10.3 \pm$   
176  $0.5$  GtC yr<sup>-1</sup> when the cement carbonation sink is not included), E<sub>LUC</sub> was  $1.0 \pm 0.7$  GtC yr<sup>-1</sup>, for a total  
177 anthropogenic CO<sub>2</sub> emission (including the cement carbonation sink) of  $11.1 \pm 0.9$  GtC yr<sup>-1</sup> ( $40.6 \pm 3.2$  GtCO<sub>2</sub>  
178 yr<sup>-1</sup>). Also, for 2023, G<sub>ATM</sub> was  $5.9 \pm 0.2$  GtC yr<sup>-1</sup> ( $2.79 \pm 0.1$  ppm yr<sup>-1</sup>), S<sub>OCEAN</sub> was  $2.9 \pm 0.4$  GtC yr<sup>-1</sup> and  
179 S<sub>LAND</sub> was  $2.3 \pm 1.0$  GtC yr<sup>-1</sup>, with a near zero B<sub>IM</sub> ( $-0.02$  GtC yr<sup>-1</sup>). The global atmospheric CO<sub>2</sub> concentration  
180 averaged over 2023 reached  $419.31 \pm 0.1$  ppm. Preliminary data for 2024, suggest an increase in E<sub>FOS</sub> relative  
181 to 2023 of +0.8% (-0.2% to 1.7%) globally, and atmospheric CO<sub>2</sub> concentration increased by 2.87 ppm  
182 reaching 422.45 ppm, 52% above pre-industrial level (around 278 ppm in 1750). Overall, the mean and trend  
183 in the components of the global carbon budget are consistently estimated over the period 1959-2023, with a  
184 near-zero overall budget imbalance, although discrepancies of up to around 1 GtC yr<sup>-1</sup> persist for the  
185 representation of annual to semi-decadal variability in CO<sub>2</sub> fluxes. Comparison of estimates from multiple  
186 approaches and observations shows: (1) a persistent large uncertainty in the estimate of land-use change  
187 emissions, (2) a low agreement between the different methods on the magnitude of the land CO<sub>2</sub> flux in the  
188 northern extra-tropics, and (3) a discrepancy between the different methods on the mean ocean sink.

189 This living data update documents changes in methods and datasets applied to this most-recent global carbon  
190 budget as well as evolving community understanding of the global carbon cycle. The data presented in this  
191 work are available at <https://doi.org/10.18160/GCP-2024> (Friedlingstein et al., 2024).

192

## 193 **Executive Summary**

194 **Global fossil CO<sub>2</sub> emissions (including cement carbonation) are expected to further increase in 2024 by**  
195 **0.8%.** The 2023 emission increase was 0.14 GtC yr<sup>-1</sup> (0.5 GtCO<sub>2</sub> yr<sup>-1</sup>) relative to 2022, bringing 2023 fossil CO<sub>2</sub>  
196 emissions to 10.1 ± 0.5 GtC yr<sup>-1</sup> (36.8 ± 1.8 GtCO<sub>2</sub> yr<sup>-1</sup>). Preliminary estimates based on data available suggest  
197 fossil CO<sub>2</sub> emissions to increase further in 2024, by 0.8% relative to 2023 (-0.2% to 1.7%), bringing emissions  
198 to 10.2 GtC yr<sup>-1</sup> (37.4 GtCO<sub>2</sub> yr<sup>-1</sup>).<sup>1</sup>

199 Emissions from coal, oil and gas in 2024 are expected to be slightly above their 2023 levels (by 0.1%, 0.9% and  
200 2.5% respectively). Regionally, fossil emissions in 2024 are expected to decrease by 2.8% in the European  
201 Union reaching 0.7 GtC (2.4 GtCO<sub>2</sub>), and by 0.9% in the United States (1.3 GtC, 4.9 GtCO<sub>2</sub>). Emissions in  
202 China are expected to increase in 2024 by 0.1% (3.3 GtC, 11.9 GtCO<sub>2</sub>). Fossil emissions are also expected to  
203 increase by 3.7% in India (0.9 GtC, 3.2 GtCO<sub>2</sub>) and by 1.2% for the rest of the world (4.0 GtC, 14.5 GtCO<sub>2</sub>) in  
204 2024. Emissions from international aviation and shipping (IAS) are also expected to increase by 7.8% (0.3 GtC,  
205 1.2 GtCO<sub>2</sub>) in 2024.

206 **Fossil CO<sub>2</sub> emissions decreased significantly in 23 countries with significantly growing economies during**  
207 **the decade 2014-2023.** Altogether, these 23 countries contribute about 2.2 GtC yr<sup>-1</sup> (8.2 GtCO<sub>2</sub>) fossil fuel CO<sub>2</sub>  
208 emissions over the last decade, representing about 23% of world CO<sub>2</sub> fossil emissions.

209 **Global CO<sub>2</sub> emissions from land-use, land-use change, and forestry (LULUCF) averaged 1.1 ± 0.7 GtC yr<sup>-1</sup>**  
210 **(4.1 ± 2.6 GtCO<sub>2</sub> yr<sup>-1</sup>) for the 2014-2023 period with a similar preliminary projection for 2024 of 1.2 ±**  
211 **0.7 GtC yr<sup>-1</sup> (4.2 ± 2.6 GtCO<sub>2</sub> yr<sup>-1</sup>).** Since the late-1990s, emissions from LULUCF show a statistically  
212 significant decrease at a rate of around 0.2 GtC per decade. Emissions from deforestation, the main driver of  
213 global gross sources, remain high at around 1.7 GtC yr<sup>-1</sup> over the 2014-2023 period, highlighting the strong  
214 potential of halting deforestation for emissions reductions. Sequestration of 1.2 GtC yr<sup>-1</sup> through re-  
215 /afforestation and forest regrowth in shifting cultivation cycles offsets two third of the deforestation emissions.  
216 Further, smaller emissions are due to other land-use transitions and peat drainage and peat fire. The highest  
217 emitters during 2014-2023 in descending order were Brazil, Indonesia, and the Democratic Republic of the  
218 Congo, with these 3 countries contributing more than half of global land-use CO<sub>2</sub> emissions.

219 **Total anthropogenic emissions (fossil and LULUCF, including the carbonation sink) were 11.1 GtC yr<sup>-1</sup>**  
220 **(40.6 GtCO<sub>2</sub> yr<sup>-1</sup>) in 2023, with a slightly higher preliminary estimate of 11.4 GtC yr<sup>-1</sup> (41.6 GtCO<sub>2</sub> yr<sup>-1</sup>)**  
221 **for 2024. Total anthropogenic emissions have been stable over the last decade (zero growth rate over the**

---

<sup>1</sup> All 2024 growth rates use a leap year adjustment that corrects for the extra day in 2024.

222 **2014-2023 period), much slower than over the previous decade (2004-2013) with an average growth rate**  
223 **of 2.0% yr<sup>-1</sup>.**

224 **The remaining carbon budget for a 50% likelihood to limit global warming to 1.5°C, 1.7°C and 2°C above**  
225 **the 1850-1900 level has respectively been reduced to 65 GtC (235 GtCO<sub>2</sub>), 160 GtC (585 GtCO<sub>2</sub>) and 305**  
226 **GtC (1110 GtCO<sub>2</sub>) from the beginning of 2025, equivalent to around 6, 14 and 27 years, assuming 2024**  
227 **emissions levels.**

228 **The concentration of CO<sub>2</sub> in the atmosphere is set to reach 422.45 ppm in 2024, 52% above pre-industrial**  
229 **levels.** The atmospheric CO<sub>2</sub> growth was  $5.2 \pm 0.02$  GtC yr<sup>-1</sup> (2.5 ppm) during the decade 2014-2023 (48% of  
230 total CO<sub>2</sub> emissions) with a preliminary 2024 growth rate estimate of around 6.1 GtC (2.87 ppm).

231 **The ocean sink, the global net uptake of CO<sub>2</sub> by the ocean, has been stagnant since 2016 after rapid**  
232 **growth during 2002-2016, largely in response to large inter-annual climate variability.** The ocean CO<sub>2</sub> sink  
233 was  $2.9 \pm 0.4$  GtC yr<sup>-1</sup> during the decade 2014-2023 (26% of total CO<sub>2</sub> emissions). A slightly higher value of 3.0  
234 GtC yr<sup>-1</sup> is preliminarily estimated for 2024, which marks an increase in the sink since 2023 due to the  
235 prevailing El Niño and neutral conditions in 2024.

236 **The land sink, the global net uptake of CO<sub>2</sub> by the land, continued to increase during the 2014-2023**  
237 **period primarily in response to increased atmospheric CO<sub>2</sub>, albeit with large interannual variability.** The  
238 land CO<sub>2</sub> sink was  $3.2 \pm 0.9$  GtC yr<sup>-1</sup> during the 2014-2023 decade (30% of total CO<sub>2</sub> emissions). The land sink  
239 in 2023 was  $2.3 \pm 1$  GtC yr<sup>-1</sup>, 1.6 GtC lower than in 2022, and the lowest estimate since 2015. This reduced sink  
240 is primarily driven by a response of tropical land ecosystems to the onset of the 2023-2024 El Niño event,  
241 combined with large wildfires in Canada in 2023. The preliminary 2024 estimate is around 3.2 GtC yr<sup>-1</sup>, similar  
242 to the decadal average, consistent with a land sink emerging from the El Niño state.

243 **So far in 2024, global fire CO<sub>2</sub> emissions have been 11-32% higher than the 2014-2023 average due to**  
244 **high fire activity in both North and South America, reaching 1.6-2.2 GtC during January-September.** In  
245 Canada, emissions through September were 0.2-0.3 GtC yr<sup>-1</sup>, down from 0.5-0.8 GtC yr<sup>-1</sup> in 2023 but still more  
246 than twice the 2014-2023 average. In Brazil, fires through September emitted 0.2-0.3 GtC yr<sup>-1</sup>, 91-118% above  
247 the 2014-2023 average due to intense drought. These fire emissions estimates should not be directly compared  
248 with the land use emissions or the land sink, because they represent a gross carbon flux to the atmosphere and  
249 do not account for post-fire recovery or distinguish between natural, climate-driven, and land-use-related fires.

250

251

## 252 1 Introduction

253 The concentration of carbon dioxide (CO<sub>2</sub>) in the atmosphere has increased from approximately 278 parts per  
254 million (ppm) in 1750 (Gulev et al., 2021), the beginning of the Industrial Era, to  $419.3 \pm 0.1$  ppm in 2023 (Lan  
255 et al., 2024a; Figure 1). The atmospheric CO<sub>2</sub> increase above pre-industrial levels was, initially, primarily  
256 caused by the release of carbon to the atmosphere from deforestation and other land-use change activities  
257 (Canadell et al., 2021). While emissions from fossil fuels started before the Industrial Era, they became the  
258 dominant source of anthropogenic emissions to the atmosphere from around 1950 and their relative share has  
259 continued to increase until present. Anthropogenic emissions occur on top of an active natural carbon cycle that  
260 circulates carbon between the reservoirs of the atmosphere, ocean, and terrestrial biosphere on time scales from  
261 sub-daily to millennial, while exchanges with geologic reservoirs occur on longer timescales (Archer et al.,  
262 2009).

263 The global carbon budget (GCB) presented here refers to the mean, variations, and trends in the perturbation of  
264 CO<sub>2</sub> in the environment, referenced to the beginning of the Industrial Era (defined here as 1750). This paper  
265 describes the components of the global carbon cycle over the historical period with a stronger focus on the  
266 recent period (since 1958, onset of robust atmospheric CO<sub>2</sub> measurements), the last decade (2014-2023), the last  
267 year (2023) and the current year (2024). Finally, it provides cumulative emissions from fossil fuels and land-use  
268 change since the year 1750, and since the year 1850 (the reference year for historical simulations in IPCC AR6)  
269 (Eyring et al., 2016).

270 We quantify the input of CO<sub>2</sub> to the atmosphere by emissions from human activities, the growth rate of  
271 atmospheric CO<sub>2</sub> concentration, and the resulting changes in the storage of carbon in the land and ocean  
272 reservoirs in response to increasing atmospheric CO<sub>2</sub> levels, climate change and variability, and other  
273 anthropogenic and natural changes (Figure 2). An understanding of this perturbation budget over time and the  
274 underlying variability and trends of the natural carbon cycle is necessary to understand the response of natural  
275 sinks to changes in climate, CO<sub>2</sub> and land-use change drivers, and to quantify emissions compatible with a given  
276 climate stabilisation target.

277 The components of the CO<sub>2</sub> budget that are reported annually in this paper include separate and independent  
278 estimates for the CO<sub>2</sub> emissions from (1) fossil fuel combustion and oxidation from all energy and industrial  
279 processes; also including cement production and carbonation ( $E_{\text{FOS}}$ ; GtC yr<sup>-1</sup>) and (2) the emissions resulting  
280 from deliberate human activities on land, including those leading to land-use change ( $E_{\text{LUC}}$ ; GtC yr<sup>-1</sup>); and their  
281 partitioning among (3) the growth rate of atmospheric CO<sub>2</sub> concentration ( $G_{\text{ATM}}$ ; GtC yr<sup>-1</sup>), and the uptake of  
282 CO<sub>2</sub> (the ‘CO<sub>2</sub> sinks’) in (4) the ocean ( $S_{\text{OCEAN}}$ ; GtC yr<sup>-1</sup>) and (5) on land ( $S_{\text{LAND}}$ ; GtC yr<sup>-1</sup>). The CO<sub>2</sub> sinks as  
283 defined here conceptually include the response of the land (including inland waters and estuaries) and ocean  
284 (including coastal and marginal seas) to elevated CO<sub>2</sub> and changes in climate and other environmental  
285 conditions, although in practice not all processes are fully accounted for (see Section 2.10). Note that the term

286 sink means that the net transfer of carbon is from the atmosphere to land or the ocean, but it does not imply any  
287 permanence of that sink in the future.

288 Global emissions and their partitioning among the atmosphere, ocean and land are in balance in the real world.  
289 Due to the combination of imperfect spatial and/or temporal data coverage, errors in each estimate, and smaller  
290 terms not included in our budget estimate (discussed in Section 2.10), the independent estimates (1) to (5) above  
291 do not necessarily add up to zero. We hence estimate a budget imbalance ( $B_{IM}$ ), which is a measure of the  
292 mismatch between the estimated emissions and the estimated changes in the atmosphere, land and ocean, as  
293 follows:

$$294 \quad B_{IM} = E_{FOS} + E_{LUC} - (G_{ATM} + S_{OCEAN} + S_{LAND}) \quad (1)$$

295  $G_{ATM}$  is usually reported in ppm yr<sup>-1</sup>, which we convert to units of carbon mass per year, GtC yr<sup>-1</sup>, using 1 ppm  
296 = 2.124 GtC (Ballantyne et al., 2012; Table 1). Units of gigatonnes of CO<sub>2</sub> (or billion tonnes of CO<sub>2</sub>) used in  
297 policy are equal to 3.664 multiplied by the value in units of GtC.

298 We also assess a set of additional lines of evidence derived from global atmospheric inversion system results  
299 (Section 2.7), observed changes in oxygen concentration (Section 2.8) and Earth System Models (ESMs)  
300 simulations (Section 2.9), all of these methods closing the global carbon balance (zero  $B_{IM}$ ).

301 We further quantify  $E_{FOS}$  and  $E_{LUC}$  by country, including both territorial and consumption-based accounting for  
302  $E_{FOS}$  (see Section 2), and discuss missing terms from sources other than the combustion of fossil fuels (see  
303 Section 2.10, Supplement S1 and S2). We also assess carbon dioxide removal (CDR) (see Sect. 2.2 and 2.3).  
304 Land-based CDR is significant, but already accounted for in  $E_{LUC}$  in equation (1) (Sect 3.2.2). Other CDR  
305 methods, not based on vegetation, are currently several orders of magnitude smaller than the other components  
306 of the budget (Sect. 3.3), hence these are not included in equation (1), or in the global carbon budget tables or  
307 figures (with the exception of Figure 2 where CDR is shown primarily for illustrative purpose).

308 The global CO<sub>2</sub> budget has been assessed by the Intergovernmental Panel on Climate Change (IPCC) in all  
309 assessment reports (Prentice et al., 2001; Schimel et al., 1995; Watson et al., 1990; Denman et al., 2007; Ciais et  
310 al., 2013; Canadell et al., 2021), and by others (e.g. Ballantyne et al., 2012). The Global Carbon Project (GCP,  
311 www.globalcarbonproject.org, last access: 21 January 2025) has coordinated this cooperative community effort  
312 for the annual publication of global carbon budgets for the year 2005 (Raupach et al., 2007; including fossil  
313 emissions only), year 2006 (Canadell et al., 2007), year 2007 (GCP, 2008), year 2008 (Le Quéré et al., 2009),  
314 year 2009 (Friedlingstein et al., 2010), year 2010 (Peters et al., 2012a), year 2012 (Le Quéré et al., 2013; Peters  
315 et al., 2013), year 2013 (Le Quéré et al., 2014), year 2014 (Le Quéré et al., 2015a; Friedlingstein et al., 2014),  
316 year 2015 (Jackson et al., 2016; Le Quéré et al., 2015b), year 2016 (Le Quéré et al., 2016), year 2017 (Le Quéré  
317 et al., 2018a; Peters et al., 2017a), year 2018 (Le Quéré et al., 2018b; Jackson et al., 2018), year 2019  
318 (Friedlingstein et al., 2019; Jackson et al., 2019; Peters et al., 2020), year 2020 (Friedlingstein et al., 2020; Le  
319 Quéré et al., 2021), year 2021 (Friedlingstein et al., 2022a; Jackson et al., 2022), year 2022 (Friedlingstein et al.,

320 2022b), and most recently the year 2023 (Friedlingstein et al., 2023). Each of these papers updated previous  
321 estimates with the latest available information for the entire time series.

322 We adopt a range of  $\pm 1$  standard deviation ( $\sigma$ ) to report the uncertainties in our global estimates, representing a  
323 likelihood of 68% that the true value will be within the provided range if the errors have a gaussian distribution,  
324 and no bias is assumed. This choice reflects the difficulty of characterising the uncertainty in the CO<sub>2</sub> fluxes  
325 between the atmosphere and the ocean and land reservoirs individually, particularly on an annual basis, as well  
326 as the difficulty of updating the CO<sub>2</sub> emissions from land-use change. A likelihood of 68% provides an  
327 indication of our current capability to quantify each term and its uncertainty given the available information.  
328 The uncertainties reported here combine statistical analysis of the underlying data, assessments of uncertainties  
329 in the generation of the datasets, and expert judgement of the likelihood of results lying outside this range. The  
330 limitations of current information are discussed in the paper and have been examined in detail elsewhere  
331 (Ballantyne et al., 2015; Zscheischler et al., 2017). We also use a qualitative assessment of confidence level to  
332 characterise the annual estimates from each term based on the type, amount, quality, and consistency of the  
333 different lines of evidence as defined by the IPCC (Stocker et al., 2013).

334 This paper provides a detailed description of the datasets and methodology used to compute the global carbon  
335 budget estimates for the industrial period, from 1750 to 2024, and in more detail for the period since 1959. This  
336 paper is updated every year using the format of ‘living data’ to keep a record of budget versions and the changes  
337 in new data, revision of data, and changes in methodology that lead to changes in estimates of the carbon  
338 budget. Additional materials associated with the release of each new version will be posted at the Global Carbon  
339 Project (GCP) website (<http://www.globalcarbonproject.org/carbonbudget>, last access: 21 January 2025), with  
340 fossil fuel emissions also available through the Global Carbon Atlas (<http://www.globalcarbonatlas.org>, last  
341 access: 21 January 2025). All underlying data used to produce the budget can also be found at  
342 <https://globalcarbonbudget.org/> (last access: 21 January 2025). With this approach, we aim to provide the  
343 highest transparency and traceability in the reporting of CO<sub>2</sub>, the key driver of climate change.

## 344 **2 Methods**

345 Multiple organisations and research groups around the world generated the original measurements and data used  
346 to complete the global carbon budget. The effort presented here is thus mainly one of synthesis, where results  
347 from individual groups are collated, analysed, and evaluated for consistency. We facilitate access to original  
348 data with the understanding that primary datasets will be referenced in future work (see Table 2 for how to cite  
349 the datasets, and Section on data availability). Descriptions of the measurements, models, and methodologies  
350 follow below, with more detailed descriptions of each component provided as Supplementary Information (S1 to  
351 S5).

352 This is the 19<sup>th</sup> version of the global carbon budget and the 13<sup>th</sup> revised version in the format of a living data  
353 update in Earth System Science Data. It builds on the latest published global carbon budget of Friedlingstein et  
354 al. (2023). The main changes this year are: the inclusion of (1) data to year 2023 and a projection for the global  
355 carbon budget for year 2024; and (2) an estimate of the 2024 projection of fossil emissions from Carbon

356 Monitor. Other methodological differences between recent annual carbon budgets (2020 to 2024) are  
357 summarised in Table 3 and previous changes since 2006 are provided in Table S9.

## 358 **2.1 Fossil CO<sub>2</sub> emissions (E<sub>FOS</sub>)**

### 359 **2.1.1 Historical period 1850-2023**

360 The estimates of global and national fossil CO<sub>2</sub> emissions (E<sub>FOS</sub>) include the oxidation of fossil fuels through  
361 both combustion (e.g., transport, heating) and chemical oxidation (e.g. carbon anode decomposition in  
362 aluminium refining) activities, and the decomposition of carbonates in industrial processes (e.g. the production  
363 of cement). We also include CO<sub>2</sub> uptake from the cement carbonation process. Several emissions sources are not  
364 estimated or not fully covered: coverage of emissions from lime production are not global, and decomposition of  
365 carbonates in glass and ceramic production are included only for the “Annex 1” countries of the United Nations  
366 Framework Convention on Climate Change (UNFCCC) for lack of activity data. These omissions are  
367 considered to be minor. Short-cycle carbon emissions - for example from combustion of biomass - are not  
368 included here but are accounted for in the CO<sub>2</sub> emissions from land use (see Section 2.2).

369 Our estimates of fossil CO<sub>2</sub> emissions rely on data collection by many other parties. Our goal is to produce the  
370 best estimate of this flux, and we therefore use a prioritisation framework to combine data from different  
371 sources that have used different methods, while being careful to avoid double counting and undercounting of  
372 emissions sources. The CDIAC-FF emissions dataset, derived largely from UN energy data, forms the  
373 foundation, and we extend emissions to 2023 using energy growth rates reported by the Energy Institute (a  
374 dataset formerly produced by BP). We then proceed to replace estimates using data from what we consider to be  
375 superior sources, for example Annex 1 countries’ official submissions to the UNFCCC. All data points are  
376 potentially subject to revision, not just the latest year. For full details see Andrew and Peters (2024).

377 Other estimates of global fossil CO<sub>2</sub> emissions exist, and these are compared by Andrew (2020a). The most  
378 common reason for differences in estimates of global fossil CO<sub>2</sub> emissions is a difference in which emissions  
379 sources are included in the datasets. Datasets such as those published by the Energy Institute, the US Energy  
380 Information Administration, and the International Energy Agency’s ‘CO<sub>2</sub> emissions from fuel combustion’ are  
381 all generally limited to emissions from combustion of fossil fuels. In contrast, datasets such as PRIMAP-hist,  
382 CEDS, EDGAR, and GCP’s dataset aim to include all sources of fossil CO<sub>2</sub> emissions. See Andrew (2020a) for  
383 detailed comparisons and discussion.

384 Cement absorbs CO<sub>2</sub> from the atmosphere over its lifetime, a process known as ‘cement carbonation’. We  
385 estimate this CO<sub>2</sub> sink, from 1931 onwards, as the average of two studies in the literature (Cao et al., 2020; Guo  
386 et al., 2021). Both studies use the same model, developed by Xi et al. (2016), with different parameterisations  
387 and input data, with the estimate of Guo and colleagues being a revision of Xi et al. (2016). The trends of the  
388 two studies are very similar. Since carbonation is a function of both current and previous cement production, we  
389 extend these estimates to 2023 by using the growth rate derived from the smoothed cement emissions (10-year

390 smoothing) fitted to the carbonation data. In the present budget, we always include the cement carbonation  
391 carbon sink in the fossil CO<sub>2</sub> emission component (E<sub>FOS</sub>).

392 We use the Kaya Identity for a simple decomposition of CO<sub>2</sub> emissions into the key drivers (Raupach et al.,  
393 2007). While there are variations (Peters et al., 2017a), we focus here on a decomposition of CO<sub>2</sub> emissions into  
394 population, GDP per person, energy use per GDP, and CO<sub>2</sub> emissions per energy. Multiplying these individual  
395 components together returns the CO<sub>2</sub> emissions. Using the decomposition, it is possible to attribute the change  
396 in CO<sub>2</sub> emissions to the change in each of the drivers. This method gives a first-order understanding of what  
397 causes CO<sub>2</sub> emissions to change each year.

### 398 **2.1.2 2024 projection**

399 We provide a projection of global fossil CO<sub>2</sub> emissions in 2024 by combining separate projections for China,  
400 USA, EU, India, and for all other countries combined. The methods are different for each of these. For China we  
401 combine monthly fossil fuel production data from the National Bureau of Statistics and trade data from the  
402 Customs Administration, giving us partial data for the growth rates to date of natural gas, petroleum, and  
403 cement, and of the apparent consumption itself for raw coal. We then use a regression model to project full-year  
404 emissions based on historical observations. For the USA our projection is taken directly from the Energy  
405 Information Administration's (EIA) Short-Term Energy Outlook (EIA, 2024), combined with the year-to-date  
406 growth rate of cement clinker production. For the EU we use monthly energy data from Eurostat to derive  
407 estimates of monthly CO<sub>2</sub> emissions, with coal emissions extended using a statistical relationship with reported  
408 electricity generation from coal and other factors. For natural gas preliminary observations are available through  
409 December. EU emissions from oil are derived using the EIA's projection of oil consumption for Europe. EU  
410 cement emissions are based on available year-to-date data from three of the largest producers, Germany, Poland,  
411 and Spain. India's projected emissions are derived from monthly estimates using the methods of Andrew  
412 (2020b) and extrapolated through December assuming seasonal patterns from before 2019. Emissions from  
413 international transportation (bunkers) are estimated separately for aviation and shipping. Changes in aviation  
414 emissions are derived primarily from OECD monthly estimates, extrapolated using the growth rates of global  
415 flight miles from Airportia, and then the final months are projected assuming normal patterns from previous  
416 years. Changes in shipping emissions are derived from OECD monthly estimates for global shipping. Emissions  
417 for the rest of the world are derived for coal and cement using projected growth in economic production from  
418 the IMF (2024) combined with extrapolated changes in emissions intensity of economic production; for oil  
419 using a global constraint from EIA; and for natural gas using a global constraint from IEA. More details on the  
420 E<sub>FOS</sub> methodology and its 2024 projection can be found in Supplement S.1.

421 For the first time this year, we cross check our 2024 projection with a 2024 projection from Carbon Monitor.  
422 Carbon Monitor is an open access dataset (<https://carbonmonitor.org/>) of daily emissions constructed using  
423 hourly to daily proxy data (e.g., electricity consumption, travel patterns, etc) instead of energy use data.  
424 Available Carbon Monitor estimated emissions from January to November are combined to a new projection for  
425 December to give a full year 2024 estimate. The December projections are estimated by leveraging seasonal



426 patterns from 2019-2023 daily CO<sub>2</sub> emission data from Carbon Monitor. A regression model is applied  
427 separately for individual countries to obtain their respective forecast. First, the seasonality component for each  
428 month is assessed based on daily average emissions from 2019 to 2023, excluding 2020 due to the COVID-19  
429 pandemic. Then, a linear regression model is constructed using the calculated seasonal components and the daily  
430 average emissions for the months from January to November 2024. The resulting model is used to project  
431 carbon emissions for the December 2024. The uncertainty range is calculated by using historical monthly  
432 variance of seasonal components.

## 433 **2.2 CO<sub>2</sub> emissions from land-use, land-use change and forestry (E<sub>LUC</sub>)**

### 434 **2.2.1 Historical period 1850-2023**

435 The net CO<sub>2</sub> flux from land-use, land-use change and forestry (E<sub>LUC</sub>, called land-use change emissions in the  
436 rest of the text) includes CO<sub>2</sub> fluxes from deforestation, afforestation, logging and forest degradation (including  
437 harvest activity), shifting cultivation (cycle of cutting forest for agriculture, then abandoning), regrowth of  
438 forests (following wood harvest or agriculture abandonment), peat burning, and peat drainage.

439 Four bookkeeping approaches were used to quantify gross emissions and gross removals and the resulting net  
440 E<sub>LUC</sub>, the updated estimates each of BLUE (Hansis et al., 2015), OSCAR (Gasser et al., 2020), and H&C2023  
441 (Houghton and Castanho, 2023), and the new estimates of LUCE (Qin et al. 2024). Emissions from peat burning  
442 and peat drainage are added from external datasets (see Supplement S.2.1): peat fire emissions from the Global  
443 Fire Emission Database (GFED4s; van der Werf et al., 2017) and peat drainage emissions averaged from  
444 estimates of the Food Agriculture Organization (Conchedda and Tubiello, 2020; FAO, 2023) and from  
445 simulations with the DGVM ORCHIDEE-PEAT (Qiu et al., 2021) and the DGVM LPX-Bern (Lienert and Joos,  
446 2018; Müller and Joos, 2021). Uncertainty estimates were derived from the Dynamic Global Vegetation Models  
447 (DGVMs) ensemble for the time period prior to 1960, and using for the recent decades an uncertainty range of  
448  $\pm 0.7 \text{ GtC yr}^{-1}$ , which is a semi-quantitative measure for annual and decadal emissions and reflects our best value  
449 judgement that there is at least 68% chance ( $\pm 1\sigma$ ) that the true land-use change emission lies within the given  
450 range, for the range of processes considered here.

451 The GCB E<sub>LUC</sub> estimates follow the CO<sub>2</sub> flux definition of global carbon cycle models and differ from IPCC  
452 definitions adopted in National GHG Inventories (NGHGI) for reporting under the UNFCCC. The latter  
453 typically include terrestrial fluxes occurring on all land that countries define as managed, following the IPCC  
454 managed land proxy approach (Grassi et al., 2018). This partly includes fluxes due to environmental change  
455 (e.g. atmospheric CO<sub>2</sub> increase), which are part of S<sub>LAND</sub> in our definition. As a result, global emission estimates  
456 are smaller for NGHGI than for the global carbon budget definition (Grassi et al., 2023). The same is the case  
457 for the FAO estimates of carbon fluxes on forest land, which include both anthropogenic and natural fluxes on  
458 managed land (Tubiello et al., 2021). We translate the GCB and NGHGI definitions to each other, to provide a  
459 comparison of the anthropogenic carbon budget as reported in GCB to the official country reporting to the  
460 UNFCCC convention. We further compare these estimates with the net atmosphere-to-land flux from  
461 atmospheric inversion systems (see Section 2.7), averaged over managed land only.

462 ELUC contains a range of fluxes that are related to Carbon Dioxide Removal (CDR). CDR is defined as the set of  
463 anthropogenic activities that remove CO<sub>2</sub> from the atmosphere, in addition to the Earth's natural processes (such  
464 as carbon uptake in response to atmospheric CO<sub>2</sub> increase), and store it in durable form, such as in forest  
465 biomass, soils, long-lived products, ocean or geological reservoirs. Here, we quantify vegetation-based CDR  
466 that is implicitly or explicitly captured by land-use fluxes (CDR not based on vegetation is discussed in Section  
467 2.3). We quantify re/afforestation from the four bookkeeping estimates by separating forest regrowth in shifting  
468 cultivation cycles from permanent increases in forest cover (see Supplement S.2.1). The latter count as CDR,  
469 but it should be noted that the permanence of the storage under climate risks such as fire is increasingly  
470 questioned. Other CDR activities related to land use but not fully accounted for in our ELUC estimate include the  
471 transfer of carbon to harvested wood products (HWP), bioenergy with carbon capture and storage (BECCS), and  
472 biochar production (Babiker et al., 2022; Smith et al., 2024). The different bookkeeping models all represent  
473 HWP but with varying details concerning product usage and their lifetimes. BECCS and biochar are currently  
474 only represented in bookkeeping and TRENDY models with regard to the CO<sub>2</sub> removal through photosynthesis,  
475 without accounting for the durable storage. HWP, BECCS, and biochar are typically counted as CDR once the  
476 transfer to the durable storage site occurs and not when the CO<sub>2</sub> is removed from the atmosphere, which  
477 complicates a direct comparison to the GCB approach to quantify annual fluxes to and from the atmosphere. We  
478 provide estimates for CDR through HWP, BECCS, and biochar based on independent studies in Section 3.2.2,  
479 but do not add them to our ELUC estimate to avoid potential double-counting that arises from the partial  
480 consideration of HWP, BECCS, and biochar in the bookkeeping and TRENDY models and to avoid  
481 inconsistencies from the temporal discrepancy between transfer to storage and removal from the atmosphere.

### 482 **2.2.2 2024 Projection**

483 We project the 2024 land-use emissions for BLUE, H&C2023, OSCAR, and LUCE based on their ELUC  
484 estimates for 2023 and adding the change in carbon emissions from peat fires and tropical deforestation and  
485 degradation fires (2024 emissions relative to 2023 emissions) estimated using active fire data (MCD14ML;  
486 Giglio et al., 2016). Peat drainage is assumed to be unaltered as it has low interannual variability. More details  
487 on the ELUC methodology can be found in Supplement S.2.

### 488 **2.3 Carbon Dioxide Removal (CDR) not based on vegetation**

489 While some CDR involves CO<sub>2</sub> fluxes via land-use and is included in our estimate of *ELUC*, (re/afforestation) or  
490 provided from other data sources (biochar, HWP, and BECCS), other CDR occurs through fluxes of CO<sub>2</sub>  
491 directly from the air to the geosphere. The majority of this derives from enhanced weathering through the  
492 application of crushed rock to soils, with a smaller contribution from Direct Air Carbon Capture and Storage  
493 (DACCS). We use data from the State of CDR Report (Smith et al., 2024), which compiles and harmonises  
494 reported removal rates from a combination of existing databases, surveys and novel research. Currently there are  
495 no internationally agreed methods for reporting these types of CDR, meaning estimates are based on self-  
496 disclosure by projects following their own protocols. As such, the fractional uncertainty on these numbers

497 should be viewed as substantial, and they are liable to change in future years as protocols are harmonised and  
498 improved.

## 499 **2.4 Growth rate in atmospheric CO<sub>2</sub> concentration (G<sub>ATM</sub>)**

### 500 **2.4.1 Historical period 1850-2023**

501 The rate of growth of the atmospheric CO<sub>2</sub> concentration is provided for years 1959-2023 by the US National  
502 Oceanic and Atmospheric Administration Global Monitoring Laboratory (NOAA/GML; Lan et al., 2024a),  
503 which includes recent revisions to the calibration scale of atmospheric CO<sub>2</sub> measurements (WMO-CO<sub>2</sub>-X2019;  
504 Hall et al., 2021). For the 1959-1979 period, the global growth rate is based on measurements of atmospheric  
505 CO<sub>2</sub> concentration averaged from the Mauna Loa and South Pole stations, as observed by the CO<sub>2</sub> Program at  
506 Scripps Institution of Oceanography (Keeling et al., 1976). For the 1980-2021 time period, the global growth  
507 rate is based on the average of multiple stations selected from the marine boundary layer sites with well-mixed  
508 background air (Lan et al., 2023), after fitting a smooth curve through the data for each station as a function of  
509 time, and averaging by latitude band (Masarie and Tans, 1995). The annual growth rate is estimated by Lan et  
510 al. (2024a) from atmospheric CO<sub>2</sub> concentration by taking the average of the most recent December-January  
511 months corrected for the average seasonal cycle and subtracting this same average one year earlier. The growth  
512 rate in units of ppm yr<sup>-1</sup> is converted to units of GtC yr<sup>-1</sup> by multiplying by a factor of 2.124 GtC per ppm,  
513 assuming instantaneous mixing of CO<sub>2</sub> throughout the atmosphere (Ballantyne et al., 2012; Table 1).

514 The uncertainty around the atmospheric growth rate is due to three main factors. First, the network composition  
515 of the marine boundary layer sites with some sites coming or going, gaps in the time series at each site, etc. This  
516 uncertainty was estimated with a bootstrap method by constructing 100 "alternative" networks (Steele et al.,  
517 1992; Masarie and Tans, 1995; Lan et al., 2024a). Second, the analytical uncertainty that describes the short-  
518 and long-term uncertainties associated with the CO<sub>2</sub> analyzers. A Monte Carlo method was used to estimate the  
519 total analytical uncertainty by randomly selecting errors to add to each observation from a normal distribution of  
520 combined short- and long-term uncertainties. Prior to the 1980s when analyzers were less precise and CO<sub>2</sub>  
521 measurement scale was slightly less well defined, larger analytical errors were assigned to account for these  
522 factors. However, the network uncertainty remains the larger term of uncertainty. The first and second  
523 uncertainties are reported as 1-sigma standard deviations (i.e., 68% confidence interval), and summed in  
524 quadrature to determine the global surface growth rate uncertainty, which averaged to 0.085 ppm (Lan et al.,  
525 2024b). Third, the uncertainty associated with using the average CO<sub>2</sub> concentration from a surface network to  
526 approximate the true atmospheric average CO<sub>2</sub> concentration (mass-weighted, in 3 dimensions) as needed to  
527 assess the total atmospheric CO<sub>2</sub> burden. In reality, CO<sub>2</sub> variations measured at the stations will not exactly  
528 track changes in total atmospheric burden, with offsets in magnitude and phasing due to vertical and horizontal  
529 mixing. This effect must be very small on decadal and longer time scales, when the atmosphere can be  
530 considered well mixed. The long-term CO<sub>2</sub> increase in the stratosphere lags the increase (meaning lower  
531 concentrations) that we observe in the marine boundary layer, while the continental boundary layer (where most  
532 of the emissions take place) leads the marine boundary layer with higher concentrations. These effects nearly

533 cancel each other. In addition, the growth rate is nearly the same everywhere (Ballantyne et al., 2012). We  
534 therefore maintain an uncertainty around the annual growth rate based on the multiple stations dataset ranges  
535 between 0.11 and 0.72 GtC yr<sup>-1</sup>, with a mean of 0.61 GtC yr<sup>-1</sup> for 1959-1979 and 0.17 GtC yr<sup>-1</sup> for 1980-2023,  
536 when more measurement sites were available (Lan et al., 2024a). We estimate the uncertainty of the  
537 decadal averaged growth rate after 1980 at 0.02 GtC yr<sup>-1</sup> based on the annual growth rate uncertainty but  
538 stretched over a 10-year interval. For years prior to 1980, we estimate the decadal averaged uncertainty to be  
539 0.07 GtC yr<sup>-1</sup> based on a factor proportional to the annual uncertainty prior and after 1980 ( $0.02 * [0.61/0.17]$   
540 GtC yr<sup>-1</sup>).

541 We assign a high confidence to the annual estimates of  $G_{ATM}$  because they are based on direct measurements  
542 from stations distributed around the world (Lan et al 2023) with all CO<sub>2</sub> measurements consistently measured  
543 against the same CO<sub>2</sub> standard scale (WMO X2019) defined by a suite of gas standards (Hall et al., 2021).

544 To estimate the total carbon accumulated in the atmosphere since 1750 or 1850, we use an atmospheric CO<sub>2</sub>  
545 concentration of  $278.3 \pm 3$  ppm or  $285.1 \pm 3$  ppm, respectively (Gulev et al., 2021). For the construction of the  
546 cumulative budget shown in Figure 3, we use the fitted estimates of CO<sub>2</sub> concentration from Joos and Spahni  
547 (2008) to estimate the annual atmospheric growth rate using the conversion factors shown in Table 1. The  
548 uncertainty of  $\pm 3$  ppm (converted to  $\pm 1\sigma$ ) is taken directly from the IPCC's AR5 assessment (Ciais et al., 2013).  
549 Typical uncertainties in the growth rate in atmospheric CO<sub>2</sub> concentration from ice core data are equivalent to  
550  $\pm 0.1$ - $0.15$  GtC yr<sup>-1</sup> as evaluated from the Law Dome data (Etheridge et al., 1996) for individual 20-year intervals  
551 over the period from 1850 to 1960 (Bruno and Joos, 1997).

#### 552 **2.4.2 2024 projection**

553 We provide an assessment of  $G_{ATM}$  for 2024 as the average of two methods. The GCB regression method  
554 models monthly global-average atmospheric CO<sub>2</sub> concentrations and derives the increment and annual average  
555 from these. The model uses lagged observations of concentration (Lan et al., 2024a): both a 12-month lag, and  
556 the lowest lag that will allow model prediction to produce an estimate for the following January, recalling that  
557 the  $G_{ATM}$  increment is derived from December/January pairs. The largest driver of interannual changes is the  
558 ENSO signal (Betts et al., 2016), so the monthly ENSO 3.4 index (Huang et al., 2023) is included in the model.  
559 Given the natural lag between sea-surface temperatures and effects on the biosphere, and in turn effects on  
560 globally mixed atmospheric CO<sub>2</sub> concentration, a lagged ENSO index is used, and we use both a 5-month and a  
561 6-month lag. The combination of the two lagged ENSO values helps reduce possible effects of noise in a single  
562 month. To help characterise the seasonal variation, we add month as a categorical variable. Finally, we flag the  
563 period affected by the Pinatubo eruption (August 1991 - November 1993) as a categorical variable. Note that  
564 while emissions of CO<sub>2</sub> are the largest driver of the trend in atmospheric CO<sub>2</sub> concentration, our goal here is to  
565 predict divergence from that trend. Because changes in emissions from year to year are relatively minor in  
566 comparison to total emissions, this has little effect on the variation of concentration from the trend line. Even the  
567 relatively large drop in emissions in 2020 due to the COVID-19 pandemic does not cause any problems for the  
568 model.

569 We also use the multi-model mean and uncertainty of the 2024  $G_{ATM}$  estimated by the ESMS prediction system  
570 (see Section 2.9). We then take the average of the GCB regression and ESMS  $G_{ATM}$  estimates, with their  
571 respective uncertainty combined quadratically.

572 Similarly, the projection of the 2024 global average  $CO_2$  concentration (in ppm), is calculated as the average of  
573 the estimates from the two methods. For the GCB regression method, it is the annual average of global  
574 concentration over the 12 months of 2024; for the ESMS, it is the observed global average  $CO_2$  concentration for  
575 2023 plus the annual increase in 2024 of the global average  $CO_2$  concentration predicted by the ESMS multi-  
576 model mean.

## 577 **2.5 Ocean $CO_2$ sink**

### 578 **2.5.1 Historical period 1850-2023**

579 The reported estimate of the global ocean anthropogenic  $CO_2$  sink  $S_{OCEAN}$  is derived as the average of two  
580 estimates. The first estimate is derived as the mean over an ensemble of ten global ocean biogeochemistry  
581 models (GOBMs, Table 4 and Table S2). The second estimate is obtained as the mean over an ensemble of eight  
582 surface ocean  $fCO_2$ -observation-based data-products (Table 4 and Table S3). A ninth  $fCO_2$ -product (UEXP-FFN-  
583 U) is shown but is not included in the ensemble average as it differs from the other products by adjusting the  
584 flux to a cool, salty ocean surface skin. In previous editions of the GCB, this product was following the Watson  
585 et al. (2020) method but has been updated following the method of Dong et al. (2022, see Supplement S.3.1 for  
586 a discussion). The GOBMs simulate both the natural and anthropogenic  $CO_2$  cycles in the ocean. They constrain  
587 the anthropogenic air-sea  $CO_2$  flux (the dominant component of  $S_{OCEAN}$ ) by the transport of carbon into the  
588 ocean interior, which is also the controlling factor of present-day ocean carbon uptake in the real world. They  
589 cover the full globe and all seasons and were evaluated against surface ocean carbon observations, suggesting  
590 they are suitable to estimate the annual ocean carbon sink (Hauck et al., 2020). The  $fCO_2$ -products are tightly  
591 linked to observations of  $fCO_2$  (fugacity of  $CO_2$ , which equals  $pCO_2$  corrected for the non-ideal behaviour of the  
592 gas; Pfeil et al., 2013), which carry imprints of temporal and spatial variability, but are also sensitive to  
593 uncertainties in gas-exchange parameterizations and data-sparsity (Fay et al., 2021, Gloege et al., 2021, Hauck  
594 et al., 2023a). Their asset is the assessment of the mean spatial pattern of variability and its seasonality (Hauck  
595 et al., 2020, Gloege et al. 2021, Hauck et al., 2023a). To benchmark trends derived from the  $fCO_2$ -products, we  
596 additionally performed a model subsampling exercise following Hauck et al. (2023a, see section S3). In  
597 addition, two diagnostic ocean models are used to estimate  $S_{OCEAN}$  over the industrial era (1781-1958).

598 The global  $fCO_2$ -based flux estimates were adjusted to remove the pre-industrial ocean source of  $CO_2$  to the  
599 atmosphere of  $0.65 \pm 0.3$  GtC  $yr^{-1}$  from river input to the ocean (Regnier et al., 2022), to satisfy our definition of  
600  $S_{OCEAN}$  (Hauck et al., 2020). The river flux adjustment was distributed over the latitudinal bands using the  
601 regional distribution of Lacroix et al. (2020; North: 0.14 GtC  $yr^{-1}$ , Tropics: 0.42 GtC  $yr^{-1}$ , South: 0.09 GtC  $yr^{-1}$ ).  
602 Acknowledging that this distribution is based on only one model, the advantage is that a gridded field is  
603 available, and the river flux adjustment can be calculated for the three latitudinal bands and the RECCAP  
604 regions (REgional Carbon Cycle Assessment and Processes (RECCAP2; Ciais et al., 2020, Poulter et al., 2022,

605 DeVries et al., 2023). This dataset suggests that more of the riverine outgassing is located in the tropics than in  
606 the Southern Ocean and is thus opposed to the previously used dataset of Aumont et al. (2001). Accordingly, the  
607 regional distribution is associated with a major uncertainty in addition to the large uncertainty around the global  
608 estimate (Crisp et al., 2022; Gruber et al., 2023). Anthropogenic perturbations of river carbon and nutrient  
609 transport to the ocean are not considered (see Section 2.10 and Supplement S.6.3).

610 We derive  $S_{\text{OCEAN}}$  from GOBMs by using a simulation (sim A) with historical forcing of climate and  
611 atmospheric  $\text{CO}_2$  from GCB (Section 2.4), accounting for model biases and drift from a control simulation (sim  
612 B) with constant atmospheric  $\text{CO}_2$  and normal year climate forcing. A third simulation (sim C) with historical  
613 atmospheric  $\text{CO}_2$  increase and normal year climate forcing is used to attribute the ocean sink to  $\text{CO}_2$  (sim C  
614 minus sim B) and climate (sim A minus sim C) effects. A fourth simulation (sim D; historical climate forcing  
615 and constant atmospheric  $\text{CO}_2$ ) is used to compare the change in anthropogenic carbon inventory in the interior  
616 ocean (sim A minus sim D) to the observational estimate of Gruber et al. (2019) with the same flux components  
617 (steady state and non-steady state anthropogenic carbon flux). The  $f\text{CO}_2$ -products are adjusted with respect to  
618 their original publications to represent the full ice-free ocean area, including coastal zones and marginal seas,  
619 when the area coverage is below 99%. This is done by either area filling following Fay et al. (2021) or a simple  
620 scaling approach. GOBMs and  $f\text{CO}_2$ -products fall within the observational constraints over the 1990s ( $2.2 \pm 0.7$   
621  $\text{GtC yr}^{-1}$ , Ciais et al., 2013) before and after applying adjustments.

622  $S_{\text{OCEAN}}$  is calculated as the average of the GOBM ensemble mean and the  $f\text{CO}_2$ -product ensemble mean from  
623 1990 onwards. Prior to 1990, it is calculated as the GOBM ensemble mean plus half of the offset between  
624 GOBMs and  $f\text{CO}_2$ -products ensemble means over 1990-2001.

625 We assign an uncertainty of  $\pm 0.4 \text{ GtC yr}^{-1}$  to the ocean sink based on a combination of random (ensemble  
626 standard deviation) and systematic uncertainties (GOBMs bias in anthropogenic carbon accumulation,  
627 previously reported uncertainties in  $f\text{CO}_2$ -products; see Supplement S.3.4). While this approach is consistent  
628 within the GCB, an independent uncertainty assessment of the  $f\text{CO}_2$ -products alone suggests a somewhat larger  
629 uncertainty of up to  $0.7 \text{ GtC yr}^{-1}$  (Ford et al. 2024, accepted). We assess a medium confidence level to the  
630 annual ocean  $\text{CO}_2$  sink and its uncertainty because it is based on multiple lines of evidence, it is consistent with  
631 ocean interior carbon estimates (Gruber et al., 2019, see Section 3.6.5) and the interannual variability in the  
632 GOBMs and data-based estimates is largely consistent and can be explained by climate variability. We refrain  
633 from assigning a high confidence because of the deviation between the GOBM and  $f\text{CO}_2$ -product trends  
634 between around 2002 and 2020. More details on the  $S_{\text{OCEAN}}$  methodology can be found in Supplement S.3.

## 635 **2.5.2 2024 Projection**

636 The ocean  $\text{CO}_2$  sink forecast for the year 2024 is based on (a) the historical (Lan et al., 2024a) and our 2024  
637 estimate of atmospheric  $\text{CO}_2$  concentration, (b) the historical and our 2024 estimate of global fossil fuel  
638 emissions, and (c) the boreal spring (March, April, May) Oceanic Niño Index (ONI) (NCEP, 2024). Using a  
639 non-linear regression approach, i.e., a feed-forward neural network, atmospheric  $\text{CO}_2$ , ONI, and the fossil fuel  
640 emissions are used as training data to best match the annual ocean  $\text{CO}_2$  sink (i.e. combined  $S_{\text{OCEAN}}$  estimate from

641 GOBMs and data products) from 1959 through 2023 from this year’s carbon budget. Using this relationship, the  
642 2024  $S_{OCEAN}$  can then be estimated from the projected 2024 input data using the non-linear relationship  
643 established during the network training. “To avoid overfitting, the neural network training was done using a  
644 Monte Carlo approach, with a variable number of artificial neurons (varying between 2-5) and 20% of the  
645 randomly selected training data were withheld for independent internal testing”

646 Based on the best output performance (tested using the 20% withheld input data), the best performing number of  
647 neurons was selected. In a second step, we trained the network 10 times using the best number of neurons  
648 identified in step 1 and different sets of randomly selected training data. The mean of the 10 trainings is  
649 considered our best forecast, whereas the standard deviation of the 10 ensembles provides a first order estimate  
650 of the forecast uncertainty. This uncertainty is then combined with the  $S_{OCEAN}$  uncertainty ( $0.4 \text{ GtC yr}^{-1}$ ) to  
651 estimate the overall uncertainty of the 2024 projection. As an additional line of evidence, we also assess the  
652 2024 atmosphere-ocean carbon flux from the ESM prediction system (see Section 2.9).

## 653 **2.6 Land CO<sub>2</sub> sink**

### 654 **2.6.1 Historical Period 1850-2023**

655 The terrestrial land sink ( $S_{LAND}$ ) is thought to be due to the combined effects of rising atmospheric CO<sub>2</sub>,  
656 increasing N inputs, and climate change, on plant growth and terrestrial carbon storage.  $S_{LAND}$  does not include  
657 land sinks directly resulting from land-use and land-use change (e.g., regrowth of vegetation) as these are part of  
658 the land-use flux ( $E_{LUC}$ ), although system boundaries make it difficult to attribute exactly CO<sub>2</sub> fluxes on land  
659 between  $S_{LAND}$  and  $E_{LUC}$  (Erb et al., 2013).

660  $S_{LAND}$  is estimated from the multi-model mean of 20 DGVMs (Table 4 and Table S1). DGVMs simulations  
661 include all climate variability and CO<sub>2</sub> effects over land. In addition to the carbon cycle represented in all  
662 DGVMs, 14 models also account for the nitrogen cycle and hence can include the effect of N inputs on  $S_{LAND}$ .  
663 The DGVMs estimate of  $S_{LAND}$  does not include the export of carbon to aquatic systems or its historical  
664 perturbation, which is discussed in Supplement S.6.3. DGVMs need to meet several criteria to be included in  
665 this assessment. In addition, we use the International Land Model Benchmarking system (ILAMB; Collier et al.,  
666 2018) for the DGVMs evaluation (see Supplement S.4.2), with an additional comparison of DGVMs with a  
667 data-informed, Bayesian model-data fusion framework (CARDAMOM) (Bloom and Williams, 2015; Bloom et  
668 al., 2016). The uncertainty on  $S_{LAND}$  is taken from the DGVMs standard deviation. More details on the  $S_{LAND}$   
669 methodology can be found in Supplement S.4.

### 670 **2.6.2 2024 Projection**

671 Like for the ocean forecast, the land CO<sub>2</sub> sink forecast for the year 2024 is based on (a) the historical (Lan et al.,  
672 2024a) and our 2024 estimate of atmospheric CO<sub>2</sub> concentration, (b) the historical and our 2024 estimate of  
673 global fossil fuel emissions, and (c) the boreal summer (June, July, August) Oceanic Niño Index (ONI) (NCEP,  
674 2024). All training data are again used to best match  $S_{LAND}$  from 1959 through 2023 from this year’s carbon

675 budget using a feed-forward neural network. To avoid overfitting, the neural network was trained with a  
676 variable number of artificial neurons (varying between 2-15), larger than for  $S_{\text{OCEAN}}$  prediction due to the  
677 stronger land carbon interannual variability. As done for  $S_{\text{OCEAN}}$ , a Monte Carlo type pre-training selects the  
678 optimal number of artificial neurons based on 20% withheld input data, and in a second step, an ensemble of  
679 10 forecasts is produced to provide the mean forecast plus uncertainty. This uncertainty is then combined with  
680 the  $S_{\text{LAND}}$  uncertainty for 2023 ( $1.0 \text{ GtC yr}^{-1}$ ) to estimate the overall uncertainty of the 2024 projection.

## 681 **2.7 Atmospheric inversion estimate**

682 The world-wide network of in-situ atmospheric measurements and satellite derived atmospheric  $\text{CO}_2$  column ( $X_{\text{CO}_2}$ ) observations put a strong constraint on changes in the atmospheric abundance of  $\text{CO}_2$ . This is true  
683 globally (hence our large confidence in  $G_{\text{ATM}}$ ), but also in regions with sufficient observational density found  
684 mostly in the extra-tropics. This allows atmospheric inversion methods to constrain the magnitude and location  
685 of the combined total surface  $\text{CO}_2$  fluxes from all sources, including fossil and land-use change emissions and  
686 land and ocean  $\text{CO}_2$  fluxes. The inversions assume  $E_{\text{FOS}}$  to be well known, and they solve for the spatial and  
687 temporal distribution of land and ocean fluxes from the residual gradients of  $\text{CO}_2$  between stations that are not  
688 explained by fossil fuel emissions. By design, such systems thus close the carbon balance ( $B_{\text{IM}} = 0$ ) and thus  
689 provide an additional perspective on the independent estimates of the ocean and land fluxes.  
690

691 This year's release includes fourteen inversion systems that are described in Table S4. Each system is rooted in  
692 Bayesian inversion principles but uses different methodologies. These differences concern the selection of  
693 atmospheric  $\text{CO}_2$  data or  $X_{\text{CO}_2}$ , and the choice of a-priori fluxes to refine. They also differ in spatial and  
694 temporal resolution, assumed correlation structures, and mathematical approach of the models (see references in  
695 Table S4 for details). Importantly, the systems use a variety of transport models, which was demonstrated to be  
696 a driving factor behind differences in atmospheric inversion-based flux estimates, and specifically their  
697 distribution across latitudinal bands (Gaubert et al., 2019; Schuh et al., 2019). Eight inversion systems used  
698 surface observations from the global measurement network (Schuldt et al., 2023, 2024). Six inversion systems  
699 (CAMs-FT24r1, CMS-flux, GONGGA, COLA, GCASv2, NTFVAR) used satellite  $X_{\text{CO}_2}$  retrievals from  
700 GOSAT and/or OCO-2, scaled to the WMO 2019 calibration scale, of which three inversions this year (CMS-  
701 Flux, COLA, NTFVAR) used these  $X_{\text{CO}_2}$  datasets in addition to the in-situ observational  $\text{CO}_2$  mole fraction  
702 records.

703 The original products delivered by the inverse modellers were modified to facilitate the comparison to the other  
704 elements of the budget, specifically on two accounts: (1) global total fossil fuel emissions including cement  
705 carbonation  $\text{CO}_2$  uptake, and (2) riverine  $\text{CO}_2$  transport. We note that with these adjustments the inverse results  
706 no longer represent the net atmosphere-surface exchange over land/ocean areas as sensed by atmospheric  
707 observations. Instead, for land, they become the net uptake of  $\text{CO}_2$  by vegetation and soils that is not exported  
708 by fluvial systems, similar to the DGVMs estimates. For oceans, they become the net uptake of anthropogenic  
709  $\text{CO}_2$ , similar to the GOBMs estimates.



710 The inversion systems prescribe global fossil fuel emissions based on e.g. the GCP's Gridded Fossil Emissions  
711 Dataset versions 2024.0 (GCP-GridFED; Jones et al., 2024a), which are updates to GCP-GridFEDv2021  
712 presented by Jones et al. (2021b). GCP-GridFEDv2024.0 scales gridded estimates of CO<sub>2</sub> emissions from  
713 EDGARv4.3.2 (Janssens-Maenhout et al., 2019) within national territories to match national emissions  
714 estimates provided by the GCB for the years 1959-2023, which were compiled following the methodology  
715 described in Section 2.1. Small differences between the systems due to for instance regridding to the transport  
716 model resolution, or use of different fossil fuel emissions than GCP-GridFEDv2024.0, are adjusted in the  
717 latitudinal partitioning we present, to ensure agreement with the estimate of E<sub>FOS</sub> in this budget. We also note  
718 that the ocean fluxes used as prior by 8 out of 14 inversions are part of the suite of the ocean process model or  
719 fCO<sub>2</sub>-products listed in Section 2.5. Although these fluxes are further adjusted by the atmospheric inversions  
720 (except for Jena CarboScope), it makes the inversion estimates of the ocean fluxes not completely independent  
721 of S<sub>OCEAN</sub> assessed here.

722 To facilitate comparisons to the independent S<sub>OCEAN</sub> and S<sub>LAND</sub>, we used the same adjustments for transport and  
723 outgassing of carbon transported from land to ocean, as done for the observation-based estimates of S<sub>OCEAN</sub> (see  
724 Supplement S.3).

725 The atmospheric inversions are evaluated using vertical profiles of atmospheric CO<sub>2</sub> concentrations (Figure S5).  
726 More than 30 aircraft programs over the globe, either regular programs or repeated surveys over at least 9  
727 months (except for SH programs), have been used to assess system performance (with space-time observational  
728 coverage sparse in the SH and tropics, and denser in NH mid-latitudes; Table S8). The fourteen systems are  
729 compared to the independent aircraft CO<sub>2</sub> measurements between 2 and 7 km above sea level between 2001 and  
730 2023. Results are shown in Figure S5 and discussed in Supplement S.5.2.

731 With a relatively small ensemble of systems that cover at least one full decade (N=10), and which moreover  
732 share some a-priori fluxes used with one another, or with the process-based models, it is difficult to justify using  
733 their mean and standard deviation as a metric for uncertainty across the ensemble. We therefore report their full  
734 range (min-max) without their mean. More details on the atmospheric inversion methodology can be found in  
735 Supplement S.5.

## 736 **2.8 Atmospheric oxygen based estimate**

737 Long-term atmospheric O<sub>2</sub> and CO<sub>2</sub> observations allow estimation of the global ocean and land carbon sinks,  
738 due to the coupling of O<sub>2</sub> and CO<sub>2</sub> with distinct exchange ratios for fossil fuel emissions and land uptake, and  
739 uncoupled O<sub>2</sub> and CO<sub>2</sub> ocean exchange (Keeling and Manning, 2014). The global ocean and net land carbon  
740 sinks were calculated following methods and constants used in Keeling and Manning (2014) but modified to  
741 also include the effective O<sub>2</sub> source from metal refining (Battle et al., 2023). For the exchange ratio of the net  
742 land sink at value of 1.05 is used, following Resplandy et al. (2019). For fossil fuels, the following values are  
743 used: gas: 1.95 (+/-) 0.04, liquid: 1.44, (+/-) 0.03, solid: 1.17 (+/-) 0.03, cement: 0 (+/-) 0, gas flaring: 1.98 (+/-)  
744 0.07 (Keeling, 1988). Atmospheric O<sub>2</sub> is observed as δ(O<sub>2</sub>/N<sub>2</sub>) and combined with CO<sub>2</sub> mole fraction observations  
745 into Atmospheric Potential Oxygen (APO, Stephens et al., 1998). The APO observations from 1990 to 2024

746 were taken from a weighted average of flask records from three stations in the Scripps O<sub>2</sub> program network  
747 (Alert, Canada (ALT), La Jolla, California (LJO), and Cape Grim, Australia (CGO), weighted per Keeling and  
748 Manning (2014). Observed CO<sub>2</sub> was taken from the globally averaged marine surface annual mean growth rate  
749 from the NOAA/GML Global Greenhouse Gas Reference Network (Lan et al., 2024a). The O<sub>2</sub> source from  
750 ocean warming is based on ocean heat content from updated data from NOAA/NCEI (Levitus et al., 2012). The  
751 effective O<sub>2</sub> source from metal refining is based on production data from Bray (2020), Flanagan (2021), and  
752 Tuck (2022). Uncertainty was determined through a Monte Carlo approach with 20,000 iterations, using  
753 uncertainties prescribed in Keeling and Manning (2014), including observational uncertainties from Keeling et  
754 al. (2007) and autoregressive errors in fossil fuel emissions (Ballantyne et al., 2015). The reported uncertainty is  
755 1 standard deviation of the ensemble. The difference between the atmospheric O<sub>2</sub> estimate for GCB2023 is due  
756 to a revision to the Scripps O<sub>2</sub> program CO<sub>2</sub> data. As for the atmospheric inversions, the O<sub>2</sub> based estimates also  
757 closes the carbon balance ( $B_{IM} = 0$ ) by design and provides another independent estimate of the ocean and land  
758 fluxes. Note that the O<sub>2</sub> method requires a correction for global air-sea O<sub>2</sub> flux, which has the largest uncertainty  
759 at annual time scales, but which is still non negligible for decadal estimates (Nevison et al., 2008).

## 760 **2.9 Earth System Models estimate**

761 Reconstructions and predictions from decadal prediction systems based on Earth system models (ESMs) provide  
762 a novel line of evidence in assessing the atmosphere-land and atmosphere-ocean carbon fluxes in the past  
763 decades and predicting their changes for the current year. The decadal prediction systems based on ESMs used  
764 here consist of three sets of simulations: (i) uninitialized freely evolving historical simulations (1850-2014); (ii)  
765 assimilation reconstruction incorporating observational data into the model (1960-2023); (iii) initialised  
766 prediction simulations for the 1981-2024 period, starting every year from initial states obtained from the above  
767 assimilation simulations. The assimilations are designed to reconstruct the actual evolution of the Earth system  
768 by assimilating essential fields from data products. The assimilations' states, which are expected to be close to  
769 observations, are used to start the initialised prediction simulations used for the current year (2024) global  
770 carbon budget. Similar initialised prediction simulations starting every year (Nov. 1st or Jan. 1st) over the 1981-  
771 2023 period (i.e., hindcasts) are also performed for predictive skill quantification and for bias correction. More  
772 details on the illustration of a decadal prediction system based on an ESM can refer to Figure 1 of Li et al.  
773 (2023).

774 By assimilating physical atmospheric and oceanic data products into the ESMs, the models are able to reproduce  
775 the historical variations of the atmosphere-sea CO<sub>2</sub> fluxes, atmosphere-land CO<sub>2</sub> fluxes, and atmospheric CO<sub>2</sub>  
776 growth rate (Li et al., 2016, 2019; Lovenduski et al., 2019a,b; Ilyina et al., 2021; Li et al., 2023). Furthermore,  
777 the ESM-based predictions have proven their skill in predicting the air-sea CO<sub>2</sub> fluxes for up to 6 years, the air-  
778 land CO<sub>2</sub> fluxes and atmospheric CO<sub>2</sub> growth for 2 years (Lovenduski et al., 2019a,b; Ilyina et al., 2021; Li et  
779 al., 2023). The reconstructions from the fully coupled model simulations ensure a closed budget within the Earth  
780 system, i.e., no budget imbalance term.

781 Five ESMs, i.e., CanESM5 (Swart et al., 2019; Sospedra-Alfonso et al., 2021), EC-Earth3-CC (Döscher et al.  
782 2021; Bilbao et al., 2021; Bernardello et al., 2024), IPSL-CM6A-CO2-LR (Boucher et al., 2020), MIROC-ES2L  
783 (Watanabe et al., 2020), and MPI-ESM1-2-LR (Mauritsen et al., 2019; Li et al., 2023), have performed the set of  
784 prediction simulations. Each ESM uses a different assimilation method and combination of data products  
785 incorporated in the system, more details on the models configuration can be found in Table 4 and Supplementary  
786 Table S5. The ESMs use external forcings from the Coupled Model Intercomparison Project Phase 6 (CMIP6)  
787 historical (1960-2014) plus SSP2-4.5 baseline and CovidMIP two-year blip scenario (2015-2024) (Eyring et al.,  
788 2016; Lamboll et al., 2021). The CO<sub>2</sub> emissions forcing from 2015-2024 are substituted by GCB-GridFED  
789 (v2024.0, Jones et al., 2024a) to provide a consistent CO<sub>2</sub> forcing. Reconstructions of atmosphere-ocean CO<sub>2</sub>  
790 fluxes ( $S_{OCEAN}$ ) and atmosphere-land CO<sub>2</sub> fluxes ( $S_{LAND-ELUC}$ ) for the time period from 1960-2023 are assessed  
791 here. Predictions of the atmosphere-ocean CO<sub>2</sub> flux, atmosphere-land CO<sub>2</sub> flux, and atmospheric CO<sub>2</sub> growth for  
792 2024 are calculated based on the predictions at a lead time of 1 year. The predictions are bias corrected using the  
793 1985-2014 climatology mean of GCB2022 (Friedlingstein et al., 2022), more details on methods can be found in  
794 Boer et al. (2016) and Li et al. (2023). The ensemble size of initialized prediction simulations is 10, and the  
795 ensemble mean for each individual model is used here. The ESMs are used here to support the assessment of  
796  $S_{OCEAN}$  and net atmosphere-land CO<sub>2</sub> flux ( $S_{LAND} - E_{LUC}$ ) over the 1960-2023 period, and to provide an estimate  
797 of the 2024 projection of  $G_{ATM}$ .

## 798 **2.10 Processes not included in the global carbon budget**

799 The contribution of anthropogenic CO and CH<sub>4</sub> to the global carbon budget is not fully accounted for in Eq. (1)  
800 and is described in Supplement S.6.1. The contributions to CO<sub>2</sub> emissions of decomposition of carbonates not  
801 accounted for is described in Supplement S.6.2. The contribution of anthropogenic changes in river fluxes is  
802 conceptually included in Eq. (1) in  $S_{OCEAN}$  and in  $S_{LAND}$ , but it is not represented in the process models used to  
803 quantify these fluxes. This effect is discussed in Supplement S.6.3. Similarly, the loss of additional sink capacity  
804 from reduced forest cover is missing in the combination of approaches used here to estimate both land fluxes  
805 ( $E_{LUC}$  and  $S_{LAND}$ ) and its potential effect is discussed and quantified in Supplement S.6.4.

## 806 **3 Results**

807 For each component of the global carbon budget, we present results for three different time periods: the full  
808 historical period, from 1850 to 2023, the decades in which we have atmospheric concentration records from  
809 Mauna Loa (1960-2023), a specific focus on last year (2023), and the projection for the current year (2024).  
810 Subsequently, we assess the estimates of the budget components of the last decades against the top-down  
811 constraints from inverse modelling of atmospheric observations, the land/ocean partitioning derived from the  
812 atmospheric O<sub>2</sub> measurements, and the budget components estimates from the ESMs assimilation simulations.  
813 Atmospheric inversions further allow for an assessment of the budget components with a regional breakdown of  
814 land and ocean sinks.

## 815 **3.1 Fossil CO<sub>2</sub> Emissions**

### 816 **3.1.1 Historical period 1850-2023**

817 Cumulative fossil CO<sub>2</sub> emissions for 1850-2023 were  $490 \pm 25$  GtC, including the cement carbonation sink  
818 (Figure 3, Table 8, with all cumulative numbers rounded to the nearest 5GtC). In this period, 46% of global  
819 fossil CO<sub>2</sub> emissions came from coal, 35% from oil, 15% from natural gas, 3% from decomposition of  
820 carbonates, and 1% from flaring. In 1850, the UK stood for 62% of global fossil CO<sub>2</sub> emissions. In 1893 the  
821 combined cumulative emissions of the current members of the European Union reached and subsequently  
822 surpassed the level of the UK. Since 1917 US cumulative emissions have been the largest. Over the entire  
823 period 1850-2023, US cumulative emissions amounted to 120GtC (24% of world total), the EU's to 80 GtC  
824 (16%), China's to 75 GtC (15%), and India's to 15 GtC (3%).

825 In addition to the estimates of fossil CO<sub>2</sub> emissions that we provide here (see Section 2.1), there are three global  
826 datasets with long time series that include all sources of fossil CO<sub>2</sub> emissions: CDIAC-FF (Hefner and Marland,  
827 2024), CEDS version 2024\_07\_08 (Hoesly et al., 2024) and PRIMAP-hist version 2.6 (Gütschow et al., 2016;  
828 Gütschow et al., 2024), although these datasets are not entirely independent from each other (Andrew, 2020a).  
829 CEDS has cumulative emissions over 1750-2022 at 480 GtC, CDIAC-FF has 481 GtC, GCP 484 GtC,  
830 PRIMAP-hist CR 490 GtC, and PRIMAP-hist TR 492 GtC. CDIAC-FF excludes emissions from lime  
831 production. CEDS estimates higher emissions from international shipping in recent years, while PRIMAP-hist  
832 has higher fugitive emissions than the other datasets. However, in general these four datasets are in relative  
833 agreement as to total historical global emissions of fossil CO<sub>2</sub>.

### 834 **3.1.2 Recent period 1960-2023**

835 Global fossil CO<sub>2</sub> emissions,  $E_{\text{FOS}}$  (including the cement carbonation sink), have increased every decade from an  
836 average of  $3.0 \pm 0.2$  GtC yr<sup>-1</sup> for the decade of the 1960s to an average of  $9.7 \pm 0.5$  GtC yr<sup>-1</sup> during 2014-2023  
837 (Table 7, Figure 2 and Figure 5). The growth rate in these emissions decreased between the 1960s and the  
838 1990s, from 4.3% yr<sup>-1</sup> in the 1960s (1960-1969), 3.2% yr<sup>-1</sup> in the 1970s (1970-1979), 1.6% yr<sup>-1</sup> in the 1980s  
839 (1980-1989), to 1.0% yr<sup>-1</sup> in the 1990s (1990-1999). After this period, the growth rate began increasing again in  
840 the 2000s at an average growth rate of 2.8% yr<sup>-1</sup>, decreasing to 0.6% yr<sup>-1</sup> for the last decade (2014-2023).  
841 China's emissions increased by +1.9% yr<sup>-1</sup> on average over the last 10 years dominating the global trend, and  
842 India's emissions increased by +3.6% yr<sup>-1</sup>, while emissions decreased in EU27 by 2.1% yr<sup>-1</sup>, and in the USA by  
843 1.2% yr<sup>-1</sup>. Figure 6 illustrates the spatial distribution of fossil fuel emissions for the 2014-2023 period.

844  $E_{\text{FOS}}$  reported here includes the uptake of CO<sub>2</sub> by cement via carbonation which has increased with increasing  
845 stocks of cement products, from an average of 20 MtC yr<sup>-1</sup> (0.02 GtC yr<sup>-1</sup>) in the 1960s to an average of 200MtC  
846 yr<sup>-1</sup> (0.2 GtC yr<sup>-1</sup>) during 2014-2023 (Figure 5).

### 847 **3.1.3 Final year 2023**

848 Global fossil CO<sub>2</sub> emissions were slightly higher, 1.4%, in 2023 than in 2022, with an increase of 0.14 GtC to  
849 reach 10.1 ± 0.5 GtC (including the 0.21 GtC cement carbonation sink) in 2023 (Figure 5), distributed among  
850 coal (41%), oil (32%), natural gas (21%), cement (4%), flaring (<1%), and others (<1%). Compared to 2022, the  
851 2023 emissions from coal, oil, and gas increased by 1.4%, 2.5%, and 0.1% respectively, while emissions from  
852 cement decreased by 2%. All annual growth rates presented are adjusted for the leap year, unless stated  
853 otherwise.

854 In 2023, the largest absolute contributions to global fossil CO<sub>2</sub> emissions were from China (31%), the USA  
855 (13%), India (8%), and the EU27 (7%). These four regions account for 59% of global fossil CO<sub>2</sub> emissions,  
856 while the rest of the world contributed 41%, including international aviation and marine bunker fuels (3% of the  
857 total). Growth rates for these countries from 2022 to 2023 were 4.9% (China), -3.3% (USA), -8.4% (EU27), and  
858 8.2% (India), with +0.7% for the rest of the world, including international aviation and marine bunker fuels  
859 (+9.5%). The per-capita fossil CO<sub>2</sub> emissions in 2023 were 1.3 tC person<sup>-1</sup> yr<sup>-1</sup> for the globe, and were 3.9  
860 (USA), 2.3 (China), 1.5 (EU27) and 0.6 (India) tC person<sup>-1</sup> yr<sup>-1</sup> for the four highest emitters (Figure 5).

### 861 **3.1.4 Year 2024 Projection**

862 Globally, we estimate that global fossil CO<sub>2</sub> emissions (including cement carbonation, -0.21 GtC) will grow by  
863 0.8% in 2024 (-0.2% to +1.7%) to 10.2 GtC (37.4 GtCO<sub>2</sub>), an historical record high<sup>2</sup>. Carbon Monitor projects a  
864 comparable 2024 increase of 0.8% (0.5% to 1.1%). GCB estimates of changes in 2024 emissions per fuel types,  
865 relative to 2023, are projected to be 0.1% (range -1.0% to 1.2%) for coal, +0.9% (range 0.3% to 1.6%) for oil,  
866 +2.5% (range 1.3% to 3.8%) for natural gas, and -3.5% (range -5.3% to -1.6%) for cement.

867 For China, projected fossil emissions in 2024 are expected to increase slightly by 0.1% (range -1.7% to 1.9%)  
868 compared with 2023 emissions, bringing 2023 emissions for China around 3.3 GtC yr<sup>-1</sup> (11.9 GtCO<sub>2</sub> yr<sup>-1</sup>). In  
869 contrast, the Carbon Monitor estimate projects a 2024 decrease of 0.8% (range -1.3% to -1.4%). Our projected  
870 changes by fuel for China are +0.4% for coal, -1.0% for oil, +7.6% for natural gas, and -9.4% for cement.

871 For the USA, using the Energy Information Administration (EIA) emissions projection for 2024 combined with  
872 cement clinker data from USGS, we project a decrease of 0.9% (range -2.1% to 0.3%) compared to 2023,  
873 bringing USA 2023 emissions to around 1.3 GtC yr<sup>-1</sup> (4.9 GtCO<sub>2</sub> yr<sup>-1</sup>). Conversely, Carbon Monitor projects a  
874 2024 increase of 1.3% (1.0% to 1.6%). Our projected changes by fuel are -5.7% for coal, -0.7% for oil, +1.1%  
875 for natural gas, and -7.1% for cement.

876 For the European Union, our projection for 2024 is for a decrease of 2.8% (range -5.2% to -0.3%) relative to  
877 2023, with 2024 emissions around 0.7 GtC yr<sup>-1</sup> (2.4 GtCO<sub>2</sub> yr<sup>-1</sup>). The Carbon Monitor projection for the EU27 is

---

<sup>2</sup> Growth rates in this section use a leap year adjustment that corrects for the extra day in 2024.

878 slightly lower than GCB with a decrease of 4.5% (-5.4% to -3.6%). Our projected changes by fuel are -11.3%  
879 for coal, -0.6% for oil, +0.4% for natural gas, and -3.1% for cement.

880 For India, our projection for 2024 is an increase of 3.7% (range of 3.3% to 4.0%) over 2023, with 2024  
881 emissions around 0.9 GtC yr<sup>-1</sup> (3.2 GtCO<sub>2</sub> yr<sup>-1</sup>). The Carbon Monitor projection for India is an increase of 5.0%  
882 (4.4% to 5.5%). Our projected changes by fuel are +3.3% for coal, +3.3% for oil, +11.8% for natural gas, and  
883 +3.8% for cement.

884 International aviation and shipping are projected to increase by 7.8% in 2024, reaching 0.3 GtC yr<sup>-1</sup> (1.2 GtCO<sub>2</sub>  
885 yr<sup>-1</sup>), with international aviation projected to be up 14% over 2023, continuing to recover from pandemic lows,  
886 and international shipping projected to rise by 3%. The Carbon Monitor projects international aviation and  
887 shipping to only increase by 2.6% in 2024.

888 For the rest of the world, the expected change for 2024 is an increase of 1.2% (range -0.7% to 3.2%) with 2024  
889 emissions around 4.0 GtC yr<sup>-1</sup> (14.5 GtCO<sub>2</sub> yr<sup>-1</sup>), similar to the Carbon Monitor projection of 1.5% (range -1.2%  
890 to 1.8%). The fuel-specific projected 2024 growth rates for the rest of the world are: +0.5% for coal, +0.8% for  
891 oil, +2.2% for natural gas, +2.0% for cement.

892 For traceability, Table S6 provides a comparison of annual projections from GCB since 2015 with the actual  
893 emissions assessed in the subsequent GCB annual report.

## 894 **3.2 Emissions from Land Use Change**

### 895 **3.2.1 Historical period 1850-2023**

896 Cumulative CO<sub>2</sub> emissions from land-use change ( $E_{LUC}$ ) for 1850-2023 were  $225 \pm 65$  GtC (Table 8; Figure 3;  
897 Figure 16). The cumulative emissions from  $E_{LUC}$  show a large spread among individual estimates of 150 GtC  
898 (H&C2023), 205 GtC (OSCAR), 250 GtC (LUCE) and 285 GtC (BLUE) for the four bookkeeping models and a  
899 similar wide estimate of  $250 \pm 85$  GtC for the DGVMs (all cumulative numbers are rounded to the nearest 5  
900 GtC). Vegetation biomass observations provide independent constraints on the  $E_{LUC}$  estimates (Li et al., 2017).  
901 Over the 1901-2012 period, the GCB bookkeeping models cumulative  $E_{LUC}$  amounts to 165 GtC [105 to 210  
902 GtC], similar to the observation-based estimate of  $155 \pm 50$  GtC (Li et al., 2017).

### 903 **3.2.2 Recent period 1960-2023**

904 In contrast to growing fossil emissions, CO<sub>2</sub> emissions from land-use, land-use change, and forestry remained  
905 relatively constant (around 1.5 GtC yr<sup>-1</sup>) over the 1960-1999 period. Since then, they have shown a statistically  
906 significant decrease of about 0.2 GtC per decade, reaching  $1.1 \pm 0.7$  GtC yr<sup>-1</sup> for the 2014-2023 period (Table  
907 7), but with significant spread, from 0.8 to 1.3 GtC yr<sup>-1</sup> across the four bookkeeping models (Table 5, Figure 7).  
908 Different from the bookkeeping average, the DGVMs average grows slightly larger over the 1980-2010 period  
909 and shows no sign of decreasing emissions in the recent decades, apart from in the most recent decade (Table 5,

910 Figure 7). This is, however, expected as DGVM-based estimates include the loss of additional sink capacity,  
911 which grows with time, while the bookkeeping estimates do not (Supplement S.6.4).

912 We separate net  $E_{LUC}$  into five component fluxes to gain further insight into the drivers of net emissions:  
913 deforestation, forest (re-)growth, wood harvest and other forest management, peat drainage and peat fires, and  
914 all other transitions (Figure 7c; supplemental Sec. S.2.1). We further decompose the deforestation and the forest  
915 (re-)growth term into contributions from shifting cultivation vs permanent forest cover changes (Figure 7d).  
916 Averaged over the 2014-2023 period and over the four bookkeeping estimates, fluxes from deforestation amount  
917 to 1.7 [1.4 to 2.3] GtC yr<sup>-1</sup> (Table 5), of which 1.0 [0.8, 1.1] GtC yr<sup>-1</sup> are from permanent deforestation. Fluxes  
918 from forest (re-)growth amount to -1.2 [-1.5, -0.9] GtC yr<sup>-1</sup> (Table 5), of which -0.5 [-0.7, -0.3] GtC yr<sup>-1</sup> are from  
919 re/afforestation and the remainder from forest regrowth in shifting cultivation cycles. Emissions from wood  
920 harvest and other forest management (0.3 [0.0, 0.6] GtC yr<sup>-1</sup>), peat drainage and peat fires (0.2 [0.2, 0.3] GtC yr<sup>-1</sup>)  
921 and the net flux from other transitions (0.1 [0.0, 0.1] GtC yr<sup>-1</sup>) are substantially less important globally (Table  
922 5). However, the small net flux from wood harvest and other forest management contains substantial gross  
923 fluxes that largely compensate each other (see Figure S8): 1.4 [0.9, 2.0] GtC yr<sup>-1</sup> emissions result from the  
924 decomposition of slash and the decay of wood products and -1.1 [-1.4, -0.8] GtC yr<sup>-1</sup> removals result from  
925 regrowth after wood harvesting.

926 The split into component fluxes clarifies the potentials for emission reduction and carbon dioxide removal: the  
927 emissions from permanent deforestation - the largest of our component fluxes - could be halted (largely) without  
928 compromising carbon uptake by forests, contributing substantially to emissions reduction. By contrast, reducing  
929 wood harvesting would have limited potential to reduce emissions as it would be associated with less forest  
930 regrowth; removals and emissions cannot be decoupled here on long timescales. A similar conclusion applies to  
931 removals and emissions from shifting cultivation, which we have therefore separated out. Carbon Dioxide  
932 Removal (CDR) in forests could instead be increased by permanently increasing the forest cover through  
933 re/afforestation. Our estimate of about -0.5 GtC yr<sup>-1</sup> removed on average each year during 2014-2023 by  
934 re/afforestation is similar to independent estimates that were derived from NGHGs for CDR in managed forests  
935 (through re/afforestation plus forest management) for 2013-2022 (-0.5 GtC yr<sup>-1</sup>, Pongratz et al., 2024).  
936 Re/afforestation constitutes the vast majority of all current CDR (Pongratz et al., 2024). Though they cannot be  
937 compared directly to annual fluxes from the atmosphere and are thus not included in our estimate of  $E_{LUC}$ ,  
938 CDR through transfers between non-atmospheric reservoirs such as in durable HWPs, biochar, or BECCS  
939 comprise much smaller amounts of carbon. 218 MtC yr<sup>-1</sup> have been estimated to be transferred to HWPs,  
940 averaged over 2013-2022 (Pongratz et al., 2024). The net flux of HWPs, considering the re-release of CO<sub>2</sub>  
941 through their decay, amounts to 91 MtC yr<sup>-1</sup> over that period (Pongratz et al., 2024). Note that some double-  
942 counting between the CDR through HWPs and the CDR through re/afforestation exists if the HWPs are derived  
943 from newly forested areas. BECCS projects have been estimated to store 0.1 MtC yr<sup>-1</sup> in geological projects  
944 worldwide in 2023, biochar projects 0.2 MtC yr<sup>-1</sup> (Pongratz et al., 2024). “Blue carbon”, i.e. coastal wetland  
945 management such as restoration of mangrove forests, saltmarshes and seagrass meadows, though at the interface  
946 of land and ocean carbon fluxes, are counted towards the land-use sector as well. Currently, bookkeeping

947 models do not include blue carbon; however, current CDR deployment in coastal wetlands is small globally, less  
948 than  $0.003\text{MtC yr}^{-1}$  (Powis et al., 2023).

949 The statistically significant decrease in  $E_{\text{LUC}}$  since the late-1990s, including the larger drop within the most  
950 recent decade, is due to the combination of decreasing emissions from deforestation (in particular permanent  
951 deforestation) and increasing removals from forest regrowth (with those from re/afforestation stagnating  
952 globally in the last decade). Emissions in 2014-2023 are 28% lower than in the late-1990s (1995-2004) and 20%  
953 lower than in 2004-2013. The steep drop in  $E_{\text{LUC}}$  after 2015 is due to the combined effect from a peak in peat  
954 fire emissions in 2015 and a long-term decline in deforestation emissions in many countries over the 2010-2020  
955 period with largest declines in the Democratic Republic of the Congo, Brazil, China, and Indonesia. Since the  
956 processes behind gross removals, foremost forest regrowth and soil recovery, are all slow, while gross emissions  
957 include a large instantaneous component, short-term changes in land-use dynamics, such as a temporary  
958 decrease in deforestation, influences gross emissions dynamics more than gross removals dynamics, which  
959 rather are a response to longer-term dynamics. Component fluxes often differ more across the four bookkeeping  
960 estimates than the net flux, which is expected due to different process representation; in particular, the treatment  
961 of shifting cultivation, which increases both gross emissions and removals, differs across models, but also net  
962 and gross wood harvest fluxes show high uncertainty. By contrast, models agree relatively well for emissions  
963 from permanent deforestation.

964 Overall, highest land-use emissions occur in the tropical regions of all three continents. The top three emitters  
965 (both cumulatively 1959-2023 and on average over 2014-2023) are Brazil (in particular the Amazon Arc of  
966 Deforestation), Indonesia and the Democratic Republic of the Congo, with these 3 countries contributing  $0.7$   
967  $\text{GtC yr}^{-1}$  or 60% of the global net land-use emissions (average over 2014-2023) (Figure 6b, Figure 7b). This is  
968 related to massive expansion of cropland, particularly in the last few decades in Latin America, Southeast Asia,  
969 and sub-Saharan Africa (Hong et al., 2021), to a substantial part for export of agricultural products (Pendrill et  
970 al., 2019). Emission intensity is high in many tropical countries, particularly of Southeast Asia, due to high rates  
971 of land conversion in regions of carbon-dense and often still pristine, undegraded natural forests (Hong et al.,  
972 2021). Emissions are further increased by peat fires in equatorial Asia (GFED4s, van der Werf et al., 2017). Our  
973 estimates of high  $E_{\text{LUC}}$  in China has been revised down since the 1980s as compared to GCB2023 related to  
974 the update of the land-use forcing, which is now based on the cropland dataset by Yu et al. (2022) (see  
975 Supplement S.2.2), which suggests lower cropland expansion and thus less deforestation than the previous  
976 datasets assumed. Uptake due to land-use change occurs in several regions of the world (Figure 6b) particularly  
977 because of re/afforestation. Highest CDR in the last decade is seen in China, where our estimates show an even  
978 larger uptake since 2010 compared to GCB2023 related to the updated land-use forcing, in the EU27, partly  
979 related to expanding forest area as a consequence of the forest transition in the 19<sup>th</sup> and 20<sup>th</sup> century and  
980 subsequent regrowth of forest (Mather 2001; McGrath et al., 2015), and in the U.S. Substantial uptake through  
981 re/afforestation also exists in other regions such as Brazil, Myanmar or Russia, where, however, emissions from  
982 deforestation and other land-use changes dominate the net flux.



983 While the mentioned patterns are robust and supported by independent literature, we acknowledge that model  
984 spread is substantially larger on regional than global levels, as has been shown for bookkeeping models (Bastos  
985 et al., 2021) as well as DGVMs (Obermeier et al., 2021). Assessments for individual regions are being  
986 performed as part of REgional Carbon Cycle Assessment and Processes (RECCAP2; Ciais et al., 2020, Poulter  
987 et al., 2022) or already exist for selected regions (e.g., for Europe by Petrescu et al., 2020, for Brazil by Rosan et  
988 al., 2021, for 8 selected countries/regions in comparison to inventory data by Schwingshackl et al., 2022). The  
989 revisions since GCB2023 reflect such uncertainties: The integration of a fourth bookkeeping model alters our  
990 estimates, though only to a limited extent given that the new model LUCE lies in between the other three  
991 models for the global ELUC estimates. Larger changes are obvious at regional level due to the revisions of the  
992 land-use forcing with a general update to more recent FAO input for agricultural areas and wood harvest, new  
993 MapBiomass input for Brazil and Indonesia and the updated cropland dataset in China.

994 The NGHGI data under the LULUCF sector and the LULUCF estimates from FAOSTAT differ from the global  
995 models' definition of ELUC (see Section 2.2.1). In the NGHGI reporting, the natural fluxes ( $S_{LAND}$ ) are counted  
996 towards ELUC when they occur on managed land (Grassi et al., 2018). To compare our results to the NGHGI  
997 approach, we perform a translation of our ELUC estimates by adding  $S_{LAND}$  in managed forest from the DGVMs  
998 simulations (following the methodology described in Grassi et al., 2023) to the bookkeeping ELUC estimate (see  
999 Supplement S.2.3). For the 2014-2023 period, we estimate that  $1.8 \text{ GtC yr}^{-1}$  of  $S_{LAND}$  occurred in managed  
1000 forests. Adding this sink to ELUC changes ELUC from being a source of  $1.1 \text{ GtC yr}^{-1}$  to a sink of  $0.7 \text{ GtC yr}^{-1}$ , very  
1001 similar to the NGHGI estimate that yields a sink of  $0.8 \text{ GtC yr}^{-1}$  (Figure 8, Table S10). We further apply a mask  
1002 of managed land to the net atmosphere-to-land flux estimate from atmospheric inversions to obtain inverse  
1003 estimates that are comparable to the NGHGI estimates and to the translated ELUC estimates from bookkeeping  
1004 models (see Supplement S.2.3). The inversion-based net flux in managed land indicates a sink of  $0.7 \text{ GtC yr}^{-1}$   
1005 for 2014-2023, which agrees very well with the NGHGI and the translated ELUC estimates (Figure 8, Table S10).  
1006 Additionally, the interannual variability of the inversion estimates and the translated ELUC estimates show a  
1007 remarkable agreement (Pearson correlation of 0.81 in 2000-2023), which supports the suggested translation  
1008 approach.

1009 The translation approach has been shown to be generally applicable also at the country-level (Grassi et al., 2023;  
1010 Schwingshackl et al., 2022). Country-level analysis suggests, e.g., that the bookkeeping method estimates higher  
1011 deforestation emissions than the national report in Indonesia, but less  $\text{CO}_2$  removal by afforestation than the  
1012 national report in China. The fraction of the natural  $\text{CO}_2$  sinks that the NGHGI estimates include differs  
1013 substantially across countries, related to varying proportions of managed vs total forest areas (Schwingshackl et  
1014 al., 2022). By comparing ELUC and NGHGI on the basis of the component fluxes used above, we find that our  
1015 estimates reproduce very closely the NGHGI estimates for emissions from permanent deforestation, peat  
1016 emissions, and other transitions (Figure 8), although a difference in sign for the latter (small source in  
1017 bookkeeping estimates, small sink in NGHGI) creates a notable difference between NGHGI and bookkeeping  
1018 estimates. Fluxes due to forest (re-)growth & other forest management, that is, (re-)growth from re/afforestation  
1019 plus the net flux from wood harvesting and other forest management and emissions and removals in shifting  
1020 cultivation cycles, constitute a large sink in the NGHGI ( $-1.9 \text{ GtC yr}^{-1}$  averaged over 2014-2023), since they

1021 also include  $S_{\text{LAND}}$  in managed forests. Summing up the bookkeeping estimates of (re-)growth from  
1022 re/afforestation, the net flux from wood harvesting and other forest management, and the emissions and  
1023 removals in shifting cultivation cycles, and adding  $S_{\text{LAND}}$  in managed forests yields a flux of  $-2.0 \text{ GtC yr}^{-1}$   
1024 (averaged over 2014-2023), which compares well with the NGHGI estimate. Though estimates between  
1025 NGHGI, FAOSTAT and the translated budget estimates still differ in value and need further analysis, the  
1026 approach suggested by Grassi et al. (2023), which we adopt here, provides a feasible way to relate the global  
1027 models' and NGHGI approach to each other and thus link the anthropogenic carbon budget estimates of land  
1028  $\text{CO}_2$  fluxes directly to the Global Stocktake, as part of the UNFCCC Paris Agreement.

### 1029 **3.2.3 Final year 2023**

1030 The global  $\text{CO}_2$  emissions from land-use change are estimated as  $1.0 \pm 0.7 \text{ GtC}$  in 2023, similar to the 2022  
1031 estimate. However, confidence in the annual change remains low. Despite El Niño conditions, which in general  
1032 lead to more fires in deforestation areas, peat fire emissions in Indonesia remained below average (GFED4.1s;  
1033 updated from van der Werf et al., 2017). In South America, emissions from tropical deforestation and  
1034 degradation fires have been about average, as effects of the El Niño in the Amazon, such as droughts, are not  
1035 expected before 2024.

### 1036 **3.2.4 Year 2024 Projection**

1037 In Southeast Asia, peat fire emissions have further dropped (from 27 Tg C in 2023 to 2 Tg C in 2024 through  
1038 December 31 2024; GFED4.1s, van der Werf et al., 2017), as have tropical deforestation and degradation fires  
1039 (from 33 Tg C to 8 Tg C) as the El Niño conditions ceased. By contrast, emissions from tropical deforestation  
1040 and degradation fires in South America have risen from 121 Tg C in 2023 to 334 Tg C in 2024 up until  
1041 December 31, as the impacts of the El Niño unfold, in particular drought conditions since 2023. The 2024 South  
1042 American fire emissions are among the highest values in the record, which started in 1997. Part of the increase  
1043 is due to elevated fire activity in the wetlands of the Pantanal. Disentangling the degree to which interannual  
1044 variability in rainfall patterns and stronger environmental protection measures in both Indonesia after their 2015  
1045 high fire season and in Brazil after the change in government play a role in fire trends is an important research  
1046 topic. Cumulative 2024 fire emission estimates through December 31 2024 are 439 Tg C for global  
1047 deforestation and degradation fires and 2 Tg C for peatland fires in Southeast Asia.

1048 Based on these estimates, we expect  $E_{\text{LUC}}$  emissions of around 1.2 GtC (4.2 Gt $\text{CO}_2$ ) in 2024, 0.17 GtC above the  
1049 2023 level. Note that although our extrapolation includes tropical deforestation and degradation fires, the  
1050 degradation attributable to selective logging, edge-effects or fragmentation is not captured. Further,  
1051 deforestation and fires in deforestation zones may become more disconnected, partly due to changes in  
1052 legislation in some regions. For example, Van Wees et al. (2021) found that the contribution from fires to forest  
1053 loss decreased in the Amazon and in Indonesia over the period of 2003-2018.

1054 **3.3 CDR not based on vegetation**

1055 Besides the CDR through land use (Sec. 3.2), the atmosphere to geosphere flux of carbon resulting from carbon  
1056 dioxide removal (CDR) activity in 2023 is estimated at 0.011 MtC/yr. This results primarily from 0.009 MtC/yr  
1057 of enhanced weathering projects and 0.001 MtC/yr of DACCS. While it represents a growth of 200% in the  
1058 anthropogenic sink, from the 0.0036 MtC/yr estimate in 2022, it remains about a million times smaller than  
1059 current fossil CO<sub>2</sub> emissions. Note that the lower estimate for DACCS is due to more accurate (lower) annual  
1060 estimates now being available, rather than lower activity. Enhanced rock weathering has gone up relative to last  
1061 year, both as a result of better coverage of projects and an actual increase in activity.

1062 **3.4 Total anthropogenic emissions**

1063 Cumulative anthropogenic CO<sub>2</sub> emissions (fossil and land use) for 1850-2023 totalled 710 ± 70 GtC (2605 ±  
1064 260 GtCO<sub>2</sub>), of which 70% (500 GtC) occurred since 1960 and 34% (240 GtC) since 2000 (Table 7 and 8).  
1065 Total anthropogenic emissions more than doubled over the last 60 years, from 4.6 ± 0.7 GtC yr<sup>-1</sup> for the decade  
1066 of the 1960s to an average of 10.8 ± 0.9 GtC yr<sup>-1</sup> during 2014-2023, and reaching 11.1 ± 0.9 GtC (40.6 ± 3.2  
1067 GtCO<sub>2</sub>) in 2023. However, total anthropogenic CO<sub>2</sub> emissions have been stable over the last decade (zero  
1068 growth rate over the 2014-2023 period), much slower than the 2.0% growth rate over the previous decade  
1069 (2004-2013).

1070 During the historical period 1850-2023, 31% of historical emissions were from land use change and 69% from  
1071 fossil emissions. However, fossil emissions have grown significantly since 1960 while land use changes have  
1072 not, and consequently the contributions of land use change to total anthropogenic emissions were smaller during  
1073 recent periods, 18% during the period 1960-2023 and down to 10% over the last decade (2014-2023).

1074 For 2024, we project global total anthropogenic CO<sub>2</sub> emissions from fossil and land use changes to be around  
1075 11.4 GtC (41.6 GtCO<sub>2</sub>), 2% above the 2023 level. All values here include the cement carbonation sink (currently  
1076 about 0.2 GtC yr<sup>-1</sup>).

1077 **3.5 Atmospheric CO<sub>2</sub>**

1078 **3.5.1 Historical period 1850-2023**

1079 Atmospheric CO<sub>2</sub> concentration was approximately 278 parts per million (ppm) in 1750, reaching 300 ppm in  
1080 the late 1900s, 350 ppm in the late 1980s, and reaching 419.31 ± 0.1 ppm in 2023 (Lan et al., 2024a; Figure 1).  
1081 The mass of carbon in the atmosphere increased by 51% from 590 GtC in 1750 to 890 GtC in 2023. Current  
1082 CO<sub>2</sub> concentrations in the atmosphere are unprecedented in the last 2 million years and the current rate of  
1083 atmospheric CO<sub>2</sub> increase is at least 10 times faster than at any other time during the last 800,000 years  
1084 (Canadell et al., 2021).

### 1085 **3.5.2 Recent period 1960-2023**

1086 The growth rate in atmospheric CO<sub>2</sub> level increased from  $1.7 \pm 0.07$  GtC yr<sup>-1</sup> in the 1960s to  $5.2 \pm 0.02$  GtC yr<sup>-1</sup>  
1087 during 2014-2023 with important decadal variations (Table 7, Figure 3 and Figure 4). During the last decade  
1088 (2014-2023), the growth rate in atmospheric CO<sub>2</sub> concentration continued to increase, albeit with large  
1089 interannual variability (Figure 4).

1090 The airborne fraction (AF) is defined as the ratio of atmospheric CO<sub>2</sub> growth rate to total anthropogenic  
1091 emissions:

$$1092 \quad AF = G_{ATM} / (E_{FOS} + E_{LUC}) \quad (2)$$

1093 It provides a diagnostic of the relative strength of the land and ocean carbon sinks in removing part of the  
1094 anthropogenic CO<sub>2</sub> perturbation. The evolution of AF over the last 60 years shows no significant trend,  
1095 remaining at around 44%, albeit showing a large interannual and decadal variability driven by the year-to-year  
1096 variability in G<sub>ATM</sub> (Figure 10). The observed stability of the airborne fraction over the 1960-2023 period  
1097 indicates that the ocean and land CO<sub>2</sub> sinks have been increasing in pace with the total anthropogenic emissions  
1098 over that period, removing on average about 56% of the emissions (see Sections 3.6.2 and 3.7.2).

### 1099 **3.5.3 Final year 2023**

1100 The growth rate in atmospheric CO<sub>2</sub> concentration was  $5.9 \pm 0.2$  GtC ( $2.79 \pm 0.08$  ppm) in 2023 (Figure 4; Lan  
1101 et al., 2024a), well above the 2022 growth rate ( $4.6 \pm 0.2$  GtC) or the 2014-2023 average ( $5.2 \pm 0.02$  GtC), as to  
1102 be expected during an El Niño year. The 2023 atmospheric CO<sub>2</sub> growth rate was the 4th largest over the 1959-  
1103 2023 atmospheric observational record, closely following 2015, 2016 and 1998, all strong El Niño years.

### 1104 **3.5.4 Year 2024 Projection**

1105 The 2024 growth in atmospheric CO<sub>2</sub> concentration (G<sub>ATM</sub>) is projected to be about 6.1 GtC (2.87 ppm), still  
1106 high, which is common for the year after a strong El Niño year. This is the average of the GCB regression  
1107 method (6.1 GtC, 2.85 ppm) and ESMs the multi-model mean (6.1 GtC, 2.88 ppm). The 2024 atmospheric CO<sub>2</sub>  
1108 concentration, averaged over the year, is expected to reach the level of 422.45 ppm, 52% over the pre-industrial  
1109 level.

## 1110 **3.6 Ocean Sink**

### 1111 **3.6.1 Historical period 1850-2023**

1112 Cumulated since 1850, the ocean sink adds up to  $185 \pm 35$  GtC, with more than two thirds of this amount ( $130 \pm$   
1113  $25$  GtC) being taken up by the global ocean since 1960. Over the historical period, the ocean sink increased in  
1114 pace with the anthropogenic emissions exponential increase (Figure 3). Since 1850, the ocean has removed 26%  
1115 of total anthropogenic emissions.

### 1116 3.6.2 Recent period 1960-2023

1117 The ocean CO<sub>2</sub> sink increased from  $1.2 \pm 0.4$  GtC yr<sup>-1</sup> in the 1960s to  $2.9 \pm 0.4$  GtC yr<sup>-1</sup> during 2014-2023  
1118 (Table 7), with interannual variations of the order of a few tenths of GtC yr<sup>-1</sup> (Figure 4, Figure 11). The ocean-  
1119 borne fraction ( $S_{\text{OCEAN}}/(E_{\text{FOS}}+E_{\text{LUC}})$ ) has been remarkably constant around 25% on average (Figure 10c), with  
1120 variations around this mean illustrating the decadal variability of the ocean carbon sink. So far, there is no  
1121 indication of a decrease in the ocean-borne fraction from 1960 to 2022. The increase of the ocean sink is  
1122 primarily driven by the increased atmospheric CO<sub>2</sub> concentration, with the strongest CO<sub>2</sub> induced signal in the  
1123 North Atlantic and the Southern Ocean (Figure 12a). The effect of climate change is much weaker, reducing the  
1124 ocean sink globally by  $0.17 \pm 0.05$  GtC yr<sup>-1</sup> (-5.9% of  $S_{\text{OCEAN}}$ ) during 2014-2023 (all models simulate a  
1125 weakening of the ocean sink by climate change, range -3.4 to -10.7%), and does not show clear spatial patterns  
1126 across the GOBMs ensemble (Figure 12b). This is the combined effect of change and variability in all  
1127 atmospheric forcing fields, previously attributed to wind and temperature changes (LeQuéré et al., 2010, Bunsen  
1128 et al., 2024). The effect of warming is smaller than expected from offline calculation due to a stabilising  
1129 feedback from limited exchange between surface and deep waters (Bunsen et al., 2024).

1130 The global net air-sea CO<sub>2</sub> flux is a residual of large natural and anthropogenic CO<sub>2</sub> fluxes into and out of the  
1131 ocean with distinct regional and seasonal variations (Figure 6 and S1). Natural fluxes dominate on regional  
1132 scales, but largely cancel out when integrated globally (Gruber et al., 2009). Mid-latitudes in all basins and the  
1133 high-latitude North Atlantic dominate the ocean CO<sub>2</sub> uptake where low temperatures and high wind speeds  
1134 facilitate CO<sub>2</sub> uptake at the surface (Takahashi et al., 2009). In these regions, formation of mode, intermediate  
1135 and deep-water masses transport anthropogenic carbon into the ocean interior, thus allowing for continued CO<sub>2</sub>  
1136 uptake at the surface. Outgassing of natural CO<sub>2</sub> occurs mostly in the tropics, especially in the equatorial  
1137 upwelling region, and to a lesser extent in the North Pacific and polar Southern Ocean, mirroring a well-  
1138 established understanding of regional patterns of air-sea CO<sub>2</sub> exchange (e.g., Takahashi et al., 2009, Gruber et  
1139 al., 2009). These patterns are also noticeable in the Surface Ocean CO<sub>2</sub> Atlas (SOCAT) dataset, where an ocean  
1140  $f\text{CO}_2$  value above the atmospheric level indicates outgassing (Figure S1). This map further illustrates the data-  
1141 sparsity in the Indian Ocean and the southern hemisphere in general.

1142 The largest variability in the ocean sink occurs on decadal time-scales (Figure 11). The ensemble means of  
1143 GOBMs and  $f\text{CO}_2$ -products show the same patterns of decadal variability, although with a larger amplitude of  
1144 variability in the  $f\text{CO}_2$ -products than in the GOBMs. The ocean sink stagnated in the 1990s and strengthened  
1145 between the early 2000s and the mid-2010s (Figure 11; Le Quéré et al., 2007; Landschützer et al., 2015, 2016;  
1146 DeVries et al., 2017; Hauck et al., 2020; McKinley et al., 2020, Gruber et al., 2023). More recently, the sink  
1147 seems to have entered a phase of stagnation since 2016, largely in response to large inter-annual climate  
1148 variability. Different explanations have been proposed for the decadal variability in the 1990s and 2000s,  
1149 ranging from the ocean's response to changes in atmospheric wind systems (e.g., Le Quéré et al., 2007, Keppler  
1150 and Landschützer, 2019), including variations in upper ocean overturning circulation (DeVries et al., 2017) to  
1151 the eruption of Mount Pinatubo in the 1990s (McKinley et al., 2020). The main origin of the decadal variability  
1152 is a matter of debate with a number of studies initially pointing to the Southern Ocean (see review in Canadell et

1153 al., 2021), but also contributions from the North Atlantic and North Pacific (Landschützer et al., 2016, DeVries  
1154 et al., 2019), or a global signal (McKinley et al., 2020) were proposed.

1155 On top of the decadal variability, interannual variability of the ocean carbon sink is driven by climate variability  
1156 with a first-order effect from a stronger ocean sink during large El Niño events (e.g., 1997-1998) (Figure 11;  
1157 Rödenbeck et al., 2014, Hauck et al., 2020; McKinley et al. 2017) leading to a reduction in CO<sub>2</sub> outgassing from  
1158 the Tropical Pacific. During 2010-2016, the ocean CO<sub>2</sub> sink appears to have intensified in line with the expected  
1159 increase from atmospheric CO<sub>2</sub> (McKinley et al., 2020). This effect is similar in the *f*CO<sub>2</sub>-products (Figure 11,  
1160 ocean sink 2016 minus 2010, GOBMs:  $+0.42 \pm 0.11$  GtC yr<sup>-1</sup>, *f*CO<sub>2</sub>-products:  $+0.44$  GtC yr<sup>-1</sup>, range 0.18 to 0.72  
1161 GtC yr<sup>-1</sup>). The reduction of  $-0.18$  GtC yr<sup>-1</sup> (range:  $-0.41$  to  $-0.03$  GtC yr<sup>-1</sup>) in the ocean CO<sub>2</sub> sink in 2017 is  
1162 consistent with the return to normal conditions after the El Niño in 2015/16, which caused an enhanced sink in  
1163 previous years. After an increasing *S*<sub>OCEAN</sub> in 2018 and 2019, the GOBM and *f*CO<sub>2</sub>-product ensemble means  
1164 suggest a decrease of *S*<sub>OCEAN</sub>, related to the triple La Niña event 2020-2022, followed by a rebound in 2023  
1165 linked to the onset of an El Niño event.

1166 Although all individual GOBMs and *f*CO<sub>2</sub>-products fall within the observational constraint, the ensemble means  
1167 of GOBMs, and *f*CO<sub>2</sub>-products (adjusted for the riverine flux) show a mean offset increasing from 0.31 GtC yr<sup>-1</sup>  
1168 in the 1990s to 0.49 GtC yr<sup>-1</sup> in the decade 2014-2023 and a slightly lower offset of 0.3 GtC yr<sup>-1</sup> in 2023. In this  
1169 version of the GCB, the *S*<sub>OCEAN</sub> positive trend diverges over time by a factor of 1.4 since 2002 (GOBMs:  $0.25 \pm$   
1170  $0.04$  GtC yr<sup>-1</sup> per decade, *f*CO<sub>2</sub>-products:  $0.35$  GtC yr<sup>-1</sup> per decade [ $0.17$  to  $0.79$  GtC yr<sup>-1</sup> per decade], *S*<sub>OCEAN</sub>:  
1171  $0.30$  GtC yr<sup>-1</sup> per decade), but the uncertainty ranges overlap. This divergence is smaller than reported in  
1172 previous GCB versions, because of the updated lower sink estimates by the *f*CO<sub>2</sub>-products for recent years. This  
1173 also leads to agreement on the trend since 2010 (GOBMs:  $0.18 \pm 0.06$  GtC yr<sup>-1</sup> per decade, *f*CO<sub>2</sub>-products:  $0.18$   
1174 GtC yr<sup>-1</sup> per decade [ $-0.36$  to  $0.73$  GtC yr<sup>-1</sup> per decade] *S*<sub>OCEAN</sub>:  $0.18$  GtC yr<sup>-1</sup> per decade). A hybrid approach  
1175 recently constrained the trend 2000-2022 to  $0.42 \pm 0.06$  GtC yr<sup>-1</sup> decade<sup>-1</sup> (Mayot et al., 2024), which aligns  
1176 with the updated trends of *S*<sub>OCEAN</sub> ( $0.39$  GtCyr<sup>-1</sup> decade<sup>-1</sup>) and of the *f*CO<sub>2</sub>-products ( $0.45$  [ $0.28, 0.84$ ] GtCyr<sup>-1</sup>  
1177 decade<sup>-1</sup>), while the GOBMs result in a lower trend ( $0.32 \pm 0.04$  GtC yr<sup>-1</sup> per decade) over the same period.

1178 In the current dataset, the discrepancy between the two types of estimates stems from a persistently larger  
1179 *S*<sub>OCEAN</sub> in the *f*CO<sub>2</sub>-products in the northern extra-tropics since around 2002 and an intermittently larger *S*<sub>OCEAN</sub>  
1180 in the southern extra-tropics in the period 2008-2020 (Figure 14). Note that the discrepancy in the mean flux,  
1181 which was located in the Southern Ocean in GCB 2022 and earlier, was reduced due to the choice of the  
1182 regional river flux adjustment (Lacroix et al., 2020 instead of Aumont et al., 2001). This comes at the expense of  
1183 a discrepancy in the mean *S*<sub>OCEAN</sub> of about 0.2 GtC yr<sup>-1</sup> in the tropics. Likely explanations for the discrepancy in  
1184 the trends and decadal variability in the high-latitudes are data sparsity and uneven data distribution (Bushinsky  
1185 et al., 2019, Gloege et al., 2021, Hauck et al., 2023a, Mayot et al., 2024). In particular, two *f*CO<sub>2</sub>-products were  
1186 shown to overestimate the Southern Ocean CO<sub>2</sub> flux trend by 50 and 130% based on current sampling in a  
1187 model subsampling experiment (Hauck et al., 2023a) and the largest trends in the *f*CO<sub>2</sub>-products occurred in a  
1188 data void region in the North Pacific (Mayot et al., 2024). In this respect it is highly worrisome that the coverage  
1189 of *f*CO<sub>2</sub> observations continues to decline (Dong et al 2024) and is now down to that of the early 2000s (Fig.

1190 11). Another likely contributor to the discrepancy between GOBMs and  $f\text{CO}_2$ -products are model biases (as  
1191 indicated by the comparison with Mayot et al., 2024, by the large model spread in the South, Figure 14, and the  
1192 larger model-data  $f\text{CO}_2$  mismatch, Figure S2).

1193 The reported  $\text{SOCEAN}$  estimate from GOBMs and  $f\text{CO}_2$ -products is  $2.2 \pm 0.4 \text{ GtC yr}^{-1}$  over the period 1994 to  
1194 2007, which is in agreement with the ocean interior estimate of  $2.2 \pm 0.4 \text{ GtC yr}^{-1}$ , which accounts for the  
1195 climate effect on the natural  $\text{CO}_2$  flux of  $-0.4 \pm 0.24 \text{ GtC yr}^{-1}$  (Gruber et al., 2019) to match the  
1196 definition of  $\text{SOCEAN}$  used here (Hauck et al., 2020). This comparison depends critically on the estimate of the  
1197 climate effect on the natural  $\text{CO}_2$  flux, which is smaller from the GOBMs ( $-0.1 \text{ GtC yr}^{-1}$ ) than in Gruber et al.  
1198 (2019). Uncertainties of these two estimates would also overlap when using the GOBM estimate of the climate  
1199 effect on the natural  $\text{CO}_2$  flux. Similarly, the  $\text{SOCEAN}$  estimates integrated over the decades 1994-2004 ( $21.5 \text{ GtC}$   
1200  $\text{yr}^{-1}$ ) and 2004-2014 ( $25.6 \text{ GtC yr}^{-1}$ ) agree with the interior ocean-based estimates of Müller et al. (2023;  $21.4 \pm$   
1201  $2.8$  and  $26.5 \pm 1.3 \text{ GtC yr}^{-1}$ ) but depend critically on assumptions of the climate effect on natural carbon, which  
1202 in turn, are based on the  $f\text{CO}_2$ -products in Müller et al. (2023).

### 1203 **3.6.3 Final year 2023**

1204 The estimated ocean  $\text{CO}_2$  sink is  $2.9 \pm 0.4 \text{ GtC}$  for 2023. This is a small increase of  $0.16 \text{ GtC}$  compared to 2022,  
1205 in line with the expected sink strengthening from the 2023 El Niño conditions. GOBM and  $f\text{CO}_2$ -product  
1206 ensemble mean estimates consistently result in an  $\text{SOCEAN}$  increase in 2023 (GOBMs:  $0.17 \pm 0.15 \text{ GtC}$ ,  $f\text{CO}_2$ -  
1207 products:  $0.14 [-0.04, 0.30] \text{ GtC}$ ). Eight GOBMs and six  $f\text{CO}_2$ -products show an increase in  $\text{SOCEAN}$ , while only  
1208 two GOBMs and two  $f\text{CO}_2$ -products show a minor decrease in  $\text{SOCEAN}$  of less than  $0.05 \text{ GtC}$  (Figure 11). The  
1209  $f\text{CO}_2$ -products have a larger uncertainty at the end of the reconstructed time series, potentially linked to  
1210 uncertainties related to fewer available observations in the final year and the shift from La Niña to El Niño (see  
1211 e.g. Watson et al 2020, Pérez et al 2024). Specifically, the  $f\text{CO}_2$ -products' estimate of the last year is regularly  
1212 adjusted in the following release owing to the tail effect and an incrementally increasing data availability. While  
1213 the monthly grid cells covered may have a lag of only about a year (Figure 11 inset), the values within grid cells  
1214 may change with 1-5 years lag (see absolute number of observations plotted in previous GCB releases),  
1215 potentially resulting in annual changes in the flux magnitude from  $f\text{CO}_2$ -products.

### 1216 **3.6.4 Year 2024 projection**

1217 Using a feed-forward neural network method (see Section 2.5.2) we project an ocean sink of  $3.0 \text{ GtC}$  for 2024,  
1218 only  $0.1 \text{ GtC}$  higher than for the year 2023, consistent with El Niño to neutral conditions in 2024. The set of  
1219 ESMS predictions support this estimate with a 2024 ocean sink of around  $3.0 [2.9, 3.1] \text{ GtC}$ .

### 1220 **3.6.5 Evaluation of ocean models and $f\text{CO}_2$ -products**

1221 The process-based model evaluation draws a generally positive picture with GOBMs scattered around the  
1222 observational values for Southern Ocean sea-surface salinity, Southern Ocean stratification index and surface

1223 ocean Revelle factor (Section S3.3 and Table S11). However, the Atlantic Meridional Overturning Circulation at  
1224 26°N is underestimated by 8 out of 10 GOBMs and overestimated by one GOBM. It is planned to derive skill  
1225 scores for the GOBMs in future releases based on these metrics.

1226 The model simulations allow to separate the anthropogenic carbon component (steady state and non-steady  
1227 state, sim D - sim A) and to compare the model flux and DIC inventory change directly to the interior ocean  
1228 estimate of Gruber et al. (2019) without further assumptions (Table S11). The GOBMs ensemble average of  
1229 anthropogenic carbon inventory changes 1994-2007 amounts to  $2.4 \text{ GtC yr}^{-1}$  and is thus lower than the  $2.6 \pm 0.3$   
1230  $\text{GtC yr}^{-1}$  estimated by Gruber et al. (2019) although within the uncertainty. Only three models fall within the  
1231 range reported by Gruber et al. (2019). This suggests that the majority of the GOBMs may underestimate  
1232 anthropogenic carbon uptake by 10-20% and some models even more. Comparison to the decadal estimates of  
1233 anthropogenic carbon accumulation (Müller et al., 2023) are close to the interior ocean data based estimate for  
1234 the decade 2004-2014 (GOBMs sim D minus sim A,  $24.7 \pm 3.6 \text{ GtC yr}^{-1}$ , Müller et al.  $27.3 \pm 2.5 \text{ GtC yr}^{-1}$ ), but  
1235 do not reproduce the supposedly higher anthropogenic carbon accumulation in the earlier period 1994-2004  
1236 (GOBMs sim D minus sim A,  $21.1 \pm 3.0 \text{ GtC yr}^{-1}$ , Müller et al.  $29.3 \pm 2.5 \text{ GtC yr}^{-1}$ ). Analysis of Earth System  
1237 Models indicate that an underestimation by about 10% may be due to biases in ocean carbon transport and  
1238 mixing from the surface mixed layer to the ocean interior (Goris et al., 2018, Terhaar et al., 2021, Bourgeois et  
1239 al., 2022, Terhaar et al., 2022), biases in the chemical buffer capacity (Revelle factor) of the ocean (Vaittinada  
1240 Ayar et al., 2022; Terhaar et al., 2022) and partly due to a late starting date of the simulations (mirrored in  
1241 atmospheric CO<sub>2</sub> chosen for the preindustrial control simulation, Table S2, Bronselaer et al., 2017, Terhaar et  
1242 al., 2022; 2024). Interestingly, and in contrast to the uncertainties in the surface CO<sub>2</sub> flux, we find the largest  
1243 mismatch in interior ocean carbon accumulation in the tropics, with smaller contributions from the north and the  
1244 south. The large discrepancy in accumulation in the tropics highlights the role of interior ocean carbon  
1245 redistribution for those inventories (Khaliwala et al., 2009, DeVries et al., 2023).

1246 The evaluation of the ocean estimates with the  $f\text{CO}_2$  observations from the SOCAT v2024 dataset for the period  
1247 1990-2023 shows an RMSE from annually detrended data of 0.2 to  $2.4 \mu\text{atm}$  for the eight  $f\text{CO}_2$ -products over  
1248 the globe (Figure S2). The GOBMs RMSEs are larger and range from 2.7 to  $4.9 \mu\text{atm}$ . The RMSEs are  
1249 generally larger at high latitudes compared to the tropics, for both the  $f\text{CO}_2$ -products and the GOBMs. The  
1250  $f\text{CO}_2$ -products have RMSEs of 0.3 to  $2.9 \mu\text{atm}$  in the Tropics, 0.6 to  $2.4 \mu\text{atm}$  in the North, and 0.8 to  $2.4 \mu\text{atm}$   
1251 in the South. Note that the  $f\text{CO}_2$ -products are based on the SOCAT v2024 database, hence SOCAT is not an  
1252 independent dataset for the evaluation of the  $f\text{CO}_2$ -products. The GOBMs RMSEs are more spread across  
1253 regions, ranging from 2.4 to  $3.9 \mu\text{atm}$  in the tropics, 2.8 to  $5.9 \mu\text{atm}$  in the North, and 2.7 to  $6.0 \mu\text{atm}$  in the  
1254 South. The higher RMSEs occur in regions with stronger climate variability, such as the northern and southern  
1255 high latitudes (poleward of the subtropical gyres). Additionally, this year we evaluate the trends derived from a  
1256 subset of  $f\text{CO}_2$ -products by subsampling four GOBMs used in Friedlingstein et al. (2023; covering the period up  
1257 to the year 2022) following the approach of Hauck et al. (2023a) and evaluating the air-sea CO<sub>2</sub> flux trend for  
1258 the 2001-2021 period, i.e. the period of strong divergence in the air-sea CO<sub>2</sub> exchange excluding the final year  
1259 to remove the tail effect, against trend biases identified by the GOBM reconstruction. The results indicate a  
1260 relationship between reconstruction bias and strength of the decadal trends (see Figure S3), indicating a



1261 tendency of the  $f\text{CO}_2$ -products ensemble to overestimate the air-sea  $\text{CO}_2$  flux trends in agreement with a recent  
1262 study by Mayot et al. (2024).

### 1263 3.7 Land Sink

#### 1264 3.7.1 Historical period 1850-2023

1265 Cumulated since 1850, the terrestrial carbon sink amounts to  $220 \pm 60$  GtC, 31% of total anthropogenic  
1266 emissions, with more than two thirds of this amount ( $150 \pm 40$  GtC) being taken up by the terrestrial ecosystems  
1267 since 1960. Over the historical period, the land sink increased in pace with the anthropogenic emissions  
1268 exponential increase (Figure 3).

#### 1269 3.7.2 Recent period 1960-2023

1270 The terrestrial  $\text{CO}_2$  sink  $S_{\text{LAND}}$  increased from  $1.2 \pm 0.5$  GtC  $\text{yr}^{-1}$  in the 1960s to  $3.2 \pm 0.9$  GtC  $\text{yr}^{-1}$  during 2014-  
1271 2023, with important interannual variations of up to 2 GtC  $\text{yr}^{-1}$  generally showing a decreased land sink during  
1272 El Niño events (Figure 9), responsible for the corresponding enhanced growth rate in atmospheric  $\text{CO}_2$   
1273 concentration. The larger land  $\text{CO}_2$  sink during 2014-2023 compared to the 1960s is reproduced by all the  
1274 DGVMs in response to the increase in both atmospheric  $\text{CO}_2$ , nitrogen deposition, and the changes in climate,  
1275 and is consistent with the residual estimated from the other budget terms ( $E_{\text{FOS}}+E_{\text{LUC}}-G_{\text{ATM}}-S_{\text{OCEAN}}$ , Table 5).

1276 Over the period 1960 to present the increase in the global terrestrial  $\text{CO}_2$  sink is largely attributed to the  $\text{CO}_2$   
1277 fertilisation effect (Prentice et al., 2001, Piao et al., 2009, Schimel et al., 2015) and increased nitrogen  
1278 deposition (Huntzinger et al., 2017, O'Sullivan et al., 2019), directly stimulating plant photosynthesis and  
1279 increased plant water use in water limited systems, with a small negative contribution of climate change (Figure  
1280 12). There is a range of evidence to support a positive terrestrial carbon sink in response to increasing  
1281 atmospheric  $\text{CO}_2$ , albeit with uncertain magnitude (Walker et al., 2021). As expected from theory, the greatest  
1282  $\text{CO}_2$  effect is simulated in the tropical forest regions, associated with warm temperatures and long growing  
1283 seasons (Hickler et al., 2008) (Figure 12a). However, evidence from tropical intact forest plots indicate an  
1284 overall decline in the land sink across Amazonia (1985-2011), attributed to enhanced mortality offsetting  
1285 productivity gains (Brienen et al., 2015, Hubau et al., 2020). During 2014-2023 the land sink is positive in all  
1286 regions (Figure 6) with the exception of eastern Brazil, Bolivia, northern Venezuela, Southwest USA, central  
1287 Europe and Central Asia, North and South Africa, and eastern Australia, where the negative effects of climate  
1288 variability and change (i.e. reduced rainfall and/or increased temperature) counterbalance  $\text{CO}_2$  effects. This is  
1289 clearly visible on Figure 12 where the effects of  $\text{CO}_2$  (Figure 12a) and climate (Figure 12b) as simulated by the  
1290 DGVMs are isolated. The negative effect of climate can be seen across the globe, and is particularly strong in  
1291 most of South America, Central America, Southwest US, Central Europe, western Sahel, southern Africa,  
1292 Southeast Asia and southern China, and eastern Australia (Figure 12b). Globally, over the 2014-2023 period,  
1293 climate change reduces the land sink by  $0.87 \pm 0.56$  GtC  $\text{yr}^{-1}$  (27% of  $S_{\text{LAND}}$ ).

1294 Most DGVMs have similar  $S_{\text{LAND}}$  averaged over 2014-2023, and 14/20 models fall within the  $1\sigma$  range of the  
1295 residual land sink [ $1.8\text{-}3.7 \text{ GtC yr}^{-1}$ ] (see Table 5), and all models but one are within the  $2\sigma$  range [ $0.8\text{-}4.6 \text{ GtC}$   
1296  $\text{yr}^{-1}$ ]. The ED model is an outlier, with a land sink estimate of  $5.1 \text{ GtC yr}^{-1}$  for the 2014-2023 period, driven by a  
1297 strong  $\text{CO}_2$  fertilisation effect ( $6.3 \text{ GtC yr}^{-1}$  in the  $\text{CO}_2$  only (S1) simulation). There are no direct global  
1298 observations of the land sink ( $S_{\text{LAND}}$ ), or the  $\text{CO}_2$  fertilisation effect, and so we are not yet in a position to rule  
1299 out models based on component fluxes if their net land sink ( $S_{\text{LAND}}\text{-ELUC}$ ) is within the observational uncertainty  
1300 provided by atmospheric inversions or  $\text{O}_2$  measurements (Table 5). Furthermore, DGVMs were compared  
1301 against a model-data fusion based analysis of the land carbon cycle (CARDAMOM) (Bloom and Williams,  
1302 2015; Bloom et al., 2016). Results suggest good correspondence between approaches at the interannual  
1303 timescales, but divergence in the recent trend in  $S_{\text{LAND}}$  with CARDAMOM simulating a stronger trend than the  
1304 DGVM multi-model mean (Figure 9).

1305 Since 2020 the globe has experienced La Niña conditions which would be expected to lead to an increased land  
1306 carbon sink. This 3-year long period of La Niña conditions came to an end by the second half of 2023 and  
1307 transitioned to an El Niño which lasted until mid-2024. A clear transition from maximum to a minimum in the  
1308 global land sink is evident in  $S_{\text{LAND}}$ , from 2022 to 2023 and we find that a El Niño- driven decrease in tropical  
1309 land sink is offset by a smaller increase in the high latitude land sink. In the past years several regions  
1310 experienced record-setting fire events (see also section 3.8.3). While global burned area has declined over the  
1311 past decades mostly due to declining fire activity in savannas (Andela et al., 2017), forest fire emissions are  
1312 rising and have the potential to counter the negative fire trend in savannas (Zheng et al., 2021). Noteworthy  
1313 extreme fire events include the 2019-2020 Black Summer event in Australia (emissions of roughly  $0.2 \text{ GtC}$ ; van  
1314 der Velde et al., 2021), Siberia in 2021, where emissions approached  $0.4 \text{ GtC}$  or three times the 1997-2020  
1315 average according to GFED4s, and Canada in 2023 (Byrne et al., 2024). While other regions, including Western  
1316 US and Mediterranean Europe, also experienced intense fire seasons in 2021 their emissions are substantially  
1317 lower.

1318 Despite these regional negative effects of climate change on  $S_{\text{LAND}}$ , the efficiency of land to remove  
1319 anthropogenic  $\text{CO}_2$  emissions has remained broadly constant over the last six decades, with a land-borne  
1320 fraction ( $S_{\text{LAND}}/(\text{E}_{\text{FOS}}+\text{E}_{\text{LUC}})$ ) of around 30% (Figure 10b).

### 1321 **3.7.3 Final year 2023**

1322 The terrestrial  $\text{CO}_2$  sink from the DGVMs ensemble  $S_{\text{LAND}}$  was  $2.3 \pm 1.0 \text{ GtC}$  in 2023, 41% below the 2022 La  
1323 Niña induced strong sink of  $3.9 \pm 1.0 \text{ GtC}$ , and also below the 2014-2023 average of  $3.2 \pm 0.9 \text{ GtC yr}^{-1}$  (Figure  
1324 4, Table 7). We estimate that the 2023 land sink was the lowest since 2015. The severe reduction in the land  
1325 sink in 2023 is likely driven by the El Niño conditions, leading to a 58% reduction in  $S_{\text{LAND}}$  in the tropics (30N-  
1326 30S) from  $2.8 \text{ GtC}$  in 2022 to  $1.2 \text{ GtC}$  in 2023. This is combined with intense wildfires in Canada that led to a  
1327 significant  $\text{CO}_2$  source (see also Section 3.8.3). We note that the  $S_{\text{LAND}}$  DGVMs estimate for 2023 of  $2.3 \pm 1.0$   
1328  $\text{GtC}$  is very similar to the  $2.2 \pm 1.0 \text{ GtC yr}^{-1}$  estimate from the residual sink from the global budget ( $\text{E}_{\text{FOS}}+\text{E}_{\text{LUC}}\text{-}$   
1329  $\text{G}_{\text{ATM-SOCEAN}}$ , Table 5).

### 1330 **3.7.4 Year 2024 projection**

1331 Using a feed-forward neural network method we project a land sink of 3.2 GtC for 2024, 0.9 GtC larger than the  
1332 2023 estimate. As for the ocean sink, we attribute this to the transition from the El Niño conditions in 2023 to a  
1333 neutral state. The ESMs do not provide an additional estimate of  $S_{\text{LAND}}$  as they only simulate the net  
1334 atmosphere-land carbon flux ( $S_{\text{LAND-ELUC}}$ ).

### 1335 **3.7.5 Evaluation of land models**

1336 The evaluation of the DGVMs shows generally higher agreement across models for runoff, and to a lesser extent  
1337 for GPP, and ecosystem respiration. These conclusions are supported by a more comprehensive analysis of  
1338 DGVM performance in comparison with benchmark data (Sitch et al., 2024). A relative comparison of DGVM  
1339 performance (Figure S4) suggests several DGVMs (CABLE-POP, CLASSIC, OCN, ORCHIDEE) may  
1340 outperform others at multiple carbon and water cycle benchmarks. However, results from Seiler et al., 2022,  
1341 also show how DGVM differences are often of similar magnitude compared with the range across observational  
1342 datasets. All models score high enough over the metrics tests to support their use here. There are a few  
1343 anomalously low scores for individual metrics from a single model, and these can direct the effort to improve  
1344 models for use in future budgets.

## 1345 **3.8 Partitioning the carbon sinks**

### 1346 **3.8.1 Global sinks and spread of estimates**

1347 In the period 2014-2023, the bottom-up view of global net ocean and land carbon sinks provided by the GCB,  
1348  $S_{\text{OCEAN}}$  for the ocean and  $S_{\text{LAND-ELUC}}$  for the land, agrees closely with the top-down global carbon sinks  
1349 delivered by the atmospheric inversions. This is shown in Figure 13, which visualises the individual decadal  
1350 mean atmosphere-land and atmosphere-ocean fluxes from each, along with the constraints on their sum offered  
1351 by the global fossil  $\text{CO}_2$  emissions flux minus the atmospheric growth rate ( $E_{\text{FOS}} - G_{\text{ATM}}$ ,  $4.4 \pm 0.5 \text{ Gt C yr}^{-1}$ ,  
1352 Table 7, shown as diagonal line on Figure 13). The GCB estimate for net atmosphere-to-surface flux ( $S_{\text{OCEAN}} +$   
1353  $S_{\text{LAND-ELUC}}$ ) during 2014-2023 is  $4.9 \pm 1.2 \text{ Gt C yr}^{-1}$  (Table 7), with the difference to the diagonal representing  
1354 the budget imbalance ( $B_{\text{IM}}$ ) of  $0.4 \text{ GtC yr}^{-1}$  discussed in Section 3.9. By virtue of the inversion methodology, the  
1355 atmospheric inversions estimate of the net atmosphere-to-surface flux during 2014-2023 is  $4.5 \text{ Gt C yr}^{-1}$ , with a  
1356  $< 0.1 \text{ GtC yr}^{-1}$  imbalance, and thus scatter across the diagonal, with inverse models trading land for ocean fluxes  
1357 in their solution. The independent constraint on the net atmosphere-to-surface flux based on atmospheric  $\text{O}_2$  by  
1358 design also closes the balance and is  $4.5 \pm 0.9 \text{ GtC yr}^{-1}$  over the 2014-2023 period (orange symbol on Figure  
1359 13), while the ESMs estimate for the net atmosphere-to-surface flux over that period average to  $4.7 [3.0, 5.8]$   
1360  $\text{GtC yr}^{-1}$  (Tables 5 and 6).

1361 The distributions based on the individual models and  $f\text{CO}_2$ -products reveal substantial spread but converge near  
1362 the decadal means quoted in Tables 5 to 7. Sink estimates for  $S_{\text{OCEAN}}$  and from inverse systems are mostly non-  
1363 Gaussian, while the ensemble of DGVMs appears more normally distributed justifying the use of a multi-model

1364 mean and standard deviation for their errors in the budget. Noteworthy is that the tails of the distributions  
1365 provided by the land and ocean bottom-up estimates would not agree with the global constraint provided by the  
1366 fossil fuel emissions and the observed atmospheric CO<sub>2</sub> growth rate. This illustrates the power of the  
1367 atmospheric joint constraint from G<sub>ATM</sub> and the global CO<sub>2</sub> observation network it is derived from.

### 1368 **3.8.1.1 Net atmosphere-to-land flux**

1369 The GCB estimate of the net atmosphere-to-land flux ( $S_{\text{LAND}} - E_{\text{LUC}}$ ), calculated as the difference between  
1370  $S_{\text{LAND}}$  from the DGVMs and  $E_{\text{LUC}}$  from the bookkeeping models, amounts to a  $2.1 \pm 1.1$  GtC yr<sup>-1</sup> sink during  
1371 2014-2023 (Table 5). Estimates of net atmosphere-to-land flux ( $S_{\text{LAND}} - E_{\text{LUC}}$ ) from the DGVMs alone ( $1.7 \pm$   
1372  $0.6$  GtC yr<sup>-1</sup>, Table 5, green symbol on Figure 13) are slightly lower, although within the uncertainty of the GCB  
1373 estimate and also within uncertainty of the global carbon budget constraint ( $E_{\text{FOS}} - G_{\text{ATM}} - S_{\text{OCEAN}}$ ,  $1.6 \pm 0.6$  GtC  
1374 yr<sup>-1</sup>; Table 7). Also, for 2014-2023, the inversions estimate the net atmosphere-to-land flux is a  $1.4$  [0.3, 2.2]  
1375 GtC yr<sup>-1</sup> sink, slightly lower than the mean of the DGVMs estimates (purple versus grey symbols on Figure 13).  
1376 The independent constraint based on atmospheric O<sub>2</sub> is even lower,  $1.0 \pm 0.8$  GtC yr<sup>-1</sup> (orange symbol in Figure  
1377 13), although its large uncertainty overlaps with the uncertainty range from other approaches. Last, the ESMs  
1378 estimate for the net atmosphere-to-land flux during 2014-2023 is a  $2.2$  [0.3, 3.6] GtC yr<sup>-1</sup> sink, more consistent  
1379 with the GCB estimates of  $S_{\text{LAND}} - E_{\text{LUC}}$  (Figure 14 top row).

1380 As discussed in Section 3.5.3, the atmospheric growth rate of CO<sub>2</sub> was very high in 2023, 5.9 GtC (2.79 ppm)  
1381 the 4<sup>th</sup> largest on record. Both DGVMs and inversions assign this large CO<sub>2</sub> growth rate to a severe decrease of  
1382 the net atmosphere to land flux, and in particular in the tropics (Figure 14). DGVMs simulate a 2023 global the  
1383 net atmosphere-to-land flux of 1.1 GtC yr<sup>-1</sup>, a 55% decline relative to the 2.4 GtC yr<sup>-1</sup> sink in 2022, primarily  
1384 driven by the severe reduction in  $S_{\text{LAND}}$  (-41%, see Section 3.7.3). The tropics (30N-30S) are recording a  
1385 dramatic decrease in the net atmosphere-to-land flux from 1.5 GtC yr<sup>-1</sup> in 2022 to 0.1 GtC yr<sup>-1</sup> in 2023. The  
1386 atmospheric inversion shows a similar story with the global net atmosphere-to-land flux declining from 2.6 GtC  
1387 yr<sup>-1</sup> in 2022 to 0.9 GtC yr<sup>-1</sup> in 2023 (-64%), with the tropics turning from a 1.0 GtC yr<sup>-1</sup> sink in 2022 to a 0.4  
1388 GtC yr<sup>-1</sup> source in 2023. Our results are broadly consistent with the Ke et al. (2024) study which reported a  
1389 global atmosphere-to-land flux of  $0.4 \pm 0.2$  GtC yr<sup>-1</sup> in 2023.

1390 In addition to the large decline of the tropical land uptake, the northern extra-tropics experienced warmer than  
1391 average conditions, in particular in the summer over North America and North Eurasia. In Canada alone, 2023  
1392 led to enhanced CO<sub>2</sub> release due to fires of 0.5-0.8 GtC yr<sup>-1</sup> (see Section 3.8.3). The atmospheric inversions do  
1393 simulate a slight reduction of the atmosphere-to-land flux in the northern extra-tropics (north of 30°N), from  
1394 1.6 GtC yr<sup>-1</sup> in 2022 to 1.4 GtC yr<sup>-1</sup> in 2023, while the DGVM fail to capture this pattern, with a simulated  
1395 northern extra-tropics net atmosphere-to-land flux larger in 2023 than in 2022 (1.0 vs 0.7 GtC yr<sup>-1</sup>).

### 1396 **3.8.1.2 Net atmosphere-to-ocean flux**

1397 For the 2014-2023 period, the GOBMs ( $2.6 \pm 0.4$  GtC yr<sup>-1</sup>) produce a lower estimate for  $S_{\text{OCEAN}}$  than the  $f\text{CO}_2$ -  
1398 products with 3.1 [2.9, 3.7] GtC yr<sup>-1</sup>, which shows up in Figure 13 as separate peaks in the distribution from the

1399 GOBMs (dark blue symbols) and from the  $f\text{CO}_2$ -products (light blue symbols). Atmospheric inversions (3.1  
1400 [2.4, 4.1]  $\text{GtC yr}^{-1}$ ) suggest an ocean uptake more in line with the  $f\text{CO}_2$ -products for the recent decade (Table 7),  
1401 although the inversions range includes both the GOBMs and  $f\text{CO}_2$ -products estimates (Figure 14 top row) and  
1402 the inversions are not fully independent as 6 out of 10 inversions covering the last decade use  $f\text{CO}_2$ -products as  
1403 ocean priors and one uses a GOBM (Table S4). The independent constraint based on atmospheric  $\text{O}_2$  ( $3.4 \pm 0.5$   
1404  $\text{GtC yr}^{-1}$ ) is at the high end of the distribution of the other methods. However, as mentioned in section 2.8, the  
1405  $\text{O}_2$  method requires a correction for global air-sea  $\text{O}_2$  flux, which induces a non-negligible uncertainty on the  
1406 decadal estimates (about  $0.5 \text{ GtC yr}^{-1}$ ). The large growth in the ocean carbon sink from  $\text{O}_2$  is compatible with  
1407 the GOBMs and  $f\text{CO}_2$ -products estimates when accounting for their uncertainty ranges. Lastly, the ESMs  
1408 estimate,  $2.5 [2.2, 2.8] \text{ GtC yr}^{-1}$ , suggest a moderate ocean carbon sink, comparable to the GOBMs estimate with  
1409 regard to mean and spread. We caution that the riverine transport of carbon taken up on land and outgassing  
1410 from the ocean, accounted for here, is a substantial ( $0.65 \pm 0.3 \text{ GtC yr}^{-1}$ ) and uncertain term (Crisp et al., 2022;  
1411 Gruber et al., 2023; DeVries et al., 2023) that separates the GOBMs, ESMs and oxygen-based estimates on the  
1412 one hand from the  $f\text{CO}_2$ -products and atmospheric inversions on the other hand.

### 1413 **3.8.2 Regional partitioning**

1414 Figure 14 shows the latitudinal partitioning of the global atmosphere-to-ocean ( $\text{SOCEAN}$ ), atmosphere-to-land  
1415 ( $\text{SLAND} - \text{ELUC}$ ), and their sum ( $\text{SOCEAN} + \text{SLAND} - \text{ELUC}$ ) according to the estimates from GOBMs and ocean  
1416  $f\text{CO}_2$ -products ( $\text{SOCEAN}$ ), DGVMs ( $\text{SLAND} - \text{ELUC}$ ), and from atmospheric inversions ( $\text{SOCEAN}$  and  $\text{SLAND} - \text{ELUC}$ ).

#### 1417 **3.8.2.1 North**

1418 Despite being one of the most densely observed and studied regions of our globe, annual mean carbon sink  
1419 estimates in the northern extra-tropics (north of  $30^\circ\text{N}$ ) continue to differ. The atmospheric inversions suggest an  
1420 atmosphere-to-surface sink ( $\text{SOCEAN} + \text{SLAND} - \text{ELUC}$ ) for 2014-2023 of  $2.6 [2.0 \text{ to } 3.4] \text{ GtC yr}^{-1}$ , which is slightly  
1421 higher than the process models' estimate of  $2.2 \pm 0.4 \text{ GtC yr}^{-1}$  (Figure 14). The GOBMs ( $1.2 \pm 0.2 \text{ GtC yr}^{-1}$ ),  
1422  $f\text{CO}_2$ -products ( $1.4 [1.3-1.5] \text{ GtC yr}^{-1}$ ), and inversion systems ( $1.2 [0.9 \text{ to } 1.4] \text{ GtC yr}^{-1}$ ) produce largely  
1423 consistent estimates of the ocean sink. However, the larger flux in the  $f\text{CO}_2$ -products may be related to data  
1424 sparsity (Mayot et al., 2024). Thus, the difference mainly arises from the net land flux ( $\text{SLAND} - \text{ELUC}$ ) estimate,  
1425 which is  $1.0 \pm 0.4 \text{ GtC yr}^{-1}$  in the DGVMs compared to  $1.5 [0.6 \text{ to } 2.3] \text{ GtC yr}^{-1}$  in the atmospheric inversions  
1426 (Figure 14, second row).

1427 Discrepancies in the northern land fluxes conforms with persistent issues surrounding the quantification of the  
1428 drivers of the global net land  $\text{CO}_2$  flux (Arneeth et al., 2017; Huntzinger et al., 2017; O'Sullivan et al., 2022) and  
1429 the distribution of atmosphere-to-land fluxes between the tropics and high northern latitudes (Baccini et al.,  
1430 2017; Schimel et al., 2015; Stephens et al., 2007; Ciais et al., 2019; Gaubert et al., 2019).

1431 In the northern extra-tropics, the process models, inversions, and  $f\text{CO}_2$ -products consistently suggest that most  
1432 of the interannual variability stems from the land (Figure 14). Inversions generally agree on the magnitude of

1433 interannual variations (IAV) over land, more so than DGVMs (0.29-0.32 vs 0.14-0.63 GtC yr<sup>-1</sup>, averaged over  
1434 1990-2023).

### 1435 3.8.2.2 Tropics

1436 In the tropics (30°S-30°N), both the atmospheric inversions and process models estimate a net carbon balance  
1437 ( $S_{\text{OCEAN}} + S_{\text{LAND}} - E_{\text{LUC}}$ ) that is relatively close to neutral over the past decade (inversions: 0.3 [-0.4, 0.9] GtC yr<sup>-1</sup>,  
1438 process models: 0.6±0.6 GtC yr<sup>-1</sup>). The GOBMs (-0.03 ± 0.3 GtC yr<sup>-1</sup>),  $f\text{CO}_2$ -products (0.3 [0.1, 0.6] GtC yr<sup>-1</sup>),  
1439 and inversion systems (0.3 [-0.1, 0.8] GtC yr<sup>-1</sup>) indicate a neutral to positive tropical ocean flux (see Figure S1  
1440 for spatial patterns). DGVMs indicate a net land sink ( $S_{\text{LAND}} - E_{\text{LUC}}$ ) of 0.6 ± 0.4 GtC yr<sup>-1</sup>, whereas the inversion  
1441 systems indicate a neutral net land flux although with large model spread (-0.0 [-0.9, 0.8] GtC yr<sup>-1</sup>, (Figure 14,  
1442 third row).

1443 The tropical lands are the origin of most of the atmospheric CO<sub>2</sub> interannual variability (Ahlström et al., 2015),  
1444 consistently among the process models and inversions (Figure 14). The interannual variability in the tropics is  
1445 similar among the ocean  $f\text{CO}_2$ -products (0.06-0.16 GtC yr<sup>-1</sup>) and the GOBMs (0.07-0.16 GtC yr<sup>-1</sup>, Figure S2).  
1446 The DGVMs and inversions indicate that atmosphere-to-land CO<sub>2</sub> fluxes are more variable than atmosphere-to-  
1447 ocean CO<sub>2</sub> fluxes in the tropics, with interannual variability of 0.37 to 1.33 and 0.86-0.96 GtC yr<sup>-1</sup> for DGVMs  
1448 and inversions, respectively.

### 1449 3.8.2.3 South

1450 In the southern extra-tropics (south of 30°S), the atmospheric inversions suggest a net atmosphere-to-surface  
1451 sink ( $S_{\text{OCEAN}} + S_{\text{LAND}} - E_{\text{LUC}}$ ) for 2014-2023 of 1.5 [1.2, 1.9] GtC yr<sup>-1</sup>, identical to the process models' estimate of  
1452 1.5 ± 0.4 GtC yr<sup>-1</sup> (Figure 14). An approximately neutral net land flux ( $S_{\text{LAND}} - E_{\text{LUC}}$ ) for the southern extra-  
1453 tropics is estimated by both the DGVMs (0.05 ± 0.1 GtC yr<sup>-1</sup>) and the inversion systems (-0.03 [-0.11, 0.08] GtC  
1454 yr<sup>-1</sup>). This means nearly all carbon uptake is due to oceanic sinks south of 30°S. The Southern Ocean flux in the  
1455  $f\text{CO}_2$ -products (1.5 [1.3, 1.7 GtC] yr<sup>-1</sup>) and inversion estimates (1.6 [1.2, 1.9] GtCyr<sup>-1</sup>) is marginally higher than  
1456 in the GOBMs (1.4 ± 0.4 GtC yr<sup>-1</sup>) (Figure 14, bottom row). This agreement is subject to the choice of the river  
1457 flux adjustment (Lacroix et al., 2020, Hauck et al., 2023b). Nevertheless, the time-series of atmospheric  
1458 inversions and  $f\text{CO}_2$ -products diverge from the GOBMs. A substantial overestimation of the trends in the  $f\text{CO}_2$ -  
1459 products could be explained by sparse and unevenly distributed observations, especially in wintertime (Figure  
1460 S1; Hauck et al., 2023a; Gloege et al., 2021). Model biases may contribute as well, with biases in mode water  
1461 formation, stratification, and the chemical buffer capacity known to play a role in Earth System Models (Terhaar  
1462 et al., 2021, Bourgeois et al., 2022, Terhaar et al., 2022).

1463 The interannual variability in the southern extra-tropics is low because of the dominance of ocean areas with  
1464 low variability compared to land areas. The split between land ( $S_{\text{LAND}} - E_{\text{LUC}}$ ) and ocean ( $S_{\text{OCEAN}}$ ) shows a  
1465 substantial contribution to variability in the south coming from the land, with no consistency between the  
1466 DGVMs and the inversions or among inversions. This is expected due to the difficulty of separating exactly the  
1467 land and oceanic fluxes when viewed from atmospheric observations alone. The  $S_{\text{OCEAN}}$  interannual variability

1468 was found to be higher in the  $f\text{CO}_2$ -products ( $0.04\text{-}0.20 \text{ GtC yr}^{-1}$ ) compared to GOBMs ( $0.04$  to  $0.06 \text{ GtC yr}^{-1}$ )  
1469 in 1990-2023 (Figure S2). Inversions give an interannual variability of  $0.10$  to  $0.13 \text{ GtC yr}^{-1}$ . Model  
1470 subsampling experiments recently illustrated that  $f\text{CO}_2$ -products may overestimate decadal variability in the  
1471 Southern Ocean carbon sink by 30% and the trend since 2000 by 50-130% due to data sparsity, based on one  
1472 and two  $f\text{CO}_2$ -products with strong variability (Gloege et al., 2021, Hauck et al., 2023a). The trend benchmark  
1473 test using the method of Hauck et al., (2023a) and a subset of 6  $f\text{CO}_2$ -products confirms the sensitivity of the  
1474 decadal trends in  $f\text{CO}_2$ -products to reconstruction biases, particularly in the Southern Ocean, indicating an  
1475 overestimation of the ensemble mean trend. However, we also find compensating positive biases in the  
1476 ensemble so that the ensemble mean bias is smaller than the bias from some individual  $f\text{CO}_2$ -products.

#### 1477 **3.8.2.4 RECCAP2 regions**

1478 Aligning with the RECCAP-2 initiative (Ciais et al., 2022; Poulter et al., 2022; DeVries et al., 2023), we  
1479 provide a breakdown of this GCB paper estimate of the  $\text{ELUC}$ ,  $\text{SLAND}$ , Net land ( $\text{SLAND} - \text{ELUC}$ ), and  $\text{SOCEAN}$  fluxes  
1480 over the 10 land, and 5 ocean RECCAP-2 regions, averaged over the period 2014-2023 (Figure 15). The  
1481 DGVMs and inversions suggest a positive net land sink in all regions, except for South America and Africa,  
1482 where the inversions indicate a small net source of respectively  $-0.1 [-0.8, 0.3] \text{ GtC yr}^{-1}$  and  $-0.3 [-0.7, -0.1]$   
1483  $\text{GtC yr}^{-1}$ , compared to a small sink of  $0.1\pm 0.3 \text{ GtC yr}^{-1}$  and  $0.3\pm 0.1 \text{ GtC yr}^{-1}$  for the DGVMs. However, for  
1484 South America, there is substantial uncertainty in both products (ensembles span zero). For the DGVMs, this is  
1485 driven by uncertainty in both  $\text{SLAND}$  ( $0.5\pm 0.4 \text{ GtC yr}^{-1}$ ) and  $\text{ELUC}$  ( $0.4\pm 0.2 \text{ GtC yr}^{-1}$ ). The bookkeeping models  
1486 also suggest an  $\text{ELUC}$  source of around  $0.4 \text{ GtC yr}^{-1}$  in South America and Africa, in line with the DGVMs  
1487 estimates. Bookkeeping models and DGVMs similarly estimate a source of  $0.3\text{-}0.4 \text{ GtC yr}^{-1}$  in Southeast Asia,  
1488 with DGVMs suggesting a small net land sink ( $0.1\pm 0.1 \text{ GtC yr}^{-1}$ ). This is similar to the inversion mean estimate  
1489 of a  $0.1 [-0.3, 0.8] \text{ GtC yr}^{-1}$  sink, although the inversion spread is substantial. The inversions suggest the largest  
1490 net land sinks are located in North America ( $0.5 [-0.1, 1.0] \text{ GtC yr}^{-1}$ ), Russia ( $0.6 [0.1, 0.9] \text{ GtC yr}^{-1}$ ), and East  
1491 Asia ( $0.4 [-0.2, 1.3] \text{ GtC yr}^{-1}$ ). This agrees well with the DGVMs in North America ( $0.4\pm 0.1 \text{ GtC yr}^{-1}$ ), which  
1492 indicate a large natural land sink ( $\text{SLAND}$ ) of  $0.6\pm 0.2 \text{ GtC yr}^{-1}$ , being slightly reduced by land-use related carbon  
1493 losses ( $0.2\pm 0.1 \text{ GtC yr}^{-1}$ ). The DGVMs suggest a smaller net land sink in Russia compared to inversions  
1494 ( $0.3\pm 0.2 \text{ GtC yr}^{-1}$ ), and a similar net sink in East Asia ( $0.2\pm 0.1 \text{ GtC yr}^{-1}$ ).

1495 There is generally a higher level of agreement in the estimates of regional  $\text{SOCEAN}$  between the different data  
1496 streams (GOBMs,  $f\text{CO}_2$ -products and atmospheric inversions) on decadal scale, compared to the agreement  
1497 between the different land flux estimates. All data streams agree that the largest contribution to  $\text{SOCEAN}$  stems  
1498 from the Southern Ocean due to a combination of high flux density and large surface area, but with important  
1499 contributions also from the Atlantic (high flux density) and Pacific (large area) basins. In the Southern Ocean,  
1500 GOBMs suggest a sink of  $1.0\pm 0.3 \text{ GtC yr}^{-1}$ , in line with the  $f\text{CO}_2$ -products ( $1.0 [0.8, 1.3] \text{ GtC yr}^{-1}$ ) and  
1501 atmospheric inversions ( $1.0 [0.7, 1.4] \text{ GtC yr}^{-1}$ ). There is similar agreement in the Pacific Ocean, with GOBMs,  
1502  $f\text{CO}_2$ -products, and atmospheric inversions indicating a sink of  $0.6\pm 0.2 \text{ GtC yr}^{-1}$ ,  $0.7 [0.6, 1.0] \text{ GtC yr}^{-1}$ , and

1503 0.6 [0.1,1.0] GtC yr<sup>-1</sup>, respectively. However, in the Atlantic Ocean, GOBMs simulate a sink of 0.5±0.1 GtC  
1504 yr<sup>-1</sup>, noticeably lower than both the *f*CO<sub>2</sub>-products (0.8 [0.7,1.0] GtC yr<sup>-1</sup>) and atmospheric inversions (0.7  
1505 [0.4,1.1] GtC yr<sup>-1</sup>). It is important to note the *f*CO<sub>2</sub>-products and atmospheric inversions have a substantial and  
1506 uncertain river flux adjustment in the Atlantic Ocean (0.3 GtC yr<sup>-1</sup>) that also leads to a mean offset between  
1507 GOBMs and *f*CO<sub>2</sub>-products/inversions in the latitude band of the tropics (Figure 14). The Indian Ocean due its  
1508 smaller size and the Arctic Ocean due to its size and sea-ice cover that prevents air-sea gas-exchange are  
1509 responsible for smaller but non negligible S<sub>OCEAN</sub> fluxes (Indian Ocean: (0.3 [0.2,0.3] GtC yr<sup>-1</sup>, 0.3 [0.3,0.4]  
1510 GtC yr<sup>-1</sup>, and 0.4 [0.3,0.6] GtC yr<sup>-1</sup> for GOBMs, *f*CO<sub>2</sub>-products, and atmospheric inversions, respectively, and  
1511 Arctic Ocean: (0.1 [0.1,0.1] GtC yr<sup>-1</sup>, 0.2 [0.1,0.2] GtC yr<sup>-1</sup>, and 0.1 [0.1,0.2] GtC yr<sup>-1</sup> for GOBMs, *f*CO<sub>2</sub>-  
1512 products, and atmospheric inversions, respectively). Note that the S<sub>OCEAN</sub> numbers presented here deviate from  
1513 numbers reported in RECCAP-2 where the net air-sea CO<sub>2</sub> flux is reported (i.e. without river flux adjustment for  
1514 *f*CO<sub>2</sub>-products and inversions, and with river flux adjustment subtracted from GOBMs in most chapters, or  
1515 comparing unadjusted datasets with discussion of uncertain regional riverine fluxes as major uncertainty, e.g.  
1516 Sarma et al., 2023, DeVries et al., 2023).

### 1517 **3.8.2.5 Tropical vs northern land uptake**

1518 A continuing conundrum is the partitioning of the global atmosphere-land flux between the northern hemisphere  
1519 land and the tropical land (Stephens et al., 2017; Pan et al., 2011; Gaubert et al., 2019). It is of importance  
1520 because each region has its own history of land-use change, climate drivers, and impact of increasing  
1521 atmospheric CO<sub>2</sub> and nitrogen deposition. Quantifying the magnitude of each sink is a prerequisite to  
1522 understanding how each individual driver impacts the tropical and mid/high-latitude carbon balance.

1523 We define the North-South (N-S) difference as net atmosphere-land flux north of 30°N minus the net  
1524 atmosphere-land flux south of 30°N. For the inversions, the N-S difference is 1.50 [0.05,3.0] GtC yr<sup>-1</sup> across  
1525 this year's inversion ensemble. An apparent clustering of six satellite-driven solutions towards a common NH  
1526 land sink noted in GCB2023 is no longer clear.

1527 In the ensemble of DGVMs the N-S difference is 0.4 ± 0.5 GtC yr<sup>-1</sup>, a much narrower range than the one from  
1528 atmospheric inversions. Only three out of twenty DGVMs have a N-S difference larger than 1.0 GtC yr<sup>-1</sup>,  
1529 compared to half of the inversion systems simulating a difference at least this large. The smaller spread across  
1530 DGVMs than across inversions is to be expected as there is no correlation between Northern and Tropical land  
1531 sinks in the DGVMs as opposed to the inversions where the sum of the two regions being well-constrained by  
1532 atmospheric observations leads to an anti-correlation between these two regions. This atmospheric N-S gradient  
1533 could be used as an additional way to evaluate tropical and NH uptake in DGVMs, if their fluxes were  
1534 combined with multiple transport models. Vice versa, the much smaller spread in the N-S difference between  
1535 the DGVMs could help to scrutinise the inverse systems further. For example, a large northern land sink and a  
1536 tropical land source in an inversion would suggest a large sensitivity to CO<sub>2</sub> fertilisation (the dominant factor  
1537 driving the land sinks) for Northern ecosystems, which would be not mirrored by tropical ecosystems. Such a



1538 combination could be hard to reconcile with the process understanding gained from the DGVM ensembles and  
1539 independent measurements (e.g. Free Air CO<sub>2</sub> Enrichment experiments).

### 1540 **3.8.3 Fire emissions in 2024**

1541 Fire emissions so far in 2024 have been above the average of recent decades, chiefly due to synchronous large  
1542 emissions fluxes from North and South America. Figure S9 shows global and regional emissions estimates for  
1543 the period 1st Jan-30th September in each year 2003-2024. Estimates derive from two global fire emissions  
1544 products: the global fire emissions database (GFED, version 4.1s; van der Werf et al., 2017), and the global fire  
1545 assimilation system (GFAS, operated by the Copernicus Atmosphere Service; Kaiser et al., 2012). The two  
1546 products estimate that global emissions from fires were 1.6-2.2 GtC yr<sup>-1</sup> during January-September 2024. These  
1547 estimates are 11-32% above the 2014-2023 average for the same months (1.5-1.7 GtC yr<sup>-1</sup>). In the GFED4.1s  
1548 product, the year-to-date emissions in 2024 were highest since 2003, exceeding even the large emissions  
1549 estimate of 2023, whereas the GFAS product showed lower emissions in 2024 than in 2023 and six other years  
1550 since 2003.

1551 The pattern of high fire emissions from Canada in 2023, which were record-breaking (Jones et al., 2024b, Byrne  
1552 et al., 2024), continued into 2024. In January-September 2024, emissions from Canada (0.2-0.3 GtC yr<sup>-1</sup>) were  
1553 half as great as in the same months of 2023 (0.5-0.8 GtC yr<sup>-1</sup>) but still 2.1-2.3 times the average of January-  
1554 September periods in 2014-2023 (and 4-6 times greater than the average of those months in 2003-2022  
1555 [excluding the record-breaking year in 2023]; Figure S9). The continued anomaly in Canada propagated to the  
1556 northern hemisphere, where emissions of 0.5-0.6 GtC yr<sup>-1</sup> were 26-44% above the average of 2014-2023.

1557 In January-September 2024, fire emissions from South America (0.4-0.6 GtC yr<sup>-1</sup>) were 94-164% above the  
1558 average of January-September periods in 2014-2023, marking 2024 out as a year with synchronous high fire  
1559 emissions across the Americas. Emissions from Brazil in January-September 2024 (0.2-0.3 GtC yr<sup>-1</sup>) were 91-  
1560 118% above the average of January-September periods of 2014-2023 and were at a level not seen since the  
1561 major drought year of 2010 (Figure S9; Aragão et al., 2018, Silva Junior et al., 2019). In 2023, deforestation fire  
1562 activity in the Brazilian Amazon was below the average levels recorded in national recording systems and  
1563 attributed to renewed environmental policy implementation, however the fall in Amazon deforestation fire  
1564 activity was largely offset by above-average wildfires related to historic drought (Mataveli et al. 2024).

1565 According to the National Center for Monitoring and Early Warning of Natural Disasters (CEMADEN), drought  
1566 conditions continued into 2024 and the current drought is the most intense and widespread Brazil has  
1567 experienced since records began in 1950 (CEMADEN, 2024), prompting large wildfires anomalies across the  
1568 Amazon, Cerrado and Pantanal regions (INPE, 2024).

1569 Emissions anomalies in Africa strongly influence global totals because the continent typically contributed 41-  
1570 47% of global fire emissions during 2014-2023 (average of January-September periods). GFAS suggests that  
1571 fire emissions in Africa through September 2024 (0.6 GtC yr<sup>-1</sup>) were slightly below the average of 2014-2023,  
1572 whereas GFED4.1s suggests that fire emissions through September 2024 were slightly above the average of  
1573 2014-2023 (0.8 GtC yr<sup>-1</sup>).

1574 Tropical fire emissions through September 2024 (1.1-1.6 GtC yr<sup>-1</sup>) accounted for 69-74% of the global total  
1575 emissions, which is close to the average of the 2014-2023 period (1.1-1.2 GtC yr<sup>-1</sup>; 72-75%). This marks a  
1576 return to a more typical distribution of fire emissions between the tropics and extra-tropics after the tropical  
1577 contribution fell to just 55-59% during January-September 2023 (Figure S9).

1578 We caution that the fire emissions fluxes presented here should not be compared directly with other fluxes of the  
1579 budget (e.g. S<sub>LAND</sub> or E<sub>LUC</sub>) due to incompatibilities between the observable fire emission fluxes and what is  
1580 quantified in the S<sub>LAND</sub> and E<sub>LUC</sub> components of the budget. The fire emission estimates from global fire  
1581 products relate to all fire types that can be observed in Earth Observations (Giglio et al., 2018; Randerson et al.,  
1582 2012; Kaiser et al., 2012), including (i) fires occurring as part of natural disturbance-recovery cycles that would  
1583 also have occurred in the pre-industrial period (Yue et al., 2016; Keeley and Pausas, 2019; Zou et al., 2019), (ii)  
1584 fires occurring above and beyond natural disturbance-recovery cycle due to changes in climate, CO<sub>2</sub> and N  
1585 fertilisation and to an increased frequency of extreme drought and heatwave events (Abatzoglou et al., 2019;  
1586 Jones et al., 2022; Zheng et al., 2021; Burton et al., 2024), and (iii) fires occurring in relation to land use and  
1587 land use change, such as deforestation fires and agricultural fires (van der Werf et al., 2010; Magi et al., 2012).  
1588 In the context of the global carbon budget, only the portion of fire emissions associated with (ii) should be  
1589 included in the S<sub>LAND</sub> component, and fire emissions associated with (iii) should already be accounted for in the  
1590 E<sub>LUC</sub> component. Emissions associated with (i) should not be included in the global carbon budget. It is not  
1591 currently possible to derive specific estimates for fluxes (i), (ii), and (iii) using global fire emission products  
1592 such as GFED or GFAS. In addition, the fire emissions estimates from global fire emissions products represent  
1593 a gross flux of carbon to the atmosphere, whereas the S<sub>LAND</sub> component of the budget is a net flux that should  
1594 also include post-fire recovery fluxes. Even if emissions from fires of type (ii) could be separated from those of  
1595 type (i), these fluxes may be partially or wholly offset in subsequent years by post-fire fluxes as vegetation  
1596 recovers, sequestering carbon from the atmosphere to the terrestrial biosphere (Yue et al., 2016; Jones et al.,  
1597 2024c). Increases in forest fire emissions and severity (emissions per unit area) from globally during the past  
1598 two decades have highlighted the increasing potential for fire emissions fluxes to outweigh post-fire recovery  
1599 fluxes, though long-term monitoring of vegetation recovery is required to quantify the net effect on terrestrial C  
1600 storage (Jones et al., 2024c).

### 1601 **3.9 Closing the global carbon cycle**

#### 1602 **3.9.1 Partitioning of cumulative emissions and sink fluxes**

1603 Emissions during the period 1850-2023 amounted to  $710 \pm 70$  GtC and were partitioned among the atmosphere  
1604 ( $285 \pm 5$  GtC; 40%), ocean ( $185 \pm 35$  GtC; 26%), and land ( $220 \pm 60$  GtC; 32%). The cumulative land sink is  
1605 almost equal to the cumulative land-use emissions ( $225 \pm 65$  GtC), making the global land nearly neutral over  
1606 the whole 1850-2023 period (Figure 3).

1607 The use of nearly independent estimates for the individual terms of the global carbon budget shows a cumulative  
1608 budget imbalance of 25 GtC (3% of total emissions) during 1850-2023 (Figure 3, Table 8), which, if correct,  
1609 suggests that emissions could be slightly too high by the same proportion or that the combined land and ocean

1610 sinks are slightly underestimated (by about 6%), although these are well within the uncertainty range of each  
1611 component of the budget. Nevertheless, part of the imbalance could originate from the estimation of significant  
1612 increase in  $E_{\text{FOS}}$  and  $E_{\text{LUC}}$  between the mid 1920s and the mid 1960s which is unmatched by a similar growth in  
1613 atmospheric  $\text{CO}_2$  concentration as recorded in ice cores (Figure 3). However, the known loss of additional sink  
1614 capacity of 30-40 GtC (over the 1850-2020 period) due to reduced forest cover has not been accounted for in  
1615 our method and would exacerbate the budget imbalance (see Section 2.10 and Supplement S.6.4).

1616 For the more recent 1960-2023 period where direct atmospheric  $\text{CO}_2$  measurements are available, total  
1617 emissions ( $E_{\text{FOS}} + E_{\text{LUC}}$ ) amounted to  $500 \pm 50$  GtC, of which  $410 \pm 20$  GtC (82%) were caused by fossil  $\text{CO}_2$   
1618 emissions, and  $90 \pm 45$  GtC (18%) by land-use change (Table 8). The total emissions were partitioned among  
1619 the atmosphere ( $220 \pm 5$  GtC; 45%), ocean ( $130 \pm 26$  GtC; 25%), and the land ( $150 \pm 40$  GtC; 30%), with a near  
1620 zero ( $<1$  GtC) unattributed budget imbalance. All components except land-use change emissions have  
1621 significantly grown since 1960, with important interannual variability in the growth rate in atmospheric  $\text{CO}_2$   
1622 concentration and in the land  $\text{CO}_2$  sink (Figure 4), and some decadal variability in all terms (Table 7).  
1623 Differences with previous budget releases are documented in Figure S6.

1624 The global carbon budget averaged over the last decade (2014-2023) is shown in Figure 2, Figure 16 (right  
1625 panel) and Table 7. For this period, 90% of the total emissions ( $E_{\text{FOS}} + E_{\text{LUC}}$ ) were from fossil  $\text{CO}_2$  emissions  
1626 ( $E_{\text{FOS}}$ ), and 10% from land-use change ( $E_{\text{LUC}}$ ). The total emissions were partitioned among the atmosphere  
1627 (48%), ocean (26%) and land (30%), with a small negative budget imbalance ( $\sim 4\%$ ,  $0.4 \text{ GtC yr}^{-1}$ ). For single  
1628 years, the budget imbalance can be larger (Figure 4). For 2023, the combination of our estimated sources ( $11.1 \pm$   
1629  $0.9 \text{ GtC yr}^{-1}$ ) and sinks ( $11.1 \pm 0.9 \text{ GtC yr}^{-1}$ ) leads to a  $B_{\text{IM}}$  of  $-0.02 \text{ GtC}$ , suggesting a near perfect closure of  
1630 the global carbon budget.

### 1631 **3.9.2 Trend and variability in the carbon budget imbalance**

1632 The carbon budget imbalance ( $B_{\text{IM}}$ ; Eq. 1, Figure 4) quantifies the mismatch between the estimated total  
1633 emissions and the estimated changes in the atmosphere, land, and ocean reservoirs. The budget imbalance from  
1634 1960 to 2023 is very small ( $0.5 \text{ GtC}$  over the period, i.e.  $<0.01 \text{ GtC yr}^{-1}$  on average) and shows no trend over the  
1635 full time series (Figure 4e). The process models (GOBMs and DGVMs) and  $f\text{CO}_2$ -products have been selected  
1636 to match observational constraints in the 1990s, but no further constraints have been applied to their  
1637 representation of trend and variability. Therefore, the near-zero mean and trend in the budget imbalance is seen  
1638 as evidence of a coherent community understanding of the emissions and their partitioning on those time scales  
1639 (Figure 4). However, the budget imbalance shows substantial variability of the order of  $\pm 1 \text{ GtC yr}^{-1}$ , particularly  
1640 over semi-decadal time scales, although most of the variability is within the uncertainty of the estimates. The  
1641 positive carbon imbalance during the 1960s, and early 1990s, indicates that either the emissions were  
1642 overestimated, or the sinks were underestimated during these periods. The reverse is true for the 1970s, and to a  
1643 lesser extent for the 1980s and 2014-2023 period (Figure 4, Table 7).

1644 We cannot attribute the cause of the variability in the budget imbalance with our analysis, we only note that the  
1645 budget imbalance is unlikely to be explained by errors or biases in the emissions alone because of its large semi-

1646 decadal variability component, a variability that is atypical of emissions and has not changed in the past 60 years  
1647 despite a near tripling in emissions (Figure 4). Errors in  $S_{\text{LAND}}$  and  $S_{\text{OCEAN}}$  are more likely to be the main cause  
1648 for the budget imbalance, especially on interannual to semi-decadal timescales. For example, underestimation of  
1649 the  $S_{\text{LAND}}$  by DGVMs has been reported following the eruption of Mount Pinatubo in 1991 possibly due to  
1650 missing responses to changes in diffuse radiation (Mercado et al., 2009). Although since GCB2021 we  
1651 accounted for aerosol effects on solar radiation quantity and quality (diffuse vs direct), most DGVMs only used  
1652 the former as input (i.e., total solar radiation) (Table S1). Thus, the ensemble mean may not capture the full  
1653 effects of volcanic eruptions, i.e. associated with high light scattering sulphate aerosols, on the land carbon sink  
1654 (O’Sullivan et al., 2021). DGVMs are suspected to overestimate the land sink in response to the wet decade of  
1655 the 1970s (Sitch et al., 2008). Quasi-decadal variability in the ocean sink has also been reported, with all  
1656 methods agreeing on a smaller than expected ocean  $\text{CO}_2$  sink in the 1990s and a larger than expected sink in the  
1657 2000s (Figure 11; Landschützer et al., 2016, DeVries et al., 2019, Hauck et al., 2020, McKinley et al., 2020,  
1658 Gruber et al., 2023) and the climate-driven variability could be substantial but is not well constrained (DeVries  
1659 et al., 2023, Müller et al., 2023). Errors in sink estimates could also be driven by errors in the climatic forcing  
1660 data, particularly precipitation for  $S_{\text{LAND}}$  and wind for  $S_{\text{OCEAN}}$ . Also, the  $B_{\text{IM}}$  shows substantial departure from  
1661 zero on yearly time scales (Figure 4e), highlighting unresolved variability of the carbon cycle, likely in the land  
1662 sink ( $S_{\text{LAND}}$ ), given its large year to year variability (Figure 4d and 9).

1663 Both the budget imbalance ( $B_{\text{IM}}$ , Table 7) and the residual land sink from the global budget ( $E_{\text{FOS}}+E_{\text{LUC}}-G_{\text{ATM}}-$   
1664  $S_{\text{OCEAN}}$ , Table 5) include an error term due to the inconsistencies that arises from combining  $E_{\text{LUC}}$  from  
1665 bookkeeping models with  $S_{\text{LAND}}$  from DGVMs, most notably the loss of additional sink capacity (see Section  
1666 2.10 and Supplement S.6.4). Other differences include a better accounting of land use changes practices and  
1667 processes in bookkeeping models than in DGVMs, or the bookkeeping models error of having present-day  
1668 observed carbon densities fixed in the past. That the budget imbalance shows no clear trend towards larger  
1669 values over time is an indication that these inconsistencies probably play a minor role compared to other errors  
1670 in  $S_{\text{LAND}}$  or  $S_{\text{OCEAN}}$ .

1671 Although the budget imbalance is near zero for the recent decades, it could be due to a compensation of errors.  
1672 We cannot exclude an overestimation of  $\text{CO}_2$  emissions, particularly from land-use change, given their large  
1673 uncertainty, as has been suggested elsewhere (Piao et al., 2018), and/or an underestimate of the sinks. A larger  
1674 DGVM estimate of the atmosphere-land  $\text{CO}_2$  flux ( $S_{\text{LAND}}-E_{\text{LUC}}$ ) over the extra-tropics would reconcile model  
1675 results with inversion estimates for fluxes in the total land during the past decade (Figure 14; Table 5).  
1676 Likewise, a larger  $S_{\text{OCEAN}}$  is also possible given the higher estimates from the  $f\text{CO}_2$ -products, inversions and  
1677 oxygen based estimates (see Section 3.6.2, Figure 11 and Figure 14), the underestimation of interior ocean  
1678 anthropogenic carbon accumulation in the GOBMs (Section 3.6.5, Müller et al., 2023), known biases of ocean  
1679 models (e.g., Terhaar et al., 2022; 2024), the role of potential temperature bias and skin effects in  $f\text{CO}_2$ -products  
1680 (Watson et al., 2020; Dong et al., 2022; Bellenger et al., 2023, Figure 11) and regionally larger estimates based  
1681 e.g. on eddy covariance measurements and aircraft data (Dong et al., 2024a; Long et al., 2021; Jin et al., 2024).  
1682 More integrated use of observations in the Global Carbon Budget, either on their own or for further constraining  
1683 model results, should help resolve some of the budget imbalance (Peters et al., 2017a).

#### 1684 4 Tracking progress towards mitigation targets

1685 The average growth in global fossil CO<sub>2</sub> emissions peaked at nearly +3% per year during the 2000s, driven by  
1686 the rapid growth in emissions in China. In the last decade, however, the global growth rate has slowly declined,  
1687 reaching a low +0.6% per year over 2014-2023. While this slowdown in global fossil CO<sub>2</sub> emissions growth is  
1688 welcome, global fossil CO<sub>2</sub> emissions continue to grow, far from the rapid emission decreases needed to be  
1689 consistent with the temperature goals of the Paris Agreement.

1690 Since the 1990s, the average growth rate of fossil CO<sub>2</sub> emissions has continuously declined across the group of  
1691 developed countries of the Organisation for Economic Co-operation and Development (OECD), with emissions  
1692 peaking in around 2005 and declining at 1.4% yr<sup>-1</sup> in the decade 2014-2023, compared to a decline of 0.9% yr<sup>-1</sup>  
1693 during the 2004-2013 period (Table 9). In the decade 2014-2023, territorial fossil CO<sub>2</sub> emissions decreased  
1694 significantly (at the 95% confidence level) in 23 countries/economies whose economies grew significantly (also  
1695 at the 95% confidence level): Belgium, Czechia, Denmark, Estonia, Finland, France, Gabon, Germany, Jordan,  
1696 Luxembourg, Netherlands, New Zealand, Norway, Portugal, South Korea, Romania, Slovenia, Somalia, Spain,  
1697 Sweden, Switzerland, United Kingdom, USA (updated from Le Quéré et al., 2019). Altogether, these 23  
1698 countries emitted 2.2 GtC yr<sup>-1</sup> (8.2 GtCO<sub>2</sub> yr<sup>-1</sup>) on average over the last decade, about 23% of world CO<sub>2</sub> fossil  
1699 emissions. For comparison, 17 countries showed a significant decrease in territorial fossil CO<sub>2</sub> emissions over  
1700 the previous decade (2004-2013).

1701 Decomposing emission changes into the components of growth, a Kaya decomposition, helps give an initial  
1702 understanding of the drivers of the changes (Peters et al., 2017b). The reduction in growth in global fossil CO<sub>2</sub>  
1703 emissions in the last decade is due to slightly weaker economic growth, accelerating declines in CO<sub>2</sub> emissions  
1704 per unit energy, and sustained declines in energy per unit GDP (Figure 17). These trends are a supposition of the  
1705 trends at the national level. Fossil CO<sub>2</sub> emission declines in the USA and the EU27 are primarily driven by  
1706 slightly weaker economic growth since the Global Financial Crisis (GFC) in 2008/2009, sustained declines in  
1707 energy per GDP, and sustained declines in CO<sub>2</sub> emissions per unit energy with a slight acceleration in the USA  
1708 in the last decade. In contrast, fossil CO<sub>2</sub> emissions continue to grow in non-OECD countries, although the  
1709 growth rate has slowed from 4.9% yr<sup>-1</sup> during the 2004-2013 decade to 1.8% yr<sup>-1</sup> in the last decade (Table 9).  
1710 Representing 47% of non-OECD emissions in 2023, a large part of this slowdown is due to China, which has  
1711 seen emissions growth decline from 7.5% yr<sup>-1</sup> in the 2004-2013 decade to 1.9% yr<sup>-1</sup> in the last decade.  
1712 Excluding China, non-OECD emissions grew at 3% yr<sup>-1</sup> in the 2004-2013 decade compared to 1.7% yr<sup>-1</sup> in the  
1713 last decade. China has had weaker economic growth in the 2000s compared to the 2010s, and the rate of  
1714 reduction in the energy intensity of economic production has weakened significantly since 2015 with  
1715 accelerating declines in CO<sub>2</sub> emissions per unit energy (Figure 17). India has had strong economic growth that is  
1716 not offset by declines in energy per GDP or declines in CO<sub>2</sub> emissions per unit energy, driving up fossil CO<sub>2</sub>  
1717 emissions. Despite the high deployment of renewables in some countries (e.g., China, India), fossil energy  
1718 sources continue to grow to meet growing energy demand (Le Quéré et al., 2019). In the rest of the world,  
1719 economic growth has slowed considerably in the last decade, but is only partly offset by declines in energy or  
1720 carbon intensity, leading to growing emissions.

1721 Globally, fossil CO<sub>2</sub> emissions growth is slowing, and this is due in part to the emergence of climate policy  
1722 (Eskander and Fankhauser 2020; Le Quere et al 2019) and technological change, which is leading to a shift from  
1723 coal to gas and growth in renewable energies, and reduced expansion of coal capacity. At the aggregated global  
1724 level, decarbonisation shows a strong and growing signal in the last decade, with smaller contributions from  
1725 lower economic growth and declines in energy per GDP (Figure 17). Altogether, global fossil CO<sub>2</sub> emissions are  
1726 still growing (average of 0.6% per year over the 2014-2023 decade), far from the reductions needed to meet the  
1727 ambitious climate goals of the UNFCCC Paris agreement.

1728 Last, we update the remaining carbon budget (RCB) based on two studies, the IPCC AR6 (Canadell et al., 2021)  
1729 and the revision of the IPCC AR6 estimates (Forster et al., 2024, Lamboll et al., 2023). We update the RCB  
1730 assessed by the IPCC AR6 (Canadell et al., 2021), accounting for the 2020 to 2024 estimated emissions from  
1731 fossil fuel combustion ( $E_{FOS}$ ) and land use changes ( $E_{LUC}$ ). From January 2025, the IPCC AR6 RCB (50%  
1732 likelihood) for limiting global warming to 1.5°C, 1.7°C and 2°C is estimated to amount to 85, 180, and 315 GtC  
1733 (305, 655, 1155 GtCO<sub>2</sub>). The Forster et al. (2024) study proposed a significantly lower RCB than IPCC AR6,  
1734 with the largest reduction being due to an update of the climate emulator (MAGICC) used to estimate the  
1735 warming contribution of non-CO<sub>2</sub> agents, and to the warming (i.e. emissions) that occurred over the 2020-2023  
1736 period. We update the Forster et al., budget accounting for the 2024 estimated emissions from fossil fuel  
1737 combustion ( $E_{FOS}$ ) and land use changes ( $E_{LUC}$ ). From January 2025, the Forster et al., (2024) RCB (50%  
1738 likelihood) for limiting global warming to 1.5°C, 1.7°C and 2°C is estimated to amount to 45, 140, and 290 GtC  
1739 (160, 510, 1060 GtCO<sub>2</sub>), significantly smaller than the updated IPCC AR6 estimate. Both the original IPCC  
1740 AR6 and Forster et al. (2024) estimates include the Earth System uncertainty on the climate response to  
1741 cumulative CO<sub>2</sub> emissions, which is reflected through the percent likelihood of exceeding the given temperature  
1742 threshold, an additional uncertainty of  $\pm 220$  GtCO<sub>2</sub> due to alternative non-CO<sub>2</sub> emission scenarios, and other  
1743 sources of uncertainties (see Canadell et al., 2021). The two sets of estimates overlap when considering all  
1744 uncertainties.

1745 Here, we take the average of our 2024 update of both IPCC AR6 and Forster et al. (2024) estimates, giving a  
1746 remaining carbon (50% likelihood) for limiting global warming to 1.5°C, 1.7°C and 2°C of respectively 65, 160,  
1747 and 305 GtC (235, 585, 1110 GtCO<sub>2</sub>) starting from January 2025. We emphasise the large uncertainties,  
1748 particularly when close to the global warming limit of 1.5°C. These 1.5°C, 1.7°C and 2°C remaining carbon  
1749 budgets correspond respectively to about 6, 14 and 27 years from the beginning of 2025, at the 2024 level of  
1750 total anthropogenic CO<sub>2</sub> emissions. Reaching net-zero CO<sub>2</sub> emissions by 2050 entails cutting total  
1751 anthropogenic CO<sub>2</sub> emissions by about 0.4 GtC (1.6 GtCO<sub>2</sub>), 3.9% of 2024 emissions, each year on average,  
1752 comparable to the decrease in  $E_{FOS}$  observed in 2020 during the COVID-19 pandemic. However, this would lead  
1753 to cumulative emissions over 2025-2050 of 145 GtC (530 GtCO<sub>2</sub>), well above the remaining carbon budget of  
1754 65 GtC to limit global warming to 1.5°C, but still within the remaining budget of 160 GtC to limit warming to  
1755 1.7°C (in phase with the “well below 2°C” ambition of the Paris Agreement). Even reaching net zero CO<sub>2</sub>  
1756 globally by 2040, which would require annual emissions cuts of 0.7 GtC (2.5 GtCO<sub>2</sub>) on average, would still  
1757 exceed the remaining carbon budget for 1.5°C, with 90 GtC (325 GtCO<sub>2</sub>) cumulative emissions over 2025-2040,

1758 unless the global emissions trajectory becomes net negative (i.e. more anthropogenic CO<sub>2</sub> sinks than emissions)  
1759 after 2040.

## 1760 **5 Discussion**

1761 Each year when the global carbon budget is published, each flux component is updated for all previous years to  
1762 consider corrections that are the result of further scrutiny and verification of the underlying data in the primary  
1763 input datasets. Annual estimates may be updated with improvements in data quality and timeliness (e.g., to  
1764 eliminate the need for extrapolation of forcing data such as land-use). Of all terms in the global budget, only the  
1765 fossil CO<sub>2</sub> emissions and the growth rate in atmospheric CO<sub>2</sub> concentration are based primarily on empirical  
1766 inputs supporting annual estimates in this carbon budget. The carbon budget imbalance, yet an imperfect  
1767 measure, provides a strong indication of the limitations in observations, in understanding and representing  
1768 processes in models, and/or in the integration of the carbon budget components.

1769 The persistent unexplained variability in the carbon budget imbalance limits our ability to verify reported  
1770 emissions (Peters et al., 2017a) and suggests we do not yet have a complete understanding of the underlying  
1771 carbon cycle dynamics on annual to decadal timescales. Resolving most of this unexplained variability should  
1772 be possible through different and complementary approaches. First, as intended with our annual updates, the  
1773 imbalance as an error term should be reduced by improvements of individual components of the global carbon  
1774 budget that follow from improving the underlying data and statistics and by improving the models through the  
1775 resolution of some of the key uncertainties detailed in Table 10. Second, additional clues to the origin and  
1776 processes responsible for the variability in the budget imbalance could be obtained through a closer scrutiny of  
1777 carbon variability in light of other Earth system data (e.g., heat balance, water balance), and the use of a wider  
1778 range of biogeochemical observations to better understand the land-ocean partitioning of the carbon imbalance  
1779 such as the constraint from atmospheric oxygen included this year. Finally, additional information could also be  
1780 obtained through better inclusion of process knowledge at the regional level, and through the introduction of  
1781 inferred fluxes such as those based on satellite XCO<sub>2</sub> retrievals. The limit of the resolution of the carbon budget  
1782 imbalance is yet unclear, but most certainly not yet reached given the possibilities for improvements that lie  
1783 ahead.

1784 Estimates of global fossil CO<sub>2</sub> emissions from different datasets are in relatively good agreement when the  
1785 different system boundaries of these datasets are considered (Andrew, 2020a). But while estimates of E<sub>FOS</sub> are  
1786 derived from reported activity data requiring much fewer complex transformations than some other components  
1787 of the budget, uncertainties remain, and one reason for the apparently low variation between datasets is precisely  
1788 the reliance on the same underlying reported energy data. The budget excludes some sources of fossil CO<sub>2</sub>  
1789 emissions, which available evidence suggests are relatively small (<1%). We have added emissions from lime  
1790 production in China and the US, but these are still absent in most other non-Annex I countries, and before 1990  
1791 in other Annex I countries.

1792 Estimates of E<sub>LUC</sub> suffer from a range of intertwined issues, including the poor quality of historical land-cover  
1793 and land-use change maps, the rudimentary representation of management processes in most models, and the

1794 confusion in methodologies and boundary conditions used across methods (e.g., Arneth et al., 2017; Pongratz et  
1795 al., 2014, see also Supplement S.6.4 on the loss of sink capacity; Bastos et al., 2021). Uncertainties in current  
1796 and historical carbon stocks in soils and vegetation also add uncertainty in the  $E_{LUC}$  estimates. Unless a major  
1797 effort to resolve these issues is made, little progress is expected in the resolution of  $E_{LUC}$ . This is particularly  
1798 concerning given the growing importance of  $E_{LUC}$  for climate mitigation strategies, and the large issues in the  
1799 quantification of the cumulative emissions over the historical period that arise from large uncertainties in  $E_{LUC}$ .

1800 By adding the DGVMs estimates of  $CO_2$  fluxes due to environmental change from countries' managed forest  
1801 areas (part of  $S_{LAND}$  in this budget) to the budget  $E_{LUC}$  estimate, we successfully reconciled the large gap  
1802 between our  $E_{LUC}$  estimate and the land use flux from NGHGs using the approach described in Grassi et al.  
1803 (2021) for future scenarios and in Grassi et al. (2023) using data from the Global Carbon Budget 2021. The  
1804 updated data presented here can be used as potential adjustment in the policy context, e.g., to help assess the  
1805 collective countries' progress towards the goal of the Paris Agreement and avoiding double-accounting for the  
1806 sink in managed forests. In the absence of this adjustment, collective progress would hence appear better than it  
1807 is (Grassi et al., 2021). The application of this adjustment is also recommended in the UNFCCC Synthesis  
1808 report for the first Global Stocktake (UNFCCC, 2022) whenever a comparison between LULUCF fluxes  
1809 reported by countries and the global emission estimates of the IPCC is conducted. However, this adjustment  
1810 should be seen as a short-term and pragmatic fix based on existing data, rather than a definitive solution to  
1811 bridge the differences between global models and national inventories. Additional steps are needed to  
1812 understand and reconcile the remaining differences, some of which are relevant at the country level (Grassi, et  
1813 al., 2023, Schwingshackl, et al., 2022).

1814 The comparison of GOBMs,  $fCO_2$ -products, and inversions highlights substantial discrepancy in the temporal  
1815 evolution of  $S_{OCEAN}$  in the Southern Ocean and northern high-latitudes (Figure 14, Hauck et al., 2023a) and in  
1816 the mean  $S_{OCEAN}$  in the tropics. A large part of the uncertainty in the mean fluxes stems from the regional  
1817 distribution of the river flux adjustment term. The current distribution simulates the largest share of the  
1818 outgassing to occur in the tropics (Lacroix et al., 2020). The long-standing sparse data coverage of  $fCO_2$   
1819 observations in the Southern compared to the Northern Hemisphere (e.g., Takahashi et al., 2009) continues to  
1820 exist (Bakker et al., 2016, 2024, Figure S1) and to lead to substantially higher uncertainty in the  $S_{OCEAN}$  estimate  
1821 for the Southern Hemisphere (Watson et al., 2020, Gloege et al., 2021, Hauck et al., 2023a). This discrepancy,  
1822 which also hampers model improvement, points to the need for increased high-quality  $fCO_2$  observations  
1823 especially in the Southern Ocean. At the same time, model uncertainty is illustrated by the large spread of  
1824 individual GOBM estimates (indicated by shading in Figure 14) and highlights the need for model  
1825 improvement. The issue of diverging trends in  $S_{OCEAN}$  from different methods is smaller this year as the trend in  
1826 the  $fCO_2$ -products was revised downwards with the data available in this GCB release, but remains a matter of  
1827 concern. Recent and on-going work suggests that the  $fCO_2$ -products may overestimate the trend (Hauck et al.,  
1828 2023a, Supplement section S3.4), though the full  $fCO_2$ -product ensemble remains to be tested. A data-  
1829 constrained model approach suggests that the GOBMs underestimate the amplitude of decadal variability, but  
1830 that the  $fCO_2$ -products overestimate the trend (Mayot et al., 2024). At the same time, evidence is accumulating  
1831 that GOBMs likely underestimate the mean flux (Section 3.6.2, Terhaar et al., 2022, DeVries et al., 2023,



1832 Müller et al., 2023, Dong et al., 2024). The independent constraint from atmospheric oxygen measurements  
1833 gives a larger sink for the past decade and a steeper trend. However, the estimate is consistent within  
1834 uncertainties with  $S_{OCEAN}$ , with the relatively larger ocean sink in the  $fCO_2$ -products and some of the GOBMs.  
1835 The assessment of the net land-atmosphere exchange from DGVMs and atmospheric inversions also shows  
1836 substantial discrepancy, particularly for the estimate of the net land flux over the northern extra-tropic. This  
1837 discrepancy highlights the difficulty to quantify complex processes (CO<sub>2</sub> fertilisation, nitrogen deposition and  
1838 fertilisers, climate change and variability, land management, etc.) that collectively determine the net land CO<sub>2</sub>  
1839 flux. Resolving the differences in the Northern Hemisphere land sink will require the consideration and  
1840 inclusion of larger volumes of observations.

1841 We provide metrics for the evaluation of the ocean and land models and the atmospheric inversions (Figures S2  
1842 to S4, Table S11). These metrics expand the use of observations in the global carbon budget, helping 1) to  
1843 support improvements in the ocean and land carbon models that produce the sink estimates, and 2) to constrain  
1844 the representation of key underlying processes in the models and to allocate the regional partitioning of the CO<sub>2</sub>  
1845 fluxes. The introduction of process-based metrics targeted to evaluate the simulation of  $S_{OCEAN}$  in the ocean  
1846 biogeochemistry models is an important addition to the evaluation based on ocean carbon observations. This is  
1847 an initial step towards the introduction of a broader range of observations and more stringent model evaluation  
1848 that we hope will support continued improvements in the annual estimates of the global carbon budget.

1849 We assessed before that a sustained decrease of –1% in global emissions could be detected at the 66%  
1850 likelihood level after a decade only (Peters et al., 2017a). Similarly, a change in behaviour of the land and/or  
1851 ocean carbon sink would take as long to detect, and much longer if it emerges more slowly. To continue  
1852 reducing the carbon imbalance on annual to decadal time scales, regionalising the carbon budget, and integrating  
1853 multiple variables are powerful ways to shorten the detection limit and ensure the research community can  
1854 rapidly identify issues of concern in the evolution of the global carbon cycle under the current rapid and  
1855 unprecedented changing environmental conditions.

## 1856 **6 Conclusions**

1857 The estimation of global CO<sub>2</sub> emissions and sinks is a major effort by the carbon cycle research community that  
1858 requires a careful compilation and synthesis of measurements, statistical estimates, and model results. The  
1859 delivery of an annual carbon budget serves two purposes. First, there is a large demand for up-to-date  
1860 information on the state of the anthropogenic perturbation of the climate system and its underpinning causes. A  
1861 broad stakeholder community relies on the datasets associated with the annual carbon budget including  
1862 scientists, policy makers, businesses, journalists, and non-governmental organisations engaged in adapting to  
1863 and mitigating human-driven climate change. Second, over the last decades we have seen unprecedented  
1864 changes in the human and biophysical environments (e.g., changes in the growth of fossil fuel emissions, impact  
1865 of COVID-19 pandemic, Earth’s warming, and strength of the carbon sinks), which call for frequent  
1866 assessments of the state of the planet, a better quantification of the causes of changes in the contemporary global  
1867 carbon cycle, and an improved capacity to anticipate its evolution in the future. Building this scientific

1868 understanding to meet the extraordinary climate mitigation challenge requires frequent, robust, transparent, and  
1869 traceable datasets and methods that can be scrutinised and replicated. This paper via ‘living data’ helps to keep  
1870 track of new budget updates.

## 1871 7 **Data availability**

1872 The data presented here are made available in the belief that their wide dissemination will lead to greater  
1873 understanding and new scientific insights of how the carbon cycle works, how humans are altering it, and how  
1874 we can mitigate the resulting human-driven climate change. Full contact details and information on how to cite  
1875 the data shown here are given at the top of each page in the accompanying database and summarised in Table 2.

1876 The accompanying database includes three Excel files organised in the following spreadsheets:

1877 File `Global_Carbon_Budget_2024v1.0.xlsx` includes the following:

- 1878 1. Summary
- 1879 2. The global carbon budget (1959-2023);
- 1880 3. The historical global carbon budget (1750-2023);
- 1881 4. Global CO<sub>2</sub> emissions from fossil fuels and cement production by fuel type, and the per-capita emissions  
1882 (1850-2023);
- 1883 5. CO<sub>2</sub> emissions from land-use change from the individual bookkeeping models (1959-2023);
- 1884 6. Ocean CO<sub>2</sub> sink from the individual global ocean biogeochemistry models and /CO<sub>2</sub>-products (1959-  
1885 2023);
- 1886 7. Terrestrial CO<sub>2</sub> sink from the individual DGVMs (1959-2023);
- 1887 8. Cement carbonation CO<sub>2</sub> sink (1959-2023).

1888 File `National_Fossil_Carbon_Emissions_2024v1.0.xlsx` includes the following:

- 1889 1. Summary
- 1890 2. Territorial country CO<sub>2</sub> emissions from fossil fuels and cement production (1850-2023);
- 1891 3. Consumption country CO<sub>2</sub> emissions from fossil fuels and cement production and emissions transfer from  
1892 the international trade of goods and services (1990-2020) using CDIAC/UNFCCC data as reference;
- 1893 4. Emissions transfers (Consumption minus territorial emissions; 1990-2020);
- 1894 5. Country definitions.

1895 File `National_LandUseChange_Carbon_Emissions_2024v1.0.xlsx` includes the following:

1896 1. Summary

1897 2. Territorial country CO<sub>2</sub> emissions from Land Use Change (1850-2023) from three bookkeeping models;

1898 All three spreadsheets are published by the Integrated Carbon Observation System (ICOS) Carbon Portal and

1899 are available at <https://doi.org/10.18160/GCP-2024> (Friedlingstein et al., 2024). National emissions data are also

1900 available at <https://doi.org/10.5281/zenodo.13981696> (Andrew and Peters, 2024), from the Global Carbon Atlas

1901 (<http://www.globalcarbonatlas.org/>, last access: 21 January 2025) and from Our World in Data

1902 (<https://ourworldindata.org/co2-emissions>, last access: 21 January 2025).

1903 **Author contributions**

1904 PF, MO, MWJ, RMA, JH, PL, CLQ, HL, ITL, AO, GPP, WP, JP, CS, and SSi designed the study, conducted

1905 the analysis, and wrote the paper with input from JGC, PCi and RBJ. RMA, GPP and JIK produced the fossil

1906 CO<sub>2</sub> emissions and their uncertainties and analysed the emissions data. MH and GMa provided fossil fuel

1907 emission data. JP, TGa, ZQ, and CS provided the bookkeeping land-use change emissions with synthesis by JP

1908 and CS. SSm provided the estimates of non-vegetation CDR fluxes. LB, MC, ÖG, NG, TI, TJ, LR, JS, RS, and

1909 HTs provided an update of the global ocean biogeochemical models; LMD, ARF, DJF, MG, LG, YI, AJ, CR,

1910 AR, JZ, and PC provided an update of the ocean fCO<sub>2</sub>-data products, with synthesis on both streams by JH, PL

1911 and NMa. SRA, NRB, MB, CFB, HCB, KC, KE, WE, RAF, TGk, SKL, NL, NMe, NMM, SN, LO, TO, DP,

1912 AJS, ST, BT, CN, and RW provided ocean fCO<sub>2</sub> measurements for the year 2023, with synthesis by AO and TS.

1913 AA, VA, PCa, THC, JD, CDR, AF, JHe, AKJ, EK, JK, PCM, LM, TN, MO, QS, HTi, XYa, WY, XYu, and SZ

1914 provided an update of the Dynamic Global Vegetation Models, with synthesis by SSi and MO. HL, RSA, OT,

1915 and ET provided estimates of land and ocean sinks from Earth System Models, as well as a projection of the

1916 atmospheric growth rate for 2024. NC, FC, ARJ, FJ, ZJ, JL, SM, YN, PIP, CR, DY, and NZ provided an

1917 updated atmospheric inversion, WP, FC, and ITL developed the protocol and produced the synthesis and

1918 evaluation of the atmospheric inversions. RMA provided projections of the 2024 fossil emissions and

1919 atmospheric CO<sub>2</sub> growth rate. PL provided the predictions of the 2024 ocean and land sinks. LPC, GCH, KKG,

1920 TMR, GRvdW, WX, and ZY provided forcing data for land-use change. FT and GG provided data for the land-

1921 use change NGHGI harmonisation. RFK provided key atmospheric CO<sub>2</sub> data. EJM and RFK provided the

1922 atmospheric oxygen constraint on surface net carbon sinks. MWJ provided the historical atmospheric CO<sub>2</sub>

1923 concentration and growth rate. MO and NB produced the aerosol diffuse radiative forcing for the DGVMs. IH

1924 provided the climate forcing data for the DGVMs. PCM provided the evaluation of the DGVMs. MWJ provided

1925 the emissions prior for use in the inversion systems. XD provided seasonal emissions data for most recent years  
1926 for the emission prior. PF, MO and MWJ coordinated the effort, revised all figures, tables, text and numbers to  
1927 ensure the update was clear from the 2023 edition and in line with the [globalcarbonatlas.org](https://globalcarbonatlas.org).

#### 1928 **Competing interests.**

1929 At least one of the (co-)authors is a member of the editorial board of Earth System Science Data

1930

#### 1931 **Acknowledgements**

1932 We thank all people and institutions who provided the data used in this global carbon budget 2024 and the Global  
1933 Carbon Project members for their input throughout the development of this publication. We thank Nigel Hawtin  
1934 for producing Figure 2 and Figure 15. We thank Alex Vermeulen and Hannah Ritchie for respectively hosting the  
1935 Global Carbon Budget datasets on the ICOS portal and the Our World in Data website. We thank Ram Alkama,  
1936 Ian G. C. Ashton, Dorothee Bakker, Raffaele Bernardello, Ida Bagus Mandhara Brasika, Sebastian Brune,  
1937 Fatemeh Cheginig, Emeric Claudel, Jason Cole, Lushanya Dayathilake, Pengyue Du, Christian Ethé, Stefanie  
1938 Falk, Kristina Frölich, Lonneke Goddijn-Murphy, Ian Harman, T. Holding, Drew Holzworth, Rajesh Janardanan,  
1939 Daniel Kennedy, Erik Kluzek, Fabrice Lacroix, Vladimir Lapin, Peter Lawrence, am Levis, Yi Liu, Damian Loher,  
1940 Zoé Lloret, Adrien Martinez, H. Nakano, Lorna Nayagam, Naiqing Pan, Shufen Pan, Tristan Quaiife, Simone  
1941 Rossi, Paridhi Rustogi, J. D. Shutler, Richard Sims, Victoria Spada, Sean Swenson, Phillip Townsend, K. Toyama,  
1942 S. L. Urakawa, Anthony P. Walker, Jing Wang, Andrew J. Watson, S Lachlan Whyborn, David K. Woolf, and  
1943 Yakun Zhu for their involvement in the development, use and analysis of the models and data-products used here.  
1944 We thank Kim Currie, Siyabulela Hamnca, Boris Herrmann, Arne Körtzinger, C. Lo Monaco, Team Malizia,  
1945 Pedro Monteiro, and Mutshutshu Tsanwani who contributed to the provision of surface ocean CO<sub>2</sub> observations  
1946 for the year 2023 (see Table S7). We also thank Stephen D. Jones of the Ocean Thematic Centre of the EU  
1947 Integrated Carbon Observation System (ICOS) Research Infrastructure, Eugene Burger of NOAA's Pacific Marine  
1948 Environmental Laboratory and Alex Kozyr of NOAA's National Centers for Environmental Information, for their  
1949 contribution to surface ocean CO<sub>2</sub> data and metadata management. We thank the scientists, institutions, and  
1950 funding agencies responsible for the collection and quality control of the data in SOCAT as well as the  
1951 International Ocean Carbon Coordination Project (IOCCP), the Surface Ocean Lower Atmosphere Study  
1952 (SOLAS) and the Integrated Marine Biosphere Research (IMBeR) program for their support. We thank Nadine

1953 Goris and Lavinia Patara for support in calculating observational ocean evaluation metrics. We thank Fortunat  
1954 Joos, Samar Khatiwala and Timothy DeVries for providing historical atmospheric and ocean data. We thank data  
1955 providers ObsPack GLOBALVIEWplus v9.0 and NRT v9.2 for atmospheric CO<sub>2</sub> observations. Ingrid T Lujckx  
1956 and Wouter Peters thank the CarbonTracker Europe team at Wageningen University, including Remco de Kok,  
1957 Joram Hooghiem, Linda Kooijmans and Auke van der Woude. Ian Harris thanks the Japan Meteorological Agency  
1958 (JMA) for producing the Japanese 55-year Reanalysis (JRA-55). Reinel Sospedra-Alfonso thanks William J.  
1959 Merryfield, Woosung Lee, Jason Cole, and Victoria Spada for their help to set up and produce CanESM5 runs.  
1960 Olivier Torres thanks Patricia Cadule, Juliette Mignot, Didier Swingedouw, and Laurent Bopp for contributions  
1961 to the IPSL-CM6-LR-ESMCO2 simulations. Yosuke Niwa thanks CSIRO, EC, EMPA, FMI, IPEN, JMA, LSCE,  
1962 NCAR, NIES, NILU, NIWA, NOAA, SIO, and TU/NIPR for providing data for NISMON-CO2. Zhe Jin thanks  
1963 Xiangjun Tian, Yilong Wang, Hongqin Zhang, Min Zhao, Tao Wang, Jinzhi Ding and Shilong Piao for their  
1964 contributions to the GONGGA inversion system. Paul I. Palmer thanks Lian Fang and acknowledges ongoing  
1965 support from the National Centre for Earth Observation. Ning Zeng thanks Zhiqiang Liu, Yun Liu, Eugenia  
1966 Kalnay, and Gassem Asrar for their contributions to the COLA system. Fei Jiang acknowledges the High-  
1967 Performance Computing Center (HPCC) of Nanjing University for doing the inversions on its blade cluster  
1968 system, and thanks Weimin Ju for updating the a priori fluxes of the terrestrial ecosystems. Meike Becker and Are  
1969 Olsen thank Sparebanken Vest / Agenda Vestlandet for their support for the observations on the Statsraad  
1970 Lehmkuhl. Wiley Evans and Katie Campbell thank the Tula Foundation for funding support. Thanos Gkritzalis  
1971 and the VLIZ ICOS team are thankful to the crew of the research vessel Simon Stevin for all the support and help  
1972 they provide. Bronte Tilbrook and Craig Neill thank Australia's Integrated Marine Observing System (IMOS) for  
1973 sourcing CO<sub>2</sub> data. FAOSTAT is funded by FAO member states through their contributions to the FAO Regular  
1974 Programme, data contributions by national experts are greatly acknowledged. The views expressed in this paper  
1975 are the authors' only and do not necessarily reflect those of FAO. Finally, we thank all funders who have supported  
1976 the individual and joint contributions to this work (see details below), as well as the two reviewers of this  
1977 manuscript, and the many researchers who have provided feedback.

#### 1978 **Financial and computing support**

1979 This research was supported by the following sources of funding: The Argentinian-Uruguayan Joint Technical  
1980 Commission of the Maritime Front (Comisión Técnica Mixta del Frente Marítimo, CTMFM) (Argentina);  
1981 Instituto Nacional de Investigación y Desarrollo Pesquero (Argentina); Australia's Integrated Marine Observing

1982 System (IMOS) which is enabled by the National Collaborative Research Infrastructure Strategy (NCRIS)  
1983 (Australia); Australian Earth-System Simulator National Research Infrastructure (ACCESS-NRI) (Australia);  
1984 Australian National Environmental Science Program, Climate Systems Hub (Australia); Research Foundation  
1985 Flanders (ICOS Flanders, grant no. I001821N) (Belgium); Tula Foundation (Canada); National Key Research and  
1986 Development Program (grant no. 2023YFF0805400) (China); National Key Research and Development Program  
1987 (grant no. 2023YFB3907404) (China); Jiangsu Provincial Science Fund for Distinguished Young Scholars (Grant  
1988 No: BK20231530) (China); National Natural Science Foundation (grant no. 42141020) (China); Carbon  
1989 Neutrality and Energy System Transformation (CNEST) Program led by Tsinghua University, granted by National  
1990 Key R&D Program of China (Grant No. 2023YFE0113000) (China); Second Tibetan Plateau Scientific  
1991 Expedition and Research Program (Grant: 2022QZKK0101) (China); CAS Project for Young Scientists in Basic  
1992 Research, Grant No.YSBR-037 (China); grant no. 2021YFD2200405 (China); Copernicus Atmosphere  
1993 Monitoring Service, implemented by ECMWF (Grant: CAMS2 55) (European Commission); Copernicus Marine  
1994 Environment Monitoring Service, implemented by MOi (Grant: CMEMS-TAC-MOB) (European Commission);  
1995 H2020 4C (grant no. 821003) (European Commission); H2020 ESM2025 – Earth System Models for the Future  
1996 (grant no. 101003536) (European Commission); H2020 GEORGE (grant no. 101094716) (European  
1997 Commission); Horizon Europe (EYE-CLIMA: grant no. 101081395) (European Commission); ERC-2022-STG  
1998 OceanPeak (Grant 101077209) (European Commission); Horizon Europe Grant 101083922 (OceanICU  
1999 Improving Carbon Understanding) (European Commission); Horizon 2020 research and innovation programme  
2000 under Grant Agreements N° 101056939 (RESCUE project) (European Commission); COMFORT project (grant  
2001 no. 820989) (European Commission); Climate Space RECCAP-2 (European Space Agency); Ocean Carbon for  
2002 Climate (European Space Agency); EO-LINCS (European Space Agency); OceanSODA project, grant no.  
2003 4000112091/14/I-LG (European Space Agency); Institut National des Sciences de l'Univers (INSU) (France);  
2004 Institut Polaire français, Paul-Emile Victor (IPEV) (France); Observatoire des sciences de l'univers Ecce-Terra  
2005 (OSU at Sorbonne Université) (France); Institut de recherché français sur les ressources marines (IFREMER)  
2006 (France); French Oceanographic Fleet (FOF) (France); ICOS-France (France); Institut de Recherche pour le  
2007 Développement (IRD) (France); Agence Nationale de la Recherche - France 2030 (PEPR TRACCS programme  
2008 under grant number ANR-22-EXTR-0009) (France); Institut de l'Océan and the Institut des Sciences du Calcul et  
2009 des Données of Sorbonne University (IDEX SUPER 11-IDEX-0004, project-team FORMAL) (France); Federal  
2010 Ministry of Education and Research, collaborative project C-SCOPE (project no. 03F0877A) (Germany);  
2011 Helmholtz Association ATMO programme (Germany); Initiative and Networking Fund of the Helmholtz  
2012 Association (grant no. VH-NG-19-33) (Germany); ICOS Germany (Germany); German Federal Ministry of  
2013 Education and Research (BMBF), project STEPSEC (grant no. 01LS2102A) (Germany); Helmholtz Young  
2014 Investigator Group Marine Carbon and Ecosystem Feedbacks in the Earth System (MarESys), grant number VH-  
2015 NG-1301 (Germany); Deutsche Forschungsgemeinschaft (DFG) under Germany's Excellence Strategy – EXC  
2016 2037 'Climate, Climatic Change, and Society' – Project Number: 390683824 (Germany); Arctic Challenge for  
2017 Sustainability phase II project (ArCS-II; grant no. JP-MXD1420318865) (Japan); Environment Research and  
2018 Technology Development Fund (grant no. JPMEERF24S12206) (Japan); CREST, Japan Science and Technology  
2019 Agency (grant no. JPMJCR23J4) (Japan); Global Environmental Research Coordination System, Ministry of the  
2020 Environment (grant no. E2252) (Japan); Meteorological Agency (Japan); Ministry of Education, Culture, Sports,

2021 Science and Technology, MEXT program for the advanced studies of climate change projection (SENTAN) (grant  
2022 numbers JPMXD0722680395 and JPMXD0722681344) (Japan); Meteorological Research Institute and the  
2023 Environment Research and Technology Development Fund (JPMEERF24S12200) (Japan); NIES GOSAT project  
2024 (Japan); Research Council of Norway (N-ICOS-2, grant no. 296012) (Norway); Research Council of Norway  
2025 (grant no. 270061) (Norway); Swiss National Science Foundation (grant no. 200020-200511) (Switzerland);  
2026 Natural Environment Research Council, National Centre for Earth Observation (NE/R016518/1) (UK); Natural  
2027 Environment Research Council, UK EO Climate Information Service (NE/X019071/1) (UK); Natural  
2028 Environment Research Council (NE/V01417X/1) (UK); Natural Environment Research Council, National Centre  
2029 for Atmospheric Science (UK); Natural Environment Research Council (NE/Y005260/1) (UK); UK Royal Society  
2030 (grant no. RP/R1\191063) (UK); Natural Environment Research Council (Grant Ref: NE/V013106/1) (UK);  
2031 National Center for Atmospheric Research (NSF Cooperative Agreement No. 1852977) (USA); NOAA Ocean  
2032 Acidification Program (grant no. 100018228) (USA); NOAA Global Ocean Monitoring and Observing Program  
2033 (grant no. 100018302) (USA); NOAA cooperative agreement NA22OAR4320151 (USA); NOAA cooperative  
2034 agreement NA20OAR4310340 (USA); NOAA (grant no. 1305M322PNRMJ0338); NASA (grant no.  
2035 80NSSC22K0150); NASA (grant no. 80NM0018D0004); National Science Foundation (NSF-2019625) (USA);  
2036 National Science Foundation (NSF-831361857) (USA); NASA Terrestrial Ecology Program (USA); NASA  
2037 Carbon Monitoring System program (80NSSC21K1059) (USA); NASA Land Cover and Land Use Change  
2038 Program (80NSSC24K0920) (USA); National Science Foundation (NSF-1903722) (USA); National Science  
2039 Foundation (NSF-1852977) (USA); The U.S. Department of Energy, Office of Science, Office of Biological and  
2040 Environmental Research (USA); The Department for Education SciDac (grant number: DESC0012972) (USA);  
2041 IDS (grant number: 80NSSC17K0348) (USA); Schmidt Sciences, LLC (USA).

2042 We also acknowledge support from the following computing facilities: The Australian Earth-System Simulator  
2043 National Research Infrastructure (ACCESS-NRI) (Australia); Deutsches Klimarechenzentrum (DKRZ) granted  
2044 by its Scientific Steering Committee (WLA) under project ID bm0891 (Germany); HPC cluster Aether at the  
2045 University of Bremen, financed by DFG within the scope of the Excellence Initiative (Germany); HPC resources  
2046 of TGCC under the allocation A0150102201 awarded by GENCI and of CCRT under the Grant CCRT2024-  
2047 p24cheva awarded by CEA/DRF (France); HPC resources of Meteo-France (France); NIES supercomputer system  
2048 (Japan); UNINETT Sigma2, National Infrastructure for High Performance Computing and Data Storage in  
2049 Norway (NN2980K/NS2980K) (Norway); UK CEDA JASMIN supercomputer (UK); UEA (University of East  
2050 Anglia) high performance computing cluster (UK); Derecho supercomputer (doi:10.5065/D6RX99HX), provided  
2051 by the Computational and Information Systems Laboratory (CISL) at NCAR (USA); Oak Ridge Leadership  
2052 Computing Facility at the Oak Ridge National Laboratory (USA); ISAM simulations were performed using  
2053 Cheyenne, NCAR HPC resources managed by CISL (doi:10.5065/D6RX99HX) (USA).

2054

**References**

- 2055 Andela, N., Morton, D. C., Giglio, L., Chen, Y., van der Werf, G. R., Kasibhatla, P. S., DeFries, R. S., Collatz, G. J.,  
 2056 Hantson, S., Kloster, S., Bachelet, D., Forrest, M., Lasslop, G., Li, F., Mangeon, S., Melton, J. R., Yue, C., and Randerson, J.  
 2057 T.: A human-driven decline in global burned area, *Science*, 356, 1356–1362, <https://doi.org/10.1126/science.aal4108>, 2017.
- 2058 Andrew, R. M.: A comparison of estimates of global carbon dioxide emissions from fossil carbon sources, *Earth Syst. Sci.*  
 2059 *Data*, 12, 1437–1465, <https://doi.org/10.5194/essd-12-1437-2020>, 2020a.
- 2060 Andrew, R. M.: Timely estimates of India’s annual and monthly fossil CO<sub>2</sub> emissions, *Earth Syst. Sci. Data*, 12, 2411–2421,  
 2061 <https://doi.org/10.5194/essd-12-2411-2020>, 2020b.
- 2062 Andrew, R. M. and Peters, G. P.: The Global Carbon Project’s fossil CO<sub>2</sub> emissions dataset (2024v17), Zenodo [dataset],  
 2063 <https://doi.org/10.5281/zenodo.13981696>, 2024.
- 2064 Aragão, L. E. O. C., Anderson, L. O., Fonseca, M. G., Rosan, T. M., Vedovato, L. B., Wagner, F. H., Silva, C. V. J., Silva  
 2065 Junior, C. H. L., Arai, E., Aguiar, A. P., Barlow, J., Berenguer, E., Deeter, M. N., Domingues, L. G., Gatti, L., Gloor, M.,  
 2066 Malhi, Y., Marengo, J. A., Miller, J. B., Phillips, O. L., and Saatchi, S.: 21st Century drought-related fires counteract the  
 2067 decline of Amazon deforestation carbon emissions, *Nat Commun*, 9, 536, <https://doi.org/10.1038/s41467-017-02771-y>,  
 2068 2018.
- 2069 Archer, D., Eby, M., Brovkin, V., Ridgwell, A., Cao, L., Mikolajewicz, U., Caldeira, K., Matsumoto, K., Munhoven, G.,  
 2070 Montenegro, A., and Tokos, K.: Atmospheric Lifetime of Fossil Fuel Carbon Dioxide, *Annu. Rev. Earth Planet. Sci.*, 37,  
 2071 117–134, <https://doi.org/10.1146/annurev.earth.031208.100206>, 2009.
- 2072 Arneeth, A., Sitch, S., Pongratz, J., Stocker, B. D., Ciais, P., Poulter, B., Bayer, A. D., Bondeau, A., Calle, L., Chini, L. P.,  
 2073 Gasser, T., Fader, M., Friedlingstein, P., Kato, E., Li, W., Lindeskog, M., Nabel, J. E. M. S., Pugh, T. A. M., Robertson, E.,  
 2074 Viovy, N., Yue, C., and Zaehle, S.: Historical carbon dioxide emissions caused by land-use changes are possibly larger than  
 2075 assumed, *Nature Geosci*, 10, 79–84, <https://doi.org/10.1038/ngeo2882>, 2017.
- 2076 Asaadi, A., Arora, V. K., Melton, J. R., and Bartlett, P.: An improved parameterization of leaf area index (LAI) seasonality  
 2077 in the Canadian Land Surface Scheme (CLASS) and Canadian Terrestrial Ecosystem Model (CTEM) modelling framework,  
 2078 *Biogeosciences*, 15, 6885–6907, <https://doi.org/10.5194/bg-15-6885-2018>, 2018.
- 2079 Aumont, O., Orr, J. C., Monfray, P., Ludwig, W., Amiotte-Suchet, P., and Probst, J.-L.: Riverine-driven interhemispheric  
 2080 transport of carbon, *Global Biogeochem. Cycles*, 15, 393–405, <https://doi.org/10.1029/1999GB001238>, 2001.
- 2081 Aumont, O., Ethé, C., Tagliabue, A., Bopp, L., and Gehlen, M.: PISCES-v2: an ocean biogeochemical model for carbon and  
 2082 ecosystem studies, *Geoscientific Model Development*, 8, 2465–2513, <https://doi.org/10.5194/gmd-8-2465-2015>, 2015.
- 2083 Babiker, M., G. Berndes, K. Blok, B. Cohen, A. Cowie, O. Geden, V. Ginzburg, A. Leip, P. Smith, M. Sugiyama, F. Yamba,  
 2084 Al Khourdjie, A., Arneeth, A., Lima de Azevedo, I. M., Bataille, C., Beerling, D., Bezner Kerr, R., Bradley, J., Buck, H. J.,  
 2085 Cabeza, L. F., Calvin, K., Campbell, D., Carnicer Cols, J., Daioglou, V., Harmsen, M., Höglund-Isaksson, L., House, J. I.,  
 2086 Keller, D., de Kleijne, K., Kugelberg, S., Makarov, I., Meza, F., Minx, J. C., Morecroft, M., Nabuurs, G. J., Neufeldt, H.,  
 2087 Novikova, A., Nugroho, S. B., Oschlies, A., Parmesan, C., Peters, G. P., Poore, J., Portugal-Pereira, J., Postigo, J. C.,  
 2088 Pradhan, P., Renforth, P., Rivera-Ferre, M. G., Roe, S., Singh, P. K., Slade, R., Smith, S. M., Tirado von der Pahlen, M. C.,  
 2089 and Toribio Ramirez, D.: Cross sectoral perspectives. In: *Climate Change 2022: Mitigation of Climate Change. Contribution*



2090 of Working Group III to the Sixth Assessment Report of the Intergovernmental Panel on Climate Change [P.R. Shukla, J.  
2091 Skea, R. Slade, A. Al Khourdajie, R. van Diemen, D. McCollum, M. Pathak, S. Some, P. Vyas, R. Fradera, M. Belkacemi,  
2092 A. Hasija, G. Lisboa, S. Luz, J. Malley, (eds.)]. Cambridge University Press, Cambridge, UK and New York, NY, USA. doi:  
2093 10.1017/9781009157926.014, 2022.

2094 Baccini, A., Walker, W., Carvalho, L., Farina, M., Sulla-Menashe, D., and Houghton, R. A.: Tropical forests are a net carbon  
2095 source based on aboveground measurements of gain and loss, *Science*, 358, 230–234,  
2096 <https://doi.org/10.1126/science.aam5962>, 2017.

2097 Bakker, D. C. E., Pfeil, B., Landa, C. S., Metzl, N., O'Brien, K. M., Olsen, A., Smith, K., Cosca, C., Harasawa, S., Jones, S.  
2098 D., Nakaoka, S., Nojiri, Y., Schuster, U., Steinhoff, T., Sweeney, C., Takahashi, T., Tilbrook, B., Wada, C., Wanninkhof, R.,  
2099 Alin, S. R., Balestrini, C. F., Barbero, L., Bates, N. R., Bianchi, A. A., Bonou, F., Boutin, J., Bozec, Y., Burger, E. F., Cai,  
2100 W.-J., Castle, R. D., Chen, L., Chierici, M., Currie, K., Evans, W., Featherstone, C., Feely, R. A., Fransson, A., Goyet, C.,  
2101 Greenwood, N., Gregor, L., Hankin, S., Hardman-Mountford, N. J., Harlay, J., Hauck, J., Hoppema, M., Humphreys, M. P.,  
2102 Hunt, C. W., Huss, B., Ibánhez, J. S. P., Johannessen, T., Keeling, R., Kitidis, V., Körtzinger, A., Kozyr, A., Krasakopoulou,  
2103 E., Kuwata, A., Landschützer, P., Lauvset, S. K., Lefèvre, N., Lo Monaco, C., Manke, A., Mathis, J. T., Merlivat, L.,  
2104 Millero, F. J., Monteiro, P. M. S., Munro, D. R., Murata, A., Newberger, T., Omar, A. M., Ono, T., Paterson, K., Pearce, D.,  
2105 Pierrot, D., Robbins, L. L., Saito, S., Salisbury, J., Schlitzer, R., Schneider, B., Schweitzer, R., Sieger, R., Skjelvan, I.,  
2106 Sullivan, K. F., Sutherland, S. C., Sutton, A. J., Tadokoro, K., Telszewski, M., Tuma, M., van Heuven, S. M. A. C.,  
2107 Vandemark, D., Ward, B., Watson, A. J., and Xu, S.: A multi-decade record of high-quality CO<sub>2</sub> data in version 3 of the  
2108 Surface Ocean CO<sub>2</sub> Atlas (SOCAT), *Earth Syst. Sci. Data*, 8, 383–413, <https://doi.org/10.5194/essd-8-383-2016>, 2016.

2109 Bakker, Dorothee C. E.; Alin, Simone R.; Bates, Nicholas; Becker, Meike; Gkritzalis, Thanos; Jones, Steve D.; Kozyr, Alex;  
2110 Lauvset, Siv K.; Metzl, Nicolas; Nakaoka, Shin-ichiro; O'Brien, Kevin M.; Olsen, Are; Pierrot, Denis; Steinhoff, Tobias;  
2111 Sutton, Adrienne J.; Takao, Shintaro; Tilbrook, Bronte; Wada, Chisato; Wanninkhof, Rik; Akl, John; Arbilla, Lisandro A.;  
2112 Arruda, Ricardo; Azetsu-Scott, Kumiko; Barbero, Leticia; Beatty, Cory M.; Berghoff, Carla F.; Bittig, Henry C.; Burger,  
2113 Eugene F.; Campbell, Katie; Cardin, Vanessa; Collins, Andrew; Coppola, Laurent; Cronin, Margot; Cross, Jessica N.;  
2114 Currie, Kim I.; Emerson, Steven R.; Enright, Matt P.; Enyo, Kazutaka; Evans, Wiley; Feely, Richard A.; Flohr, Anita;  
2115 Gehrung, Martina; Glockzin, Michael; González-Dávila, Melchor; Hamna, Siyabulela; Hartman, Sue; Howden, Stephan D.;  
2116 Kam, Kitty; Kamb, Linus; Körtzinger, Arne; Kosugi, Naohiro; Lefèvre, Nathalie; Lo Monaco, Claire; Macovei, Vlad A.;  
2117 Maenner Jones, Stacy; Manalang, Dana; Martz, Todd R.; Mdokwana, Baxolele; Monacci, Natalie M.; Monteiro, Pedro M.  
2118 S.; Mordy, Calvin; Morell, Julio M.; Murata, Akihiko; Neill, Craig; Noh, Jae-Hoon; Nojiri, Yukihiko; Ohman, Mark; Olivier,  
2119 Léa; Ono, Tsuneo; Petersen, Wilhelm; Plueddemann, Albert J.; Prytherch, John; Rehder, Gregor; Rutgersson, Anna;  
2120 Santana-Casiano, J. Magdalena; Schlitzer, Reiner; Send, Uwe; Skjelvan, Ingunn; Sullivan, Kevin F.; T'Jampens, Michiel;  
2121 Tadokoro, Kazuaki; Telszewski, Maciej; Theetaert, Hannelore; Tsanwani, Mutshutshu; Vandemark, Douglas; van Ooijen,  
2122 Erik; Vecchia, Martín H.; Voynova, Yoana G.; Wang, Hongjie; Weller, Robert A.; Woosley, Ryan J.: Surface Ocean CO<sub>2</sub>  
2123 Atlas Database Version 2024 (SOCATv2024) (NCEI Accession 0293257). NOAA National Centers for Environmental  
2124 Information, <https://doi.org/10.25921/9wpm-th28>, last access: 21 January 2025, 2024.

2125 Ballantyne, A. P., Alden, C. B., Miller, J. B., Tans, P. P., and White, J. W. C.: Increase in observed net carbon dioxide  
2126 uptake by land and oceans during the past 50 years, *Nature*, 488, 70–72, <https://doi.org/10.1038/nature11299>, 2012.

2127 Ballantyne, A. P., Andres, R., Houghton, R., Stocker, B. D., Wanninkhof, R., Anderegg, W., Cooper, L. A., DeGrandpre,  
2128 M., Tans, P. P., Miller, J. B., Alden, C., and White, J. W. C.: Audit of the global carbon budget: estimate errors and their  
2129 impact on uptake uncertainty, *Biogeosciences*, 12, 2565–2584, <https://doi.org/10.5194/bg-12-2565-2015>, 2015.

2130 Bastos, A., Hartung, K., Nützel, T. B., Nabel, J. E. M. S., Houghton, R. A., and Pongratz, J.: Comparison of uncertainties in  
2131 land-use change fluxes from bookkeeping model parameterisation, *12*, 745–762, <https://doi.org/10.5194/esd-12-745-2021>,  
2132 2021.

2133 Battle, M. O., Raynor, R., Kesler, S., and Keeling, R.: Technical Note: The impact of industrial activity on the amount of  
2134 atmospheric O<sub>2</sub>, *Atmospheric Chem. Phys. Discuss.*, 1–17, <https://doi.org/10.5194/acp-2022-765>, 2023.  
2135

2136 Bellenger, H., Bopp, L., Ethé, C., Ho, D., Duvel, J. P., Flavoni, S., Guez, L., Kataoka, T., Perrot, X., Parc, L., and Watanabe,  
2137 M.: Sensitivity of the Global Ocean Carbon Sink to the Ocean Skin in a Climate Model, *J. Geophys. Res. Oceans*, *128*,  
2138 e2022JC019479, <https://doi.org/10.1029/2022JC019479>, 2023.  
2139

2140 Bennington, V., Gloege, L., and McKinley, G. A.: Variability in the Global Ocean Carbon Sink From 1959 to 2020 by  
2141 Correcting Models with Observations, *Geophys. Res. Lett.*, *49*, e2022GL098632, <https://doi.org/10.1029/2022GL098632>,  
2142 2022.

2143 Bernardello, R., Sicardi, V., Lapin, V., Ortega, P., Ruprich-Robert, Y., Tourigny, E. and Ferrer, E.: Ocean biogeochemical  
2144 reconstructions to estimate historical ocean CO<sub>2</sub> uptake. *Earth System Dynamics*, *15*(5), pp.1255-1275,  
2145 <https://doi.org/10.5194/esd-15-1255-2024>, 2024.

2146 Berthet, S., Séférian, R., Bricaud, C., Chevallier, M., Voldoire, A., and Ethé, C.: Evaluation of an Online Grid-Coarsening  
2147 Algorithm in a Global Eddy-Admitting Ocean Biogeochemical Model, *J. Adv. Model Earth Sy.*, *11*, 1759–1783,  
2148 <https://doi.org/10.1029/2019MS001644>, 2019.

2149 Betts, R. A., Jones, C. D., Knight, J. R., Keeling, R. F., and Kennedy, J. J.: El Niño and a record CO<sub>2</sub> rise, *Nat. Clim.*  
2150 *Change*, *6*, 806–810, <https://doi.org/10.1038/nclimate3063>, 2016.

2151 Bilbao, R., Wild, S., Ortega, P., Acosta-Navarro, J., Arsouze, T., Bretonnière, P.A., Caron, L.P., Castrillo, M., Cruz-García,  
2152 R., Cvijanovic, I. and Doblas-Reyes, F.J.: Assessment of a full-field initialised decadal climate prediction system with the  
2153 CMIP6 version of EC-Earth. *Earth System Dynamics Discussions*, 2020, pp.1-30, <https://doi.org/10.5194/esd-12-173-2021>,  
2154 2020.

2155 Bloom, A. A. and Williams, M.: Constraining ecosystem carbon dynamics in a data-limited world: integrating ecological  
2156 “common sense” in a model–data fusion framework, *Biogeosciences*, *12*, 1299–1315, [https://doi.org/10.5194/bg-12-1299-](https://doi.org/10.5194/bg-12-1299-2015)  
2157 2015, 2015.  
2158

2159 Bloom, A. A., Exbrayat, J.-F., van der Velde, I. R., Feng, L., and Williams, M.: The decadal state of the terrestrial carbon  
2160 cycle: Global retrievals of terrestrial carbon allocation, pools, and residence times, *Proc. Natl. Acad. Sci.*, *113*, 1285–1290,  
2161 <https://doi.org/10.1073/pnas.1515160113>, 2016.  
2162

2163 Boer, G. J., Smith, D. M., Cassou, C., Doblas-Reyes, F., Danabasoglu, G., Kirtman, B., Kushnir, Y., Kimoto, M., Meehl, G.  
2164 A., Msadek, R., Mueller, W. A., Taylor, K. E., Zwiers, F., Rixen, M., Ruprich-Robert, Y., and Eade, R.: The Decadal  
2165 Climate Prediction Project (DCPP) contribution to CMIP6, *Geosci. Model Dev.*, *9*, 3751–3777, [https://doi.org/10.5194/gmd-](https://doi.org/10.5194/gmd-9-3751-2016)  
2166 9-3751-2016, 2016.  
2167

- 2168 Boucher, O., Servonnat, J., Albright, A. L., Aumont, O., Balkanski, Y., Bastrikov, V., Bekki, S., Bonnet, R., Bony, S., Bopp,  
2169 L., Braconnot, P., Brockmann, P., Cadule, P., Caubel, A., Cheruy, F., Codron, F., Cozic, A., Cugnet, D., D'Andrea, F.,  
2170 Davini, P., de Lavergne, C., Denvil, S., Deshayes, J., Devilliers, M., Ducharne, A., Dufresne, J.-L., Dupont, E., Éthé, C.,  
2171 Fairhead, L., Falletti, L., Flavoni, S., Foujols, M.-A., Gardoll, S., Gastineau, G., Ghattas, J., Grandpeix, J.-Y., Guenet, B.,  
2172 Guez, E., Lionel, Guilyardi, E., Guimberteau, M., Hauglustaine, D., Hourdin, F., Idelkadi, A., Joussaume, S., Kageyama, M.,  
2173 Khodri, M., Krinner, G., Lebas, N., Levvasseur, G., Lévy, C., Li, L., Lott, F., Lurton, T., Luysaert, S., Madec, G.,  
2174 Madeleine, J.-B., Maignan, F., Marchand, M., Marti, O., Mellul, L., Meurdesoif, Y., Mignot, J., Musat, I., Ottlé, C., Peylin,  
2175 P., Planton, Y., Polcher, J., Rio, C., Rochetin, N., Rousset, C., Sepulchre, P., Sima, A., Swingedouw, D., Thiéblemont, R.,  
2176 Traore, A. K., Vancoppenolle, M., Vial, J., Vialard, J., Viovy, N., and Vuichard, N.: Presentation and Evaluation of the  
2177 IPSL-CM6A-LR Climate Model, *J. Adv. Model. Earth Syst.*, 12, e2019MS002010, <https://doi.org/10.1029/2019MS002010>,  
2178 2020.
- 2179 Bourgeois, T., Goris, N., Schwinger, J., and Tjiputra, J. F.: Stratification constrains future heat and carbon uptake in the  
2180 Southern Ocean between 30°S and 55°S, *Nat. Commun.*, 13, 340, <https://doi.org/10.1038/s41467-022-27979-5>, 2022.
- 2181 Bray, E.: 2017 Minerals Yearbook: Aluminum [Advance Release], Tech. rep., U.S. Geological Survey, [https://d9-wret.s3-us-](https://d9-wret.s3-us-west-2.amazonaws.com/assets/palladium/production/atoms/files/myb1-2017-alumi.pdf)  
2182 [west-2.amazonaws.com/assets/palladium/production/atoms/files/myb1-2017-alumi.pdf](https://d9-wret.s3-us-west-2.amazonaws.com/assets/palladium/production/atoms/files/myb1-2017-alumi.pdf), 2020.
- 2183 Brienens, R. J. W., Caldwell, L., Duchesne, L., Voelker, S., Barichivich, J., Baliva, M., Ceccantini, G., Di Filippo, A.,  
2184 Helama, S., Locosselli, G. M., Lopez, L., Piovesan, G., Schöngart, J., Villalba, R., and Gloor, E.: Forest carbon sink  
2185 neutralized by pervasive growth-lifespan trade-offs, *Nat. Commun.*, 11, 4241, <https://doi.org/10.1038/s41467-020-17966-z>,  
2186 2020.
- 2187 Brienens, R. J. W., Phillips, O. L., Feldpausch, T. R., Gloor, E., Baker, T. R., Lloyd, J., Lopez-Gonzalez, G., Monteagudo-  
2188 Mendoza, A., Malhi, Y., Lewis, S. L., Vásquez Martínez, R., Alexiades, M., Álvarez Dávila, E., Alvarez-Loayza, P.,  
2189 Andrade, A., Aragão, L. E. O. C., Araujo-Murakami, A., Arets, E. J. M. M., Arroyo, L., Aymard C., G. A., Bánki, O. S.,  
2190 Baraloto, C., Barroso, J., Bonal, D., Boot, R. G. A., Camargo, J. L. C., Castilho, C. V., Chama, V., Chao, K. J., Chave, J.,  
2191 Comiskey, J. A., Cornejo Valverde, F., da Costa, L., de Oliveira, E. A., Di Fiore, A., Erwin, T. L., Fauset, S., Forsthofer, M.,  
2192 Galbraith, D. R., Grahame, E. S., Groot, N., Hérault, B., Higuchi, N., Honorio Coronado, E. N., Keeling, H., Killeen, T. J.,  
2193 Laurance, W. F., Laurance, S., Licona, J., Magnussen, W. E., Marimon, B. S., Marimon-Junior, B. H., Mendoza, C., Neill,  
2194 D. A., Nogueira, E. M., Núñez, P., Pallqui Camacho, N. C., Parada, A., Pardo-Molina, G., Peacock, J., Peña-Claros, M.,  
2195 Pickavance, G. C., Pitman, N. C. A., Poorter, L., Prieto, A., Quesada, C. A., Ramírez, F., Ramírez-Angulo, H., Restrepo, Z.,  
2196 Roopsind, A., Rudas, A., Salomão, R. P., Schwarz, M., Silva, N., Silva-Espejo, J. E., Silveira, M., Stropp, J., Talbot, J., ter  
2197 Steege, H., Teran-Aguilar, J., Terborgh, J., Thomas-Caesar, R., Toledo, M., Torello-Raventos, M., Umetsu, R. K., van der  
2198 Heijden, G. M. F., van der Hout, P., Guimarães Vieira, I. C., Vieira, S. A., Vilanova, E., Vos, V. A., and Zagt, R. J.: Long-  
2199 term decline of the Amazon carbon sink, 519, 344–348, <https://doi.org/10.1038/nature14283>, 2015.
- 2200 Bronselaer, B., Winton, M., Russell, J., Sabine, C. L., and Khatiwala, S.: Agreement of CMIP5 Simulated and Observed  
2201 Ocean Anthropogenic CO<sub>2</sub> Uptake, *Geophys. Res. Lett.*, 44, 12,298-12,305, <https://doi.org/10.1002/2017GL074435>, 2017.
- 2202 Bruno, M. and Joos, F.: Terrestrial carbon storage during the past 200 years: A Monte Carlo Analysis of CO<sub>2</sub> data from ice  
2203 core and atmospheric measurements, *Global Biogeochem. Cycles*, 11, 111–124, <https://doi.org/10.1029/96GB03611>, 1997.
- 2204 Burrows, S. M., Maltrud, M., Yang, X., Zhu, Q., Jeffery, N., Shi, X., Ricciuto, D., Wang, S., Bisht, G., Tang, J., Wolfe, J.,  
2205 Harrop, B. E., Singh, B., Brent, L., Baldwin, S., Zhou, T., Cameron-Smith, P., Keen, N., Collier, N., Xu, M., Hunke, E. C.,

- 2206 Elliott, S. M., Turner, A. K., Li, H., Wang, H., Golaz, J.-C., Bond-Lamberty, B., Hoffman, F. M., Riley, W. J., Thornton, P.  
2207 E., Calvin, K., and Leung, L. R.: The DOE E3SM v1.1 Biogeochemistry Configuration: Description and Simulated  
2208 Ecosystem-Climate Responses to Historical Changes in Forcing, *J. Adv. Model. Earth Syst.*, 12, e2019MS001766,  
2209 <https://doi.org/10.1029/2019MS001766>, 2020.
- 2210 Bunsen, F., Nissen, C., and Hauck, J.: The Impact of Recent Climate Change on the Global Ocean Carbon Sink. *Geophysical*  
2211 *Research Letters*, 51(4), e2023GL107030, <https://doi.org/10.1029/2023GL107030>, 2024.
- 2212 Burton, C., Betts, R., Cardoso, M., Feldpausch, T. R., Harper, A., Jones, C. D., Kelley, D. I., Robertson, E., and Wiltshire,  
2213 A.: Representation of fire, land-use change and vegetation dynamics in the Joint UK Land Environment Simulator vn4.9  
2214 (JULES), *Geosci. Model Dev.*, 12, 179–193, <https://doi.org/10.5194/gmd-12-179-2019>, 2019.
- 2215 Burton, C., Lampe, S., Kelley, D. I., Thiery, W., Hantson, S., Christidis, N., Gudmundsson, L., Forrest, M., Burke, E.,  
2216 Chang, J., Huang, H., Ito, A., Kou-Giesbrecht, S., Lasslop, G., Li, W., Nieradzki, L., Li, F., Chen, Y., Randerson, J., Reyer,  
2217 C. P. O., and Mengel, M.: Global burned area increasingly explained by climate change, *Nature Climate Change*,  
2218 <https://doi.org/10.1038/s41558-024-02140-w>, 2024.
- 2219 Bushinsky, S. M., Landschützer, P., Rödenbeck, C., Gray, A. R., Baker, D., Mazloff, M. R., Resplandy, L., Johnson, K. S.,  
2220 and Sarmiento, J. L.: Reassessing Southern Ocean Air-Sea CO<sub>2</sub> Flux Estimates With the Addition of Biogeochemical Float  
2221 Observations, *Global Biogeochem. Cycles*, 33, 1370–1388, <https://doi.org/10.1029/2019GB006176>, 2019.
- 2222 Byrne, B., Liu, J., Bowman, K. W., Pascolini-Campbell, M., Chatterjee, A., Pandey, S., Miyazaki, K., van der Werf, G. R.,  
2223 Wunch, D., Wennberg, P. O., Roehl, C. M., and Sinha, S.: Carbon emissions from the 2023 Canadian wildfires. *Nature*, 633,  
2224 835–839, <https://doi.org/10.1038/s41586-024-07878-z>, 2024.
- 2225 Canadell, J. G., Le Quere, C., Raupach, M. R., Field, C. B., Buitenhuis, E. T., Ciais, P., Conway, T. J., Gillett, N. P.,  
2226 Houghton, R. A., and Marland, G.: Contributions to accelerating atmospheric CO<sub>2</sub> growth from economic activity, carbon  
2227 intensity, and efficiency of natural sinks, *Proceedings of the National Academy of Sciences*, 104, 18866–18870,  
2228 <https://doi.org/10.1073/pnas.0702737104>, 2007.
- 2229 Canadell, J. G., Monteiro, P. M. S., Costa, M. H., Cotrim da Cunha, L., Cox, P. M., Eliseev, A. V., Henson, S., Ishii, M.,  
2230 Jaccard, S., Koven, C., Lohila, A., Patra, P. K., Piao, S., Rogelj, J., Syampungani, S., Zaehle, S., and Zickfeld, K.: Global  
2231 Carbon and other Biogeochemical Cycles and Feedbacks. In: *Climate Change 2021: The Physical Science Basis.*  
2232 *Contribution of Working Group I to the Sixth Assessment Report of the Intergovernmental Panel on Climate Change*  
2233 [Masson-Delmotte, V., P. Zhai, A. Pirani, S. L. Connors, C. Péan, S. Berger, N. Caud, Y. Chen, L. Goldfarb, M. I. Gomis,  
2234 M. Huang, K. Leitzell, E. Lonnoy, J. B. R. Matthews, T. K. Maycock, T. Waterfield, O. Yelekçi, R. Yu and B. Zhou (eds.)].  
2235 Cambridge University Press, Cambridge, United Kingdom and New York, NY, USA, pp. 673–816,  
2236 <https://doi.org/10.1017/9781009157896.007>, 2021.
- 2237 Cao, Z., Myers, R. J., Lupton, R. C., Duan, H., Sacchi, R., Zhou, N., Reed Miller, T., Cullen, J. M., Ge, Q., and Liu, G.: The  
2238 sponge effect and carbon emission mitigation potentials of the global cement cycle, *Nat Commun*, 11, 3777,  
2239 <https://doi.org/10.1038/s41467-020-17583-w>, 2020.
- 2240 Centro Nacional de Monitoramento e Alertas de Desastres Naturais (CEMADEN): Monitoramento de secas e impactos no  
2241 Brasil - Agosto 2024, available at: [https://www.gov.br/cemaden/pt-br/assuntos/monitoramento/monitoramento-de-seca-para-](https://www.gov.br/cemaden/pt-br/assuntos/monitoramento/monitoramento-de-seca-para-o-brasil/monitoramento-de-secas-e-impactos-no-brasil-agosto-2024)  
2242 [o-brasil/monitoramento-de-secas-e-impactos-no-brasil-agosto-2024](https://www.gov.br/cemaden/pt-br/assuntos/monitoramento/monitoramento-de-seca-para-o-brasil/monitoramento-de-secas-e-impactos-no-brasil-agosto-2024), last access: 21 January 2025.

- 2243 Céspedes, J., Sylvester, J. M., Pérez-Marulanda, L., Paz-García, P., Reymondin, L., Khodadadi, M., Tello, J. J., and Castro-  
 2244 Nunez, A.: Has global deforestation accelerated due to the COVID-19 pandemic?, *J. For. Res.*, 34, 1153–1165,  
 2245 <https://doi.org/10.1007/s11676-022-01561-7>, 2023.
- 2246 Chandra, N., Patra, P. K., Niwa, Y., Ito, A., Iida, Y., Goto, D., Morimoto, S., Kondo, M., Takigawa, M., Hajima, T., and  
 2247 Watanabe, M.: Estimated regional CO<sub>2</sub> flux and uncertainty based on an ensemble of atmospheric CO<sub>2</sub> inversions,  
 2248 *Atmospheric Chem. Phys.*, 22, 9215–9243, <https://doi.org/10.5194/acp-22-9215-2022>, 2022.
- 2249 Chatfield, C.: The Holt-Winters Forecasting Procedure, *J. Roy. Stat. Soc. C.*, 27, 264–279, <https://doi.org/10.2307/2347162>,  
 2250 1978.
- 2251 Chau, T. T. T., Gehlen, M., and Chevallier, F.: A seamless ensemble-based reconstruction of surface ocean *p*CO<sub>2</sub> and air–sea  
 2252 CO<sub>2</sub> fluxes over the global coastal and open oceans, *Biogeosciences*, 19, 1087–1109, [https://doi.org/10.5194/bg-19-1087-](https://doi.org/10.5194/bg-19-1087-2022)  
 2253 2022, 2022.
- 2254 Chevallier, F., Fisher, M., Peylin, P., Serrar, S., Bousquet, P., Bréon, F.-M., Chédin, A., and Ciais, P.: Inferring CO<sub>2</sub>  
 2255 sources and sinks from satellite observations: Method and application to TOVS data, *J. Geophys. Res.*, 110, D24309,  
 2256 <https://doi.org/10.1029/2005JD006390>, 2005.
- 2257 Ciais, P., Sabine, C., Bala, G., Bopp, L., Brovkin, V., Canadell, J. G., Chhabra, A., DeFries, R., Galloway, J., Heimann, M.,  
 2258 Jones, C., Le Quéré, C., Myneni, R., Piao, S., Thornton, P., Willem, J., Friedlingstein, P., and Munhoven, G.: Carbon and  
 2259 Other Biogeochemical Cycles, in *Climate Change 2013: The Physical Science Basis, Contribution of Working Group I to the*  
 2260 *Fifth Assessment Report of the Intergovernmental Panel on Climate Change*, edited by: Intergovernmental Panel on Climate  
 2261 Change, Cambridge University Press, Cambridge, United Kingdom and New York, NY, USA,  
 2262 <https://doi.org/10.1017/CBO9781107415324.015>, 2013.
- 2263 Ciais, P., Tan, J., Wang, X., Roedenbeck, C., Chevallier, F., Piao, S.-L., Moriarty, R., Broquet, G., Le Quéré, C., Canadell, J.  
 2264 G., Peng, S., Poulter, B., Liu, Z., and Tans, P.: Five decades of northern land carbon uptake revealed by the interhemispheric  
 2265 CO<sub>2</sub> gradient, *Nature*, 568, 221–225, <https://doi.org/10.1038/s41586-019-1078-6>, 2019.
- 2266 Ciais, P., Bastos, A., Chevallier, F., Lauerwald, R., Poulter, B., Canadell, P., Hugelius, G., Jackson, R. B., Jain, A., Jones,  
 2267 M., Kondo, M., Luijkx, I. T., Patra, P. K., Peters, W., Pongratz, J., Petrescu, A. M. R., Piao, S., Qiu, C., Von Randow, C.,  
 2268 Regnier, P., Saunois, M., Scholes, R., Shvidenko, A., Tian, H., Yang, H., Wang, X., and Zheng, B.: Definitions and methods  
 2269 to estimate regional land carbon fluxes for the second phase of the REgional Carbon Cycle Assessment and Processes  
 2270 Project (RECCAP-2), *Geosci. Model Dev.*, 15, 1289–1316, <https://doi.org/10.5194/gmd-15-1289-2022>, 2022.
- 2271 Collier, N., Hoffman, F. M., Lawrence, D. M., Keppel-Aleks, G., Koven, C. D., Riley, W. J., Mu, M., and Randerson, J. T.:  
 2272 The International Land Model Benchmarking (ILAMB) System: Design, Theory, and Implementation, *J. Adv. Model. Earth*  
 2273 *Syst.*, 10, 2731–2754, <https://doi.org/10.1029/2018MS001354>, 2018.
- 2274 Conchedda, G. and Tubiello, F. N.: Drainage of organic soils and GHG emissions: Validation with country data, *Biosphere –*  
 2275 *Biogeosciences*, <https://doi.org/10.5194/essd-2020-202>, 2020.
- 2276 Cox, P. M., Pearson, D., Booth, B. B., Friedlingstein, P., Huntingford, C., Jones, C. D., and Luke, C. M.: Sensitivity of  
 2277 tropical carbon to climate change constrained by carbon dioxide variability, *Nature*, 494, 341–344,  
 2278 <https://doi.org/10.1038/nature11882>, 2013.

- 2279 De Kauwe, M. G., Medlyn, B. E., Zaehle, S., Walker, A. P., Dietze, M. C., Wang, Y.-P., Luo, Y., Jain, A. K., El-Masri, B.,  
 2280 Hickler, T., Wårlind, D., Weng, E., Parton, W. J., Thornton, P. E., Wang, S., Prentice, I. C., Asao, S., Smith, B., McCarthy,  
 2281 H. R., Iversen, C. M., Hanson, P. J., Warren, J. M., Oren, R., and Norby, R. J.: Where does the carbon go? A model–data  
 2282 intercomparison of vegetation carbon allocation and turnover processes at two temperate forest free-air CO<sub>2</sub> enrichment  
 2283 sites, *New Phytol.*, 203, 883–899, <https://doi.org/10.1111/nph.12847>, 2014.
- 2284 Delire, C., Séférian, R., Decharme, B., Alkama, R., Calvet, J.-C., Carrer, D., Gibelin, A.-L., Joetzjer, E., Morel, X., Rocher,  
 2285 M., and Tzanos, D.: The Global Land Carbon Cycle Simulated With ISBA-CTRIP: Improvements Over the Last Decade, *J.*  
 2286 *Adv. Model. Earth Syst.*, 12, e2019MS001886, <https://doi.org/10.1029/2019MS001886>, 2020.
- 2287 Denman, K. L., Brasseur, G., Chidthaisong, A., Ciais, P., Cox, P. M., Dickinson, R. E., Hauglustaine, D., Heinze, C.,  
 2288 Holland, E., Jacob, D., Lohmann, U., Ramachandran, S., Leite da Silva Dias, P., Wofsy, S. C., and Zhang, X.: Couplings  
 2289 Between Changes in the Climate System and Biogeochemistry, in: *Climate Change 2007: The Physical Science Basis.*  
 2290 *Contribution of Working Group I to the Fourth Assessment Report of the Intergovernmental Panel on Climate Change,*  
 2291 edited by: Solomon, S., Qin, D., Manning, M., Marquis, M., Averyt, K., Tignor, M. M. B., Miller, H. L., and Chen, Z. L.,  
 2292 Cambridge University Press, Cambridge, UK and New York, USA, 499–587, ISBN: 9780521705967, 2007.
- 2293 Denvil-Sommer, A., Gehlen, M., and Vrac, M.: Observation system simulation experiments in the Atlantic Ocean for  
 2294 enhanced surface ocean pCO<sub>2</sub> reconstructions, *Ocean Sci.*, 17, 1011–1030, <https://doi.org/10.5194/os-17-1011-2021>, 2021.
- 2295 DeVries, T., Holzer, M., and Primeau, F.: Recent increase in oceanic carbon uptake driven by weaker upper-ocean  
 2296 overturning, *Nature*, 542, 215–218, <https://doi.org/10.1038/nature21068>, 2017.
- 2297 DeVries, T., Quéré, C. L., Andrews, O., Berthet, S., Hauck, J., Ilyina, T., Landschützer, P., Lenton, A., Lima, I. D., Nowicki,  
 2298 M., Schwinger, J., and Séférian, R.: Decadal trends in the ocean carbon sink, *PNAS*, 116, 11646–11651,  
 2299 <https://doi.org/10.1073/pnas.1900371116>, 2019.
- 2300 DeVries, T., Yamamoto, K., Wanninkhof, R., Gruber, N., Hauck, J., Müller, J. D., Bopp, L., Carroll, D., Carter, B., Chau,  
 2301 T.-T.-T., Doney, S. C., Gehlen, M., Gloege, L., Gregor, L., Henson, S., Kim, J. H., Iida, Y., Ilyina, T., Landschützer, P., Le  
 2302 Quéré, C., Munro, D., Nissen, C., Patara, L., Pérez, F. F., Resplandy, L., Rodgers, K. B., Schwinger, J., Séférian, R., Sicardi,  
 2303 V., Terhaar, J., Triñanes, J., Tsujino, H., Watson, A., Yasunaka, S., and Zeng, J.: Magnitude, trends, and variability of the  
 2304 global ocean carbon sink from 1985–2018, *Glob. Biogeochem. Cycles*, n/a, e2023GB007780,  
 2305 <https://doi.org/10.1029/2023GB007780>, 2023.
- 2306  
 2307 Döscher, R., Acosta, M., Alessandri, A., Anthoni, P., Arneeth, A., Arsouze, T., Bergmann, T., Bernadello, R., Bousetta, S.,  
 2308 Caron, L.P. and Carver, G.: The EC-earth3 Earth system model for the climate model intercomparison project 6.  
 2309 *Geoscientific Model Development Discussions*, 2021, pp.1-90, <https://doi.org/10.5194/gmd-15-2973-2022>, 2021.
- 2310  
 2311 Forster, P. M., Smith, C., Walsh, T., Lamb, W. F., Lamboll, R., Hall, B., Hauser, M., Ribes, A., Rosen, D., Gillett, N. P.,  
 2312 Palmer, M. D., Rogelj, J., von Schuckmann, K., Trewin, B., Allen, M., Andrew, R., Betts, R. A., Borger, A., Boyer, T.,  
 2313 Broersma, J. A., Buontempo, C., Burgess, S., Cagnazzo, C., Cheng, L., Friedlingstein, P., Gettelman, A., Gütschow, J., Ishii,  
 2314 M., Jenkins, S., Lan, X., Morice, C., Mühle, J., Kadow, C., Kennedy, J., Killick, R. E., Krummel, P. B., Minx, J. C., Myhre,  
 2315 G., Naik, V., Peters, G. P., Pirani, A., Pongratz, J., Schleussner, C.-F., Seneviratne, S. I., Szopa, S., Thorne, P., Kovilakam,  
 2316 M. V. M., Majamäki, E., Jalkanen, J.-P., van Marle, M., Hoesly, R. M., Rohde, R., Schumacher, D., van der Werf, G., Vose,  
 2317 R., Zickfeld, K., Zhang, X., Masson-Delmotte, V., and Zhai, P.: *Indicators of Global Climate Change 2023: annual update of*

- 2318 key indicators of the state of the climate system and human influence, *Earth Syst. Sci. Data*, 16, 2625–2658,  
2319 <https://doi.org/10.5194/essd-16-2625-2024>, 2024.
- 2320 Doney, S. C., Lima, I., Feely, R. A., Glover, D. M., Lindsay, K., Mahowald, N., Moore, J. K., and Wanninkhof, R.:  
2321 Mechanisms governing interannual variability in upper-ocean inorganic carbon system and air–sea CO<sub>2</sub> fluxes: Physical  
2322 climate and atmospheric dust, *Deep Sea Research Part II: Topical Studies in Oceanography*, 56, 640–655,  
2323 <https://doi.org/10.1016/j.dsr2.2008.12.006>, 2009.
- 2324 Dong, Y., Bakker, D. C. E., Bell, T. G., Huang, B., Landschützer, P., Liss, P. S., and Yang, M.: Update on the Temperature  
2325 Corrections of Global Air–Sea CO<sub>2</sub> Flux Estimates, *Glob. Biogeochem. Cycles*, 36, e2022GB007360,  
2326 <https://doi.org/10.1029/2022GB007360>, 2022.  
2327
- 2328 Dong, Y., Bakker, D. C. E., Bell, T. G., Yang, M., Landschützer, P., Hauck, J., Rödenbeck, C., Kitidis, V., Bushinsky, S. M.,  
2329 and Liss, P. S. (2024). Direct observational evidence of strong CO<sub>2</sub> uptake in the Southern Ocean. *Science Advances*,  
2330 10(30), eadn5781, <https://doi.org/10.1126/sciadv.adn5781>, 2024a.  
2331
- 2332 Dong, Y., Bakker, D. C. E., and Landschützer, P.: Accuracy of ocean CO<sub>2</sub> uptake estimates at a risk by a reduction in the  
2333 data collection. *Geophysical Research Letters*, 51, e2024GL108502, <https://doi.org/10.1029/2024GL108502>, 2024b.  
2334
- 2335 Dorgeist, L., Schwingshackl, C., Bultan, S., and Pongratz, J.: A consistent budgeting of terrestrial carbon fluxes. *Nature*  
2336 *Communications*, 15(1), 7426, <https://doi.org/10.1038/s41467-024-51126-x>, 2024.  
2337
- 2338 Dou, X., Wang, Y., Ciais, P., Chevallier, F., Davis, S. J., Crippa, M., Janssens-Maenhout, G., Guizzardi, D., Solazzo, E.,  
2339 Yan, F., Huo, D., Zheng, B., Zhu, B., Cui, D., Ke, P., Sun, T., Wang, H., Zhang, Q., Gentine, P., Deng, Z., and Liu, Z.: Near-  
2340 real-time global gridded daily CO<sub>2</sub> emissions, *The Innovation*, 3, 100182, <https://doi.org/10.1016/j.xinn.2021.100182>, 2022.
- 2341 Edson, J. B., Jampana, V., Weller, R. A., Bigorre, S. P., Plueddemann, A. J., Fairall, C. W., Miller, S. D., Mahrt, L., Vickers,  
2342 D., and Hersbach, H.: On the Exchange of Momentum over the Open Ocean, *J. Phys. Oceanogr.*, 43, 1589–1610,  
2343 <https://doi.org/10.1175/JPO-D-12-0173.1>, 2013.
- 2344 EIA. Short-Term Energy Outlook: September 2023. U.S. Energy Information Administration [dataset]. Available at:  
2345 <http://www.eia.gov/forecasts/steo/outlook.cfm>, last access: 21 January 2025, 2023.
- 2346 Embury, O., Merchant, C.J., Good, S.A., Rayner, N.A., Hoyer, J.L., Atkinson, C., Block, T., Alerskans, E., Pearson, K.J.,  
2347 Worsfold, M. and McCarroll, N. and Donlon, C.: Satellite-based time-series of sea-surface temperature since 1980 for  
2348 climate applications. *Scientific Data*, 11(1), 326, <https://doi.org/10.1038/s41597-024-03147-w>, 2024.
- 2349 Erb, K.-H., Kastner, T., Luyssaert, S., Houghton, R. A., Kuemmerle, T., Olofsson, P., and Haberl, H.: Bias in the attribution  
2350 of forest carbon sinks, *Nature Clim Change*, 3, 854–856, <https://doi.org/10.1038/nclimate2004>, 2013.
- 2351 Erb, K.-H., Kastner, T., Plutzer, C., Bais, A. L. S., Carvalhais, N., Fetzl, T., Gingrich, S., Haberl, H., Lauk, C.,  
2352 Niedertscheider, M., Pongratz, J., Thurner, M., and Luyssaert, S.: Unexpectedly large impact of forest management and  
2353 grazing on global vegetation biomass, *Nature*, 553, 73–76, <https://doi.org/10.1038/nature25138>, 2018.

- 2354 Eskander, S. M. S. U. and Fankhauser, S.: Reduction in greenhouse gas emissions from national climate legislation, *Nat.*  
2355 *Clim. Chang.*, 10, 750–756, <https://doi.org/10.1038/s41558-020-0831-z>, 2020.
- 2356 Etheridge, D. M., Steele, L. P., Langenfelds, R. L., Francey, R. J., Barnola, J.-M., and Morgan, V. I.: Natural and  
2357 anthropogenic changes in atmospheric CO<sub>2</sub> over the last 1000 years from air in Antarctic ice and firn, *J. Geophys. Res.*,  
2358 101, 4115–4128, <https://doi.org/10.1029/95JD03410>, 1996.
- 2359 Eyring, V., Bony, S., Meehl, G. A., Senior, C. A., Stevens, B., Stouffer, R. J., and Taylor, K. E.: Overview of the Coupled  
2360 Model Intercomparison Project Phase 6 (CMIP6) experimental design and organization, *Geosci. Model Dev.*, 9, 1937–1958,  
2361 <https://doi.org/10.5194/gmd-9-1937-2016>, 2016.
- 2362 FAO, Food and Agriculture Organization of the United Nations (FAO): Impact of the Ukraine-Russia conflict on global food  
2363 security and related matters under the mandate of the Food and Agriculture Organization of the United Nations (FAO),  
2364 Hundred and Seventieth Session of the Council, <https://www.fao.org/3/nj164en/nj164en.pdf>, last access: 21 January 2025,  
2365 2023.
- 2366 FAO: FAOSTAT Climate Change: Agrifood systems emissions, Emissions from Drained, available at  
2367 <http://www.fao.org/faostat/en/#data/GV>, last access: 12 January 2025, 2023.
- 2368 Fay, A. R., Gregor, L., Landschützer, P., McKinley, G. A., Gruber, N., Gehlen, M., Iida, Y., Laruelle, G. G., Rödenbeck, C.,  
2369 Roobaert, A., and Zeng, J.: SeaFlux: harmonization of air–sea CO<sub>2</sub> fluxes from surface pCO<sub>2</sub> data products using a  
2370 standardized approach, *Earth System Science Data*, 13, 4693–4710, <https://doi.org/10.5194/essd-13-4693-2021>, 2021.
- 2371 Feng, L., Palmer, P. I., Bösch, H., and Dance, S.: Estimating surface CO<sub>2</sub> fluxes from space-borne CO<sub>2</sub> dry air mole fraction  
2372 observations using an ensemble Kalman Filter, *Atmospheric Chem. Phys.*, 9, 2619–2633, [https://doi.org/10.5194/acp-9-](https://doi.org/10.5194/acp-9-2619-2009)  
2373 2619-2009, 2009.
- 2374 Feng, L., Palmer, P. I., Parker, R. J., Deutscher, N. M., Feist, D. G., Kivi, R., Morino, I., and Sussmann, R.: Estimates of  
2375 European uptake of CO<sub>2</sub> inferred from GOSAT XCO<sub>2</sub> retrievals: sensitivity to measurement bias inside and outside Europe,  
2376 *Atmos. Chem. Phys.*, 16, 1289–1302, <https://doi.org/10.5194/acp-16-1289-2016>, 2016.
- 2377 Flanagan, D.: 2017 Minerals Yearbook: Copper [Advance Release], Tech. rep., U.S. Geological Survey,  
2378 <https://pubs.usgs.gov/myb/vol1/2017/myb1-2017-copper.pdf>, 2021.
- 2379 Ford, D., Blannin, J., Watts, J., Watson, A., Landschützer, P., Jersild, A. and Shutler, J.: A comprehensive analysis of air-sea  
2380 CO<sub>2</sub> flux uncertainties constructed from surface ocean data products, *Global Biogeochemical Cycles*, accepted, 2024.
- 2381 Friedlingstein, P., Houghton, R. A., Marland, G., Hackler, J., Boden, T. A., Conway, T. J., Canadell, J. G., Raupach, M. R.,  
2382 Ciais, P., and Le Quéré, C.: Update on CO<sub>2</sub> emissions, *Nature Geosci.*, 3, 811–812, <https://doi.org/10.1038/ngeo1022>, 2010.
- 2383 Friedlingstein, P., Andrew, R. M., Rogelj, J., Peters, G. P., Canadell, J. G., Knutti, R., Luderer, G., Raupach, M. R.,  
2384 Schaeffer, M., van Vuuren, D. P., and Le Quéré, C.: Persistent growth of CO<sub>2</sub> emissions and implications for reaching  
2385 climate targets, *Nature Geosci.*, 7, 709–715, <https://doi.org/10.1038/ngeo2248>, 2014.
- 2386 Friedlingstein, P., Jones, M. W., O’Sullivan, M., Andrew, R. M., Hauck, J., Peters, G. P., Peters, W., Pongratz, J., Sitch, S.,  
2387 Le Quéré, C., Bakker, D. C. E., Canadell, J. G., Ciais, P., Jackson, R. B., Anthoni, P., Barbero, L., Bastos, A., Bastrikov, V.,  
2388 Becker, M., Bopp, L., Buitenhuis, E., Chandra, N., Chevallier, F., Chini, L. P., Currie, K. I., Feely, R. A., Gehlen, M.,



2389 Gilfillan, D., Gkritzalis, T., Goll, D. S., Gruber, N., Gutekunst, S., Harris, I., Haverd, V., Houghton, R. A., Hurtt, G., Ilyina,  
2390 T., Jain, A. K., Joetzjer, E., Kaplan, J. O., Kato, E., Klein Goldewijk, K., Korsbakken, J. I., Landschützer, P., Lauvset, S. K.,  
2391 Lefèvre, N., Lenton, A., Lienert, S., Lombardozi, D., Marland, G., McGuire, P. C., Melton, J. R., Metzl, N., Munro, D. R.,  
2392 Nabel, J. E. M. S., Nakaoka, S.-I., Neill, C., Omar, A. M., Ono, T., Peregon, A., Pierrot, D., Poulter, B., Rehder, G.,  
2393 Resplandy, L., Robertson, E., Rödenbeck, C., Séférian, R., Schwinger, J., Smith, N., Tans, P. P., Tian, H., Tilbrook, B.,  
2394 Tubiello, F. N., van der Werf, G. R., Wiltshire, A. J., and Zaehle, S.: Global Carbon Budget 2019, *Earth Syst. Sci. Data*, 11,  
2395 1783–1838, <https://doi.org/10.5194/essd-11-1783-2019>, 2019.

2396 Friedlingstein, P., O’Sullivan, M., Jones, M. W., Andrew, R. M., Hauck, J., Olsen, A., Peters, G. P., Peters, W., Pongratz, J.,  
2397 Sitch, S., Le Quéré, C., Canadell, J. G., Ciais, P., Jackson, R. B., Alin, S., Aragão, L. E. O. C., Arneeth, A., Arora, V., Bates,  
2398 N. R., Becker, M., Benoit-Cattin, A., Bittig, H. C., Bopp, L., Bultan, S., Chandra, N., Chevallier, F., Chini, L. P., Evans, W.,  
2399 Florentie, L., Forster, P. M., Gasser, T., Gehlen, M., Gilfillan, D., Gkritzalis, T., Gregor, L., Gruber, N., Harris, I., Hartung,  
2400 K., Haverd, V., Houghton, R. A., Ilyina, T., Jain, A. K., Joetzjer, E., Kadono, K., Kato, E., Kitidis, V., Korsbakken, J. I.,  
2401 Landschützer, P., Lefèvre, N., Lenton, A., Lienert, S., Liu, Z., Lombardozi, D., Marland, G., Metzl, N., Munro, D. R.,  
2402 Nabel, J. E. M. S., Nakaoka, S.-I., Niwa, Y., O’Brien, K., Ono, T., Palmer, P. I., Pierrot, D., Poulter, B., Resplandy, L.,  
2403 Robertson, E., Rödenbeck, C., Schwinger, J., Séférian, R., Skjelvan, I., Smith, A. J. P., Sutton, A. J., Tanhua, T., Tans, P. P.,  
2404 Tian, H., Tilbrook, B., van der Werf, G., Vuichard, N., Walker, A. P., Wanninkhof, R., Watson, A. J., Willis, D., Wiltshire,  
2405 A. J., Yuan, W., Yue, X., and Zaehle, S.: Global Carbon Budget 2020, *Earth Syst. Sci. Data*, 12, 3269–3340,  
2406 <https://doi.org/10.5194/essd-12-3269-2020>, 2020.

2407 Friedlingstein, P., Jones, M. W., O’Sullivan, M., Andrew, R. M., Bakker, D. C. E., Hauck, J., Le Quéré, C., Peters, G. P.,  
2408 Peters, W., Pongratz, J., Sitch, S., Canadell, J. G., Ciais, P., Jackson, R. B., Alin, S. R., Anthoni, P., Bates, N. R., Becker, M.,  
2409 Bellouin, N., Bopp, L., Chau, T. T. T., Chevallier, F., Chini, L. P., Cronin, M., Currie, K. I., Decharme, B., Djeutchouang, L.  
2410 M., Dou, X., Evans, W., Feely, R. A., Feng, L., Gasser, T., Gilfillan, D., Gkritzalis, T., Grassi, G., Gregor, L., Gruber, N.,  
2411 Gürses, Ö., Harris, I., Houghton, R. A., Hurtt, G. C., Iida, Y., Ilyina, T., Luijkx, I. T., Jain, A., Jones, S. D., Kato, E.,  
2412 Kennedy, D., Klein Goldewijk, K., Knauer, J., Korsbakken, J. I., Körtzinger, A., Landschützer, P., Lauvset, S. K., Lefèvre,  
2413 N., Lienert, S., Liu, J., Marland, G., McGuire, P. C., Melton, J. R., Munro, D. R., Nabel, J. E. M. S., Nakaoka, S.-I., Niwa,  
2414 Y., Ono, T., Pierrot, D., Poulter, B., Rehder, G., Resplandy, L., Robertson, E., Rödenbeck, C., Rosan, T. M., Schwinger, J.,  
2415 Schwingshackl, C., Séférian, R., Sutton, A. J., Sweeney, C., Tanhua, T., Tans, P. P., Tian, H., Tilbrook, B., Tubiello, F., van  
2416 der Werf, G. R., Vuichard, N., Wada, C., Wanninkhof, R., Watson, A. J., Willis, D., Wiltshire, A. J., Yuan, W., Yue, C.,  
2417 Yue, X., Zaehle, S., and Zeng, J.: Global Carbon Budget 2021, *Earth Syst. Sci. Data*, 14, 1917–2005,  
2418 <https://doi.org/10.5194/essd-14-1917-2022>, 2022a.

2419 Friedlingstein, P., O’Sullivan, M., Jones, M. W., Andrew, R. M., Gregor, L., Hauck, J., Le Quéré, C., Luijkx, I. T., Olsen, A.,  
2420 Peters, G. P., Peters, W., Pongratz, J., Schwingshackl, C., Sitch, S., Canadell, J. G., Ciais, P., Jackson, R. B., Alin, S. R.,  
2421 Alkama, R., Arneeth, A., Arora, V. K., Bates, N. R., Becker, M., Bellouin, N., Bittig, H. C., Bopp, L., Chevallier, F., Chini, L.  
2422 P., Cronin, M., Evans, W., Falk, S., Feely, R. A., Gasser, T., Gehlen, M., Gkritzalis, T., Gloege, L., Grassi, G., Gruber, N.,  
2423 Gürses, Ö., Harris, I., Hefner, M., Houghton, R. A., Hurtt, G. C., Iida, Y., Ilyina, T., Jain, A. K., Jersild, A., Kadono, K.,  
2424 Kato, E., Kennedy, D., Klein Goldewijk, K., Knauer, J., Korsbakken, J. I., Landschützer, P., Lefèvre, N., Lindsay, K., Liu,  
2425 J., Liu, Z., Marland, G., Mayot, N., McGrath, M. J., Metzl, N., Monacci, N. M., Munro, D. R., Nakaoka, S., Niwa, Y.,  
2426 O’Brien, K., Ono, T., Palmer, P. I., Pan, N., Pierrot, D., Pockock, K., Poulter, B., Resplandy, L., Robertson, E., Rödenbeck,  
2427 C., Rodriguez, C., Rosan, T. M., Schwinger, J., Séférian, R., Shutler, J. D., Skjelvan, I., Steinhoff, T., Sun, Q., Sutton, A. J.,  
2428 Sweeney, C., Takao, S., Tanhua, T., Tans, P. P., Tian, X., Tian, H., Tilbrook, B., Tsujino, H., Tubiello, F., van der Werf, G.  
2429 R., Walker, A. P., Wanninkhof, R., Whitehead, C., Willstrand Wranne, A., Wright, R., Yuan, W., Yue, C., Yue, X., Zaehle,

2430 S., Zeng, J., and Zheng, B.: Global Carbon Budget 2022, *Earth Syst. Sci. Data*, 14, 4811–4900, [https://doi.org/10.5194/essd-](https://doi.org/10.5194/essd-14-4811-2022)  
2431 14-4811-2022, 2022b.

2432

2433 Friedlingstein, P., O'Sullivan, M., Jones, M. W., Andrew, R. M., Bakker, D. C. E., Hauck, J., Landschützer, P., Le Quéré, C.,  
2434 Luijkx, I. T., Peters, G. P., Peters, W., Pongratz, J., Schwingshackl, C., Sitch, S., Canadell, J. G., Ciais, P., Jackson, R. B.,  
2435 Alin, S. R., Anthoni, P., Barbero, L., Bates, N. R., Becker, M., Bellouin, N., Decharme, B., Bopp, L., Brasika, I. B. M.,  
2436 Cadule, P., Chamberlain, M. A., Chandra, N., Chau, T.-T.-T., Chevallier, F., Chini, L. P., Cronin, M., Dou, X., Enyo, K.,  
2437 Evans, W., Falk, S., Feely, R. A., Feng, L., Ford, D. J., Gasser, T., Ghattas, J., Gkritzalis, T., Grassi, G., Gregor, L., Gruber,  
2438 N., Gürses, Ö., Harris, I., Hefner, M., Heinke, J., Houghton, R. A., Hurtt, G. C., Iida, Y., Ilyina, T., Jacobson, A. R., Jain, A.  
2439 K., Jarníková, T., Jersild, A., Jiang, F., Jin, Z., Joos, F., Kato, E., Keeling, R. F., Kennedy, D., Klein Goldewijk, K., Knauer,  
2440 J., Korsbakken, J. I., Körtzinger, A., Lan, X., Lefèvre, N., Li, H., Liu, J., Liu, Z., Ma, L., Marland, G., Mayot, N., McGuire,  
2441 P. C., McKinley, G. A., Meyer, G., Morgan, E. J., Munro, D. R., Nakaoka, S., Niwa, Y., O'Brien, K. M., Olsen, A., Omar, A.  
2442 M., Ono, T., Paulsen, M., Pierrot, D., Pockock, K., Poulter, B., Powis, C. M., Rehder, G., Resplandy, L., Robertson, E.,  
2443 Rödenbeck, C., Rosan, T. M., Schwinger, J., Séférian, R., Smallman, T. L., Smith, S. M., Sospedra-Alfonso, R., Sun, Q.,  
2444 Sutton, A. J., Sweeney, C., Takao, S., Tans, P. P., Tian, H., Tilbrook, B., Tsujino, H., Tubiello, F., van der Werf, G. R., van  
2445 Ooijen, E., Wanninkhof, R., Watanabe, M., Wimart-Rousseau, C., Yang, D., Yang, X., Yuan, W., Yue, X., Zaehle, S., Zeng,  
2446 J., and Zheng, B.: Global Carbon Budget 2023, *Earth Syst. Sci. Data*, 15, 5301–5369, [https://doi.org/10.5194/essd-15-5301-](https://doi.org/10.5194/essd-15-5301-2023)  
2447 2023, 2023.

2448 Friedlingstein, P., O'Sullivan, M., Jones, M. W., Andrew, R. M., Hauck, J., Landschützer, P., Le Quéré, C., Li, H., Luijkx, I.  
2449 T., Olsen, A., Peters, G. P., Peters, W., Pongratz, J., Schwingshackl, C., Sitch, S., Canadell, J. G., Ciais, P., Jackson, R. B.,  
2450 Alin, S. R., Arneeth, A., Arora, V., Bates, N. R., Becker, M., Bellouin, N., Berghoff, C. F., Bittig, H. C., Bopp, L., Cadule, P.,  
2451 Campbell, K., Chamberlain, M. A., Chandra, N., Chevallier, F., Chini, L. P., Colligan, T., Decayeux, J., Djeutchouang, L.  
2452 M., Dou, X., Duran Rojas, C., Enyo, K., Evans, W., Fay, A. R., Feely, R. A., Ford, D. J., Foster, A., Gasser, T., Gehlen, M.,  
2453 Gkritzalis, T., Grassi, G., Gregor, L., Gruber, N., Gürses, Ö., Harris, I., Hefner, M., Heinke, J., Hurtt, G. C., Iida, Y., Ilyina,  
2454 T., Jacobson, A. R., Jain, A. K., Jarníková, T., Jersild, A., Jiang, F., Jin, Z., Kato, E., Keeling, R. F., Klein Goldewijk, K.,  
2455 Knauer, J., Korsbakken, J. I., Lauvset, S. K., Lefèvre, N., Liu, Z., Liu, J., Ma, L., Maksyutov, S., Marland, G., Mayot, N.,  
2456 McGuire, P. C., Metzl, N., Monacci, N. M., Morgan, E. J., Nakaoka, S., Neill, C., Niwa, Y., Nützel, T., Olivier, L., Ono, T.,  
2457 Palmer, P. I., Pierrot, D., Qin, Z., Resplandy, L., Roobaert, A., Rosan, T. M., Rödenbeck, C., Schwinger, J., Smallman, T. L.,  
2458 Smith, S. M., Sospedra-Alfonso, R., Steinhoff, T., Sun, Q., Sutton, A. J., Séférian, R., Takao, S., Tatebe, H., Tian, H.,  
2459 Tilbrook, B., Torres, O., Tourigny, E., Tsujino, H., Tubiello, F., van der Werf, G., Wanninkhof, R., Wang, X., Yang, D.,  
2460 Yang, X., Yu, Z., Yuan, W., Yue, X., Zaehle, S., Zeng, N., Zeng, J.: Supplemental data of the Global Carbon Budget 2024,  
2461 ICOS-ERIC Carbon Portal, <https://doi.org/10.18160/GCP-2024>, 2024.

2462 Ganzenmüller, R., Bultan, S., Winkler, K., Fuchs, R., Zabel, F., and Pongratz, J.: Land-use change emissions based on high-  
2463 resolution activity data substantially lower than previously estimated, *Environ. Res. Lett.*, 17, 064050,  
2464 <https://doi.org/10.1088/1748-9326/ac70d8>, 2022.

2465 Gasser, T., Crepin, L., Quilcaille, Y., Houghton, R. A., Ciais, P., and Obersteiner, M.: Historical CO<sub>2</sub> emissions from land  
2466 use and land cover change and their uncertainty, *Biogeosciences*, 17, 4075–4101, <https://doi.org/10.5194/bg-17-4075-2020>,  
2467 2020.

2468 Gaubert, B., Stephens, B. B., Basu, S., Chevallier, F., Deng, F., Kort, E. A., Patra, P. K., Peters, W., Rödenbeck, C., Saeki,  
2469 T., Schimel, D., Van der Laan-Luijkx, I., Wofsy, S., and Yin, Y.: Global atmospheric CO<sub>2</sub> inverse models converging on

2470 neutral tropical land exchange, but disagreeing on fossil fuel and atmospheric growth rate, *Biogeosciences*, 16, 117–134,  
2471 <https://doi.org/10.5194/bg-16-117-2019>, 2019.

2472 GCP: The Global Carbon Budget 2007, available at: <http://www.globalcarbonproject.org/carbonbudget/archive.htm>, last  
2473 access: 21 January 2025, 2007.

2474 Giglio, L., Schroeder, W., and Justice, C. O.: The collection 6 MODIS active fire detection algorithm and fire products,  
2475 *Remote Sensing of Environment*, 178, 31–41, <https://doi.org/10.1016/j.rse.2016.02.054>, 2016.

2476 Gloege, L., McKinley, G. A., Landschützer, P., Fay, A. R., Frölicher, T. L., Fyfe, J. C., Ilyina, T., Jones, S., Lovenduski, N.  
2477 S., Rodgers, K. B., Schlunegger, S., and Takano, Y.: Quantifying Errors in Observationally Based Estimates of Ocean  
2478 Carbon Sink Variability, *Global Biogeochem. Cy.*, 35, e2020GB006788, <https://doi.org/10.1029/2020GB006788>, 2021.

2479 Gloege, L., Yan, M., Zheng, T., and McKinley, G. A.: Improved Quantification of Ocean Carbon Uptake by Using Machine  
2480 Learning to Merge Global Models and pCO<sub>2</sub> Data, *J. Adv. Model. Earth Syst.*, 14, e2021MS002620,  
2481 <https://doi.org/10.1029/2021MS002620>, 2022.

2482 Golar, G., Malik, A., Muis, H., Herman, A., Nurudin, N., and Lukman, L.: The social-economic impact of COVID-19  
2483 pandemic: implications for potential forest degradation, *Heliyon*, 6, e05354, <https://doi.org/10.1016/j.heliyon.2020.e05354>,  
2484 2020.

2485 Goris, N., Tjiputra, J. F., Olsen, A., Schwinger, J., Lauvset, S. K., and Jeansson, E.: Constraining Projection-Based Estimates  
2486 of the Future North Atlantic Carbon Uptake, *J. Clim.*, 31, 3959–3978, <https://doi.org/10.1175/JCLI-D-17-0564.1>, 2018.

2487 Grassi, G., House, J., Kurz, W. A., Cescatti, A., Houghton, R. A., Peters, G. P., Sanz, M. J., Viñas, R. A., Alkama, R.,  
2488 Arneeth, A., Bondeau, A., Dentener, F., Fader, M., Federici, S., Friedlingstein, P., Jain, A. K., Kato, E., Koven, C. D., Lee,  
2489 D., Nabel, J. E. M. S., Nassikas, A. A., Perugini, L., Rossi, S., Sitch, S., Viovy, N., Wiltshire, A., and Zaehle, S.:  
2490 Reconciling global-model estimates and country reporting of anthropogenic forest CO<sub>2</sub> sinks, *Nature Clim Change*, 8, 914–  
2491 920, <https://doi.org/10.1038/s41558-018-0283-x>, 2018.

2492 Grassi, G., Stehfest, E., Rogelj, J., van Vuuren, D., Cescatti, A., House, J., Nabuurs, G.-J., Rossi, S., Alkama, R., Viñas, R.  
2493 A., Calvin, K., Ceccherini, G., Federici, S., Fujimori, S., Gusti, M., Hasegawa, T., Havlik, P., Humpenöder, F., Korosuo, A.,  
2494 Perugini, L., Tubiello, F. N., and Popp, A.: Critical adjustment of land mitigation pathways for assessing countries' climate  
2495 progress, *Nat. Clim. Chang.*, 11, 425–434, <https://doi.org/10.1038/s41558-021-01033-6>, 2021.

2496 Grassi, G., Schwingshackl, C., Gasser, T., Houghton, R. A., Sitch, S., Canadell, J. G., Cescatti, A., Ciais, P., Federici, S.,  
2497 Friedlingstein, P., Kurz, W. A., Sanz Sanchez, M. J., Abad Viñas, R., Alkama, R., Bultan, S., Ceccherini, G., Falk, S., Kato,  
2498 E., Kennedy, D., Knauer, J., Korosuo, A., Melo, J., McGrath, M. J., Nabel, J. E. M. S., Poulter, B., Romanovskaya, A. A.,  
2499 Rossi, S., Tian, H., Walker, A. P., Yuan, W., Yue, X., and Pongratz, J.: Harmonising the land-use flux estimates of global  
2500 models and national inventories for 2000–2020, *Earth Syst. Sci. Data*, 15, 1093–1114, [https://doi.org/10.5194/essd-15-1093-](https://doi.org/10.5194/essd-15-1093-2023)  
2501 2023, 2023.

2502 Gregor, L., Lebehot, A. D., Kok, S., and Scheel Monteiro, P. M.: A comparative assessment of the uncertainties of global  
2503 surface ocean CO<sub>2</sub> estimates using a machine-learning ensemble (CSIR-ML6 version 2019a)—have we hit the  
2504 wall?. *Geoscientific Model Development*, 12(12), 5113–5136, <https://doi.org/10.5194/gmd-12-5113-2019>, 2019.

- 2505 Gregor, L., Shutler, J., and Gruber, N.: High-resolution variability of the ocean carbon sink. *Global Biogeochemical Cycles*,  
2506 38(8), e2024GB008127, <https://doi.org/10.1029/2024GB008127>, 2024.
- 2507 Gruber, N., Bakker, D. C. E., DeVries, T., Gregor, L., Hauck, J., Landschützer, P., McKinley, G. A., and Müller, J. D.:  
2508 Trends and variability in the ocean carbon sink, *Nat. Rev. Earth Environ.*, 4, 119–134, [https://doi.org/10.1038/s43017-022-](https://doi.org/10.1038/s43017-022-00381-x)  
2509 00381-x, 2023.
- 2510 Gruber, N., Clement, D., Carter, B. R., Feely, R. A., van Heuven, S., Hoppema, M., Ishii, M., Key, R. M., Kozyr, A.,  
2511 Lauvset, S. K., Lo Monaco, C., Mathis, J. T., Murata, A., Olsen, A., Perez, F. F., Sabine, C. L., Tanhua, T., and Wanninkhof,  
2512 R.: The oceanic sink for anthropogenic CO<sub>2</sub> from 1994 to 2007, 363, 1193–1199, <https://doi.org/10.1126/science.aau5153>,  
2513 2019.
- 2514 Guan, D., Liu, Z., Geng, Y., Lindner, S., and Hubacek, K.: The gigatonne gap in China’s carbon dioxide inventories, *Nature*  
2515 *Clim Change*, 2, 672–675, <https://doi.org/10.1038/nclimate1560>, 2012.
- 2516 Gulev, S. K., Thorne, P. W., Ahn, J., Dentener, F. J., Domingues, C. M., Gerland, S., Gong, D. S., Kaufman, S., Nnamchi,  
2517 H. C., Quaas, J., Rivera, J. A., Sathyendranath, S., Smith, S. L., Trewin, B., von Shuckmann, K., and Vose, R. S.: Changing  
2518 State of the Climate System. In: *Climate Change 2021: The Physical Science Basis. Contribution of Working Group I to the*  
2519 *Sixth Assessment Report of the Intergovernmental Panel on Climate Change* [Masson-Delmotte, V., Zhai, P., Pirani, A.,  
2520 Connors, S. L., Péan, C., Berger, S., Caud, N., Chen, Y., Goldfarb, L., Gomis, M. I., Huang, M., Leitzell, K., Lonnoy, E.,  
2521 Matthews, J.B.R., Maycock, T.K., Waterfield, T., Yelekçi, O., Yu, R. and Zhou, B. (eds.)]. Cambridge University Press,  
2522 Cambridge, United Kingdom and New York, NY, USA, pp. 287–422, <https://doi.org/10.1017/9781009157896.004>, 2021.
- 2523 Guo, R., Wang, J., Bing, L., Tong, D., Ciais, P., Davis, S. J., Andrew, R. M., Xi, F., and Liu, Z.: Global CO<sub>2</sub> uptake by  
2524 cement from 1930 to 2019, 13, 1791–1805, <https://doi.org/10.5194/essd-13-1791-2021>, 2021.
- 2525 Gürses, Ö., Oziel, L., Karakuş, O., Sidorenko, D., Völker, C., Ye, Y., Zeising, M., Butzin, M., and Hauck, J.: Ocean  
2526 biogeochemistry in the coupled ocean–sea ice–biogeochemistry model FESOM2.1–REcoM3, *Geosci. Model Dev.*, 16,  
2527 4883–4936, <https://doi.org/10.5194/gmd-16-4883-2023>, 2023.
- 2528 Gütschow, J., Jeffery, M. L., Gieseke, R., Gebel, R., Stevens, D., Krapp, M., and Rocha, M.: The PRIMAP-hist national  
2529 historical emissions time series, 8, 571–603, <https://doi.org/10.5194/essd-8-571-2016>, 2016.
- 2530 Gütschow, J., Busch, D. and Pflüger, M.: The PRIMAP-hist national historical emissions time series (1750–2023) v2.6,  
2531 Zenodo [dataset], <https://doi.org/10.5281/zenodo.13752654>, 2023.
- 2532 Hall, B. D., Crotwell, A. M., Kitzi, D. R., Mefford, T., Miller, B. R., Schibig, M. F., and Tans, P. P.: Revision of the World  
2533 Meteorological Organization Global Atmosphere Watch (WMO/GAW) CO<sub>2</sub> calibration scale, 14, 3015–3032,  
2534 <https://doi.org/10.5194/amt-14-3015-2021>, 2021.
- 2535 Hansis, E., Davis, S. J., and Pongratz, J.: Relevance of methodological choices for accounting of land use change carbon  
2536 fluxes, *Global Biogeochem. Cycles*, 29, 1230–1246, <https://doi.org/10.1002/2014GB004997>, 2015.
- 2537 Hauck, J., Nissen, C., Landschützer, P., Rödenbeck, C., Bushinsky, S., and Olsen, A.: Sparse observations induce large  
2538 biases in estimates of the global ocean CO<sub>2</sub> sink: an ocean model subsampling experiment, *Philos. Trans. R. Soc. Math.*  
2539 *Phys. Eng. Sci.*, 381, 20220063, <https://doi.org/10.1098/rsta.2022.0063>, 2023a.

2540

2541 Hauck, J., Gregor, L., Nissen, C., Patara, L., Hague, M., Mongwe, P., Bushinsky, S., Doney, S. C., Gruber, N., Le Quéré, C.,  
 2542 Manizza, M., Mazloff, M., Monteiro, P. M. S., and Terhaar, J.: The Southern Ocean Carbon Cycle 1985–2018: Mean,  
 2543 Seasonal Cycle, Trends, and Storage. *Global Biogeochemical Cycles*, 37(11), e2023GB007848,  
 2544 <https://doi.org/10.1029/2023GB007848>, 2023b.

2545 Hauck, J., Zeising, M., Le Quéré, C., Gruber, N., Bakker, D. C. E., Bopp, L., Chau, T. T. T., Gürses, Ö., Ilyina, T.,  
 2546 Landschützer, P., Lenton, A., Resplandy, L., Rödenbeck, C., Schwinger, J., and Séférian, R.: Consistency and Challenges in  
 2547 the Ocean Carbon Sink Estimate for the Global Carbon Budget, *Front. Mar. Sci.*, 7, 571720,  
 2548 <https://doi.org/10.3389/fmars.2020.571720>, 2020.

2549 Haverd, V., Smith, B., Nieradzick, L., Briggs, P. R., Woodgate, W., Trudinger, C. M., Canadell, J. G., and Cuntz, M.: A new  
 2550 version of the CABLE land surface model (Subversion revision r4601) incorporating land use and land cover change, woody  
 2551 vegetation demography, and a novel optimisation-based approach to plant coordination of photosynthesis, *Geosci. Model*  
 2552 *Dev.*, 11, 2995–3026, <https://doi.org/10.5194/gmd-11-2995-2018>, 2018.

2553 Heinke, J., Rolinski, S., and Müller, C.: Modelling the role of livestock grazing in C and N cycling in grasslands with  
 2554 LPJmL5.0-grazing, *Geosci. Model Dev.*, 16, 2455–2475, <https://doi.org/10.5194/gmd-16-2455-2023>, 2023.

2555 Hefner, M., Marland, G., Boden, T., Andres, R.: Global, Regional, and National Fossil-Fuel CO<sub>2</sub> Emissions: 1751-2020  
 2556 CDIAC-FF [dataset], available at: <https://energy.appstate.edu/cdiac-appstate/data-products>, last access: 21 January 2025,  
 2557 2023.

2558 Hefner, M; Marland G; (2023): Global, Regional, and National Fossil-Fuel CO<sub>2</sub> Emissions: 1751-2020 CDIAC-FF,  
 2559 Research Institute for Environment, Energy, and Economics, Appalachian State University,  
 2560 <https://rieec.appstate.edu/projects-programs/cdiac>

2561 Hickler, T., Smith, B., Prentice, I. C., Mjöfors, K., Miller, P., Arneth, A., and Sykes, M. T.: CO<sub>2</sub> fertilization in temperate  
 2562 FACE experiments not representative of boreal and tropical forests, *Glob. Change Biol.*, 14, 1531–1542,  
 2563 <https://doi.org/10.1111/j.1365-2486.2008.01598.x>, 2008.

2564 Hoesly, R. M., Smith, S. J., Feng, L., Klimont, Z., Janssens-Maenhout, G., Pitkanen, T., Seibert, J. J., Vu, L., Andres, R. J.,  
 2565 Bolt, R. M., Bond, T. C., Dawidowski, L., Kholod, N., Kurokawa, J., Li, M., Liu, L., Lu, Z., Moura, M. C. P., O'Rourke, P.  
 2566 R., and Zhang, Q.: Historical (1750–2014) anthropogenic emissions of reactive gases and aerosols from the Community  
 2567 Emissions Data System (CEDS), *Geosci. Model Dev.*, 11, 369–408, <https://doi.org/10.5194/gmd-11-369-2018>, 2018.

2568 Hoesly, R., Smith, S. J., Prime, N., Ahsan, H., Suchyta, H., O'Rourke, P., Crippa, M., Klimont, Z., Guizzardi, D., Behrendt,  
 2569 J., Feng, L., Harkins, C., McDonald, B., Mott, A., McDuffie, A., Nicholson, M. and Wang, S.: CEDS v\_2024\_07\_08  
 2570 Release Emission Data, Zenodo [dataset], <https://doi.org/10.5281/zenodo.12803196>, 2024.

2571 Hong, C., Burney, J. A., Pongratz, J., Nabel, J. E. M. S., Mueller, N. D., Jackson, R. B., and Davis, S. J.: Global and regional  
 2572 drivers of land-use emissions in 1961–2017, *Nature*, 589, 554–561, <https://doi.org/10.1038/s41586-020-03138-y>, 2021.

2573 Holding, T., Ashton, I. G., Shutler, J. D., Land, P. E., Nightingale, P. D., Rees, A. P., Brown, I., Piolle, J.-F., Kock, A.,  
 2574 Bange, H. W., Woolf, D. K., Goddijn-Murphy, L., Pereira, R., Paul, F., Girard-Ardhuin, F., Chapron, B., Rehder, G.,

- 2575 Arduin, F., and Donlon, C. J.: The FluxEngine air–sea gas flux toolbox: simplified interface and extensions for in situ  
2576 analyses and multiple sparingly soluble gases, *Ocean Sci.*, 15, 1707–1728, <https://doi.org/10.5194/os-15-1707-2019>, 2019.
- 2577 Houghton, R. A. and Castanho, A.: Annual emissions of carbon from land use, land-use change, and forestry from 1850 to  
2578 2020, *Earth Syst. Sci. Data*, 15, 2025–2054, <https://doi.org/10.5194/essd-15-2025-2023>, 2023.
- 2579 Houghton, R. A., House, J. I., Pongratz, J., van der Werf, G. R., DeFries, R. S., Hansen, M. C., Le Quéré, C., and  
2580 Ramankutty, N.: Carbon emissions from land use and land-cover change, *Biogeosciences*, 9, 5125–5142,  
2581 <https://doi.org/10.5194/bg-9-5125-2012>, 2012.
- 2582 Huang, B., Thorne, P. W., Banzon, V. F., Boyer, T., Chepurin, G., Lawrimore, J. H., Menne, M. J., Smith, T. M., Vose, R.  
2583 S., and Zhang, H.-M.: NOAA Extended Reconstructed Sea Surface Temperature (ERSST), Version 5,  
2584 <https://doi.org/10.7289/V5T72FNM>, 2017.
- 2585 Hubau, W., Lewis, S.L., Phillips, O.L., Affum-Baffoe, K., Beeckman, H., Cuní-Sanchez, A., Daniels, A.K., Ewango, C.E.N.,  
2586 Fauset, S., Mukinzi, J.M., Sheil, D., Sonké, B., Sullivan, M.J.P., Sunderland, T.C.H., Taedoumg, H., Thomas, S.C., White,  
2587 L.J.T., Abernethy, K.A., Adu-Bredu, S., Amani, C.A., Baker, T.R., Banin, L.F., Baya, F., Begne, S.K., Bennett, A.C.,  
2588 Benedet, F., Bitariho, R., Bocko, Y.E., Boeckx, P., Boundja, P., Brienen, R.J.W., Brncic, T., Chezeaux, E., Chuyong, G.B.,  
2589 Clark, C.J., Collins, M., Comiskey, J.A., Coomes, D.A., Dargie, G.C., de Haulleville, T., Kamdem, M.N.D., Doucet, J.-L.,  
2590 Esquivel-Muelbert, A., Feldpausch, T.R., Fofanah, A., Foli, E.G., Gilpin, M., Gloor, E., Gonmadje, C., Gourlet-Fleury, S.,  
2591 Hall, J.S., Hamilton, A.C., Harris, D.J., Hart, T.B., Hockemba, M.B.N., Hladik, A., Ifo, S.A., Jeffery, K.J., Jucker, T.,  
2592 Yakusu, E.K., Kearsley, E., Kenfack, D., Koch, A., Leal, M.E., Levesley, A., Lindsell, J.A., Lisingo, J., Lopez-Gonzalez, G.,  
2593 Lovett, J.C., Makana, J.-R., Malhi, Y., Marshall, A.R., Martin, J., Martin, E.H., Mbayu, F.M., Medjibe, V.P., Mihindou, V.,  
2594 Mitchard, E.T.A., Moore, S., Munishi, P.K.T., Bengone, N.N., Ojo, L., Ondo, F.E., Peh, K.S.-H., Pickavance, G.C., Poulsen,  
2595 A.D., Poulsen, J.R., Qie, L., Reitsma, J., Rovero, F., Swaine, M.D., Talbot, J., Taplin, J., Taylor, D.M., Thomas, D.W.,  
2596 Toirambe, B., Mukendi, J.T., Tuagben, D., Umunay, P.M., van der Heijden, G.M.F., Verbeeck, H., Vleminckx, J., Willcock,  
2597 S., Wöll, H., Woods, J.T., Zomagho, L.: Asynchronous carbon sink saturation in African and Amazonian tropical forests,  
2598 *Nature*, 579, 80–87, <https://doi.org/10.1038/s41586-020-2035-0>, 2020.
- 2599 Humphrey, V., Zscheischler, J., Ciais, P., Gudmundsson, L., Sitch, S., and Seneviratne, S. I.: Sensitivity of atmospheric CO<sub>2</sub>  
2600 growth rate to observed changes in terrestrial water storage, *Nature*, 560, 628–631, <https://doi.org/10.1038/s41586-018->  
2601 0424-4, 2018.
- 2602 Humphrey, V., Berg, A., Ciais, P., Gentine, P., Jung, M., Reichstein, M., Seneviratne, S. I., and Frankenberg, C.: Soil  
2603 moisture–atmosphere feedback dominates land carbon uptake variability, *Nature*, 592, 65–69,  
2604 <https://doi.org/10.1038/s41586-021-03325-5>, 2021.
- 2605 Huntzinger, D. N., Michalak, A. M., Schwalm, C., Ciais, P., King, A. W., Fang, Y., Schaefer, K., Wei, Y., Cook, R. B.,  
2606 Fisher, J. B., Hayes, D., Huang, M., Ito, A., Jain, A. K., Lei, H., Lu, C., Maignan, F., Mao, J., Parazoo, N., Peng, S., Poulter,  
2607 B., Ricciuto, D., Shi, X., Tian, H., Wang, W., Zeng, N., and Zhao, F.: Uncertainty in the response of terrestrial carbon sink to  
2608 environmental drivers undermines carbon-climate feedback predictions, *Sci Rep*, 7, 4765, <https://doi.org/10.1038/s41598->  
2609 017-03818-2, 2017.

- 2610 Iida, Y., Takatani, Y., Kojima, A., and Ishii, M.: Global trends of ocean CO<sub>2</sub> sink and ocean acidification: an observation-  
2611 based reconstruction of surface ocean inorganic carbon variables, *J Oceanogr*, 77, 323–358, [https://doi.org/10.1007/s10872-](https://doi.org/10.1007/s10872-020-00571-5)  
2612 020-00571-5, 2021.
- 2613 Ilyina, T., Li, H., Spring, A., Müller, W. A., Bopp, L., Chikamoto, M. O., Danabasoglu, G., Dobrynin, M., Dunne, J.,  
2614 Fransner, F., Friedlingstein, P., Lee, W., Lovenduski, N. S., Merryfield, W. J., Mignot, J., Park, J. Y., Séférian, R., Sospedra-  
2615 Alfonso, R., Watanabe, M., and Yeager, S.: Predictable Variations of the Carbon Sinks and Atmospheric CO<sub>2</sub> Growth in a  
2616 Multi-Model Framework, *Geophys. Res. Lett.*, 48, e2020GL090695, <https://doi.org/10.1029/2020GL090695>, 2021.
- 2617 IMF: International Monetary Fund: World Economic Outlook, available at: <http://www.imf.org>, last access: 21 January  
2618 2025, 2024.
- 2619 Instituto Nacional de Pesquisas Espaciais (INPE): Portal TerraBrasilis, available at: <http://terrabrasilis.dpi.inpe.br/en/home->  
2620 [page/](http://terrabrasilis.dpi.inpe.br/en/home-), last access: 21 January 2025.
- 2621 Ito, A. and Inatomi, M.: Use of a process-based model for assessing the methane budgets of global terrestrial ecosystems and  
2622 evaluation of uncertainty, 9, 759–773, <https://doi.org/10.5194/bg-9-759-2012>, 2012.
- 2623 Jackson, R. B., Canadell, J. G., Le Quéré, C., Andrew, R. M., Korsbakken, J. I., Peters, G. P., and Nakicenovic, N.:  
2624 Reaching peak emissions, *Nature Clim Change*, 6, 7–10, <https://doi.org/10.1038/nclimate2892>, 2016.
- 2625 Jackson, R. B., Le Quéré, C., Andrew, R. M., Canadell, J. G., Korsbakken, J. I., Liu, Z., Peters, G. P., and Zheng, B.: Global  
2626 energy growth is outpacing decarbonization, *Environ. Res. Lett.*, 13, 120401, <https://doi.org/10.1088/1748-9326/aaf303>,  
2627 2018.
- 2628 Jackson, R. B., Friedlingstein, P., Andrew, R. M., Canadell, J. G., Le Quéré, C., and Peters, G. P.: Persistent fossil fuel  
2629 growth threatens the Paris Agreement and planetary health, *Environ. Res. Lett.*, 14, 121001, [https://doi.org/10.1088/1748-](https://doi.org/10.1088/1748-9326/ab57b3)  
2630 9326/ab57b3, 2019.
- 2631 Jackson, R. B., Friedlingstein, P., Quéré, C. L., Abernethy, S., Andrew, R. M., Canadell, J. G., Ciais, P., Davis, S. J., Deng,  
2632 Z., Liu, Z., Korsbakken, J. I., and Peters, G. P.: Global fossil carbon emissions rebound near pre-COVID-19 levels, *Environ.*  
2633 *Res. Lett.*, 17, 031001, <https://doi.org/10.1088/1748-9326/ac55b6>, 2022.
- 2634 Jacobson, A. R., Schuldt, K. N., Tans, P., Andrews, A., Miller, J. B., Oda, T., Basu, S., Mund, J., Weir, B., Ott, L., Aalto, T.,  
2635 Abshire, J. B., Aikin, K., Aoki, S., Apadula, F., Arnold, S., Baier, B., Bartyzel, J., Beyersdorf, A., Biermann, T., Biraud, S.  
2636 C., Boenisch, H., Brailsford, G., Brand, W. A., Chen, G., Chen, H., Chmura, L., Clark, S., Colomb, A., Commane, R., Conil,  
2637 S., Couret, C., Cox, A., Cristofanelli, P., Cuevas, E., Curcoll, R., Daube, B., Davis, K. J., De Wekker, S., Della Coletta, J.,  
2638 Delmotte, M., DiGangi, E., DiGangi, J. P., di Sarra, A. G., Dlugokencky, E., Elkins, J. W., Emmenegger, L., Fang, S.,  
2639 Fischer, M. L., Forster, G., Frumau, A., Galkowski, M., Gatti, L. V., Gehrlein, T., Gerbig, C., Gheusi, F., Gloor, E., Gomez-  
2640 Trueba, V., Goto, D., Griffis, T., Hammer, S., Hanson, C., Haszpra, L., Hatakka, J., Heimann, M., Heliasz, M., Hensen, A.,  
2641 Hermansen, O., Hintsa, E., Holst, J., Ivakhov, V., Jaffé, D. A., Jordan, A., Joubert, W., Karion, A., Kawa, S. R., Kazan, V.,  
2642 Keeling, R. F., Keronen, P., Kneuer, T., Kolari, P., Komínková, K., Kort, E., Kozlova, E., Krummel, P., Kubistin, D.,  
2643 Labuschagne, C., Lam, D. H. Y., Lan, X., Langenfelds, R. L., Laurent, O., Laurila, T., Lauvaux, T., Lavric, J., Law, B. E.,  
2644 Lee, J., Lee, O. S. M., Lehner, I., Lehtinen, K., Leppert, R., Leskinen, A., Leuenberger, M., Levin, I., Levula, J., Lin, J.,  
2645 Lindauer, M., Loh, Z., Lopez, M., Luijkx, I. T., Lunder, C. R., Machida, T., Mammarella, I., Manca, G., Manning, A.,

- 2646 Manning, A., Marek, M. V., Martin, M. Y., Matsueda, H., McKain, K., Meijer, H., Meinhardt, F., Merchant, L.,  
 2647 Mihalopoulos, N., Miles, N. L., Miller, C. E., Mitchell, L., Mölder, M., Montzka, S., Moore, F., Moossen, H., Morgan, E.,  
 2648 Morgui, J.-A., Morimoto, S., Müller-Williams, J., Munger, J. W., Munro, D., Myhre, C. L., Nakaoka, S.-I., Necki, J.,  
 2649 Newman, S., Nichol, S., Niwa, Y., Obersteiner, F., O'Doherty, S., Paplawsky, B., Peischl, J., Peltola, O., Piacentino, S.,  
 2650 Pichon, J.-M., Pickers, P., Piper, S., Pitt, J., Plass-Dülmer, C., Platt, S. M., Prinzivalli, S., Ramonet, M., Ramos, R., Reyes-  
 2651 Sanchez, E., Richardson, S. J., Riris, H., Rivas, P. P., Ryerson, T., Saito, K., Sargent, M., Sasakawa, M., Scheeren, B.,  
 2652 Schuck, T., Schumacher, M., Seifert, T., Sha, M. K., Shepson, P., Shook, M., Sloop, C. D., Smith, P., Stanley, K.,  
 2653 Steinbacher, M., Stephens, B., Sweeney, C., Thoning, K., Timas, H., Torn, M., Tørseth, K., Trisolino, P., Turnbull, J., van  
 2654 den Bulk, P., van Dinter, D., Vermeulen, A., Viner, B., Vitkova, G., Walker, S., Watson, A., Wofsy, S. C., Worsley, J.,  
 2655 Worthy, D., Young, D., Zaehle, S., Zahn, A., and Zimnoch, M.: CarbonTracker CT2022, NOAA GML [dataset],  
 2656 <https://doi.org/10.25925/Z1GJ-3254>, 2023a.
- 2657 Jacobson, A. R., Schuldt, K. N., Tans, P., Andrews, A., Miller, J. B., Oda, T., Basu, S., Mund, J., Weir, B., Ott, L., Aalto, T.,  
 2658 Abshire, J. B., Aikin, K., Aoki, S., Apadula, F., Arnold, S., Baier, B., Bartyzel, J., Beyersdorf, A., Biermann, T., Biraud, S.  
 2659 C., Boenisch, H., Brailsford, G., Brand, W. A., Chen, G., Chen, H., Chmura, L., Clark, S., Colomb, A., Commane, R., Conil,  
 2660 S., Couret, C., Cox, A., Cristofanelli, P., Cuevas, E., Curcoll, R., Daube, B., Davis, K. J., De Wekker, S., Della Coletta, J.,  
 2661 Delmotte, M., DiGangi, E., DiGangi, J. P., di Sarra, A. G., Dlugokencky, E., Elkins, J. W., Emmenegger, L., Fang, S.,  
 2662 Fischer, M. L., Forster, G., Frumau, A., Galkowski, M., Gatti, L. V., Gehrlein, T., Gerbig, C., Gheusi, F., Gloor, E., Gomez-  
 2663 Trueba, V., Goto, D., Griffis, T., Hammer, S., Hanson, C., Haszpra, L., Hatakka, J., Heimann, M., Heliasz, M., Hensen, A.,  
 2664 Hermansen, O., Hints, E., Holst, J., Ivakhov, V., Jaffe, D. A., Jordan, A., Joubert, W., Karion, A., Kawa, S. R., Kazan, V.,  
 2665 Keeling, R. F., Keronen, P., Kneuer, T., Kolari, P., Komínková, K., Kort, E., Kozlova, E., Krummel, P., Kubistin, D.,  
 2666 Labuschagne, C., Lam, D. H. Y., Lan, X., Langenfelds, R. L., Laurent, O., Laurila, T., Lauvaux, T., Lavric, J., Law, B. E.,  
 2667 Lee, J., Lee, O. S. M., Lehner, I., Lehtinen, K., Leppert, R., Leskinen, A., Leuenberger, M., Levin, I., Levula, J., Lin, J.,  
 2668 Lindauer, M., Loh, Z., Lopez, M., Luijkx, I. T., Lunder, C. R., Machida, T., Mammarella, I., Manca, G., Manning, A.,  
 2669 Manning, A., Marek, M. V., Martin, M. Y., Matsueda, H., McKain, K., Meijer, H., Meinhardt, F., Merchant, L.,  
 2670 Mihalopoulos, N., Miles, N. L., Miller, C. E., Mitchell, L., Mölder, M., Montzka, S., Moore, F., Moossen, H., Morgan, E.,  
 2671 Morgui, J.-A., Morimoto, S., Müller-Williams, J., Munger, J. W., Munro, D., Myhre, C. L., Nakaoka, S.-I., Necki, J.,  
 2672 Newman, S., Nichol, S., Niwa, Y., Obersteiner, F., O'Doherty, S., Paplawsky, B., Peischl, J., Peltola, O., Piacentino, S.,  
 2673 Pichon, J.-M., Pickers, P., Piper, S., Pitt, J., Plass-Dülmer, C., Platt, S. M., Prinzivalli, S., Ramonet, M., Ramos, R., Reyes-  
 2674 Sanchez, E., Richardson, S. J., Riris, H., Rivas, P. P., Ryerson, T., Saito, K., Sargent, M., Sasakawa, M., Scheeren, B.,  
 2675 Schuck, T., Schumacher, M., Seifert, T., Sha, M. K., Shepson, P., Shook, M., Sloop, C. D., Smith, P., Stanley, K.,  
 2676 Steinbacher, M., Stephens, B., Sweeney, C., Thoning, K., Timas, H., Torn, M., Tørseth, K., Trisolino, P., Turnbull, J., van  
 2677 den Bulk, P., van Dinter, D., Vermeulen, A., Viner, B., Vitkova, G., Walker, S., Watson, A., Wofsy, S. C., Worsley, J.,  
 2678 Worthy, D., Young, D., Zaehle, S., Zahn, A., and Zimnoch, M.: CarbonTracker CT-NRT.v2023-3, NOAA GML [dataset],  
 2679 <https://doi.org/10.25925/7TAF-J322>, 2023b.
- 2680 Jain, P., Barber, Q. E., Taylor, S. W., Whitman, E., Castellanos Acuna, D., Boulanger, Y., Chavardès, R. D., Chen, J.,  
 2681 Englefield, P., Flannigan, M., Girardin, M. P., Hanes, C. C., Little, J., Morrison, K., Skakun, R. S., Thompson, D. K., Wang,  
 2682 X., Parisien, M.-A.: Drivers and Impacts of the Record-Breaking 2023 Wildfire Season in Canada. *Nature Communications*,  
 2683 15(1), p.6764, <https://doi.org/10.1038/s41467-024-51154-7>, 2024.
- 2684 Janssens-Maenhout, G., Crippa, M., Guizzardi, D., Muntean, M., Schaaf, E., Dentener, F., Bergamaschi, P., Pagliari, V.,  
 2685 Olivier, J. G. J., Peters, J. A. H. W., van Aardenne, J. A., Monni, S., Doering, U., Petrescu, A. M. R., Solazzo, E., and



2686 Oreggioni, G. D.: EDGAR v4.3.2 Global Atlas of the three major greenhouse gas emissions for the period 1970–2012, *Earth*  
2687 *Syst. Sci. Data*, 11, 959–1002, <https://doi.org/10.5194/essd-11-959-2019>, 2019.

2688 Jean-Michel, L., Eric, G., Romain, B.-B., Gilles, G., Angélique, M., Marie, D., Clément, B., Mathieu, H., Olivier, L. G.,  
2689 Charly, R., Tony, C., Charles-Emmanuel, T., Florent, G., Giovanni, R., Mounir, B., Yann, D., and Pierre-Yves, L. T.: The  
2690 Copernicus Global 1/12° Oceanic and Sea Ice GLORYS12 Reanalysis, *Front. Earth Sci.*, 9, 2021.

2691 Jiang, F., Ju, W., He, W., Wu, M., Wang, H., Wang, J., Jia, M., Feng, S., Zhang, L., and Chen, J. M.: A 10-year global  
2692 monthly averaged terrestrial net ecosystem exchange dataset inferred from the ACOS GOSAT v9 XCO<sub>2</sub> retrievals  
2693 (GCAS2021), *Earth Syst. Sci. Data*, 14, 3013–3037, <https://doi.org/10.5194/essd-14-3013-2022>, 2022.

2694 Jiang, F., Wang, H., Chen, J. M., Ju, W., Tian, X., Feng, S., Li, G., Chen, Z., Zhang, S., Lu, X., Liu, J., Wang, H., Wang, J.,  
2695 He, W., and Wu, M.: Regional CO<sub>2</sub> fluxes from 2010 to 2015 inferred from GOSAT XCO<sub>2</sub> retrievals using a new version of  
2696 the Global Carbon Assimilation System, *Atmospheric Chem. Phys.*, 21, 1963–1985, [https://doi.org/10.5194/acp-21-1963-](https://doi.org/10.5194/acp-21-1963-2021)  
2697 [2021](https://doi.org/10.5194/acp-21-1963-2021), 2021.

2698

2699 Jin, Y., Keeling, R. F., Stephens, B. B., Long, M. C., Patra, P. K., Rödenbeck, C., Morgan, E. J., Kort, E. A., and Sweeney,  
2700 C.: Improved atmospheric constraints on Southern Ocean CO<sub>2</sub> exchange. *Proceedings of the National Academy of*  
2701 *Sciences*, 121(6), e2309333121, <https://doi.org/10.1073/pnas.2309333121>, 2024.

2702

2703 Jin, Z., Wang, T., Zhang, H., Wang, Y., Ding, J., and Tian, X.: Constraint of satellite CO<sub>2</sub> retrieval on the global carbon  
2704 cycle from a Chinese atmospheric inversion system, *Sci. China Earth Sci.*, 66, 609–618, [https://doi.org/10.1007/s11430-022-](https://doi.org/10.1007/s11430-022-1036-7)  
2705 [1036-7](https://doi.org/10.1007/s11430-022-1036-7), 2023.

2706 Joos, F. and Spahni, R.: Rates of change in natural and anthropogenic radiative forcing over the past 20,000 years,  
2707 *Proceedings of the National Academy of Sciences*, 105, 1425–1430, <https://doi.org/10.1073/pnas.0707386105>, 2008.

2708 Jones, C. D., Hickman, J. E., Rumbold, S. T., Walton, J., Lamboll, R. D., Skeie, R. B., Fiedler, S., Forster, P. M., Rogelj, J.,  
2709 Abe, M., Botzet, M., Calvin, K., Cassou, C., Cole, J. N. S., Davini, P., Deushi, M., Dix, M., Fyfe, J. C., Gillett, N. P., Ilyina,  
2710 T., Kawamiya, M., Kelley, M., Kharin, S., Koshiro, T., Li, H., Mackallah, C., Müller, W. A., Nabat, P., van Noije, T., Nolan,  
2711 P., Ohgaito, R., Olivie, D., Oshima, N., Parodi, J., Reerink, T. J., Ren, L., Romanou, A., Séférian, R., Tang, Y., Timmreck,  
2712 C., Tjiputra, J., Tourigny, E., Tsigaridis, K., Wang, H., Wu, M., Wyser, K., Yang, S., Yang, Y., and Ziehn, T.: The Climate  
2713 Response to Emissions Reductions Due to COVID-19: Initial Results From CovidMIP, *Geophys. Res. Lett.*, 48,  
2714 e2020GL091883, <https://doi.org/10.1029/2020GL091883>, 2021a.

2715

2716 Jones, M. W., Abatzoglou, J. T., Veraverbeke, S., Andela, N., Lasslop, G., Forkel, M., Smith, A. J. P., Burton, C., Betts, R.  
2717 A., van der Werf, G. R., Sitch, S., Canadell, J. G., Santín, C., Kolden, C., Doerr, S. H., and Le Quéré, C.: Global and  
2718 Regional Trends and Drivers of Fire Under Climate Change, *Rev. Geophys.*, 60, e2020RG000726,  
2719 <https://doi.org/10.1029/2020RG000726>, 2022.

2720 Jones, M. W., Andrew, R. M., Peters, G. P., Janssens-Maenhout, G., De-Gol, A. J., Ciais, P., Patra, P. K., Chevallier, F., and  
2721 Le Quéré, C.: Gridded fossil CO<sub>2</sub> emissions and related O<sub>2</sub> combustion consistent with national inventories 1959–2018, *Sci*  
2722 *Data*, 8, 2, <https://doi.org/10.1038/s41597-020-00779-6>, 2021b.

- 2723 Jones, M. W., Andrew, R. M., Peters, G. P., Janssens-Maenhout, G., De-Gol, A. J., Dou, X., Liu, Z., Pickers, P., Ciais, P.,  
 2724 Patra, P. K., Chevallier, F., and Le Quéré, C.: Gridded fossil CO<sub>2</sub> emissions and related O<sub>2</sub> combustion consistent with  
 2725 national inventories, Zenodo [dataset], <https://doi.org/10.5281/zenodo.13909046>, 2024a.
- 2726 Jones, M. W., Kelley, D. I., Burton, C. A., Di Giuseppe, F., Barbosa, M. L. F., Brambleby, E., Hartley, A. J., Lombardi, A.,  
 2727 Mataveli, G., McNorton, J. R., Spuler, F. R., Wessel, J. B., Abatzoglou, J. T., Anderson, L. O., Andela, N., Archibald, S.,  
 2728 Armenteras, D., Burke, E., Carmenta, R., Chuvieco, E., Clarke, H., Doerr, S. H., Fernandes, P. M., Giglio, L., Hamilton, D.  
 2729 S., Hantson, S., Harris, S., Jain, P., Kolden, C. A., Kurvits, T., Lampe, S., Meier, S., New, S., Parrington, M., Perron, M. M.  
 2730 G., Qu, Y., Ribeiro, N. S., Saharjo, B. H., San-Miguel-Ayanz, J., Shuman, J. K., Tanpipat, V., van der Werf, G. R.,  
 2731 Veraverbeke, S., and Xanthopoulos, G.: State of Wildfires 2023–2024, Earth System Science Data, 16, 3601–3685,  
 2732 <https://doi.org/10.5194/essd-16-3601-2024>, 2024b.
- 2733 Jones, M.W., Veraverbeke, S., Andela, N., Doerr, S.H., Kolden, C., Mataveli, G., Pettinari, M.L., Le Quéré, C., Rosan, T.M.,  
 2734 van der Werf, G.R. and van Wees, D.: Global rise in forest fire emissions linked to climate change in the extratropics.  
 2735 Science, 386(6719), p.ead15889, 2024c.
- 2736 Jung, M., Reichstein, M., Schwalm, C. R., Huntingford, C., Sitch, S., Ahlström, A., Arneth, A., Camps-Valls, G., Ciais, P.,  
 2737 Friedlingstein, P., Gans, F., Ichii, K., Jain, A. K., Kato, E., Papale, D., Poulter, B., Raduly, B., Rödenbeck, C., Tramontana,  
 2738 G., Viovy, N., Wang, Y.-P., Weber, U., Zaehle, S., and Zeng, N.: Compensatory water effects link yearly global land CO<sub>2</sub>  
 2739 sink changes to temperature, Nature, 541, 516–520, <https://doi.org/10.1038/nature20780>, 2017.
- 2740 Kaiser, J. W., Heil, A., Andreae, M. O., Benedetti, A., Chubarova, N., Jones, L., Morcrette, J.-J., Razinger, M., Schultz, M.  
 2741 G., Suttie, M., and van der Werf, G. R.: Biomass burning emissions estimated with a global fire assimilation system based  
 2742 on observed fire radiative power, Biogeosciences, 9, 527–554, <https://doi.org/10.5194/bg-9-527-2012>, 2012.
- 2743 Kato, E., Kinoshita, T., Ito, A., Kawamiya, M., and Yamagata, Y.: Evaluation of spatially explicit emission scenario of land-  
 2744 use change and biomass burning using a process-based biogeochemical model, J. Land Use Sci., 8, 104–122,  
 2745 <https://doi.org/10.1080/1747423X.2011.628705>, 2013.
- 2746 Kawasaki, T., Hasumi, H., and Tanaka, Y.: Role of tide-induced vertical mixing in the deep Pacific Ocean circulation, J.  
 2747 Oceanogr., 77, 173–184, <https://doi.org/10.1007/s10872-020-00584-0>, 2021.
- 2748 Ke, P., Ciais, P., Sitch, S., Li, W., Bastos, A., Liu, Z., Xu, Y., Gui, X., Bian, J., Goll, D. S., Xi, Y., Li, W., O'Sullivan, M.,  
 2749 Goncalves de Souza, J., Friedlingstein, P., Chevallier, F.: Low latency carbon budget analysis reveals a large decline of the  
 2750 land carbon sink in 2023. National Science Review, p.nwae367, <https://doi.org/10.1093/nsr/nwae367>, 2024.  
 2751
- 2752 Keeley, J. E. and Pausas, J. G.: Distinguishing disturbance from perturbations in fire-prone ecosystems, Int. J. Wildland Fire,  
 2753 28, 282–287, <https://doi.org/10.1071/WF18203>, 2019.
- 2754 Keeling, C. D., Bacastow, R. B., Bainbridge, A. E., Ekdahl, C. A., Guenther, P. R., Waterman, L. S., and Chin, J. F. S.:  
 2755 Atmospheric carbon dioxide variations at Mauna Loa Observatory, Hawaii, Tellus A., 28, 538–551,  
 2756 <https://doi.org/10.1111/j.2153-3490.1976.tb00701.x>, 1976.

- 2757 Keeling R.F.: Development of an Interferometric Oxygen Analyzer for Precise Measurement of the Atmospheric O<sub>2</sub> Mole  
2758 Fraction, PhD thesis, Harvard University, Cambridge, Massachusetts, available at:  
2759 [https://bluemoon.ucsd.edu/publications/ralph/34\\_PhDthesis.pdf](https://bluemoon.ucsd.edu/publications/ralph/34_PhDthesis.pdf), last access: 21 January 2025, 1988.
- 2760 Keeling, R. F., Manning, A. C., Paplawsky, W. J., and Cox, A. C.: On the long-term stability of reference gases for  
2761 atmospheric O<sub>2</sub>/N<sub>2</sub> and CO<sub>2</sub> measurements, *Tellus B Chem. Phys. Meteorol.*, 59, 3–14, <https://doi.org/10.1111/j.1600-0889.2006.00196.x>, 2007.
- 2762  
2763
- 2764 Keeling, R. F. and Manning, A. C.: 5.15 - Studies of Recent Changes in Atmospheric O<sub>2</sub> Content, in: *Treatise on*  
2765 *Geochemistry (Second Edition)*, edited by: Holland, H. D. and Turekian, K. K., Elsevier, Oxford, 385–404,  
2766 <https://doi.org/10.1016/B978-0-08-095975-7.00420-4>, 2014.
- 2767 Keppler, L. and Landschützer, P.: Regional Wind Variability Modulates the Southern Ocean Carbon Sink, *Sci Rep*, 9, 7384,  
2768 <https://doi.org/10.1038/s41598-019-43826-y>, 2019.
- 2769 Khatiwala, S., Primeau, F., and Hall, T.: Reconstruction of the history of anthropogenic CO<sub>2</sub> concentrations in the ocean,  
2770 *Nature*, 462, 346–349, <https://doi.org/10.1038/nature08526>, 2009.
- 2771 Khatiwala, S., Tanhua, T., Mikaloff Fletcher, S., Gerber, M., Doney, S. C., Graven, H. D., Gruber, N., McKinley, G. A.,  
2772 Murata, A., Ríos, A. F., and Sabine, C. L.: Global ocean storage of anthropogenic carbon, *Biogeosciences*, 10, 2169–2191,  
2773 <https://doi.org/10.5194/bg-10-2169-2013>, 2013.
- 2774 Kong, Y., Zheng, B., Zhang, Q., and He, K.: Global and regional carbon budget for 2015–2020 inferred from OCO-2 based  
2775 on an ensemble Kalman filter coupled with GEOS-Chem, *Atmospheric Chem. Phys.*, 22, 10769–10788,  
2776 <https://doi.org/10.5194/acp-22-10769-2022>, 2022.
- 2777 Korsbakken, J. I., Peters, G. P., and Andrew, R. M.: Uncertainties around reductions in China’s coal use and CO<sub>2</sub> emissions,  
2778 *Nature Clim Change*, 6, 687–690, <https://doi.org/10.1038/nclimate2963>, 2016.
- 2779 Krinner, G., Viovy, N., de Noblet-Ducoudré, N., Ogée, J., Polcher, J., Friedlingstein, P., Ciais, P., Sitch, S., and Prentice, I.  
2780 C.: A dynamic global vegetation model for studies of the coupled atmosphere-biosphere system: DVGCM for coupled climate  
2781 studies, *Global Biogeochem. Cycles*, 19, GB1015, <https://doi.org/10.1029/2003GB002199>, 2005.
- 2782 Lacroix, F., Ilyina, T., and Hartmann, J.: Oceanic CO<sub>2</sub> outgassing and biological production hotspots induced by pre-  
2783 industrial river loads of nutrients and carbon in a global modeling approach, *Biogeosciences*, 17, 55–88,  
2784 <https://doi.org/10.5194/bg-17-55-2020>, 2020.
- 2785 Lacroix, F., Ilyina, T., Mathis, M., Laruelle, G. G., and Regnier, P.: Historical increases in land-derived nutrient inputs may  
2786 alleviate effects of a changing physical climate on the oceanic carbon cycle, *Glob Change Biol*, 27, 5491–5513,  
2787 <https://doi.org/10.1111/gcb.15822>, 2021.
- 2788 Lamboll, R. D., Nicholls, Z. R. J., Smith, C. J., Kikstra, J. S., Byers, E., and Rogelj, J.: Assessing the size and uncertainty of  
2789 remaining carbon budgets, *Nat. Clim. Change*, <https://doi.org/10.1038/s41558-023-01848-5>, 2023.
- 2790

2791 Lamboll, R. D., Jones, C. D., Skeie, R. B., Fiedler, S., Samset, B. H., Gillett, N. P., Rogelj, J., Forster, P. M., 2021:  
2792 Modifying emissions scenario projections to account for the effects of COVID-19: protocol for CovidMIP, *Geosci. Model*  
2793 *Dev.*, 14, 3683–3695, <https://doi.org/10.5194/gmd-14-3683-2021>, 2021.

2794 Lan, X., Tans, P. and Thoning, K.: NOAA Greenhouse Gas Marine Boundary Layer Reference - CO2 [Data set]. NOAA  
2795 Global Monitoring Laboratory, <https://doi.org/10.15138/DVNP-F961>, 2023.

2796 Lan, X., Tans, P. and K.W. Thoning: Trends in globally-averaged CO2 determined from NOAA Global Monitoring  
2797 Laboratory measurements, Version 2024-09. National Oceanic and Atmospheric Administration, Global Monitoring  
2798 Laboratory (NOAA/GML) [dataset], available at: <https://gml.noaa.gov/ccgg/trends/global.html>, last access: 21 January 2025,  
2799 2024a.

2800 Lan, X., Tans, P. and Thoning, K. W.: Trends in globally-averaged CO2 determined from NOAA Global Monitoring  
2801 Laboratory measurements, <https://doi.org/10.15138/9N0H-ZH07>, 2024b.

2802 Landschützer, P., Gruber, N., Haumann, F. A., Rödenbeck, C., Bakker, D. C. E., van Heuven, S., Hoppema, M., Metzl, N.,  
2803 Sweeney, C., Takahashi, T., Tilbrook, B., and Wanninkhof, R.: The reinvigoration of the Southern Ocean carbon sink,  
2804 *Science*, 349, 1221–1224, <https://doi.org/10.1126/science.aab2620>, 2015.

2805 Landschützer, P., Gruber, N., and Bakker, D. C. E.: Decadal variations and trends of the global ocean carbon sink: decadal  
2806 air-sea CO2 flux variability, *Global Biogeochem. Cycles*, 30, 1396–1417, <https://doi.org/10.1002/2015GB005359>, 2016.

2807 Lapola, D. M., Pinho, P., Barlow, J., Aragão, L. E. O. C., Berenguer, E., Carmenta, R., Liddy, H. M., Seixas, H., Silva, C. V.  
2808 J., Silva-Junior, C. H. L., Alencar, A. A. C., Anderson, L. O., Armenteras, D., Brovkin, V., Calders, K., Chambers, J., Chini,  
2809 L., Costa, M. H., Faria, B. L., Fearnside, P. M., Ferreira, J., Gatti, L., Gutierrez-Velez, V. H., Han, Z., Hibbard, K., Koven,  
2810 C., Lawrence, P., Pongratz, J., Portela, B. T. T., Rounsevell, M., Ruane, A. C., Schaldach, R., da Silva, S. S., von Randow,  
2811 C., Walker, W. S.: The drivers and impacts of Amazon forest degradation. *Science*, 379(6630), p.eabp8622,  
2812 <https://doi.org/10.1126/science.abp8622>, 2023.

2813 Law, R. M., Ziehn, T., Matear, R. J., Lenton, A., Chamberlain, M. A., Stevens, L. E., Wang, Y.-P., Sribinovsky, J., Bi, D.,  
2814 Yan, H., and Vohralik, P. F.: The carbon cycle in the Australian Community Climate and Earth System Simulator  
2815 (ACCESS-ESM1) – Part 1: Model description and pre-industrial simulation, *Geosci. Model Dev.*, 10, 2567–2590,  
2816 <https://doi.org/10.5194/gmd-10-2567-2017>.

2817 Lawrence, D. M., Fisher, R. A., Koven, C. D., Oleson, K. W., Swenson, S. C., Bonan, G., Collier, N., Ghimire, B., van  
2818 Kampenhout, L., Kennedy, D., Kluzek, E., Lawrence, P. J., Li, F., Li, H., Lombardozzi, D., Riley, W. J., Sacks, W. J., Shi,  
2819 M., Vertenstein, M., Wieder, W. R., Xu, C., Ali, A. A., Badger, A. M., Bisht, G., van den Broeke, M., Brunke, M. A., Burns,  
2820 S. P., Buzan, J., Clark, M., Craig, A., Dahlin, K., Drewniak, B., Fisher, J. B., Flanner, M., Fox, A. M., Gentine, P., Hoffman,  
2821 F., Keppel-Aleks, G., Knox, R., Kumar, S., Lenaerts, J., Leung, L. R., Lipscomb, W. H., Lu, Y., Pandey, A., Pelletier, J. D.,  
2822 Perket, J., Randerson, J. T., Ricciuto, D. M., Sanderson, B. M., Slater, A., Subin, Z. M., Tang, J., Thomas, R. Q., Val Martin,  
2823 M., and Zeng, X.: The Community Land Model Version 5: Description of New Features, Benchmarking, and Impact of  
2824 Forcing Uncertainty, *J. Adv. Model Earth, Sy.*, 11, 4245–4287, <https://doi.org/10.1029/2018MS001583>, 2019.

2825 Le Quééré, C., Rödenbeck, C., Buitenhuis, E. T., Conway, T. J., Langenfelds, R., Gomez, A., Labuschagne, C., Ramonet, M.,  
2826 Nakazawa, T., Metzl, N., Gillett, N., and Heimann, M.: Saturation of the Southern Ocean CO2 Sink Due to Recent Climate  
2827 Change, *Science*, 316, 1735–1738, <https://doi.org/10.1126/science.1136188>, 2007.

2828 Le Quéré, C., Raupach, M. R., Canadell, J. G., Marland, G., Bopp, L., Ciais, P., Conway, T. J., Doney, S. C., Feely, R. A.,  
2829 Foster, P., Friedlingstein, P., Gurney, K., Houghton, R. A., House, J. I., Huntingford, C., Levy, P. E., Lomas, M. R., Majkut,  
2830 J., Metzl, N., Ometto, J. P., Peters, G. P., Prentice, I. C., Randerson, J. T., Running, S. W., Sarmiento, J. L., Schuster, U.,  
2831 Sitch, S., Takahashi, T., Viovy, N., van der Werf, G. R., and Woodward, F. I.: Trends in the sources and sinks of carbon  
2832 dioxide, *Nature Geosci*, 2, 831–836, <https://doi.org/10.1038/ngeo689>, 2009.

2833 Le Quéré, C., Andres, R. J., Boden, T., Conway, T., Houghton, R. A., House, J. I., Marland, G., Peters, G. P., van der Werf,  
2834 G. R., Ahlström, A., Andrew, R. M., Bopp, L., Canadell, J. G., Ciais, P., Doney, S. C., Enright, C., Friedlingstein, P.,  
2835 Huntingford, C., Jain, A. K., Jourdain, C., Kato, E., Keeling, R. F., Klein Goldewijk, K., Levis, S., Levy, P., Lomas, M.,  
2836 Poulter, B., Raupach, M. R., Schwinger, J., Sitch, S., Stocker, B. D., Viovy, N., Zaehle, S., and Zeng, N.: The global carbon  
2837 budget 1959–2011, *Earth Syst. Sci. Data*, 5, 165–185, <https://doi.org/10.5194/essd-5-165-2013>, 2013.

2838 Le Quéré, C., Peters, G. P., Andres, R. J., Andrew, R. M., Boden, T. A., Ciais, P., Friedlingstein, P., Houghton, R. A.,  
2839 Marland, G., Moriarty, R., Sitch, S., Tans, P., Arneeth, A., Arvanitis, A., Bakker, D. C. E., Bopp, L., Canadell, J. G., Chini, L.  
2840 P., Doney, S. C., Harper, A., Harris, I., House, J. I., Jain, A. K., Jones, S. D., Kato, E., Keeling, R. F., Klein Goldewijk, K.,  
2841 Körtzinger, A., Koven, C., Lefèvre, N., Maignan, F., Omar, A., Ono, T., Park, G.-H., Pfeil, B., Poulter, B., Raupach, M. R.,  
2842 Regnier, P., Rödenbeck, C., Saito, S., Schwinger, J., Segschneider, J., Stocker, B. D., Takahashi, T., Tilbrook, B., van  
2843 Heuven, S., Viovy, N., Wanninkhof, R., Wiltshire, A., and Zaehle, S.: Global carbon budget 2013, *Earth Syst. Sci. Data*, 6,  
2844 235–263, <https://doi.org/10.5194/essd-6-235-2014>, 2014.

2845 Le Quéré, C., Moriarty, R., Andrew, R. M., Peters, G. P., Ciais, P., Friedlingstein, P., Jones, S. D., Sitch, S., Tans, P.,  
2846 Arneeth, A., Boden, T. A., Bopp, L., Bozec, Y., Canadell, J. G., Chini, L. P., Chevallier, F., Cosca, C. E., Harris, I.,  
2847 Hoppema, M., Houghton, R. A., House, J. I., Jain, A. K., Johannessen, T., Kato, E., Keeling, R. F., Kitidis, V., Klein  
2848 Goldewijk, K., Koven, C., Landa, C. S., Landschützer, P., Lenton, A., Lima, I. D., Marland, G., Mathis, J. T., Metzl, N.,  
2849 Nojiri, Y., Olsen, A., Ono, T., Peng, S., Peters, W., Pfeil, B., Poulter, B., Raupach, M. R., Regnier, P., Rödenbeck, C., Saito,  
2850 S., Salisbury, J. E., Schuster, U., Schwinger, J., Séférian, R., Segschneider, J., Steinhoff, T., Stocker, B. D., Sutton, A. J.,  
2851 Takahashi, T., Tilbrook, B., van der Werf, G. R., Viovy, N., Wang, Y.-P., Wanninkhof, R., Wiltshire, A., and Zeng, N.:  
2852 Global carbon budget 2014, *Earth Syst. Sci. Data*, 7, 47–85, <https://doi.org/10.5194/essd-7-47-2015>, 2015a.

2853 Le Quéré, C., Moriarty, R., Andrew, R. M., Canadell, J. G., Sitch, S., Korsbakken, J. I., Friedlingstein, P., Peters, G. P.,  
2854 Andres, R. J., Boden, T. A., Houghton, R. A., House, J. I., Keeling, R. F., Tans, P., Arneeth, A., Bakker, D. C. E., Barbero,  
2855 L., Bopp, L., Chang, J., Chevallier, F., Chini, L. P., Ciais, P., Fader, M., Feely, R. A., Gkritzalis, T., Harris, I., Hauck, J.,  
2856 Ilyina, T., Jain, A. K., Kato, E., Kitidis, V., Klein Goldewijk, K., Koven, C., Landschützer, P., Lauvset, S. K., Lefèvre, N.,  
2857 Lenton, A., Lima, I. D., Metzl, N., Millero, F., Munro, D. R., Murata, A., Nabel, J. E. M. S., Nakaoka, S., Nojiri, Y.,  
2858 O'Brien, K., Olsen, A., Ono, T., Pérez, F. F., Pfeil, B., Pierrot, D., Poulter, B., Rehder, G., Rödenbeck, C., Saito, S.,  
2859 Schuster, U., Schwinger, J., Séférian, R., Steinhoff, T., Stocker, B. D., Sutton, A. J., Takahashi, T., Tilbrook, B., van der  
2860 Laan-Luijkx, I. T., van der Werf, G. R., van Heuven, S., Vandemark, D., Viovy, N., Wiltshire, A., Zaehle, S., and Zeng, N.:  
2861 Global Carbon Budget 2015, *Earth Syst. Sci. Data*, 7, 349–396, <https://doi.org/10.5194/essd-7-349-2015>, 2015b.

2862 Le Quéré, C., Andrew, R. M., Canadell, J. G., Sitch, S., Korsbakken, J. I., Peters, G. P., Manning, A. C., Boden, T. A., Tans,  
2863 P. P., Houghton, R. A., Keeling, R. F., Alin, S., Andrews, O. D., Anthoni, P., Barbero, L., Bopp, L., Chevallier, F., Chini, L.  
2864 P., Ciais, P., Currie, K., Delire, C., Doney, S. C., Friedlingstein, P., Gkritzalis, T., Harris, I., Hauck, J., Haverd, V.,  
2865 Hoppema, M., Klein Goldewijk, K., Jain, A. K., Kato, E., Körtzinger, A., Landschützer, P., Lefèvre, N., Lenton, A., Lienert,  
2866 S., Lombardozi, D., Melton, J. R., Metzl, N., Millero, F., Monteiro, P. M. S., Munro, D. R., Nabel, J. E. M. S., Nakaoka, S.,

2867 O'Brien, K., Olsen, A., Omar, A. M., Ono, T., Pierrot, D., Poulter, B., Rödenbeck, C., Salisbury, J., Schuster, U., Schwinger,  
2868 J., Séférian, R., Skjelvan, I., Stocker, B. D., Sutton, A. J., Takahashi, T., Tian, H., Tilbrook, B., van der Laan-Luijkx, I. T.,  
2869 van der Werf, G. R., Viovy, N., Walker, A. P., Wiltshire, A. J., and Zaehe, S.: Global Carbon Budget 2016, *Earth Syst. Sci.*  
2870 *Data*, 8, 605–649, <https://doi.org/10.5194/essd-8-605-2016>, 2016.

2871 Le Quéré, C., Andrew, R. M., Friedlingstein, P., Sitch, S., Pongratz, J., Manning, A. C., Korsbakken, J. I., Peters, G. P.,  
2872 Canadell, J. G., Jackson, R. B., Boden, T. A., Tans, P. P., Andrews, O. D., Arora, V. K., Bakker, D. C. E., Barbero, L.,  
2873 Becker, M., Betts, R. A., Bopp, L., Chevallier, F., Chini, L. P., Ciais, P., Cosca, C. E., Cross, J., Currie, K., Gasser, T.,  
2874 Harris, I., Hauck, J., Haverd, V., Houghton, R. A., Hunt, C. W., Hurtt, G., Ilyina, T., Jain, A. K., Kato, E., Kautz, M.,  
2875 Keeling, R. F., Klein Goldewijk, K., Körtzinger, A., Landschützer, P., Lefèvre, N., Lenton, A., Lienert, S., Lima, I.,  
2876 Lombardozi, D., Metzl, N., Millero, F., Monteiro, P. M. S., Munro, D. R., Nabel, J. E. M. S., Nakaoka, S., Nojiri, Y., Padin,  
2877 X. A., Pregon, A., Pfeil, B., Pierrot, D., Poulter, B., Rehder, G., Reimer, J., Rödenbeck, C., Schwinger, J., Séférian, R.,  
2878 Skjelvan, I., Stocker, B. D., Tian, H., Tilbrook, B., Tubiello, F. N., van der Laan-Luijkx, I. T., van der Werf, G. R., van  
2879 Heuven, S., Viovy, N., Vuichard, N., Walker, A. P., Watson, A. J., Wiltshire, A. J., Zaehe, S., and Zhu, D.: Global Carbon  
2880 Budget 2017, *Earth Syst. Sci. Data*, 10, 405–448, <https://doi.org/10.5194/essd-10-405-2018>, 2018a.

2881 Le Quéré, C., Andrew, R. M., Friedlingstein, P., Sitch, S., Hauck, J., Pongratz, J., Pickers, P. A., Korsbakken, J. I., Peters, G.  
2882 P., Canadell, J. G., Arneeth, A., Arora, V. K., Barbero, L., Bastos, A., Bopp, L., Chevallier, F., Chini, L. P., Ciais, P., Doney,  
2883 S. C., Gkritzalis, T., Goll, D. S., Harris, I., Haverd, V., Hoffman, F. M., Hoppema, M., Houghton, R. A., Hurtt, G., Ilyina, T.,  
2884 Jain, A. K., Johannessen, T., Jones, C. D., Kato, E., Keeling, R. F., Klein Goldewijk, K., Landschützer, P., Lefèvre, N.,  
2885 Lienert, S., Liu, Z., Lombardozi, D., Metzl, N., Munro, D. R., Nabel, J. E. M. S., Nakaoka, S., Neill, C., Olsen, A., Ono, T.,  
2886 Patra, P., Pregon, A., Peters, W., Peylin, P., Pfeil, B., Pierrot, D., Poulter, B., Rehder, G., Resplandy, L., Robertson, E.,  
2887 Rocher, M., Rödenbeck, C., Schuster, U., Schwinger, J., Séférian, R., Skjelvan, I., Steinhoff, T., Sutton, A., Tans, P. P.,  
2888 Tian, H., Tilbrook, B., Tubiello, F. N., van der Laan-Luijkx, I. T., van der Werf, G. R., Viovy, N., Walker, A. P., Wiltshire,  
2889 A. J., Wright, R., Zaehe, S., and Zheng, B.: Global Carbon Budget 2018, *Earth Syst. Sci. Data*, 10, 2141–2194,  
2890 <https://doi.org/10.5194/essd-10-2141-2018>, 2018b.

2891 Le Quéré, C., Korsbakken, J. I., Wilson, C., Tosun, J., Andrew, R., Andres, R. J., Canadell, J. G., Jordan, A., Peters, G. P.,  
2892 and van Vuuren, D. P.: Drivers of declining CO<sub>2</sub> emissions in 18 developed economies, *Nat. Clim. Chang.*, 9, 213–217,  
2893 <https://doi.org/10.1038/s41558-019-0419-7>, 2019.

2894 Le Quéré, C., Peters, G. P., Friedlingstein, P., Andrew, R. M., Canadell, J. G., Davis, S. J., Jackson, R. B., and Jones, M. W.:  
2895 Fossil CO<sub>2</sub> emissions in the post-COVID-19 era, *Nat. Clim. Chang.*, 11, 197–199, [https://doi.org/10.1038/s41558-021-](https://doi.org/10.1038/s41558-021-01001-0)  
2896 [01001-0](https://doi.org/10.1038/s41558-021-01001-0), 2021.

2897 Levitus, S., Antonov, J. I., Boyer, T. P., Baranova, O. K., Garcia, H. E., Locarnini, R. A., Mishonov, A. V., Reagan, J. R.,  
2898 Seidov, D., Yarosh, E. S., and Zweng, M. M.: World ocean heat content and thermocline sea level change (0–2000 m),  
2899 1955–2010, *Geophys. Res. Lett.*, 39, <https://doi.org/10.1029/2012GL051106>, 2012.

2900

2901 Li, H., Ilyina, T., Müller, W. A., and Sienz, F.: Decadal predictions of the North Atlantic CO<sub>2</sub> uptake, *Nat. Commun.*, 7,  
2902 11076, <https://doi.org/10.1038/ncomms11076>, 2016.

2903

2904 Li, H., Ilyina, T., Müller, W. A., and Landschützer, P.: Predicting the variable ocean carbon sink, *Sci. Adv.*, 5, eaav6471,  
2905 <https://doi.org/10.1126/sciadv.aav6471>, 2019.

2906

2907 Li, H., Ilyina, T., Loughran, T., Spring, A., and Pongratz, J.: Reconstructions and predictions of the global carbon budget  
 2908 with an emission-driven Earth system model, *Earth Syst. Dyn.*, 14, 101–119, <https://doi.org/10.5194/esd-14-101-2023>, 2023.

2909 Li, W., Ciais, P., Peng, S., Yue, C., Wang, Y., Thurner, M., Saatchi, S. S., Arneeth, A., Avitabile, V., Carvalhais, N., Harper,  
 2910 A. B., Kato, E., Koven, C., Liu, Y. Y., Nabel, J. E. M. S., Pan, Y., Pongratz, J., Poulter, B., Pugh, T. A. M., Santoro, M.,  
 2911 Sitch, S., Stocker, B. D., Viovy, N., Wiltshire, A., Yousefpour, R., and Zaehle, S.: Land-use and land-cover change carbon  
 2912 emissions between 1901 and 2012 constrained by biomass observations, *Biogeosciences*, 14, 5053–5067,  
 2913 <https://doi.org/10.5194/bg-14-5053-2017>, 2017.

2914 Liao, E., Resplandy, L., Liu, J., and Bowman, K. W.: Amplification of the Ocean Carbon Sink During El Niños: Role of  
 2915 Poleward Ekman Transport and Influence on Atmospheric CO<sub>2</sub>, *Global Biogeochem. Cy.*, 34, e2020GB006574,  
 2916 <https://doi.org/10.1029/2020GB006574>, 2020.

2917 Lienert, S. and Joos, F.: A Bayesian ensemble data assimilation to constrain model parameters and land-use carbon  
 2918 emissions, *Biogeosciences*, 15, 2909–2930, <https://doi.org/10.5194/bg-15-2909-2018>, 2018.

2919 Liu, J., Baskaran, L., Bowman, K., Schimel, D., Bloom, A. A., Parazoo, N. C., Oda, T., Carroll, D., Menemenlis, D., Joiner,  
 2920 J., Commane, R., Daube, B., Gatti, L. V., McKain, K., Miller, J., Stephens, B. B., Sweeney, C., and Wofsy, S.: Carbon  
 2921 Monitoring System Flux Net Biosphere Exchange 2020 (CMS-Flux NBE 2020), 13, 299–330, [https://doi.org/10.5194/essd-](https://doi.org/10.5194/essd-13-299-2021)  
 2922 [13-299-2021](https://doi.org/10.5194/essd-13-299-2021), 2021.

2923 Liu, Z., Guan, D., Wei, W., Davis, S. J., Ciais, P., Bai, J., Peng, S., Zhang, Q., Hubacek, K., Marland, G., Andres, R. J.,  
 2924 Crawford-Brown, D., Lin, J., Zhao, H., Hong, C., Boden, T. A., Feng, K., Peters, G. P., Xi, F., Liu, J., Li, Y., Zhao, Y.,  
 2925 Zeng, N., and He, K.: Reduced carbon emission estimates from fossil fuel combustion and cement production in China,  
 2926 *Nature*, 524, 335–338, <https://doi.org/10.1038/nature14677>, 2015.

2927 Liu, Z., Zeng, N., Liu, Y., Kalnay, E., Asrar, G., Wu, B., Cai, Q., Liu, D., and Han, P.: Improving the joint estimation of  
 2928 CO<sub>2</sub> and surface carbon fluxes using a constrained ensemble Kalman filter in COLA (v1.0), *Geosci. Model Dev.*, 15, 5511–  
 2929 5528, <https://doi.org/10.5194/gmd-15-5511-2022>, 2022.

2930

2931 Long, M. C., Stephens, B. B., McKain, K., Sweeney, C., Keeling, R. F., Kort, E. A., Morgan, E. J., Bent, J. D., Chandra, N.,  
 2932 Chevallier, F., Commane, R., Daube, B. C., Krummel, P. B., Loh, Z., Luijkx, I. T., Munro, D., Patra, P., Peters, W.,  
 2933 Ramonet, M., Rödenbeck, C., Stavert, A., Tans, P., Wofsy, S. C.: Strong Southern Ocean carbon uptake evident in airborne  
 2934 observations. *Science*, 374(6572), 1275–1280, <https://doi.org/10.1126/science.abi4355>, 2021.

2935

2936 Lovenduski, N. S., Bonan, G. B., Yeager, S. G., Lindsay, K., and Lombardozzi, D. L.: High predictability of terrestrial  
 2937 carbon fluxes from an initialized decadal prediction system, *Environ. Res. Lett.*, 14, 124074, [https://doi.org/10.1088/1748-](https://doi.org/10.1088/1748-9326/ab5c55)  
 2938 [9326/ab5c55](https://doi.org/10.1088/1748-9326/ab5c55), 2019a.

2939

2940 Lovenduski, N. S., Yeager, S. G., Lindsay, K., and Long, M. C.: Predicting near-term variability in ocean carbon uptake,  
 2941 *Earth Syst. Dyn.*, 10, 45–57, <https://doi.org/10.5194/esd-10-45-2019>, 2019b.

- 2942 Lutz, F., Herzfeld, T., Heinke, J., Rolinski, S., Schaphoff, S., von Bloh, W., Stoorvogel, J. J., and Müller, C.: Simulating the  
2943 effect of tillage practices with the global ecosystem model LPJmL (version 5.0-tillage), *Geosci. Model Dev.*, 12, 2419–2440,  
2944 <https://doi.org/10.5194/gmd-12-2419-2019>, 2019.
- 2945 Ma, L., Hurtt, G., Ott, L., Sahajpal, R., Fisk, J., Lamb, R., Tang, H., Flanagan, S., Chini, L., Chatterjee, A., and Sullivan, J.:  
2946 Global evaluation of the Ecosystem Demography model (ED v3.0), *Geosci. Model Dev.*, 15, 1971–1994,  
2947 <https://doi.org/10.5194/gmd-15-1971-2022>, 2022.
- 2948
- 2949 Magi, B. I., Rabin, S., Shevliakova, E., and Pacala, S.: Separating agricultural and non-agricultural fire seasonality at  
2950 regional scales, *Biogeosciences*, 9, 3003–3012, <https://doi.org/10.5194/bg-9-3003-2012>, 2012.
- 2951
- 2952 Maksyutov, S., Oda, T., Saito, M., Janardanan, R., Belikov, D., Kaiser, J. W., Zhuravlev, R., Ganshin, A., Valsala, V. K.,  
2953 Andrews, A., Chmura, L., Dlugokencky, E., Haszpra, L., Langenfelds, R. L., Machida, T., Nakazawa, T., Ramonet, M.,  
2954 Sweeney, C., and Worthy, D.: Technical note: A high-resolution inverse modelling technique for estimating surface CO<sub>2</sub>  
2955 fluxes based on the NIES-TM–FLEXPART coupled transport model and its adjoint, *Atmos. Chem. Phys.*, 21, 1245–1266,  
2956 <https://doi.org/10.5194/acp-21-1245-2021>, 2021.
- 2957 Masarie, K. A. and Tans, P. P.: Extension and integration of atmospheric carbon dioxide data into a globally consistent  
2958 measurement record, *J. Geophys. Res.*, 100, 11593, <https://doi.org/10.1029/95JD00859>, 1995.
- 2959 Mataveli, G., Jones, M.W., Carmenta, R., Sanchez, A., Dutra, D.J., Chaves, M., de Oliveira, G., Anderson, L.O. and Aragão,  
2960 L.E.: Deforestation falls but rise of wildfires continues degrading Brazilian Amazon forests. *Global Change Biology*, 30(2),  
2961 p.e17202, <https://doi.org/10.1111/gcb.17202>, 2024.
- 2962 Mather, A. S.: The transition from deforestation to reforestation in Europe, in: *Agricultural technologies and tropical*  
2963 *deforestation* (eds. Angelsen, A.; Kaimowitz, D.), CABI in association with centre for international Forestry Research, 35–  
2964 52, 2001.
- 2965 Mauritsen, T., Bader, J., Becker, T., Behrens, J., Bittner, M., Brokopf, R., Brovkin, V., Claussen, M., Crueger, T., Esch, M.,  
2966 Fast, I., Fiedler, S., Fläschner, D., Gayler, V., Giorgetta, M., Goll, D. S., Haak, H., Hagemann, S., Hedemann, C.,  
2967 Hohenegger, C., Ilyina, T., Jahns, T., Jimenez-de-la-Cuesta, D., Jungclaus, J., Kleinen, T., Kloster, S., Kracher, D., Kinne,  
2968 S., Kleberg, D., Lasslop, G., Kornbluh, L., Marotzke, J., Matei, D., Meraner, K., Mikolajewicz, U., Modali, K., Möbis, B.,  
2969 Müller, W. A., Nabel, J. E. M. S., Nam, C. C. W., Notz, D., Nyawira, S.-S., Paulsen, H., Peters, K., Pincus, R., Pohlmann,  
2970 H., Pongratz, J., Popp, M., Raddatz, T. J., Rast, S., Redler, R., Reick, C. H., Rohrschneider, T., Schemann, V., Schmidt, H.,  
2971 Schnur, R., Schulzweida, U., Six, K. D., Stein, L., Stemmler, I., Stevens, B., von Storch, J.-S., Tian, F., Voigt, A., Vrese, P.,  
2972 Wieners, K.-H., Wilkenskjaeld, S., Winkler, A., and Roeckner, E.: Developments in the MPI-M Earth System Model version  
2973 1.2 (MPI-ESM1.2) and Its Response to Increasing CO<sub>2</sub>, *J. Adv. Model Earth Sy.*, 11, 998–1038,  
2974 <https://doi.org/10.1029/2018MS001400>, 2019.
- 2975 Mayot, N., Buitenhuis, E. T., Wright, R. M., Hauck, J., Bakker, D. C. E., and Le Quéré, C.: Constraining the trend in the  
2976 ocean CO<sub>2</sub> sink during 2000–2022. *Nat Commun* 15, 8429, <https://doi.org/10.1038/s41467-024-52641-7>, 2024.
- 2977 McGrath, M. J., Luyssaert, S., Meyfroidt, P., Kaplan, J. O., Bürgi, M., Chen, Y., Erb, K., Gimmi, U., McInerney, D., Naudts,  
2978 K., Otto, J., Pasztor, F., Ryder, J., Schelhaas, M.-J., and Valade, A.: Reconstructing European forest management from 1600  
2979 to 2010, 12, 4291–4316, <https://doi.org/10.5194/bg-12-4291-2015>, 2015.



- 2980 McKinley, G. A., Fay, A. R., Eddebbbar, Y. A., Gloege, L., and Lovenduski, N. S.: External Forcing Explains Recent  
 2981 Decadal Variability of the Ocean Carbon Sink, *AGU Advances*, 1, e2019AV000149,  
 2982 <https://doi.org/10.1029/2019AV000149>, 2020.
- 2983 McKinley, G. A., Fay, A. R., Lovenduski, N. S., and Pilcher, D. J.: Natural Variability and Anthropogenic Trends in the  
 2984 Ocean Carbon Sink, *Annu. Rev. Mar. Sci.*, 9, 125–150, <https://doi.org/10.1146/annurev-marine-010816-060529>, 2017.
- 2985 Meiyappan, P., Jain, A. K., and House, J. I.: Increased influence of nitrogen limitation on CO<sub>2</sub> emissions from future land  
 2986 use and land use change, *Global Biogeochem. Cycles*, 29, 1524–1548, <https://doi.org/10.1002/2015GB005086>, 2015.
- 2987 Melton, J. R., Arora, V. K., Wisernig-Cojoc, E., Seiler, C., Fortier, M., Chan, E., and Teckentrup, L.: CLASSIC v1.0: the  
 2988 open-source community successor to the Canadian Land Surface Scheme (CLASS) and the Canadian Terrestrial Ecosystem  
 2989 Model (CTEM) – Part 1: Model framework and site-level performance, *Geosci. Model Dev.*, 13, 2825–2850,  
 2990 <https://doi.org/10.5194/gmd-13-2825-2020>, 2020.
- 2991 Mercado, L. M., Bellouin, N., Sitch, S., Boucher, O., Huntingford, C., Wild, M., and Cox, P. M.: Impact of changes in  
 2992 diffuse radiation on the global land carbon sink, *Nature*, 458, 1014–1017, <https://doi.org/10.1038/nature07949>, 2009.
- 2993 Merchant, C. J., Embury, O., Bulgin, C. E., Block, T., Corlett, G. K., Fiedler, E., Good, S. A., Mittaz, J., Rayner, N. A.,  
 2994 Berry, D., Eastwood, S., Taylor, M., Tsushima, Y., Waterfall, A., Wilson, R., and Donlon, C.: Satellite-based time-series of  
 2995 sea-surface temperature since 1981 for climate applications, *Sci. Data*, 6, 223, <https://doi.org/10.1038/s41597-019-0236-x>,  
 2996 2019.
- 2997 Moorcroft, P. R., Hurtt, G. C., and Pacala, S. W.: A Method for Scaling Vegetation Dynamics: The Ecosystem Demography  
 2998 Model (ed), *Ecol. Monogr.*, 71, 557–586, [https://doi.org/10.1890/0012-9615\(2001\)071\[0557:AMFSVD\]2.0.CO;2](https://doi.org/10.1890/0012-9615(2001)071[0557:AMFSVD]2.0.CO;2), 2001.
- 2999 Müller, J. D., Gruber, N., Carter, B., Feely, R., Ishii, M., Lange, N., Lauvset, S. K., Murata, A., Olsen, A., Pérez, F. F.,  
 3000 Sabine, C., Tanhua, T., Wanninkhof, R., and Zhu, D.: Decadal Trends in the Oceanic Storage of Anthropogenic Carbon  
 3001 From 1994 to 2014, *AGU Adv.*, 4, e2023AV000875, <https://doi.org/10.1029/2023AV000875>, 2023.  
 3002
- 3003 Müller, J. and Joos, F.: Committed and projected future changes in global peatlands – continued transient model simulations  
 3004 since the Last Glacial Maximum, *Biogeosciences*, 18, 3657–3687, <https://doi.org/10.5194/bg-18-3657-2021>, 2021.
- 3005 Nayagam, L., Maksyutov, S., Oda, T., Janardanan, R., Trisolino, P., Zeng J., Kaiser, J.W. and Matsunaga, T.: A top-down  
 3006 estimation of subnational CO<sub>2</sub> budget using a global high-resolution inverse model with data from regional surface  
 3007 networks, *Environ. Res. Lett.*, 19, 0140312024, <https://doi.org/10.1088/1748-9326/ad0f74>, 2024.
- 3008 NCEP: National Centers for Environmental Prediction. ONI Index. Cold & Warm Episodes by Season [dataset], available at:  
 3009 [https://origin.cpc.ncep.noaa.gov/products/analysis\\_monitoring/ensostuff/ONI\\_v5.php](https://origin.cpc.ncep.noaa.gov/products/analysis_monitoring/ensostuff/ONI_v5.php), last access: 21 January 2025, 2023.
- 3010 Nevison, C.D., Mahowald, N.M., Doney, S.C., Lima, I.D. and Cassar, N.: Impact of variable air-sea O<sub>2</sub> and CO<sub>2</sub> fluxes on  
 3011 atmospheric potential oxygen (APO) and land-ocean carbon sink partitioning. *Biogeosciences*, 5(3), pp.875-889,  
 3012 <https://doi.org/10.5194/bg-5-875-2008>, 2008.
- 3013 Niu, G.-Y., Yang, Z.-L., Mitchell, K. E., Chen, F., Ek, M. B., Barlage, M., Kumar, A., Manning, K., Niyogi, D., Rosero, E.,  
 3014 Tewari, M., and Xia, Y.: The community Noah land surface model with multiparameterization options (Noah-MP): 1. Model

3015 description and evaluation with local-scale measurements, *J. Geophys. Res. Atmospheres*, 116,  
3016 <https://doi.org/10.1029/2010JD015139>, 2011.

3017 Niwa, Y., Ishijima, K., Ito, A., and Iida, Y.: Toward a long-term atmospheric CO<sub>2</sub> inversion for elucidating natural carbon  
3018 fluxes: technical notes of NISMON-CO<sub>2</sub> v2021.1, *Prog. Earth Planet Sci.*, 9, 42, [https://doi.org/10.1186/s40645-022-00502-](https://doi.org/10.1186/s40645-022-00502-6)  
3019 6, 2022.

3020 Niwa, Y., Langenfelds, R., Krummel, P., Loh, Z., Worthy, Doug, Hatakka, Juha, Aalto, Tuula, Ramonet, Michel,  
3021 Delmotte, Marc, Schmidt, Martina, Gheusi, Francois, Mihalopoulos, N., Morgui, J.A., Andrews, Arlyn, Dlugokencky, Ed,  
3022 Lee, John, Sweeney, Colm, Thoning, Kirk, Tans, Pieter, De Wekker, Stephan, Fischer, Marc L., Jaffe, Dan, McKain,  
3023 Kathryn, Viner, Brian, Miller, John B., Karion, Anna, Miller, Charles, Sloop, Christopher D., Saito, Kazuyuki, Aoki, Shuji,  
3024 Morimoto, Shinji, Goto, Daisuke, Steinbacher, Martin, Myhre, Cathrine Lund, Hermanssen, Ove, Stephens, Britton, Keeling,  
3025 Ralph, Afshar, Sara, Paplawsky, Bill, Cox, Adam, Walker, Stephen, Schuldt, Kenneth, Mukai, Hitoshi, Machida, Toshinobu,  
3026 Sasakawa, Motoki, Nomura, Shohei, Ito, Akihiko, Iida, Yosuke, and Jones, Matthew W.: Long-term global CO<sub>2</sub> fluxes  
3027 estimated by NICAM-based Inverse Simulation for Monitoring CO<sub>2</sub> (NISMON-CO<sub>2</sub>) (ver.2022.1), National Institute for  
3028 Environmental Studies Japan [dataset], <https://doi.org/10.17595/20201127.001>, 2020.

3029 Obermeier, W. A., Nabel, J. E. M. S., Loughran, T., Hartung, K., Bastos, A., Havermann, F., Anthoni, P., Arneth, A., Goll,  
3030 D. S., Lienert, S., Lombardozzi, D., Luysaert, S., McGuire, P. C., Melton, J. R., Poulter, B., Sitch, S., Sullivan, M. O., Tian,  
3031 H., Walker, A. P., Wiltshire, A. J., Zaehle, S., and Pongratz, J.: Modelled land use and land cover change emissions – a  
3032 spatio-temporal comparison of different approaches, 12, 635–670, <https://doi.org/10.5194/esd-12-635-2021>, 2021.

3033 O'Rourke, P. R., Smith, S. J., Mott, A., Ahsan, H., McDuffie, E. E., Crippa, M., Klimont, Z., McDonald, B., Wang, S.,  
3034 Nicholson, M. B., Feng, L., and Hoesly, R. M.: CEDS v\_2021\_04\_21 Release Emission Data, Zenodo [dataset],  
3035 <https://doi.org/10.5281/zenodo.4741285>, 2021.

3036 O'Sullivan, M., Zhang, Y., Bellouin, N., Harris, I., Mercado, L. M., Sitch, S., Ciais, P., and Friedlingstein, P.: Aerosol–light  
3037 interactions reduce the carbon budget imbalance, *Environ. Res. Lett.*, 16, 124072, <https://doi.org/10.1088/1748-9326/ac3b77>,  
3038 2021.

3039 O'Sullivan, M., Friedlingstein, P., Sitch, S., Anthoni, P., Arneth, A., Arora, V. K., Bastrikov, V., Delire, C., Goll, D. S., Jain,  
3040 A., Kato, E., Kennedy, D., Knauer, J., Lienert, S., Lombardozzi, D., McGuire, P. C., Melton, J. R., Nabel, J. E. M. S.,  
3041 Pongratz, J., Poulter, B., Séférian, R., Tian, H., Vuichard, N., Walker, A. P., Yuan, W., Yue, X., and Zaehle, S.: Process-  
3042 oriented analysis of dominant sources of uncertainty in the land carbon sink, *Nat. Commun.*, 13, 4781,  
3043 <https://doi.org/10.1038/s41467-022-32416-8>, 2022.

3044 O'Sullivan, M., Spracklen, D. V., Batterman, S. A., Arnold, S. R., Gloor, M., and Buermann, W.: Have Synergies Between  
3045 Nitrogen Deposition and Atmospheric CO<sub>2</sub> Driven the Recent Enhancement of the Terrestrial Carbon Sink?, *Glob.*  
3046 *Biogeochem. Cycles*, 33, 163–180, <https://doi.org/10.1029/2018GB005922>, 2019.

3047 Palmer, P. I., Feng, L., Baker, D., Chevallier, F., Bösch, H., and Somkuti, P.: Net carbon emissions from African biosphere  
3048 dominate pan-tropical atmospheric CO<sub>2</sub> signal, *Nat Commun*, 10, 3344, <https://doi.org/10.1038/s41467-019-11097-w>, 2019.

3049 Pan, Y., Birdsey, R. A., Fang, J., Houghton, R., Kauppi, P. E., Kurz, W. A., Phillips, O. L., Shvidenko, A., Lewis, S. L.,  
3050 Canadell, J. G., Ciais, P., Jackson, R. B., Pacala, S. W., McGuire, A. D., Piao, S., Rautiainen, A., Sitch, S., and Hayes, D.: A

- 3051 Large and Persistent Carbon Sink in the World's Forests, *Science*, 333, 988–993, <https://doi.org/10.1126/science.1201609>,  
3052 2011.
- 3053 Pendrill, F., Persson, U. M., Godar, J., Kastner, T., Moran, D., Schmidt, S., and Wood, R.: Agricultural and forestry trade  
3054 drives large share of tropical deforestation emissions, *Global Environmental Change*, 56, 1–10,  
3055 <https://doi.org/10.1016/j.gloenvcha.2019.03.002>, 2019.
- 3056 Pérez, F. F., Becker, M., Goris, N., Gehlen, M., López-Mozos, M., Tjiputra, J., Olsen, A., Müller, J. D., Huertas, I. E., Chau,  
3057 T. T. T., Cainzos, V., Velo, A., Benard, G., Hauck, J., Gruber, N., and Wanninkhof, R.: An Assessment of CO<sub>2</sub> Storage and  
3058 Sea-Air Fluxes for the Atlantic Ocean and Mediterranean Sea Between 1985 and 2018. *Global Biogeochemical Cycles*,  
3059 38(4), e2023GB007862, <https://doi.org/10.1029/2023GB007862>, 2024.
- 3060 Peters, G. P., Minx, J. C., Weber, C. L., and Edenhofer, O.: Growth in emission transfers via international trade from 1990 to  
3061 2008, *Proceedings of the National Academy of Sciences*, 108, 8903–8908, <https://doi.org/10.1073/pnas.1006388108>, 2011a.
- 3062 Peters, G. P., Marland, G., Le Quéré, C., Boden, T., Canadell, J. G., and Raupach, M. R.: Rapid growth in CO<sub>2</sub> emissions  
3063 after the 2008–2009 global financial crisis, *Nature Clim Change*, 2, 2–4, <https://doi.org/10.1038/nclimate1332>, 2012a.
- 3064 Peters, G. P., Andrew, R. M., Boden, T., Canadell, J. G., Ciais, P., Le Quéré, C., Marland, G., Raupach, M. R., and Wilson,  
3065 C.: The challenge to keep global warming below 2 °C, *Nature Clim Change*, 3, 4–6, <https://doi.org/10.1038/nclimate1783>,  
3066 2013.
- 3067 Peters, G. P., Le Quéré, C., Andrew, R. M., Canadell, J. G., Friedlingstein, P., Ilyina, T., Jackson, R. B., Joos, F.,  
3068 Korsbakken, J. I., McKinley, G. A., Sitch, S., and Tans, P.: Towards real-time verification of CO<sub>2</sub> emissions, *Nature Clim  
3069 Change*, 7, 848–850, <https://doi.org/10.1038/s41558-017-0013-9>, 2017a.
- 3070 Peters, G. P., Andrew, R. M., Canadell, J. G., Fuss, S., Jackson, R. B., Korsbakken, J. I., Le Quéré, C. and Nakicenovic, N.:  
3071 Key indicators to track current progress and future ambition of the Paris Agreement, 7, 118–122,  
3072 <https://doi.org/10.1038/nclimate3202>, 2017b.
- 3073 Peters, G. P., Andrew, R. M., Canadell, J. G., Friedlingstein, P., Jackson, R. B., Korsbakken, J. I., Le Quéré, C., and  
3074 Pregon, A.: Carbon dioxide emissions continue to grow amidst slowly emerging climate policies, *Nat. Clim. Chang.*, 10, 3–  
3075 6, <https://doi.org/10.1038/s41558-019-0659-6>, 2020.
- 3076 Peters, W., Miller, J. B., Whitaker, J., Denning, A. S., Hirsch, A., Krol, M. C., Zupanski, D., Bruhwiler, L., and Tans, P. P.:  
3077 An ensemble data assimilation system to estimate CO<sub>2</sub> surface fluxes from atmospheric trace gas observations, *J. Geophys.  
3078 Res. Atmospheres*, 110, <https://doi.org/10.1029/2005JD006157>, 2005.
- 3079 Petrescu, A. M. R., Peters, G. P., Janssens-Maenhout, G., Ciais, P., Tubiello, F. N., Grassi, G., Nabuurs, G.-J., Leip, A.,  
3080 Carmona-Garcia, G., Winiwarter, W., Höglund-Isaksson, L., Günther, D., Solazzo, E., Kiesow, A., Bastos, A., Pongratz, J.,  
3081 Nabel, J. E. M. S., Conchedda, G., Pilli, R., Andrew, R. M., Schelhaas, M.-J., and Dolman, A. J.: European anthropogenic  
3082 AFOLU greenhouse gas emissions: a review and benchmark data, *Earth Syst. Sci. Data*, 12, 961–1001,  
3083 <https://doi.org/10.5194/essd-12-961-2020>, 2020.
- 3084 Pfeil, B., Olsen, A., Bakker, D. C. E., Hankin, S., Koyuk, H., Kozyr, A., Malczyk, J., Manke, A., Metz, N., Sabine, C. L.,  
3085 Akl, J., Alin, S. R., Bates, N., Bellerby, R. G. J., Borges, A., Boutin, J., Brown, P. J., Cai, W.-J., Chavez, F. P., Chen, A.,

- 3086 Cosca, C., Fassbender, A. J., Feely, R. A., González-Dávila, M., Goyet, C., Hales, B., Hardman-Mountford, N., Heinze, C.,  
3087 Hood, M., Hoppema, M., Hunt, C. W., Hydes, D., Ishii, M., Johannessen, T., Jones, S. D., Key, R. M., Körtzinger, A.,  
3088 Landschützer, P., Lauvset, S. K., Lefèvre, N., Lenton, A., Lourantou, A., Merlivat, L., Midorikawa, T., Mintrop, L.,  
3089 Miyazaki, C., Murata, A., Nakadate, A., Nakano, Y., Nakaoka, S., Nojiri, Y., Omar, A. M., Padin, X. A., Park, G.-H.,  
3090 Paterson, K., Perez, F. F., Pierrot, D., Poisson, A., Ríos, A. F., Santana-Casiano, J. M., Salisbury, J., Sarma, V. V. S. S.,  
3091 Schlitzer, R., Schneider, B., Schuster, U., Sieger, R., Skjelvan, I., Steinhoff, T., Suzuki, T., Takahashi, T., Tedesco, K.,  
3092 Telszewski, M., Thomas, H., Tilbrook, B., Tjiputra, J., Vandemark, D., Veness, T., Wanninkhof, R., Watson, A. J., Weiss,  
3093 R., Wong, C. S., and Yoshikawa-Inoue, H.: A uniform, quality controlled Surface Ocean CO<sub>2</sub> Atlas (SOCAT), *Earth Syst.*  
3094 *Sci. Data*, 5, 125–143, <https://doi.org/10.5194/essd-5-125-2013>, 2013.
- 3095 Piao, S., Ciais, P., Friedlingstein, P., de Noblet-Ducoudré, N., Cadule, P., Viovy, N., and Wang, T.: Spatiotemporal patterns  
3096 of terrestrial carbon cycle during the 20th century, *Global Biogeochem. Cy.*, 23, GB4026,  
3097 <https://doi.org/10.1029/2008GB003339>, 2009.
- 3098 Piao, S., Huang, M., Liu, Z., Wang, X., Ciais, P., Canadell, J. G., Wang, K., Bastos, A., Friedlingstein, P., Houghton, R. A.,  
3099 Le Quéré, C., Liu, Y., Myneni, R. B., Peng, S., Pongratz, J., Sitch, S., Yan, T., Wang, Y., Zhu, Z., Wu, D., and Wang, T.:  
3100 Lower land-use emissions responsible for increased net land carbon sink during the slow warming period, *Nature Geosci.* 11,  
3101 739–743, <https://doi.org/10.1038/s41561-018-0204-7>, 2018.
- 3102 Pongratz, J., Reick, C. H., Houghton, R. A., and House, J. I.: Terminology as a key uncertainty in net land use and land  
3103 cover change carbon flux estimates, *Earth Syst. Dynam.*, 5, 177–195, <https://doi.org/10.5194/esd-5-177-2014>, 2014.
- 3104 Pongratz, J., Smith, S. M., Schwingshackl, C., Dayathilake, L., Gasser, T., Grassi, G. and Pilli, R.: Chapter 7: Current levels  
3105 of CDR. in *The State of Carbon Dioxide Removal 2024 – 2nd Edition*, <https://doi.org/10.17605/OSF.IOZXSKB>, 2024.
- 3106 Poulter, B., Bastos, A., Canadell, J., Ciais, P., Gruber, N., Hauck, J., Jackson, R., Ishii, M., Müller, J., Patra, P., and Tian, H.:  
3107 Inventorying Earth's Land and Ocean Greenhouse Gases, *Eos*, 103, <https://doi.org/10.1029/2022EO179084>, 2022.
- 3108 Poulter, B., Frank, D. C., Hodson, E. L., and Zimmermann, N. E.: Impacts of land cover and climate data selection on  
3109 understanding terrestrial carbon dynamics and the CO<sub>2</sub> airborne fraction, *Biogeosciences*, 8, 2027–2036,  
3110 <https://doi.org/10.5194/bg-8-2027-2011>, 2011.
- 3111 Poulter, B., Freeborn, P. H., Jolly, W. M., and Varner, J. M.: COVID-19 lockdowns drive decline in active fires in  
3112 southeastern United States, *PNAS*, 118, e2105666118, <https://doi.org/10.1073/pnas.2105666118>, 2021.
- 3113 Powis, C. M., Smith, S. M., Minx, J. C., and Gasser, T.: Quantifying global carbon dioxide removal deployment, *Environ.*  
3114 *Res. Lett.*, 18, 024022, <https://doi.org/10.1088/1748-9326/acb450>, 2023.
- 3115 Prentice, I. C., Farquhar, G. D., Fasham, M. J. R., Goulden, M. L., Heimann, M., Jaramillo, V. J., Kheshgi, H. S., Le Quéré,  
3116 C., Scholes, R. J., and Wallace, D. W. R.: The Carbon Cycle and Atmospheric Carbon Dioxide, in *Climate Change 2001:  
3117 The Scientific Basis. Contribution of Working Group I to the Third Assessment Report of the Intergovernmental Panel on  
3118 Climate Change*, edited by: Houghton, J. T., Ding, Y., Griggs, D. J., Noguer, M., van der Linden, P. J., Dai, X., Maskell, K.,  
3119 and Johnson, C. A., Cambridge University Press, Cambridge, United Kingdom and New York, NY, USA, 183–237, ISBN:  
3120 978-0521014953, 2001.

- 3121 Price, J. T. and Warren, R.: Literature Review of the Potential of “Blue Carbon” Activities to Reduce Emissions, available  
3122 at: [https://avoid-net-uk.cc.ic.ac.uk/wp-content/uploads/delightful-downloads/2016/03/Literature-review-of-the-potential-of-](https://avoid-net-uk.cc.ic.ac.uk/wp-content/uploads/delightful-downloads/2016/03/Literature-review-of-the-potential-of-blue-carbon-activities-to-reduce-emissions-AVOID2-WPE2.pdf)  
3123 [blue-carbon-activities-to-reduce-emissions-AVOID2-WPE2.pdf](https://avoid-net-uk.cc.ic.ac.uk/wp-content/uploads/delightful-downloads/2016/03/Literature-review-of-the-potential-of-blue-carbon-activities-to-reduce-emissions-AVOID2-WPE2.pdf), last access: 21 January 2025, 2016.
- 3124 Qin, Y., Xiao, X., Wigneron, J.-P., Ciais, P., Brandt, M., Fan, L., Li, X., Crowell, S., Wu, X., Doughty, R., Zhang, Y., Liu,  
3125 F., Sitch, S., and Moore, B.: Carbon loss from forest degradation exceeds that from deforestation in the Brazilian Amazon,  
3126 *Nat. Clim. Chang.*, 11, 442–448, <https://doi.org/10.1038/s41558-021-01026-5>, 2021.
- 3127 Qin, Z., Zhu, Y., Canadell, J.G., Chen, M., Li, T., Mishra, U. and Yuan, W.: Global spatially explicit carbon emissions from  
3128 land-use change over the past six decades (1961–2020). *One Earth*, 7(5), pp.835-847,  
3129 <https://doi.org/10.1016/j.oneear.2024.04.002>, 2024.
- 3130 Qiu, C., Ciais, P., Zhu, D., Guenet, B., Peng, S., Petrescu, A. M. R., Lauerwald, R., Makowski, D., Gallego-Sala, A. V.,  
3131 Charman, D. J., and Brewer, S. C.: Large historical carbon emissions from cultivated northern peatlands, *Sci. Adv.*, 7,  
3132 eabf1332, <https://doi.org/10.1126/sciadv.abf1332>, 2021.
- 3133 Randerson, J. T., Chen, Y., van der Werf, G. R., Rogers, B. M., and Morton, D. C.: Global burned area and biomass burning  
3134 emissions from small fires: BURNED AREA FROM SMALL FIRES, *J. Geophys. Res. Biogeosciences*, 117, n/a-n/a,  
3135 <https://doi.org/10.1029/2012JG002128>, 2012.
- 3136 Raupach, M. R., Marland, G., Ciais, P., Le Quere, C., Canadell, J. G., Klepper, G., and Field, C. B.: Global and regional  
3137 drivers of accelerating CO<sub>2</sub> emissions, *Proceedings of the National Academy of Sciences*, 104, 10288–10293,  
3138 <https://doi.org/10.1073/pnas.0700609104>, 2007.
- 3139 Regnier, P., Resplandy, L., Najjar, R. G., and Ciais, P.: The land-to-ocean loops of the global carbon cycle, *Nature*, 603,  
3140 401–410, <https://doi.org/10.1038/s41586-021-04339-9>, 2022.
- 3141 Reick, C. H., Gayler, V., Goll, D., Hagemann, S., Heidkamp, M., Nabel, J. E. M. S., Raddatz, T., Roeckner, E., Schnur, R.,  
3142 110 and Wilkenskjeld, S.: JSBACH 3 – The land component of the MPI Earth System Model: documentation of version 3.2,  
3143 available at: <https://doi.org/10.17617/2.3279802>, 2021.
- 3144 Remaud, M., Chevallier, F., Cozic, A., Lin, X., and Bousquet, P.: On the impact of recent developments of the LMDz  
3145 atmospheric general circulation model on the simulation of CO<sub>2</sub> transport, 11, 4489, [https://doi.org/10.5194/gmd-11-4489-](https://doi.org/10.5194/gmd-11-4489-2018)  
3146 2018, 2018.
- 3147 Resplandy, L., Keeling, R. F., Rödenbeck, C., Stephens, B. B., Khatiwala, S., Rodgers, K. B., Long, M. C., Bopp, L., and  
3148 Tans, P. P.: Revision of global carbon fluxes based on a reassessment of oceanic and riverine carbon transport, *Nature*  
3149 *Geosci*, 11, 504–509, <https://doi.org/10.1038/s41561-018-0151-3>, 2018.
- 3150 Resplandy, L., Keeling, R. F., Eddebbar, Y., Brooks, M., Wang, R., Bopp, L., Long, M. C., Dunne, J. P., Koeve, W., and  
3151 Oeschlies, A.: Quantification of ocean heat uptake from changes in atmospheric O<sub>2</sub> and CO<sub>2</sub> composition, *Scientific Reports*,  
3152 9, 20244, <https://doi.org/10.1038/s41598-019-56490-z>, 2019.
- 3153 Rodenbeck, C., Houweling, S., Gloor, M., and Heimann, M.: CO<sub>2</sub> flux history 1982–2001 inferred from atmospheric data  
3154 using a global inversion of atmospheric transport, *Atmos Chem Phys*, 3, 1919–1964, 2003.

- 3155 Rödenbeck, C., Bakker, D. C. E., Metzl, N., Olsen, A., Sabine, C., Cassar, N., Reum, F., Keeling, R. F., and Heimann, M.:  
 3156 Interannual sea–air CO<sub>2</sub> flux variability from an observation-driven ocean mixed-layer scheme, 11, 4599–4613,  
 3157 <https://doi.org/10.5194/bg-11-4599-2014>, 2014.
- 3158 Rödenbeck, C., Zachle, S., Keeling, R., and Heimann, M.: History of El Niño impacts on the global carbon cycle 1957–  
 3159 2017: a quantification from atmospheric CO<sub>2</sub> data, 373, 20170303, <https://doi.org/10.1098/rstb.2017.0303>, 2018.
- 3160 Rödenbeck, C., DeVries, T., Hauck, J., Le Quéré, C., and Keeling, R. F.: Data-based estimates of interannual sea–air CO<sub>2</sub>  
 3161 flux variations 1957–2020 and their relation to environmental drivers, *Biogeosciences*, 19, 2627–2652,  
 3162 <https://doi.org/10.5194/bg-19-2627-2022>, 2022.
- 3163 Rosan, T. M., Klein Goldewijk, K., Ganzenmüller, R., O’Sullivan, M., Pongratz, J., Mercado, L. M., Aragao, L. E. O. C.,  
 3164 Heinrich, V., Randow, C. V., Wiltshire, A., Tubiello, F. N., Bastos, A., Friedlingstein, P., and Sitch, S.: A multi-data  
 3165 assessment of land use and land cover emissions from Brazil during 2000–2019, *Environ. Res. Lett.*, 16, 074004,  
 3166 <https://doi.org/10.1088/1748-9326/ac08c3>, 2021.
- 3167 Sakamoto, K., H. Nakano, S. Urakawa, T. Toyoda, Y. Kawakami, H. Tsujino, G. Yamanaka, 2023: Reference manual for the  
 3168 Meteorological Research Institute Community Ocean Model version 5 (MRI.COMv5), Technical Reports of the  
 3169 Meteorological Research Institute, No.87, <https://doi.org/10.11483/mritechrepo.87>.
- 3170 Sarma, V. V. S. S., Sridevi, B., Metzl, N., Patra, P. K., Lachkar, Z., Chakraborty, K., Goyet, C., Levy, M., Mehari, M., and  
 3171 Chandra, N.: Air-Sea Fluxes of CO<sub>2</sub> in the Indian Ocean Between 1985 and 2018: A Synthesis Based on Observation-Based  
 3172 Surface CO<sub>2</sub>, Hindcast and Atmospheric Inversion Models, *Glob. Biogeochem. Cycles*, 37, e2023GB007694,  
 3173 <https://doi.org/10.1029/2023GB007694>, 2023.
- 3174 Schaphoff, S., von Bloh, W., Rammig, A., Thonicke, K., Biemans, H., Forkel, M., Gerten, D., Heinke, J., Jägermeyr, J.,  
 3175 Knauer, J., Langerwisch, F., Lucht, W., Müller, C., Rolinski, S., and Waha, K.: LPJmL4 – a dynamic global vegetation  
 3176 model with managed land – Part 1: Model description, *Geosci. Model Dev.*, 11, 1343–1375, [https://doi.org/10.5194/gmd-11-](https://doi.org/10.5194/gmd-11-1343-2018)  
 3177 1343-2018, 2018.
- 3178 Schimel, D., Alves, D., Enting, I. G., Heimann, M., Joos, F., Raynaud, D., Wigley, T., Prater, M., Derwent, R., Ehhalt, D.,  
 3179 Fraser, P., Sanhueza, E., Zhou, X., Jonas, P., Charlson, R., Rodhe, H., Sadasivan, S., Shine, K. P., Fouquart, Y.,  
 3180 Ramaswamy, V., Solomon, S., Srinivasan, J., Albritton, D., Derwent, R., Isaksen, I., Lal, M., and Wuebbles, D.: Radiative  
 3181 Forcing of Climate Change, in: *Climate Change 1995: The Science of Climate Change*, Contribution of Working Group I to  
 3182 the Second Assessment Report of the Intergovernmental Panel on Climate Change [Houghton, J. T., Meira Rilho, L. G.,  
 3183 Callander, B. A., Harris, N., Kattenberg, A., and Maskell, K. (eds.)], Cambridge University Press, Cambridge, United  
 3184 Kingdom and New York, NY, USA, ISBN: 978-0521559621, 1995.
- 3185 Schimel, D., Stephens, B. B., and Fisher, J. B.: Effect of increasing CO<sub>2</sub> on the terrestrial carbon cycle, *Proc Natl Acad Sci*  
 3186 USA, 112, 436–441, <https://doi.org/10.1073/pnas.1407302112>, 2015.
- 3187 Schuh, A. E., Jacobson, A. R., Basu, S., Weir, B., Baker, D., Bowman, K., Chevallier, F., Crowell, S., Davis, K. J., Deng, F.,  
 3188 Denning, S., Feng, L., Jones, D., Liu, J., and Palmer, P. I.: Quantifying the Impact of Atmospheric Transport Uncertainty on  
 3189 CO<sub>2</sub> Surface Flux Estimates, *Global Biogeochem. Cycles*, 33, 484–500, <https://doi.org/10.1029/2018GB006086>, 2019.

3190 Schuld, K. N., Mund, J., Aalto, T., Abshire, J. B., Aikin, K., Allen, G., Andrews, A., Apadula, F., Arnold, S., Baier, B.,  
3191 Bakwin, P., Bartyzel, J., Bentz, G., Bergamaschi, P., Beyersdorf, A., Biermann, T., Biraud, S. C., Blanc, P.-E., Boenisch, H.,  
3192 Bowling, D., Brailsford, G., Brand, W. A., Brunner, D., Bui, T. P., Bani, L., Calzolari, F., Chang, C. S., Chen, H., Chen, G.,  
3193 Chmura, L., Clark, S., Climadat, S., Colomb, A., Commane, R., Conen, F., Conil, S., Couret, C., Cristofanelli, P., Cuevas,  
3194 E., Curcoll, R., Daube, B., Davis, K. J., De Mazière, M., De Wekker, S., Dean-Day, J. M., Della Coletta, J., Delmotte, M.,  
3195 Di Iorio, T., DiGangi, E., DiGangi, J. P., Elkins, J. W., Elsasser, M., Emmenegger, L., Fang, S., Fischer, M. L., Forster, G.,  
3196 France, J., Frumau, A., Fuente-Lastra, M., Galkowski, M., Gatti, L. V., Gehrlein, T., Gerbig, C., Gheusi, F., Gloor, E., Goto,  
3197 D., Griffis, T., Hammer, S., Hanisco, T. F., Hanson, C., Haszpra, L., Hatakka, J., Heimann, M., Heliasz, M., Heltai, D.,  
3198 Henne, S., Hensen, A., Hermans, C., Hermansen, O., Hints, E., Hoheisel, A., Holst, J., Iraci, L. T., Ivakhov, V., Jaffe, D.  
3199 A., Jordan, A., Joubert, W., Karion, A., Kawa, S. R., Kazan, V., Keeling, R. F., Keronen, P., Kim, J., Klausen, J., Kneuer, T.,  
3200 Kolari, P., Kominkova, K., Kort, E., Kozlova, E., Krummel, P. B., Kubistin, D., Kulawik, S. S., Kumps, N., Labuschagne,  
3201 C., Lam, D. H., Lan, X., Langenfelds, R. L., Lanza, A., Laurent, O., Laurila, T., Lauvaux, T., Lavric, J., Law, B. E., Lee, J.,  
3202 Lehner, I., Lehtinen, K., Leppert, R., Leskinen, A., Leuenberger, M., Leung, W. H., Levin, I., Levula, J., Lin, J., Lindauer,  
3203 M., Lindroth, A., Loh, Z. M., Lopez, M., Lunder, C. R., Löfvenius, M. O., Machida, T., Mammarella, I., Manca, G.,  
3204 Manning, A., Manning, A., Marek, M. V., Marklund, P., Marrero, J. E., Martin, D., Martin, M. Y., Martins, G. A., Matsueda,  
3205 H., McKain, K., Meijer, H., Meinhardt, F., Merchant, L., Metzger, J.-M., Mihalopoulos, N., Miles, N. L., Miller, J. B.,  
3206 Miller, C. E., Mitchell, L., Monteiro, V., Montzka, S., Moore, F., Moossen, H., Morgan, E., Morgui, J.-A., Morimoto, S.,  
3207 Munger, J. W., Munro, D., Mutuku, M., Myhre, C. L., Mölder, M., Müller-Williams, J., Necki, J., Newman, S., Nichol, S.,  
3208 Nisbet, E., Niwa, Y., Njiru, D. M., Noe, S. M., Nojiri, Y., O'Doherty, S., Obersteiner, F., Paplawsky, B., Parworth, C. L.,  
3209 Peischl, J., Peltola, O., Peters, W., Philippon, C., Piacentino, S., Pichon, J. M., Pickers, P., Piper, S., Pitt, J., Plass-Dülmer,  
3210 C., Platt, S. M., Prinzivalli, S., Ramonet, M., Ramos, R., Reyes-Sanchez, E., Richardson, S. J., Rigoubeau, L.-J., Riris, H.,  
3211 Rivas, P. P., Rothe, M., Roulet, Y.-A., Ryerson, T., Ryoo, J.-M., Sargent, M., Sasakawa, M., Scheeren, B., Schmidt, M.,  
3212 Schuck, T., Schumacher, M., Seibel, J., Seifert, T., Sha, M. K., Shepson, P., Shook, M., Sloop, C. D., Smith, P. D., Spain,  
3213 G., St. Clair, J. M., Steger, D., Steinbacher, M., Stephens, B., Sweeney, C., Sørensen, L. L., Taipale, R., Takatsui, S., Tans,  
3214 P., Thoning, K., Timas, H., Torn, M., Trisolino, P., Turnbull, J., Vermeulen, A., Viner, B., Vitkova, G., Walker, S., Watson,  
3215 A., Weiss, R., Weyrauch, D., Wofsy, S. C., Worsley, J., Worthy, D., Xueref-Remy, I., Yates, E. L., Young, D., Yver-Kwok,  
3216 C., Zaehle, S., Zahn, A., Zellweger, C., Zimnoch, M., de Souza, R. A., di Sarra, A. G., van Dinter, D., and van den Bulk, P.  
3217 (2023) Multi-laboratory compilation of atmospheric carbon dioxide data for the period 1957-2022;  
3218 obspack\_co2\_1\_GLOBALVIEWplus\_v9.0\_2023-09-09; NOAA Earth System Research Laboratory, Global Monitoring  
3219 Laboratory, <http://doi.org/10.25925/20230801>.

3220 Schuld, K. N., Jacobson, A. R., Aalto, T., Andrews, A., Apadula, F., Arnold, S., Bakwin, P., Bartyzel, J., Bergamaschi, P.,  
3221 Biermann, T., Biraud, S. C., Blanc, P.-E., Bani, L., Calzolari, F., Chen, H., Chmura, L., Colomb, A., Condori, L., Conen, F.,  
3222 Conil, S., Couret, C., Cristofanelli, P., Cuevas, E., De Mazière, M., De Wekker, S., Della Coletta, J., Delmotte, M., Di Iorio,  
3223 T., Elsasser, M., Emmenegger, L., Fischer, M. L., Forster, G., Frumau, A., Fuente-Lastra, M., Galkowski, M., Gheusi, F.,  
3224 Hammer, S., Hatakka, J., Heliasz, M., Heltai, D., Hensen, A., Hermans, C., Hermansen, O., Hoheisel, A., Holst, J., Jaffe, D.  
3225 A., Karion, A., Kazan, V., Keronen, P., Kneuer, T., Kolari, P., Kominkova, K., Krummel, P. B., Kubistin, D., Kumps, N.,  
3226 Lan, X., Langenfelds, R. L., Lanza, A., Laurent, O., Laurila, T., Lee, J., Lehner, I., Lehtinen, K., Leskinen, A., Leuenberger,  
3227 M., Levin, I., Levula, J., Lindauer, M., Lindroth, A., Loh, Z. M., Lopez, M., Lunder, C. R., Löfvenius, M. O., Mammarella,  
3228 I., Manca, G., Manning, A., Manning, A., Marek, M. V., Marklund, P., McKain, K., Meijer, H., Meinhardt, F., Metzger, J.-  
3229 M., Miller, C. E., Miller, J. B., Myhre, C. L., Mölder, M., Müller-Williams, J., Necki, J., O'Doherty, S., Peltola, O.,  
3230 Philippon, C., Piacentino, S., Pichon, J. M., Pickers, P., Pitt, J., Plass-Dülmer, C., Platt, S. M., Ramonet, M., Ramos, R.,  
3231 Reyes-Sanchez, E., Rigoubeau, L.-J., Rivas, P. P., Roulet, Y.-A., Scheeren, B., Schmidt, M., Schumacher, M., Sha, M. K.,

- 3232 Sloop, C. D., Smith, P. D., Steger, D., Steinbacher, M., Sweeney, C., Sørensen, L. L., Taipale, R., Tans, P., Thoning, K.,  
3233 Trisolino, P., Turnbull, J., Vermeulen, A., Viner, B., Vitkova, G., Weyrauch, D., Worthy, D., Xueref-Remy, I., Young, D.,  
3234 Yver-Kwok, C., Zimnoch, M., di Sarra, A. G., van Dinter, D., and van den Bulk, P. (2024) Multi-laboratory compilation of  
3235 atmospheric carbon dioxide data for the period 2023-2024; obspack\_co2\_1\_NRT\_v9.2\_2024-03-25; NOAA Earth System  
3236 Research Laboratory, Global Monitoring Laboratory, <http://doi.org/10.25925/20240215>.
- 3237 Schwinger, J., Goris, N., Tjiputra, J. F., Kriest, I., Bentsen, M., Bethke, I., Ilicak, M., Assmann, K. M., and Heinze, C.:  
3238 Evaluation of NorESM-OC (versions 1 and 1.2), the ocean carbon-cycle stand-alone configuration of the Norwegian Earth  
3239 System Model (NorESM1), *Geosci. Model Dev.*, 9, 2589–2622, <https://doi.org/10.5194/gmd-9-2589-2016>, 2016.
- 3240 Schwingshackl, C., Obermeier, W. A., Bultan, S., Grassi, G., Canadell, J. G., Friedlingstein, P., Gasser, T., Houghton, R. A.,  
3241 Kurz, W. A., Sitch, S., and Pongratz, J.: Differences in land-based mitigation estimates reconciled by separating natural and  
3242 land-use CO<sub>2</sub> fluxes at the country level, *One Earth*, 5, 1367–1376, <https://doi.org/10.1016/j.oneear.2022.11.009>, 2022.
- 3243 Séférian, R., Nabat, P., Michou, M., Saint-Martin, D., Voltaire, A., Colin, J., Decharme, B., Delire, C., Berthet, S.,  
3244 Chevallier, M., Sénési, S., Franchisteguy, L., Vial, J., Mallet, M., Joetzjer, E., Geoffroy, O., Guérémy, J.-F., Moine, M.-P.,  
3245 Msadek, R., Ribes, A., Rocher, M., Roehrig, R., Salas-y-Méla, D., Sanchez, E., Terray, L., Valcke, S., Waldman, R.,  
3246 Aumont, O., Bopp, L., Deshayes, J., Éthé, C., and Madec, G.: Evaluation of CNRM Earth System Model, CNRM-ESM2-1:  
3247 Role of Earth System Processes in Present-Day and Future Climate, *Journal of Advances in Modeling Earth Systems*, 11,  
3248 4182–4227, <https://doi.org/10.1029/2019MS001791>, 2019.
- 3249 Seiler, C., Melton, J. R., Arora, V. K., Sitch, S., Friedlingstein, P., Anthoni, P., Goll, D., Jain, A. K., Joetzjer, E., Lienert, S.,  
3250 Lombardozi, D., Luysaert, S., Nabel, J. E. M. S., Tian, H., Vuichard, N., Walker, A. P., Yuan, W., and Zaehle, S.: Are  
3251 Terrestrial Biosphere Models Fit for Simulating the Global Land Carbon Sink?, *J. Adv. Model. Earth Syst.*, 14,  
3252 e2021MS002946, <https://doi.org/10.1029/2021MS002946>, 2022.
- 3253 Sellar, A. A., Jones, C. G., Mulcahy, J. P., Tang, Y., Yool, A., Wiltshire, A., O'Connor, F. M., Stringer, M., Hill, R.,  
3254 Palmieri, J., Woodward, S., Mora, L., Kuhlbrodt, T., Rumbold, S. T., Kelley, D. I., Ellis, R., Johnson, C. E., Walton, J.,  
3255 Abraham, N. L., Andrews, M. B., Andrews, T., Archibald, A. T., Berthou, S., Burke, E., Blockley, E., Carslaw, K., Dalvi,  
3256 M., Edwards, J., Folberth, G. A., Gedney, N., Griffiths, P. T., Harper, A. B., Hendry, M. A., Hewitt, A. J., Johnson, B.,  
3257 Jones, A., Jones, C. D., Keeble, J., Liddicoat, S., Morgenstern, O., Parker, R. J., Predoi, V., Robertson, E., Sahaan, A.,  
3258 Smith, R. S., Swaminathan, R., Woodhouse, M. T., Zeng, G., and Zerroukat, M.: UKESM1: Description and Evaluation of  
3259 the U.K. Earth System Model, *J. Adv. Model. Earth Syst.*, 11, 4513–4558, <https://doi.org/10.1029/2019MS001739>, 2019.
- 3260 Shu, S., Jain, A. K., Koven, C. D., and Mishra, U.: Estimation of Permafrost SOC Stock and Turnover Time Using a Land  
3261 Surface Model With Vertical Heterogeneity of Permafrost Soils, *Global Biogeochem. Cy.*, 34, e2020GB006585,  
3262 <https://doi.org/10.1029/2020GB006585>, 2020.
- 3263 Shutler, J. D., Land, P. E., Piolle, J.-F., Woolf, D. K., Goddijn-Murphy, L., Paul, F., Girard-Ardhuin, F., Chapron, B., and  
3264 Donlon, C. J.: FluxEngine: A Flexible Processing System for Calculating Atmosphere–Ocean Carbon Dioxide Gas Fluxes  
3265 and Climatologies, *J. Atmospheric Ocean. Technol.*, 33, 741–756, <https://doi.org/10.1175/JTECH-D-14-00204.1>, 2016.
- 3266 Silva Junior, C.H., Anderson, L.O., Silva, A.L., Almeida, C.T., Dalagnol, R., Pletsch, M.A., Penha, T.V., Paloschi, R.A. and  
3267 Aragão, L.E.: Fire responses to the 2010 and 2015/2016 Amazonian droughts. *Frontiers in Earth Science*, 7, p.97,  
3268 <https://doi.org/10.3389/feart.2019.00097>, 2019.



- 3269 Sitch, S., Huntingford, C., Gedney, N., Levy, P. E., Lomas, M., Piao, S. L., Betts, R., Ciais, P., Cox, P., Friedlingstein, P.,  
3270 Jones, C. D., Prentice, I. C., and Woodward, F. I.: Evaluation of the terrestrial carbon cycle, future plant geography and  
3271 climate-carbon cycle feedbacks using five Dynamic Global Vegetation Models (DGVMs): Uncertainty In Land Carbon  
3272 Cycle Feedbacks, *Glob. Change Biol.*, 14, 2015–2039, <https://doi.org/10.1111/j.1365-2486.2008.01626.x>, 2008.
- 3273 Sitch, S., O’Sullivan, M., Robertson, E., Friedlingstein, P., Albergel, C., Anthoni, P., Arneeth, A., Arora, V. K., Bastos, A.,  
3274 Bastrikov, V., Bellouin, N., Canadell, J. G., Chini, L., Ciais, P., Falk, S., Harris, I., Hurtt, G., Ito, A., Jain, A. K., Jones, M.  
3275 W., Joos, F., Kato, E., Kennedy, D., Klein Goldewijk, K., Kluzek, E., Knauer, J., Lawrence, P. J., Lombardozzi, D., Melton,  
3276 J. R., Nabel, J. E. M. S., Pan, N., Peylin, P., Pongratz, J., Poulter, B., Rosan, T. M., Sun, Q., Tian, H., Walker, A. P., Weber,  
3277 U., Yuan, W., Yue, X., Zaehle, S.: Trends and Drivers of Terrestrial Sources and Sinks of Carbon Dioxide: An Overview of  
3278 the TRENDY Project, *Global Biogeochemical Cycles*, 38(7), e2024GB008102, <https://doi.org/10.1029/2024GB008102>,  
3279 2024.
- 3280 Smallman, T. L., Milodowski, D. T., Neto, E. S., Koren, G., Ometto, J., and Williams, M.: Parameter uncertainty dominates  
3281 C-cycle forecast errors over most of Brazil for the 21st century, *Earth Syst. Dyn.*, 12, 1191–1237,  
3282 <https://doi.org/10.5194/esd-12-1191-2021>, 2021.
- 3283 Smith, B., Wårlind, D., Arneeth, A., Hickler, T., Leadley, P., Siltberg, J., and Zaehle, S.: Implications of incorporating N  
3284 cycling and N limitations on primary production in an individual-based dynamic vegetation model, *Biogeosciences*, 11,  
3285 2027–2054, <https://doi.org/10.5194/bg-11-2027-2014>, 2014.
- 3286 Smith, S. M., Geden, O., Gidden, M. J., Lamb, W. F., Nemet, G. F., Minx, J. C., Buck, H., Burke, J., Cox, E., Edwards, M.  
3287 R., Fuss, S., Johnstone, I., Müller-Hansen, F., Pongratz, J., Probst, B. S., Roe, S., Schenuit, F., Schulte, I., and Vaughan, N.  
3288 E. The State of Carbon Dioxide Removal 2024 - 2nd Edition, <http://dx.doi.org/10.17605/OSF.IO/F85QJ>, 2024.
- 3289 Sospedra-Alfonso, R., Merryfield, W. J., Boer, G. J., Kharin, V. V., Lee, W.-S., Seiler, C., and Christian, J. R.: Decadal  
3290 climate predictions with the Canadian Earth System Model version 5 (CanESM5), *Geosci. Model Dev.*, 14, 6863–6891,  
3291 <https://doi.org/10.5194/gmd-14-6863-2021>, 2021.
- 3292 Steele, L. P., Dlugokencky, E. J., Lang, P. M., Tans, P. P., Martin, R. C., and Masarie, K. A.: Slowing down of the global  
3293 accumulation of atmospheric methane during the 1980s, *Nature* 358, 313–316, <https://doi.org/10.1038/358313a0>, 1992.
- 3294 Stephens, B. B., Gurney, K. R., Tans, P. P., Sweeney, C., Peters, W., Bruhwiler, L., Ciais, P., Ramonet, M., Bousquet, P.,  
3295 Nakazawa, T., Aoki, S., Machida, T., Inoue, G., Vinnichenko, N., Lloyd, J., Jordan, A., Heimann, M., Shibistova, O.,  
3296 Langenfelds, R. L., Steele, L. P., Francey, R. J., and Denning, A. S.: Weak Northern and Strong Tropical Land Carbon  
3297 Uptake from Vertical Profiles of Atmospheric CO<sub>2</sub>, *Science*, 316, 1732–1735, <https://doi.org/10.1126/science.1137004>,  
3298 2007.
- 3299 Stephens, B. B., Keeling, R. F., Heimann, M., Six, K. D., Murnane, R., and Caldeira, K.: Testing global ocean carbon cycle  
3300 models using measurements of atmospheric O<sub>2</sub> and CO<sub>2</sub> concentration, *Glob. Biogeochem. Cycles*, 12, 213–230,  
3301 <https://doi.org/10.1029/97GB03500>, 1998.
- 3302 Stocker, T., Qin, D., and Platner, G.-K.: *Climate Change 2013: The Physical Science Basis. Contribution of Working Group*  
3303 *I to the Fifth Assessment Report of the Intergovernmental Panel on Climate Change [Intergovernmental Panel on Climate*  
3304 *Change (eds.)]*, Cambridge University Press, Cambridge, ISBN: 9789291691388, 2013.\

- 3305 Swart, N. C., Cole, J. N. S., Kharin, V. V., Lazare, M., Scinocca, J. F., Gillett, N. P., Anstey, J., Arora, V., Christian, J. R.,  
3306 Hanna, S., Jiao, Y., Lee, W. G., Majaess, F., Saenko, O. A., Seiler, C., Seinen, C., Shao, A., Sigmond, M., Solheim, L., von  
3307 Salzen, K., Yang, D., and Winter, B.: The Canadian Earth System Model version 5 (CanESM5.0.3), *Geosci. Model Dev.*, 12,  
3308 4823–4873, <https://doi.org/10.5194/gmd-12-4823-2019>, 2019.
- 3309 SX Coal: Monthly coal consumption estimates, <http://www.sxcoal.com/>, last access: 21 January 2025, 2022.
- 3310 Takahashi, T., Sutherland, S. C., Wanninkhof, R., Sweeney, C., Feely, R. A., Chipman, D. W., Hales, B., Friederich, G.,  
3311 Chavez, F., Sabine, C., Watson, A., Bakker, D. C. E., Schuster, U., Metzl, N., Yoshikawa-Inoue, H., Ishii, M., Midorikawa,  
3312 T., Nojiri, Y., Körtzinger, A., Steinhoff, T., Hoppema, M., Olafsson, J., Arnarson, T. S., Tilbrook, B., Johannessen, T.,  
3313 Olsen, A., Bellerby, R., Wong, C. S., Delille, B., Bates, N. R., and de Baar, H. J. W.: Climatological mean and decadal  
3314 change in surface ocean pCO<sub>2</sub>, and net sea–air CO<sub>2</sub> flux over the global oceans, *Deep Sea Research Part II: Topical Studies*  
3315 *in Oceanography*, 56, 554–577, <https://doi.org/10.1016/j.dsr2.2008.12.009>, 2009.
- 3316 Terhaar, J., Frölicher, T. L., and Joos, F.: Southern Ocean anthropogenic carbon sink constrained by sea surface salinity, *Sci.*  
3317 *Adv.*, 7, eabd5964, <https://doi.org/10.1126/sciadv.abd5964>, 2021.
- 3318 Terhaar, J., Frölicher, T. L., and Joos, F.: Observation-constrained estimates of the global ocean carbon sink from Earth  
3319 system models, *Biogeosciences*, 19, 4431–4457, <https://doi.org/10.5194/bg-19-4431-2022>, 2022.
- 3320 Terhaar, J., Goris, N., Müller, J. D., DeVries, T., Gruber, N., Hauck, J., Perez, F. F., and Séférian, R.: Assessment of Global  
3321 Ocean Biogeochemistry Models for Ocean Carbon Sink Estimates in RECCAP2 and Recommendations for Future Studies.  
3322 *Journal of Advances in Modeling Earth Systems*, 16(3), e2023MS003840, <https://doi.org/10.1029/2023MS003840>, 2024.
- 3323 Tian, H., Xu, X., Lu, C., Liu, M., Ren, W., Chen, G., Melillo, J., and Liu, J.: Net exchanges of CO<sub>2</sub>, CH<sub>4</sub>, and N<sub>2</sub>O between  
3324 China’s terrestrial ecosystems and the atmosphere and their contributions to global climate warming, *J. Geophys. Res.*  
3325 *Biogeosciences*, 116, G02011, <https://doi.org/10.1029/2010JG001393>, 2011.
- 3326 Tian, H., Chen, G., Lu, C., Xu, X., Hayes, D. J., Ren, W., Pan, S., Huntzinger, D. N., and Wofsy, S. C.: North American  
3327 terrestrial CO<sub>2</sub> uptake largely offset by CH<sub>4</sub> and N<sub>2</sub>O emissions: toward a full accounting of the greenhouse gas budget,  
3328 *Climatic Change*, 129, 413–426, <https://doi.org/10.1007/s10584-014-1072-9>, 2015.
- 3329 Tsujino, H., Nakano, H., Sakamoto, K., Urakawa, L.S., Toyama, K., Kosugi, N., Kitamura, Y., Ishii, M., Nishikawa, S.,  
3330 Nishikawa, H., Sugiyama, T., and Ishikawa, Y.: Impact of increased horizontal resolution of an ocean model on carbon  
3331 circulation in the North Pacific Ocean. *Journal of Advances in Modeling Earth Systems*, 16, e2023MS003720,  
3332 <https://doi.org/10.1029/2023MS003720>, 2024.
- 3333 Tubiello, F. N., Conchedda, G., Wanner, N., Federici, S., Rossi, S., and Grassi, G.: Carbon emissions and removals from  
3334 forests: new estimates, 1990–2020, *Earth Syst. Sci. Data*, 13, 1681–1691, <https://doi.org/10.5194/essd-13-1681-2021>, 2021.
- 3335 Tuck, C.: 2022 Mineral Commodity Summary: Iron Ore, Tech. rep., U.S. Geological Survey,  
3336 <https://pubs.usgs.gov/periodicals/mcs2022/mcs2022-iron-ore.pdf>, 2022.
- 3337 UNFCCC: Synthesis report for the technical assessment component of the first global stocktake, available at:  
3338 <https://unfccc.int/documents/461466>, last access: 21 January 2025, 2022.

- 3339 Vale, M. M., Berenguer, E., Argollo de Menezes, M., Viveiros de Castro, E. B., Pugliese de Siqueira, L., and Portela, R. de  
3340 C. Q.: The COVID-19 pandemic as an opportunity to weaken environmental protection in Brazil, *Biological Conservation*,  
3341 255, 108994, <https://doi.org/10.1016/j.biocon.2021.108994>, 2021.
- 3342 van der Laan-Luijkx, I. T., van der Velde, I. R., van der Veen, E., Tsuruta, A., Stanislawski, K., Babenhauserheide, A.,  
3343 Zhang, H. F., Liu, Y., He, W., Chen, H., Masarie, K. A., Krol, M. C., and Peters, W.: The CarbonTracker Data Assimilation  
3344 Shell (CTDAS) v1.0: implementation and global carbon balance 2001–2015, *Geosci. Model Dev.*, 10, 2785–2800,  
3345 <https://doi.org/10.5194/gmd-10-2785-2017>, 2017.
- 3346 van der Velde, I. R., van der Werf, G. R., Houweling, S., Maasackers, J. D., Borsdorff, T., Landgraf, J., Tol, P., van  
3347 Kempen, T. A., van Hees, R., Hoogeveen, R., Veeffkind, J. P., and Aben, I.: Vast CO<sub>2</sub> release from Australian fires in 2019–  
3348 2020 constrained by satellite, *Nature*, 597, 366–369, <https://doi.org/10.1038/s41586-021-03712-y>, 2021.
- 3349 van der Werf, G. R., Randerson, J. T., Giglio, L., Collatz, G. J., Mu, M., Kasibhatla, P. S., Morton, D. C., DeFries, R. S., Jin,  
3350 Y., and van Leeuwen, T. T.: Global fire emissions and the contribution of deforestation, savanna, forest, agricultural, and  
3351 peat fires (1997–2009), *Atmospheric Chem. Phys.*, 10, 11707–11735, <https://doi.org/10.5194/acp-10-11707-2010>, 2010.
- 3352 van der Werf, G. R., Randerson, J. T., Giglio, L., van Leeuwen, T. T., Chen, Y., Rogers, B. M., Mu, M., van Marle, M. J. E.,  
3353 Morton, D. C., Collatz, G. J., Yokelson, R. J., and Kasibhatla, P. S.: Global fire emissions estimates during 1997–2016,  
3354 *Earth Syst. Sci. Data*, 9, 697–720, <https://doi.org/10.5194/essd-9-697-2017>, 2017.
- 3355 van Wees, D., van der Werf, G. R., Randerson, J. T., Andela, N., Chen, Y., and Morton, D. C.: The role of fire in global  
3356 forest loss dynamics, *Glob. Change Biol.*, 27, 2377–2391, <https://doi.org/10.1111/gcb.15591>, 2021.
- 3357 von Bloh, W., Schaphoff, S., Müller, C., Rolinski, S., Waha, K., and Zaehle, S.: Implementing the nitrogen cycle into the  
3358 dynamic global vegetation, hydrology, and crop growth model LPJmL (version 5.0), *Geosci. Model Dev.*, 11, 2789–2812,  
3359 <https://doi.org/10.5194/gmd-11-2789-2018>, 2018.
- 3360 Vaittinada Ayar, P., Bopp, L., Christian, J. R., Ilyina, T., Krasting, J. P., Séférian, R., Tsujino, H., Watanabe, M., Yool, A.,  
3361 and Tjiputra, J.: Contrasting projections of the ENSO-driven CO<sub>2</sub> flux variability in the equatorial Pacific under high-  
3362 warming scenario, *Earth Syst. Dynam.*, 13, 1097–1118, <https://doi.org/10.5194/esd-13-1097-2022>, 2022.
- 3363 Vuichard, N., Messina, P., Luysaert, S., Guenet, B., Zaehle, S., Ghattas, J., Bastrikov, V., and Peylin, P.: Accounting for  
3364 carbon and nitrogen interactions in the global terrestrial ecosystem model ORCHIDEE (trunk version, rev 4999): multi-scale  
3365 evaluation of gross primary production, *Geosci. Model Dev.*, 12, 4751–4779, <https://doi.org/10.5194/gmd-12-4751-2019>,  
3366 2019.
- 3367 Walker, A. P., Quaipe, T., Bodegom, P. M., De Kauwe, M. G., Keenan, T. F., Joiner, J., Lomas, M. R., MacBean, N., Xu, C.,  
3368 Yang, X., and Woodward, F. I.: The impact of alternative trait-scaling hypotheses for the maximum photosynthetic  
3369 carboxylation rate (  $V_{cmax}$  ) on global gross primary production, *New Phytol.*, 215, 1370–1386,  
3370 <https://doi.org/10.1111/nph.14623>, 2017.
- 3371 Walker, A. P., De Kauwe, M. G., Bastos, A., Belmecheri, S., Georgiou, K., Keeling, R. F., McMahon, S. M., Medlyn, B. E.,  
3372 Moore, D. J. P., Norby, R. J., Zaehle, S., Anderson-Teixeira, K. J., Battipaglia, G., Brienen, R. J. W., Cabugao, K. G.,  
3373 Cailleret, M., Campbell, E., Canadell, J. G., Ciais, P., Craig, M. E., Ellsworth, D. S., Farquhar, G. D., Fatichi, S., Fisher, J.  
3374 B., Frank, D. C., Graven, H., Gu, L., Haverd, V., Heilman, K., Heimann, M., Hungate, B. A., Iversen, C. M., Joos, F., Jiang,

- 3375 M., Keenan, T. F., Knauer, J., Körner, C., Leshyk, V. O., Leuzinger, S., Liu, Y., MacBean, N., Malhi, Y., McVicar, T. R.,  
 3376 Penuelas, J., Pongratz, J., Powell, A. S., Riutta, T., Sabot, M. E. B., Schleucher, J., Sitch, S., Smith, W. K., Sulman, B.,  
 3377 Taylor, B., Terrer, C., Torn, M. S., Treseder, K. K., Trugman, A. T., Trumbore, S. E., van Mantgem, P. J., Voelker, S. L.,  
 3378 Whelan, M. E., and Zuidema, P. A.: Integrating the evidence for a terrestrial carbon sink caused by increasing atmospheric  
 3379 CO<sub>2</sub>, *New Phytol.*, 229, 2413–2445, <https://doi.org/10.1111/nph.16866>, 2021.
- 3380 Watanabe, M., Tatebe, H., Koyama, H., Hajima, T., Watanabe, M., and Kawamiya, M.: Importance of El Niño  
 3381 reproducibility for reconstructing historical CO<sub>2</sub> flux variations in the equatorial Pacific, *Ocean Sci.*, 16, 1431–1442,  
 3382 <https://doi.org/10.5194/os-16-1431-2020>, 2020.
- 3383 Watson, A. J., Schuster, U., Shutler, J. D., Holding, T., Ashton, I. G. C., Landschützer, P., Woolf, D. K., and Goddijn-  
 3384 Murphy, L.: Revised estimates of ocean-atmosphere CO<sub>2</sub> flux are consistent with ocean carbon inventory, *Nat Commun*, 11,  
 3385 4422, <https://doi.org/10.1038/s41467-020-18203-3>, 2020.
- 3386 Watson, R. T., Rohde, H., Oeschger, H., and Siegenthaler, U.: Greenhouse Gases and Aerosols, in: *Climate Change: The*  
 3387 *IPCC Scientific Assessment. Intergovernmental Panel on Climate Change (IPCC)*, edited by: Houghton, J. T., Jenkins, G. J.,  
 3388 and Ephraums, J. J., Cambridge University Press, Cambridge, ISBN: 978-0521403603, 1990.
- 3389 Wenzel, S., Cox, P. M., Eyring, V., and Friedlingstein, P.: Projected land photosynthesis constrained by changes in the  
 3390 seasonal cycle of atmospheric CO<sub>2</sub>, *Nature*, 538, 499–501, <https://doi.org/10.1038/nature19772>, 2016.
- 3391 Wilkenskjeld, S., Kloster, S., Pongratz, J., Raddatz, T., and Reick, C. H.: Comparing the influence of net and gross  
 3392 anthropogenic land-use and land-cover changes on the carbon cycle in the MPI-ESM, *Biogeosciences*, 11, 4817–4828,  
 3393 <https://doi.org/10.5194/bg-11-4817-2014>, 2014.
- 3394 Wiltshire, A. J., Burke, E. J., Chadburn, S. E., Jones, C. D., Cox, P. M., Davies-Barnard, T., Friedlingstein, P., Harper, A. B.,  
 3395 Liddicoat, S., Sitch, S., and Zaehle, S.: JULES-CN: a coupled terrestrial carbon–nitrogen scheme (JULES vn5.1), 14, 2161–  
 3396 2186, <https://doi.org/10.5194/gmd-14-2161-2021>, 2021.
- 3397 Winkler, K., Yang, H., Ganzenmüller, R., Fuchs, R., Ceccherini, G., Duveiller, G., Grassi, G., Pongratz, J., Bastos, A.,  
 3398 Shvidenko, A., Araza, A., Herold, M., Wigneron, J.-P., and Ciais, P.: Changes in land use and management led to a decline  
 3399 in Eastern Europe’s terrestrial carbon sink, *Commun. Earth Environ.*, 4, 1–14, <https://doi.org/10.1038/s43247-023-00893-4>,  
 3400 2023.
- 3401 Woodward, F. I. and Lomas, M. R.: Vegetation dynamics – simulating responses to climatic change, *Biol. Rev.*, 79, 643–  
 3402 670, <https://doi.org/10.1017/S1464793103006419>, 2004.
- 3403 Wright, R. M., Le Quéré, C., Buitenhuis, E., Pitois, S., and Gibbons, M. J.: Role of jellyfish in the plankton ecosystem  
 3404 revealed using a global ocean biogeochemical model, 18, 1291–1320, <https://doi.org/10.5194/bg-18-1291-2021>, 2021.
- 3405 Wunder, S., Kaimowitz, D., Jensen, S., and Feder, S.: Coronavirus, macroeconomy, and forests: What likely impacts?, *For.*  
 3406 *Policy Econ.*, 131, 102536, <https://doi.org/10.1016/j.forpol.2021.102536>, 2021.
- 3407 Xi, F., Davis, S. J., Ciais, P., Crawford-Brown, D., Guan, D., Pade, C., Shi, T., Syddall, M., Lv, J., Ji, L., Bing, L., Wang, J.,  
 3408 Wei, W., Yang, K.-H., Lagerblad, B., Galan, I., Andrade, C., Zhang, Y., and Liu, Z.: Substantial global carbon uptake by  
 3409 cement carbonation, *Nature Geosci*, 9, 880–883, <https://doi.org/10.1038/ngeo2840>, 2016.

- 3410 Xia, J., Chen, Y., Liang, S., Liu, D., and Yuan, W.: Global simulations of carbon allocation coefficients for deciduous  
3411 vegetation types, *Tellus B*, 67, 28016, <https://doi.org/10.3402/tellusb.v67.28016>, 2015.
- 3412 Yang, D., Liu, Y., Feng, L., Wang, J., Yao, L., Cai, Z., Zhu, S., Lu, N., and Lyu, D.: The First Global Carbon Dioxide Flux  
3413 Map Derived from TanSat Measurements, *Adv. Atmospheric Sci.*, 38, 1433–1443, [https://doi.org/10.1007/s00376-021-](https://doi.org/10.1007/s00376-021-1179-7)  
3414 1179-7, 2021.
- 3415 Yang, X., Thornton, P., Ricciuto, D., Wang, Y., and Hoffman, F.: Global evaluation of terrestrial biogeochemistry in the  
3416 Energy Exascale Earth System Model (E3SM) and the role of the phosphorus cycle in the historical terrestrial carbon  
3417 balance, *Biogeosciences*, 20, 2813–2836, <https://doi.org/10.5194/bg-20-2813-2023>, 2023.
- 3418 Yu, Z., Ciais, P., Piao, S., Houghton, R. A., Lu, C., Tian, H., Agathokleous, E., Kattel, G. R., Sitch, S., Goll, D., Yue, X.,  
3419 Walker, A., Friedlingstein, P., Jain, A. K., Liu, S., and Zhou, G.: Forest expansion dominates China’s land carbon sink since  
3420 1980, *Nat. Commun.*, 13, 5374, <https://doi.org/10.1038/s41467-022-32961-2>, 2022.
- 3421 Yue, X. and Unger, N.: The Yale Interactive terrestrial Biosphere model version 1.0: description, evaluation and  
3422 implementation into NASA GISS ModelE2, *Geosci. Model Dev.*, 8, 2399–2417, <https://doi.org/10.5194/gmd-8-2399-2015>,  
3423 2015.
- 3424 Yuan, W., Liu, D., Dong, W., Liu, S., Zhou, G., Yu, G., Zhao, T., Feng, J., Ma, Z., Chen, J., Chen, Y., Chen, S., Han, S.,  
3425 Huang, J., Li, L., Liu, H., Liu, S., Ma, M., Wang, Y., Xia, J., Xu, W., Zhang, Q., Zhao, X., and Zhao, L.: Multiyear  
3426 precipitation reduction strongly decreases carbon uptake over northern China, *J. Geophys. Res.-Biogeo.*, 119, 881–896,  
3427 <https://doi.org/10.1002/2014JG002608>, 2014.
- 3428 Yue, C., Ciais, P., Zhu, D., Wang, T., Peng, S. S., and Piao, S. L.: How have past fire disturbances contributed to the current  
3429 carbon balance of boreal ecosystems?, *Biogeosciences*, 13, 675–690, <https://doi.org/10.5194/bg-13-675-2016>, 2016.
- 3430 Zaehle, S. and Friend, A. D.: Carbon and nitrogen cycle dynamics in the O-CN land surface model: 1. Model description,  
3431 site-scale evaluation, and sensitivity to parameter estimates: Site-scale evaluation of a C-N model, *Global Biogeochem.*  
3432 *Cycles*, 24, GB1005, <https://doi.org/10.1029/2009GB003521>, 2010.
- 3433 Zaehle, S., Ciais, P., Friend, A. D., and Prieur, V.: Carbon benefits of anthropogenic reactive nitrogen offset by nitrous oxide  
3434 emissions, *Nature Geosci*, 4, 601–605, <https://doi.org/10.1038/ngeo1207>, 2011.
- 3435 Zaehle, S., Medlyn, B. E., De Kauwe, M. G., Walker, A. P., Dietze, M. C., Hickler, T., Luo, Y., Wang, Y.-P., El-Masri, B.,  
3436 Thornton, P., Jain, A., Wang, S., Warlind, D., Weng, E., Parton, W., Iversen, C. M., Gallet-Budynek, A., McCarthy, H.,  
3437 Finzi, A., Hanson, P. J., Prentice, I. C., Oren, R., and Norby, R. J.: Evaluation of 11 terrestrial carbon–nitrogen cycle models  
3438 against observations from two temperate Free-Air CO<sub>2</sub> Enrichment studies, *New Phytol.*, 202, 803–822,  
3439 <https://doi.org/10.1111/nph.12697>, 2014.
- 3440 Zeng, J., Iida, Y., Matsunaga, T., and Shirai, T.: Surface ocean CO<sub>2</sub> concentration and air-sea flux estimate by machine  
3441 learning with modelled variable trends, *Front. Mar. Sci.*, 9, <https://doi.org/10.3389/fmars.2022.989233>, 2022.
- 3442 Zheng, B., Ciais, P., Chevallier, F., Chuvieco, E., Chen, Y., and Yang, H.: Increasing forest fire emissions despite the  
3443 decline in global burned area, *Sci. Adv.*, 7, eabh2646, <https://doi.org/10.1126/sciadv.abh2646>, 2021.

- 3444 Zou, Y., Wang, Y., Ke, Z., Tian, H., Yang, J., and Liu, Y.: Development of a REgion-Specific Ecosystem Feedback Fire  
3445 (RESFire) Model in the Community Earth System Model, *J. Adv. Model. Earth Syst.*, 11, 417–445,  
3446 <https://doi.org/10.1029/2018MS001368>, 2019.
- 3447 Zscheischler, J., Mahecha, M. D., Avitabile, V., Calle, L., Carvalhais, N., Ciais, P., Gans, F., Gruber, N., Hartmann, J.,  
3448 Herold, M., Ichii, K., Jung, M., Landschützer, P., Laruelle, G. G., Lauerwald, R., Papale, D., Peylin, P., Poulter, B., Ray, D.,  
3449 Regnier, P., Rödenbeck, C., Roman-Cuesta, R. M., Schwalm, C., Tramontana, G., Tyukavina, A., Valentini, R., van der  
3450 Werf, G., West, T. O., Wolf, J. E., and Reichstein, M.: Reviews and syntheses: An empirical spatiotemporal description of  
3451 the global surface–atmosphere carbon fluxes: opportunities and data limitations, *Biogeosciences*, 14, 3685–3703,  
3452 <https://doi.org/10.5194/bg-14-3685-2017>, 2017.

3453 **Tables**

3454 **Table 1.** Factors used to convert carbon in various units (by convention, Unit 1 = Unit 2 × conversion).

Unit 1	Unit 2	Conversion	Source
GtC (gigatonnes of carbon)	ppm (parts per million) (a)	2.124 (b)	Ballantyne et al. (2012)
GtC (gigatonnes of carbon)	PgC (petagrams of carbon)		1 SI unit conversion
GtCO <sub>2</sub> (gigatonnes of carbon dioxide)	GtC (gigatonnes of carbon)	3.664	44.01/12.011 in mass equivalent
(a) Measurements of atmospheric CO <sub>2</sub> concentration have units of dry-air mole fraction. 'ppm' is an abbreviation for micromole/mol, dry air.			
(b) The use of a factor of 2.124 assumes that all the atmosphere is well mixed within one year. In reality, only the troposphere is well mixed and the growth rate of CO <sub>2</sub> concentration in the less well-mixed stratosphere is not measured by sites from the NOAA network. Using a factor of 2.124 makes the approximation that the growth rate of CO <sub>2</sub> concentration in the stratosphere equals that of the troposphere on a yearly basis.			

3455

3456

3457

3458

**Table 2.** How to cite the individual components of the global carbon budget presented here.

<b>Component</b>	<b>Primary reference</b>
Global fossil CO <sub>2</sub> emissions (EFOS), total and by fuel type	Andrew and Peters (2024)
National territorial fossil CO <sub>2</sub> emissions (EFOS)	Hefner and Marland (2023), UNFCCC (2024)
National consumption-based fossil CO <sub>2</sub> emissions (EFOS) by country (consumption)	Peters et al. (2011a) updated as described in this paper
Net land-use change flux (ELUC)	This paper (see Table 4 for individual model references)
Growth rate in atmospheric CO <sub>2</sub> concentration (GATM)	Lan et al. (2024a)
Ocean and land CO <sub>2</sub> sinks (SOCEAN and SLAND)	This paper (see Table 4 for individual model and data products references)

3459

3460



**Table 3.** Main methodological changes in the global carbon budget since 2020. Methodological changes introduced in one year are kept for the following years unless noted. Empty cells mean there were no methodological changes introduced that year. Table S9 lists methodological changes from the first global carbon budget publication up to 2019.

Publication year	Fossil fuel emissions		LUC emissions	Reservoirs			Other changes
	Global	Country (territorial)		Atmosphere	Ocean	Land	
2020	Cement carbonation now included in the EFOS estimate, reducing EFOS by about 0.2GtC yr <sup>-1</sup> for the last decade	India's emissions from Andrew (2020: India); Corrections to Netherland Antilles and Aruba and Soviet emissions before 1950 as per Andrew (2020: CO <sub>2</sub> ); China's coal emissions in 2019 derived from official statistics, emissions now shown for EU27 instead of EU28. Projection for 2020 based on assessment of four approaches.	Average of three bookkeeping models; use of 17 DGVMs. Estimate of gross land use sources and sinks provided	Use of six atmospheric inversions	Based on nine models. River flux revised and partitioned NH, Tropics, SH	Based on 17 models	
Friedlingstein et al. (2020) GCB2020							
2021	Projections are no longer an assessment of four approaches.	Official data included for a number of additional countries, new estimates for South Korea, added emissions from lime production in China.	ELUC estimate compared to the estimates adopted in national GHG inventories		Average of means of eight models and means of seven data-products. Current year prediction of SOCEAN using a feed-forward neural network method	Current year prediction of SLAND using a feed-forward neural network method	
Friedlingstein et al. (2022a) GCB2021							
2022			ELUC provided at country level. Revised components decomposition of ELUC fluxes. Revision of LUC	Use of nine atmospheric inversions	Average of means of ten models and means of seven data-products	Based on 16 models. Revision of LUC maps for Brazil.	
Friedlingstein et al. (2022) GCB2022							

			maps for Brazil. New datasets for peat drainage.				
2023			Refined components decomposition of ELUC. Revision of LUC maps for Indonesia. Use of updated peat drainage estimates.	Use of 14 atmospheric inversions. Additional use of 4 Earth System Models to estimate current year CO2	Additional use of 4 Earth System Models and atmospheric oxygen method to assess SOCEAN. Regional distribution of river flux adjustment revised.	Based on 20 models. Additional use of 4 Earth System Models and atmospheric oxygen method to assess the net atmosphere-land flux.	Inclusion of an estimate of Carbon Dioxide Removal
Friedlingstein et al. (2023) GCB2023							
2024			Fourth bookkeeping estimate (LUCE). Update in land-use data (HYDE3.4) including revision of LUC maps for China. Updated definition of forest (re-)growth fluxes (consistent with 2nd State of CDR Report).	Use of 14 atmospheric inversions models	Use of 10 GOBMs, 8 fCO2-products. Added evaluation for fCO2-products.	Use of 20 DGVMs	
This study	Inclusion of 2024 projections from Carbon Monitor	Inclusion of 2024 projections from Carbon Monitor for China, USA, EU27, India, and Rest of the World					

**Table 4.** References for the process models, bookkeeping models, ocean data products, and atmospheric inversions. All models and products are updated with new data to the end of year 2023.

Model/data name	Reference	Change from Global Carbon Budget 2023 (Friedlingstein et al., 2023)
<b><i>Bookkeeping models for land-use change emissions</i></b>		
BLUE	Hansis et al. (2015)	No change to model, but simulations performed with LUH2-GCB2024 forcing. Update in added peat drainage emissions.
H&C2023	Houghton and Castanho (2023)	No change to model. Data for years after last modelled year (2020) extrapolated based on anomalies in deforestation fires from GFED. Update in added peat drainage emissions.
OSCAR	Gasser et al. (2020)	No change to model, but land-use forcing changed to LUH2-GCB2024 and FRA2020 extrapolated to 2023. Constraining based on GCB2023 data for SLAND over 1960-2022. Update in added peat drainage emissions.
LUCE	Qin et al. (2024)	New model in GCB2024.
<b><i>Dynamic global vegetation models</i></b>		
CABLE-POP	Haverd et al. (2018)	Bug fix applied to land use change calculations enabling variable crop and pasture fractions; corrections to the pre-industrial primary forest fraction in Europe; minor parameter changes
CLASSIC	Melton et al. (2020), Asaadi et al. (2018)	Permeable soil depth reduced to 4 m ; 15 soil layers in the top 4 m permeable soil and 5 bed rock layers from 4 m to 62 m; saturated hydraulic conductivity decreases with depth in the permeable soil layers; transpiration occurs from a partially-wet canopy leaves. These changes yield better runoff seasonality and a more realistic partitioning of precipitation into runoff and evapotranspiration.
CLM6.0	Lawrence et al. (2019)	Updates to surface datasets; improvement of roughness length calculation; updates to snow optical properties and snow thermal conductivity; improved excess ice; improved simulation of burial of vegetation by snow; urban updates, including transient urban, urban properties, and air conditioning; improvements to biomass heat storage; tillage and residue removal; crop phenology and planting dates; improvement to irrigation methods; PFT parameter update.

DLEM	Tian et al. (2015), You et al. (2022)	Incorporate mechanistic representations of dynamic crop growth and development processes, such as crop-specific phenological development, carbon allocation, yield formation, and biological N fixation. Agricultural management practices such as N fertiliser use, irrigation, tillage, manure application, dynamic crop rotation, cover cropping, and genetic improvements are also included (You et al. 2022).
EDv3	Moorcroft et al. (2001), Ma et al. (2022)	Minor bug fixes, updated fire submodule
ELM	Yang et al.(2023), Burrows et al.(2020)	No change
IBIS	Xia et al., (2024)	Improved algorithm of leaf area index
iMAPLE	Yue et al. (2024)	The updated version of YIBs model with dynamic coupling between carbon and water cycles.
ISAM	Jain et al. (2013), Meiyappan et al. (2015), Shu et al. (2020)	Vertically resolved soil biogeochemistry (carbon and nitrogen) module, following Shu et al. (2020),
ISBA-CTrip	Delire et al. (2020)	No change.
JSBACH	Mauritsen et al. (2019), Reick et al. (2021)	Minor bug fixes in post-processing
JULES-ES	Wiltshire et al. (2021), Sellar et al. (2019), Burton et al. (2019)	Minor bug fixes. (Using JULES v7.4)
LPJ-GUESS	Smith et al. (2014)	No change.
LPJml	Schaphoff et al., 2018, von Bloh et al., 2018, Lutz et al., 2019 (tillage), Heinke et al., 2023 (livestock grazing)	No change
LPJwsl	Poulter et al. (2011) (d)	Minor bug fixes, weighting of fire carbon by GFED to simulate annual cycle
LPX-Bern	Lienert and Joos (2018)	No change.
OCN	Zaehle and Friend (2010), Zaehle et al. (2011)	No change.
ORCHIDEEv3	Krinner et al. (2005), Zaehle and Friend (2010), Vuichard et al. (2019)	No change.
SDGVM	Woodward and Lomas (2004), Walker et al. (2017)	Parameter adjustment for reducing evaporation from vegetation that intercepted precipitation, as well as other adjustments to the calculation of evapotranspiration; bug fix in output of monthly NEP, NBP, soilr, and rh; bug fix on cLeaf monthly output; further development on gross land-use transitions, tracking of carbon from wood & crop harvest, and tracking of primary & secondary vegetation.
VISIT	Ito and Inatomi (2012), Kato et al. (2013)	No change.

<b>Intermediate complexity land carbon cycle model</b>		
CARDAMOM	Bloom et al. (2016), Smallman et al. (2021)	No change.
<b>Global ocean biogeochemistry models</b>		
NEMO-PlankTOM12	Wright et al. (2021)	Minor bug fixes, change to salinity restoring and restart file. New atmospheric CO2 input for simulations A and C.
NEMO4.2-PISCES (IPSL)	Aumont et al. (2015)	Switch to the new model version NEMO4.2-PISCES. Update following the new protocol (with 1750 preindustrial CO2 for spin-up). New atmospheric CO2 input for simulations A and C.
MICOM-HAMOCC (NorESM1-OCv1.2)	Schwinger et al. (2016)	No change in model set-up. New atmospheric CO2 file for simulations A and C. Corrected diagnostic output for pco2atm; diagnostic output for sfco2 and spco2 provided at the air-sea interface (not with respect to dry air at 1 atm).
MPIOM-HAMOCC6	Lacroix et al. Global Change Biology 2021	No change; only updated atmosphere CO2 input for A and C experiments and run 1948-2023.
NEMO3.6-PISCESv2-gas (CNRM)	Berthet et al. (2019) S��ferian et al. (2019)	Updated simulations using 1750 preindustrial conditions instead of 1850. No change in model configuration. New atmospheric CO2 input for simulations A and C
FESOM2.1-REcoM3	G�urses et al. (2023)	Updated atmospheric CO2 for simulations A and C.
MOM6-COBALT (Princeton)	Liao et al. (2020)	No change.
CESM-ETHZ	Doney et al. (2009)	Compared to the 2023 submission, the spinup was extended to 1422 years before 1750. Also, starting at 1751 the new atmospheric CO2 concentrations provided by GCB have been used for simulations A and C.
MRI-ESM2-3	Tsujino et al. (2024), Sakamoto et al. (2023)	Iron circulation and its limitation on primary production are introduced. Updated atmospheric CO2 for simulations A and C
ACCESS (CSIRO)	Law et al. (2017)	No change in model set-up (since GCB2023). Updated atmospheric CO2 for simulations A and C.
<b>fCO2-products</b>		
VLIZ-SOMFFN (former MPI-SOM-FFN)	Landsch�tzer et al. (2016)	Time period 1982-2023; The estimate now covers the full open ocean and coastal domain as well as the Arctic Ocean extension by merging 2 MLD proxies for year round full coverage. Additionally, in the SOM step, the Seaflux climatology is now used
Jena-MLS	R�odenbeck et al. (2014) updated to	Time period extended to 2023

	Rödenbeck et al (2022)	
CMEMS-LSCE-FFNNv2	Chau et al. (2022)	Time period now 1985-2023
UEXP-FNN-U (previously Watson et al.)	Watson et al. (2020) and Ford et al. (accepted)	Updated CCI-SST to v3 (Embury et al. 2024), with cool bias with respect to global drifter observations corrected following recommendations in Dong et al. (2022). Updated SOM-FFN implementation to Python.
NIES-ML3	Zeng et al. (2022)	Updated time period 1982-2023.
JMA-MLR	Iida et al. (2021)	Time period extended to 2023
OceanSODA-ETHZv2	Gregor et al. (2024)	Updated method following Gregor et al 2024 and time period extended to 2023
LDEO-HPD	Gloege et al. 2022 and Bennington et al. 2022	Timeperiod extended to 2023
CSIR-ML6	Gregor et al. (2019)	Time period 1982-2023.

### ***Atmospheric inversions***

Jena CarboScope	Rödenbeck et al. (2018), Stephens et al. (2007)	Extension to end of year 2023. Slight change in station set. In the NBE-T inversion, removal of the relaxation term, instead, filtering out decadal variations from air temperature. Adding an additive correction to the result of the NBE-T inversion, to account for CO2 flux IAV not related to air temperature, based on 8 long atmospheric records available near-continuously since at least 1976. TM3 driven by ERA5 rather than NCEP.
CAMS	Chevallier et al. (2005), Remaud et al. (2018)	Extension to year 2023. Increase of the 3D resolution with hexagonal prisms rather than rectangular parallelepipeds (3 times more 3D cells than the previous submission). Update of the prior fluxes.
CarbonTracker Europe (CTE)	van der Laan-Luijkx et al. (2017)	Extension to 2023, update of prior fluxes.
NISMON-CO2	Niwa et al. (2022), Niwa et al. (2017).	Extension to 2023, update of prior fluxes.
CT-NOAA	Jacobson et al. (2023a), Jacobson et al. (2024), Byrne et al. (2023), Krol et al. (2005), Peiro et al. (2022)	Extended to 2023 using the CarbonTracker Near-Real Time release CT-NRT.v2024-1 (Jacobson et al. 2024).
CMS-Flux	Liu et al. (2021)	Extension to 2023, update of prior fluxes.
CAMS-Satellite	Chevallier et al. (2005), Remaud et al. (2018)	Extension to year 2023. Increase of the 3D resolution with hexagonal prisms rather than rectangular parallelepipeds (3 times more 3D cells than the previous submission). Update of the prior fluxes.

GONGGA	Jin et al. (2023), Nassar et al. (2010)	Extension to 2023, update of prior fluxes.
COLA	Liu et al. (2022)	Extension to 2023, update of prior fluxes.
GCASv2	Jiang et al. (2021) & Emmons et al. (2010)	Extension to 2023, update of prior fluxes.
UoE in-situ	Feng et al. (2016) & Palmer et al. (2019)	Extension to 2023, update of prior fluxes.
IAPCAS	Yang et al. (2021) & Feng et al. (2016)	Extension to 2023, update of prior fluxes.
MIROC4-ACTM	Chandra et al. (2022) & Patra et al. (2018)	Extension to 2023, update of prior fluxes using only CASA and not VISIT. Less observation sites used in the assimilation (46 instead of 50).
NTFVAR	Nayagam et al. (2024) & Maksyutov et al. (2021)	New this year
<b>Earth System Models</b>		
CanESM5	Swart et al. (2019), Sospedra-Alfonso et al. (2021)	Reconstructions are extended to 1960-2023, and predictions are extended to 2024.
EC-Earth3-CC	Döscher et al. (2021), Bilbao et al. (2021), Bernardello et al. (2024)	New this year.
IPSL-CM6A-CO2-LR	Boucher et al. (2020)	Reconstructions are extended to 1960-2023, and predictions are extended to 2024. No change to model, the CMIP6 CovidMIP CO2 emissions after 2015 are used.
MIROC-ES2L	Watanabe et al. (2020)	Reconstructions are extended to 1960-2023, and predictions are extended to 2024. No change to model, the simulations were rerun including a long spinup.
MPI-ESM1-2-LR	Mauritsen et al. (2019), Li et al. (2023)	Reconstructions are extended to 1960-2023, and predictions are extended to 2024.

**Table 5.** Comparison of results from the bookkeeping method and budget residuals with results from the DGVMs, as well as additional estimates from atmospheric oxygen, atmospheric inversions and Earth System Models (ESMs) for different periods, the last decade, and the last year available. All values are in GtCyr<sup>-1</sup>. See Figure 7 for explanation of the bookkeeping component fluxes. The DGVM uncertainties represent  $\pm 1\sigma$  of the decadal or annual (for 2023) estimates from the individual DGVMs: for the inverse systems the mean and range of available results is given. All values are rounded to the nearest 0.1 GtC and therefore columns do not necessarily add to zero.

		<i>Mean (GtC/yr)</i>						
		1960s	1970s	1980s	1990s	2000s	2014-2023	2023
Land-use change emissions (ELUC)	Bookkeeping (BK) Net flux (1a)	1.6±0.7	1.4±0.7	1.4±0.7	1.6±0.7	1.4±0.7	1.1±0.7	1±0.7
	BK - deforestation (total)	1.7 [1.3,2.2]	1.6 [1.2,2]	1.6 [1.3,1.9]	1.8 [1.6,2]	1.9 [1.6,2.2]	1.7 [1.4,2.3]	1.7 [1.3,2.3]
	BK - forest regrowth (total)	-0.8 [-1.1,-0.6]	-0.9 [-1.1,-0.7]	-0.9 [-1,-0.7]	-0.9 [-1.1,-0.8]	-1.1 [-1.2,-0.9]	-1.2 [-1.5,-0.9]	-1.2 [-1.5,-0.9]
	BK - other transitions	0.3 [0.3,0.4]	0.2 [0.2,0.3]	0.2 [0.1,0.3]	0.1 [0,0.2]	0.1 [0,0.1]	0.1 [0,0.1]	0 [0,0.1]
	BK - peat drainage & peat fires	0.2 [0.1,0.2]	0.2 [0.1,0.2]	0.2 [0.2,0.2]	0.3 [0.2,0.3]	0.2 [0.2,0.3]	0.2 [0.2,0.3]	0.2 [0.2,0.3]
	BK - wood harvest & forest management	0.2 [-0.2,0.6]	0.3 [-0.2,0.6]	0.3 [-0.2,0.7]	0.3 [-0.1,0.6]	0.3 [-0.1,0.6]	0.3 [0,0.6]	0.3 [0,0.7]
	DGVMs-net flux (1b)	1.5±0.5	1.5±0.5	1.5±0.5	1.7±0.5	1.7±0.6	1.5±0.6	1.2±0.7
Terrestrial sink (SLAND)	Residual sink from global budget (E <sub>FOS</sub> +E <sub>ELUC</sub> (1a)-G <sub>ATM</sub> -S <sub>OCEAN</sub> ) (2a)	1.7±0.8	1.9±0.8	1.6±0.9	2.6±0.9	2.8±0.9	2.7±0.9	2.3±1
	DGVMs (2b)	1.2±0.5	2±0.8	1.8±0.8	2.5±0.6	2.8±0.7	3.2±0.9	2.3±1
Net land fluxes (SLAND-ELUC)	GCB2024 Budget (2b-1a)	-0.4±0.9	0.5±1.1	0.4±1.1	0.9±0.9	1.4±1	2.1±1.1	1.3±1.2
	Atmospheric O <sub>2</sub>	---	---	---	1.3±0.7	1±0.7	1±0.8	-
	DGVMs-net (2b-1b)	-0.3±0.5	0.5±0.7	0.3±0.6	0.8±0.4	1.1±0.4	1.7±0.6	1.1±0.8
	Inversions*	- [-,-]	- [-,-]	0.3 [0.3,0.4] (2)	0.9 [0.6,1.1] (3)	1.2 [0.6,1.5] (4)	1.4 [0.3,2.2] (10)	0.9 [-0.1,-2.7] (14)
	ESMs	0 [-0.7,0.5]	1.5 [1.2,2]	1 [0.5,1.4]	1.7 [1.2,2.4]	1.8 [0.4,2.7]	2.2 [0.3,3.6]	1.8 [-2.9,-3.7]

\*Estimates are adjusted for the pre-industrial influence of river fluxes, for the cement carbonation sink, and adjusted to common EFOS (Sect. 2.7). The ranges given include varying numbers (in parentheses) of inversions in each decade (Table A4)



**Table 6:** Comparison of results for the ocean sink from the  $f\text{CO}_2$ -products, from global ocean biogeochemistry models (GOBMs), the best estimate for GCB2024 as calculated from  $f\text{CO}_2$ -products and GOBMs that is used in the budget Table 7, as well as additional estimates from atmospheric oxygen, atmospheric inversions and Earth System Models (ESMs) for different periods, the last decade, and the last year available. All values are in  $\text{GtCyr}^{-1}$ . Uncertainties represent  $\pm 1\sigma$  of the estimates from the GOBMs ( $N > 10$ ) and range of ensemble members is given for ensembles with  $N < 10$  ( $f\text{CO}_2$ -products, inversions, ESMs). The uncertainty of the GCB2024 budget estimate is based on expert judgement (Section 2 and Supplementary S1 to S4) and for oxygen it is the standard deviation of a Monte Carlo ensemble (Section 2.8).

<i>Mean (GtC/yr)</i>							
Product	1960s	1970s	1980s	1990s	2000s	2014-2023	2023
$f\text{CO}_2$ -products	---	---	---	2.3 [1.9,2.9]	2.5 [2.3,2.7]	3.1 [2.9,3.7]	3 [2.3,4]
GOBMs	1 $\pm$ 0.2	1.3 $\pm$ 0.3	1.8 $\pm$ 0.3	2 $\pm$ 0.3	2.2 $\pm$ 0.3	2.6 $\pm$ 0.4	2.7 $\pm$ 0.4
GCB2024 Budget	1.2 $\pm$ 0.4	1.5 $\pm$ 0.4	1.9 $\pm$ 0.4	2.1 $\pm$ 0.4	2.3 $\pm$ 0.4	2.9 $\pm$ 0.4	2.9 $\pm$ 0.4
Atmospheric O <sub>2</sub>	---	---	---	2 $\pm$ 0.5	2.8 $\pm$ 0.4	3.4 $\pm$ 0.5	-
Inversions	- [-,-]	- [-,-]	1.8 [1.8,1.9] (2)	2.3 [2.1,2.5] (3)	2.5 [2.3,3.1] (4)	3.1 [2.4,4.1] (10)	3 [1.8-4.1] (14)
ESMs	0.7 [0.1,1.1]	1 [0.4,1.4]	1.4 [0.7,1.7]	1.7 [1.1,2.2]	1.9 [1.5,2.2]	2.5 [2.2,2.8]	2.5 [2.2-3]

b.

**Table 7:** Decadal mean in the five components of the anthropogenic CO<sub>2</sub> budget for different periods, and last year available. All values are in GtC yr<sup>-1</sup>, and uncertainties are reported as  $\pm 1\sigma$ . Fossil CO<sub>2</sub> emissions include cement carbonation. The table also shows the budget imbalance (B<sub>IM</sub>), which provides a measure of the discrepancies among the nearly independent estimates. A positive imbalance means the emissions are overestimated and/or the sinks are too small. All values are rounded to the nearest 0.1 GtC and therefore columns do not necessarily add to zero.

		<i>Mean (GtC/yr)</i>							
		1960s	1970s	1980s	1990s	2000s	2014-2023	2023	2024 (Projection)
Total emissions (EFOS + ELUC)	Fossil CO <sub>2</sub> emissions (EFOS)*	3±0.2	4.7±0.2	5.5±0.3	6.4±0.3	7.8±0.4	9.7±0.5	10.1±0.5	10.2±0.5
	Land-use change emissions (ELUC)	1.6±0.7	1.4±0.7	1.4±0.7	1.6±0.7	1.4±0.7	1.1±0.7	1±0.7	1.2±0.7
	Total emissions	4.6±0.7	6.1±0.7	6.9±0.8	7.9±0.8	9.2±0.8	10.8±0.9	11.1±0.9	11.4±0.9
Partitioning	Growth rate in atmospheric CO <sub>2</sub> (GATM)	1.7±0.07	2.8±0.07	3.4±0.02	3.1±0.02	4±0.02	5.2±0.02	5.9±0.2	6.0±0.3
	Ocean sink (SOCEAN)	1.2±0.4	1.5±0.4	1.9±0.4	2.1±0.4	2.3±0.4	2.9±0.4	2.9±0.4	3±0.6
	Terrestrial sink (SLAND)	1.2±0.5	2±0.8	1.8±0.8	2.5±0.6	2.8±0.7	3.2±0.9	2.3±1	3.2±1.5
Budget Imbalance	BIM=E FOS+E LUC-(GATM +SOCE)	0.5	-0.1	-0.2	0.1	0	-0.4	0	-0.9

	1960s	1970s	1980s	1990s	2000s	2014-2023	2023	2024 (Projection)
AN+SL AND)								

\*Fossil emissions excluding the cement carbonation sink amount to  $3\pm 0.2$  GtC/yr,  $4.7\pm 0.2$  GtC/yr,  $5.5\pm 0.3$  GtC/yr,  $6.4\pm 0.3$  GtC/yr,  $7.9\pm 0.4$  GtC/yr, and  $9.9\pm 0.5$  GtC/yr for the decades 1960s to 2010s respectively and to  $10.3\pm 0.5$  GtC/yr for 2023, and  $10.4\pm 0.5$  GtC/yr for 2024.

**Table 8.** Cumulative CO<sub>2</sub> for different time periods in gigatonnes of carbon (GtC). Fossil CO<sub>2</sub> emissions include cement carbonation. The budget imbalance (BIM) provides a measure of the discrepancies among the nearly independent estimates. All values are rounded to the nearest 5 GtC and therefore columns do not necessarily add to zero. Uncertainties are reported as follows: E<sub>FOS</sub> is 5% of cumulative emissions; E<sub>LUC</sub> prior to 1959 is 1 $\sigma$  spread from the DGVMs, E<sub>LUC</sub> post-1959 is 0.7\*number of years (where 0.7 GtC/yr is the uncertainty on the annual E<sub>LUC</sub> flux estimate); G<sub>ATM</sub> uncertainty is held constant at 5 GtC for all time periods; S<sub>OCEAN</sub> uncertainty is 20% of the cumulative sink (20% relates to the annual uncertainty of 0.4 GtC/yr, which is ~20% of the current ocean sink); and S<sub>LAND</sub> is the 1 $\sigma$  spread from the DGVMs estimates.

		1750-2023	1850-2014	1850-2023	1960-2023	1850-2024
Emissions	Fossil CO <sub>2</sub> emissions (EFOS)	490±25	400±20	490±25	410±20	500±25
	Land-use change emissions (ELUC)	255±75	215±60	225±65	90±45	225±65
	Total emissions	745±80	615±65	710±70	500±50	725±70
Partitioning	Growth rate in atmos CO <sub>2</sub> (G <sub>ATM</sub> )	305±5	235±5	285±5	220±5	290±5
	Ocean sink (S <sub>OCEAN</sub> )	195±40	160±30	185±35	130±25	185±35
	Terrestrial sink (S <sub>LAND</sub> )	245±65	190±55	220±60	150±40	225±60
Budget imbalance	BIM=EFOS+ELUC-(G <sub>ATM</sub> +S <sub>OCEAN</sub> +S <sub>LAND</sub> )	0	30	25	0	20

**Table 9.** Average annual growth rate in fossil CO<sub>2</sub> emissions over the most recent decade (2014-2023) and the previous decade (2004-2013). The data for the World include the cement carbonation sink. IAS are emissions from international aviation and shipping. Rest of the World is World minus China, USA, EU27, India and IAS..

	World	China	USA	EU27	India	OECD	Non-OECD	IAS	Rest of the World
2004-2013	2.4%	7.5%	-1.4%	-1.8%	6.4%	-0.9%	4.9%	2.6%	1.9%
2014-2023	0.6%	1.9%	-1.2%	-2.1%	3.6%	-1.4%	1.8%	-1.6%	0.4%

**Table 10.** Major known sources of uncertainties in each component of the Global Carbon Budget, defined as input data or processes that have a demonstrated effect of at least  $\pm 0.3$  GtC yr<sup>-1</sup>.

Source of uncertainty	Time scale (years)	Location	Evidence
<b>Fossil CO<sub>2</sub> emissions (EFOS; Section 2.1)</b>			
energy statistics	annual to decadal	global, but mainly China & major developing countries	(Korsbakken et al., 2016, Guan et al., 2012)
carbon content of coal	annual to decadal	global, but mainly China & major developing countries	(Liu et al., 2015)
system boundary	annual to decadal	all countries	(Andrew, 2020a)
<b>Net land-use change flux (ELUC; section 2.2)</b>			
land-cover and land-use change statistics	continuous	global; in particular tropics	(Houghton et al., 2012, Gasser et al., 2020, Ganzenmüller et al., 2022, Yu et al. 2022)
sub-grid-scale transitions	annual to decadal	global	(Wilkenskjeld et al., 2014, Bastos et al., 2021)
vegetation biomass	annual to decadal	global; in particular tropics	(Houghton et al., 2012, Bastos et al., 2021)
forest degradation (fire, selective logging)	annual to decadal	tropics; Amazon	(Aragão et al., 2018, Qin et al., 2021, Lapola et al., 2023)
wood and crop harvest	annual to decadal	global; SE Asia	(Arneth et al., 2017, Erb et al., 2018)
peat burning	multi-decadal trend	global	(van der Werf et al., 2010, 2017)

loss of additional sink capacity	multi-decadal trend	global	(Pongratz et al., 2014, Gasser et al., 2020; Obermeier et al., 2021; Dorgeist et al., 2024)
environmental effects	multi-decadal trend	global	(Gasser et al. 2020, Dorgeist et al., 2024)
Atmospheric growth rate (GATM; section 2.4) no demonstrated uncertainties larger than $\pm 0.3$ GtC yr <sup>-1</sup> . The uncertainties in GATM have been estimated as $\pm 0.2$ GtC yr <sup>-1</sup> , although the conversion of the growth rate into a global annual flux assuming instantaneous mixing throughout the atmosphere introduces additional errors that have not yet been quantified.			
Ocean sink (SOCEAN; section 2.5)			
sparsity in surface fCO <sub>2</sub> observations	mean, decadal variability and trend	global, in particular southern hemisphere	(Gloege et al., 2021, Denvil-Sommer et al., 2021, Hauck et al., 2023a; Dong et al., 2024b)
riverine carbon outgassing and its anthropogenic perturbation	annual to decadal	global, in particular partitioning between Tropics and South	(Aumont et al., 2001, Lacroix et al., 2020, Crisp et al., 2022)
Models underestimate interior ocean anthropogenic carbon storage	annual to decadal	global	(Friedlingstein et al., 2022a, this study, DeVries et al., 2023, Müller et al., 2023)
near-surface temperature and salinity gradients	mean on all time-scales	global	(Watson et al., 2020, Dong et al., 2022, Bellenger et al., 2023, Dong et al., 2024a)
Land sink (SLAND; section 2.6)			
strength of CO <sub>2</sub> fertilisation	multi-decadal trend	global	(Wenzel et al., 2016; Walker et al., 2021)
response to variability in temperature and rainfall	annual to decadal	global; in particular tropics	(Cox et al., 2013; Jung et al., 2017; Humphrey et al., 2018; 2021)
nutrient limitation and supply	annual to decadal	global	(Zaehle et al., 2014)
carbon allocation and tissue	annual to decadal	global	(De Kauwe et al., 2014; O'Sullivan et al., 2022)

turnover rates			
tree mortality	annual	global in particular tropics	(Hubau et al., 2021; Brienen et al., 2020)
response to diffuse radiation	annual	global	(Mercado et al., 2009; O'Sullivan et al., 2021)
estimation under constant pre-industrial land cover	multi-decadal trend	global	(Gasser et al. 2020, Dorgeist et al., 2024)

## Figures

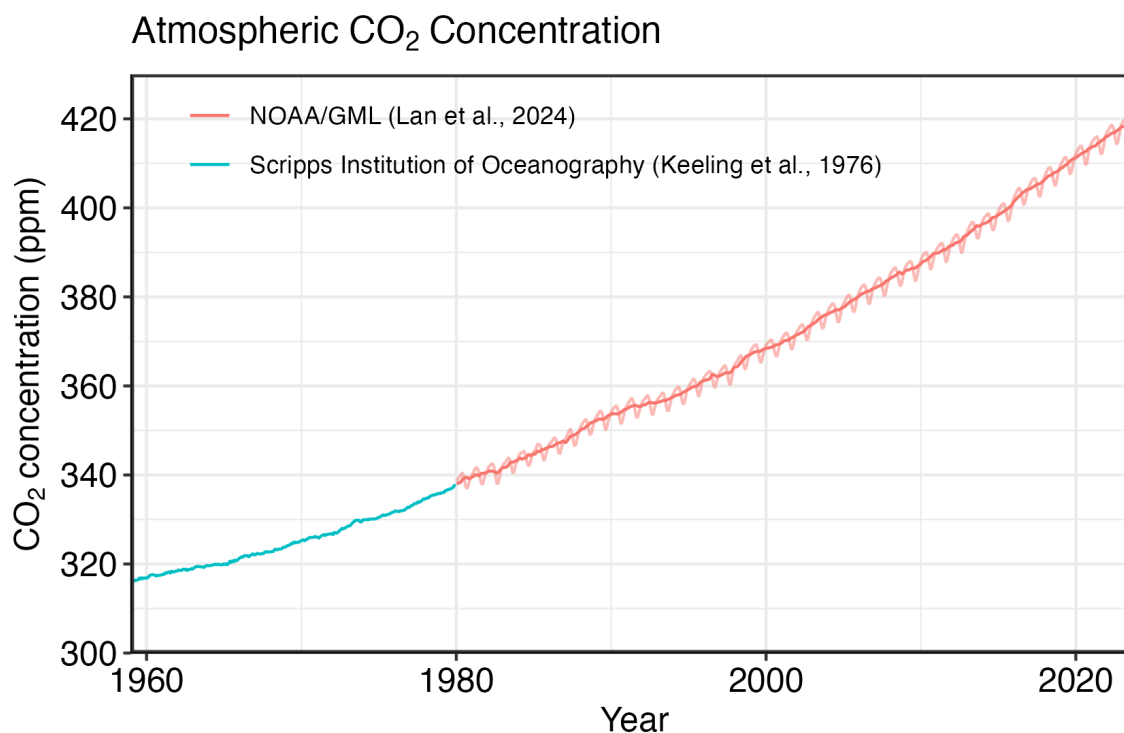


**Figure 1.** Surface average atmospheric CO<sub>2</sub> concentration (ppm). Since 1980, monthly data are from NOAA/GML (Lan et al., 2024a) and are based on an average of direct atmospheric CO<sub>2</sub> measurements from multiple stations in the marine boundary layer (Masarie and Tans, 1995). The 1958-1979 monthly data are from the Scripps Institution of Oceanography, based on an average of direct atmospheric CO<sub>2</sub> measurements from the Mauna Loa and South Pole stations (Keeling et al., 1976). To account for the difference of mean CO<sub>2</sub> and seasonality between the NOAA/GML and the Scripps station networks used here, the Scripps surface average (from two stations) was de-seasonalised and adjusted to match the NOAA/GML surface average (from multiple stations) by adding the mean difference of 0.667 ppm, calculated here from overlapping data during 1980-2012.



# The global carbon cycle

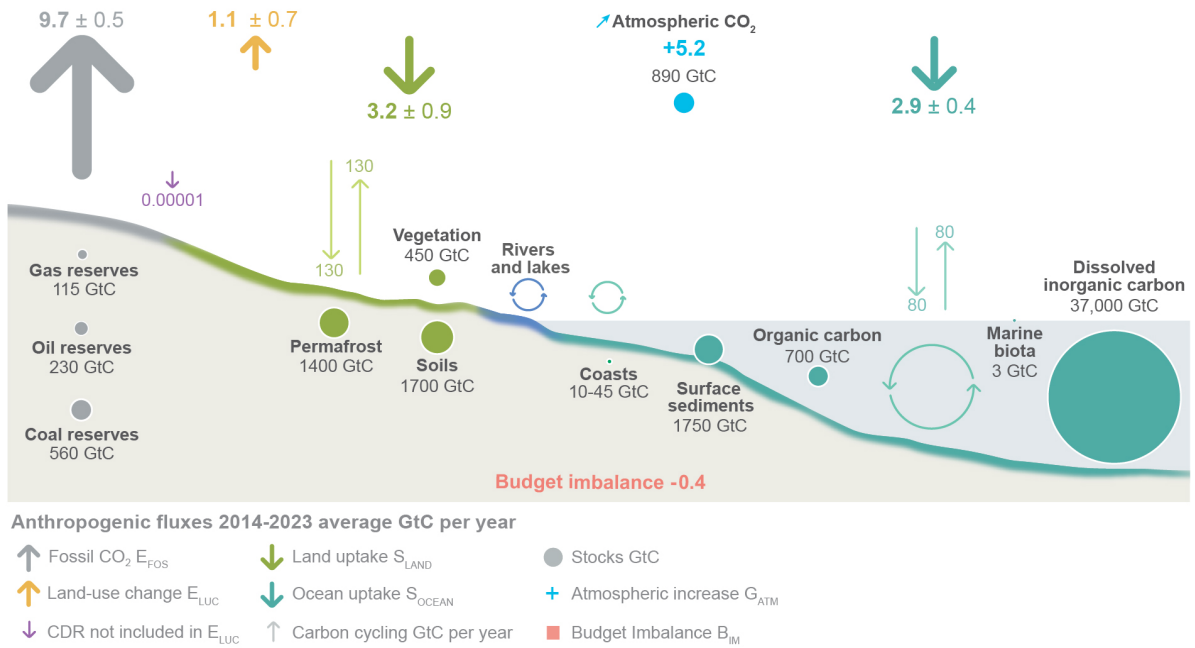


**Figure 2.** Schematic representation of the overall perturbation of the global carbon cycle caused by anthropogenic activities, averaged globally for the decade 2014-2023. See legends for the corresponding arrows. Fluxes estimates and their 1 standard deviation uncertainty are as reported in Table 7. The CDR estimate is for the year 2023 only. The uncertainty in the atmospheric CO<sub>2</sub> growth rate is very small ( $\pm 0.02$  GtC yr<sup>-1</sup>) and is neglected for the figure. The anthropogenic perturbation occurs on top of an active carbon cycle, with fluxes and stocks represented in the background and taken from Canadell et al. (2021) for all numbers, except for the carbon stocks in coasts which is from a literature review of coastal marine sediments (Price and Warren, 2016). Fluxes are in GtC yr<sup>-1</sup> and reservoirs in GtC.

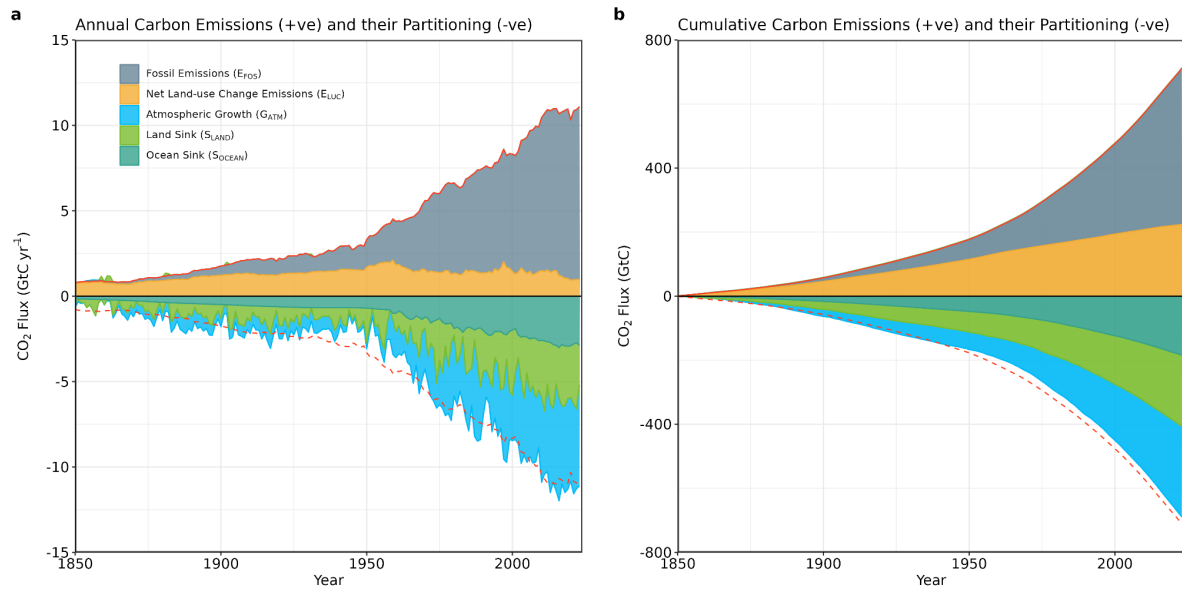


**Figure 3.** Combined components of the global carbon budget as a function of time, for fossil CO<sub>2</sub> emissions (E<sub>FOS</sub>, including a small sink from cement carbonation; grey) and emissions from land-use change (E<sub>LUC</sub>; brown), as well as their partitioning among the atmosphere (G<sub>ATM</sub>; cyan), ocean (S<sub>OCEAN</sub>; blue), and land (S<sub>LAND</sub>; green). Panel (a) shows annual estimates of each flux (in GtC yr<sup>-1</sup>) and panel (b) the cumulative flux (the sum of all prior annual fluxes, in GtC) since the year 1850. The partitioning is based on nearly independent estimates from observations (for G<sub>ATM</sub>) and from process model ensembles constrained by data (for S<sub>OCEAN</sub> and S<sub>LAND</sub>) and does not exactly add up to the sum of the emissions, resulting in a budget imbalance (B<sub>IM</sub>) which is represented by the difference between the bottom red line (mirroring total emissions) and the sum of carbon fluxes in the ocean, land, and atmosphere reservoirs. All data are in GtC yr<sup>-1</sup> (panel a) and GtC (panel b). The E<sub>FOS</sub> estimate is based on a mosaic of different datasets, and has an uncertainty of  $\pm 5\%$  ( $\pm 1\sigma$ ). The E<sub>LUC</sub> estimate is from four bookkeeping models (Table 4) with uncertainty of  $\pm 0.7$  GtC yr<sup>-1</sup>. The G<sub>ATM</sub> estimates prior to 1959 are from Joos and Spahni (2008) with uncertainties equivalent to about  $\pm 0.1$ - $0.15$  GtC yr<sup>-1</sup> and from Lan et al. (2024a) since 1959 with uncertainties of about  $\pm 0.07$  GtC yr<sup>-1</sup> during 1959-1979 and  $\pm 0.02$  GtC yr<sup>-1</sup> since 1980. The S<sub>OCEAN</sub> estimate is the average from Khatiwala et al. (2013) and DeVries (2014) with uncertainty of about  $\pm 30\%$  prior to 1959, and the average of an ensemble of models and an ensemble of fCO<sub>2</sub>-products (Table 4) with uncertainties of about  $\pm 0.4$  GtC yr<sup>-1</sup> since 1959. The S<sub>LAND</sub> estimate is the average of an ensemble of models (Table 4) with uncertainties of about  $\pm 1$  GtC yr<sup>-1</sup>. See the text for more details of each component and their uncertainties.

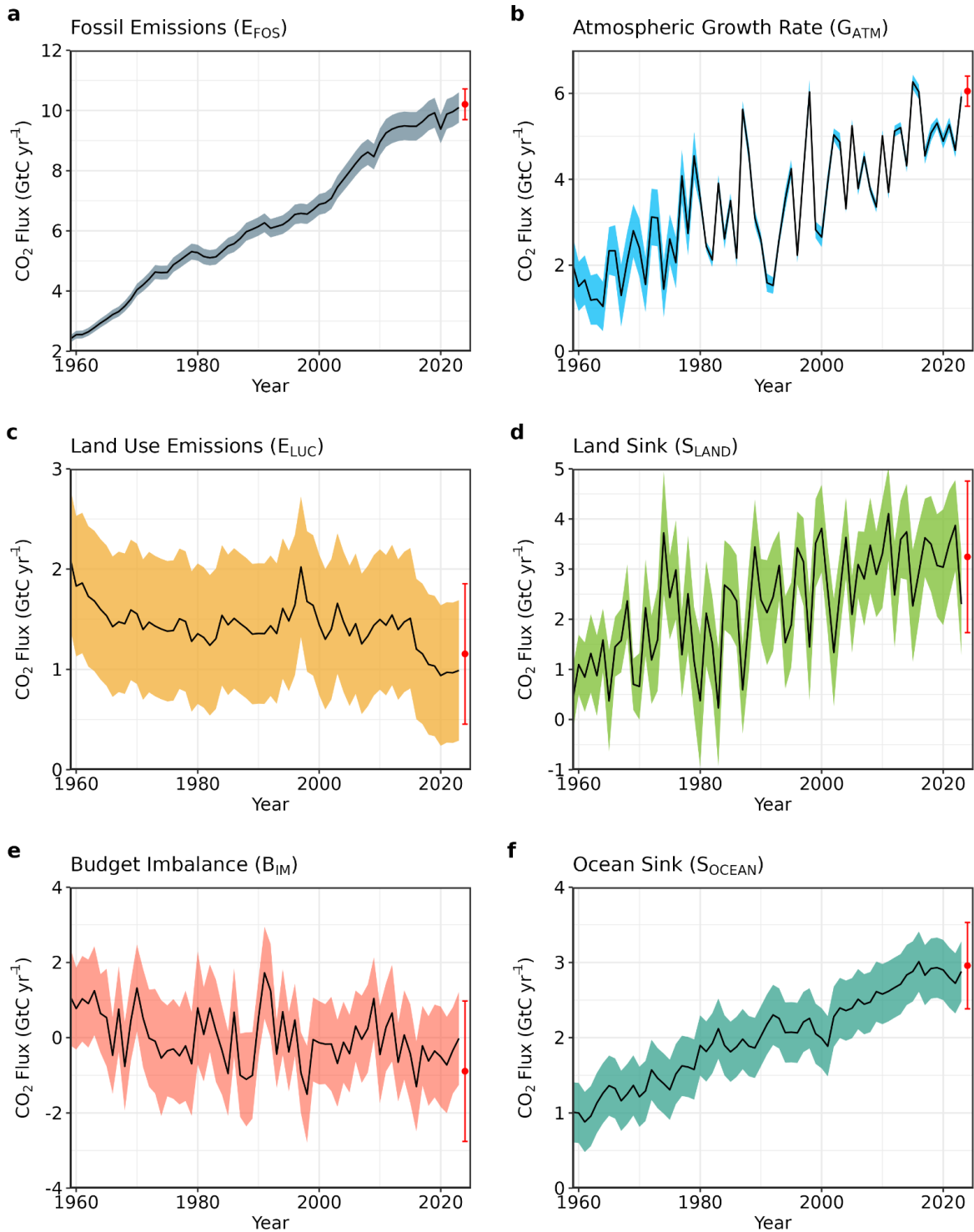


**Figure 4.** Components of the global carbon budget and their uncertainties as a function of time, presented individually for (a) fossil CO<sub>2</sub>, including cement carbonation emissions ( $E_{FOS}$ ), (b) growth rate in atmospheric CO<sub>2</sub> concentration ( $G_{ATM}$ ), (c) emissions from land-use change ( $E_{LUC}$ ), (d) the land CO<sub>2</sub> sink ( $S_{LAND}$ ), (e) the ocean CO<sub>2</sub> sink ( $S_{OCEAN}$ ), (f) the budget imbalance ( $B_{IM}$ ) that is not accounted for by the other terms. Positive values of  $S_{LAND}$  and  $S_{OCEAN}$  represent a flux from the atmosphere to land or the ocean. All data are in GtC yr<sup>-1</sup> with the uncertainty bounds representing  $\pm 1$  standard deviation in shaded colour. Data sources are as in Figure

3. The red dots indicate our projections for the year 2024 and the red error bars the uncertainty in the 2024 projections (see methods).

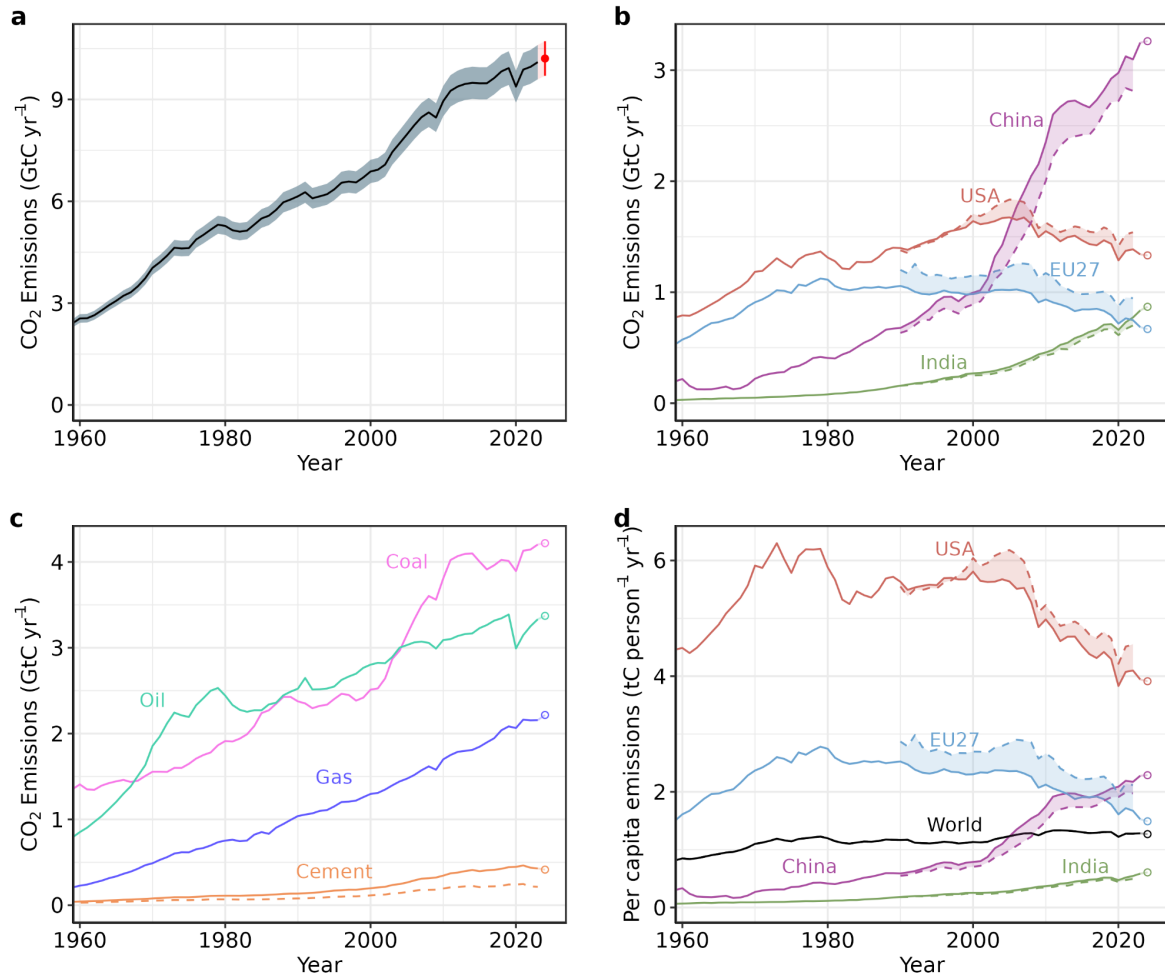


**Figure 5.** Fossil CO<sub>2</sub> emissions for (a) the globe, including an uncertainty of  $\pm 5\%$  (grey shading) and a projection through the year 2024 (red dot and uncertainty range), (b) territorial (solid lines) and consumption (dashed lines) emissions for the top three country emitters (USA, China, India) and for the European Union (EU27), (c) global emissions by fuel type, including coal, oil, gas, and cement, and cement minus cement carbonation (dashed), and (d) per-capita emissions the world and for the large emitters as in panel (b). Territorial emissions are primarily from a draft update of Hefner and Marland (2023) except for national data for most Annex I countries for 1990-2022, which are reported to the UNFCCC as detailed in the text, as well as some improvements in individual countries, and extrapolated forward to 2023 using data from Energy Institute. Consumption-based emissions are updated from Peters et al. (2011a). See Section 2.1 and Supplement S.1 for details of the calculations and data sources.

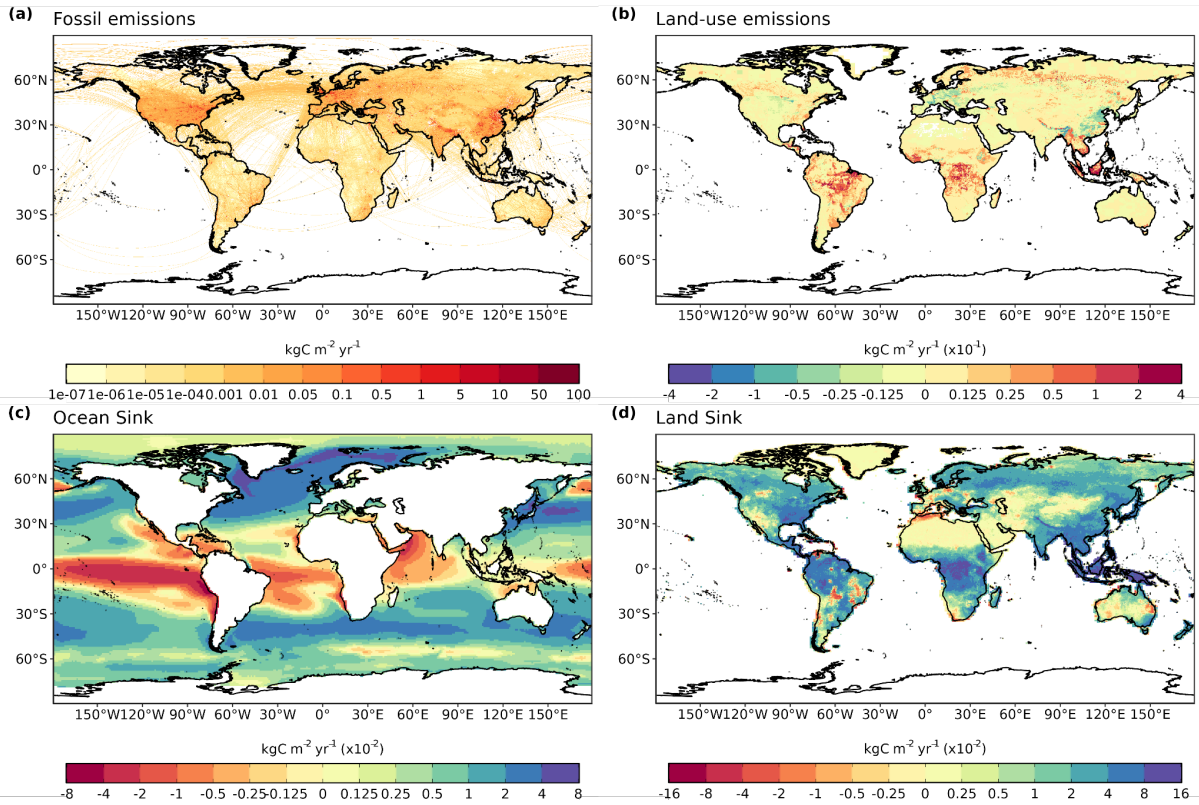


**Figure 6.** The 2014-2023 decadal mean components of the global carbon budget, presented for (a) fossil CO<sub>2</sub> emissions ( $E_{FOS}$ ), (b) land-use change emissions ( $E_{LUC}$ ), (c) the ocean CO<sub>2</sub> sink ( $S_{OCEAN}$ ), and (d) the land CO<sub>2</sub> sink ( $S_{LAND}$ ). Positive values for  $E_{FOS}$  and  $E_{LUC}$  represent a flux to the atmosphere, whereas positive values of  $S_{OCEAN}$  and  $S_{LAND}$  represent a flux from the atmosphere to the ocean or the land (carbon sink). In all panels, yellow/red colours represent a source (flux from the land/ocean to the atmosphere), green/blue colours represent a sink (flux from the atmosphere into the land/ocean). All units are in  $\text{kgC m}^{-2} \text{yr}^{-1}$ . Note the different scales in each panel.  $E_{FOS}$  data shown is from GCP-GridFEDv2024.0 and does not include cement carbonation. The  $E_{LUC}$  map shows the average  $E_{LUC}$  from the four bookkeeping models plus emissions from peat drainage and peat fires. BLUE and LUCE provide spatially explicit estimates at  $0.25^\circ$  resolution. Gridded  $E_{LUC}$  estimates for H&C2023 and OSCAR are derived by spatially distributing their national data based on the spatial patterns of BLUE gross fluxes in each country (see Schwingshackl et al., 2022, for more details about the methodology).  $S_{OCEAN}$  data shown is the average of GOBMs and  $f_{CO_2}$ -products means, using GOBMs simulation A, no adjustment for bias and drift applied to the gridded fields (see Section 2.5).  $S_{LAND}$  data shown is the average of the DGVMs for simulation S2 (see Section 2.6).

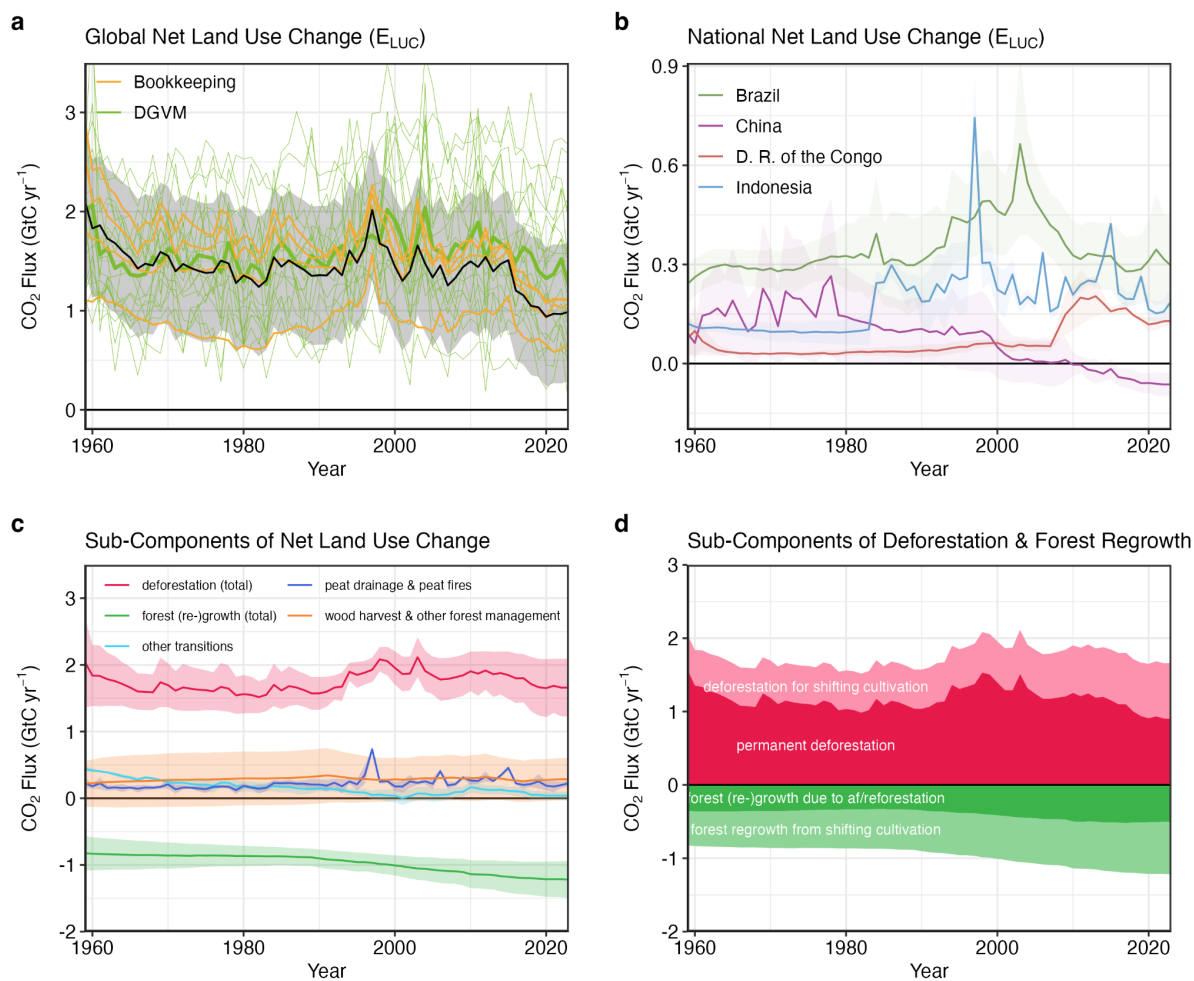


**Figure 7.** Net  $CO_2$  exchanges between the atmosphere and the terrestrial biosphere related to land use change. (a) Net  $CO_2$  emissions from land-use change ( $E_{LUC}$ ) with estimates from the four bookkeeping models (yellow lines) and the budget estimate (black with  $\pm 1\sigma$  uncertainty), which is the average of the four bookkeeping models. Estimates from individual DGVMs (narrow green lines) and the DGVM ensemble mean (thick green line) are also shown. (b) Net  $CO_2$  emissions from land-use change from the four countries with largest cumulative emissions since 1959. Values shown are the average of the four bookkeeping models, with shaded regions as  $\pm 1\sigma$  uncertainty. (c) Sub-components of  $E_{LUC}$ : (i) emissions from deforestation (including permanent deforestation and deforestation in shifting cultivation cycles), (ii) emissions from peat drainage & peat fires, (iii) removals from forest (re-)growth (including forest (re-)growth due to afforestation and reforestation and forest regrowth in shifting cultivation cycles), (iv) fluxes from wood harvest and other forest management (comprising slash and product decay following wood harvest, regrowth after wood harvest, and fire suppression), and (v) emissions and removals related to other land-use transitions. The sum of the five components is  $E_{LUC}$  shown in panel (a). (d) Sub-components of ‘deforestation (total)’ and of ‘forest (re-)growth (total)’: (i) deforestation in shifting cultivation cycles, (ii) permanent deforestation, (iii) forest (re-)growth due to afforestation and/or reforestation, and (iv) forest regrowth in shifting cultivation cycles.

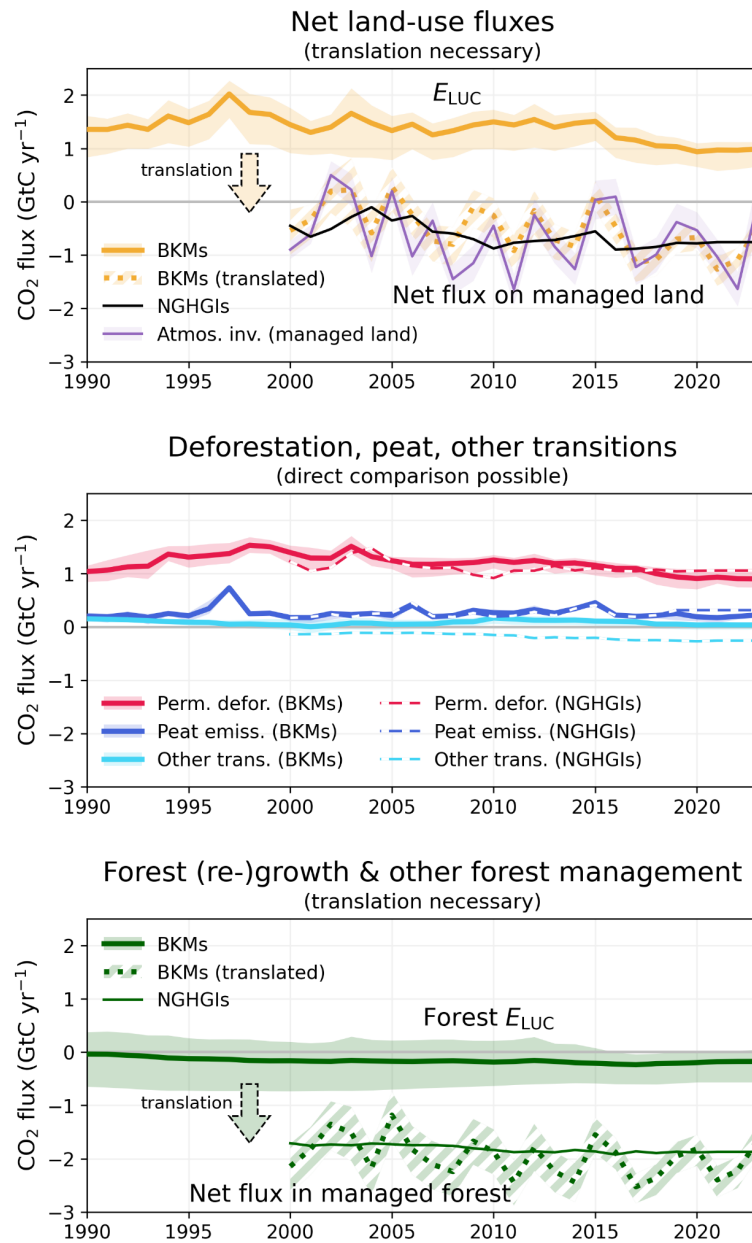


**Figure 8.** Comparison of land-use flux estimates from bookkeeping models (BKMs; following the GCB definition of  $E_{LUC}$ ), national GHG inventories (NGHGIs; following IPCC guidelines and thus including all carbon fluxes on managed land), and atmospheric inversion systems (considering fluxes on managed land only). To compare BKM results with NGHGIS, a translation is necessary for some subcomponents. (a) Net land-use fluxes, for which a translation of BKMs is necessary, (b) subcomponents permanent deforestation, peat drainage & peat fires, and other transitions, which can be directly compared and (c) subcomponent forest (re-)growth & other forest management, for which a translation is necessary. The lines represent the mean of 4 BKMs and 14 atmospheric inversion estimates, respectively; Shaded areas denote the full range across BKM estimates and the standard deviation for atmospheric inversions, respectively. The subcomponent forest (re-)growth & other forest management includes removals from forest (re-)growth (permanent), emissions and removals from wood harvest & other forest management, and emissions and removals in shifting cultivation cycles. The translation of

BKM estimates to NGHGI estimates in (a) and (c) is done by adding the natural land sink in managed forests to the BKM estimates (see also Table S10). The GCB definition of ELUC and the NGHGI definition of land-use fluxes are equally valid, each in its own context. For illustrative purposes we only show the translation of BKM estimates to the NGHGI definition.



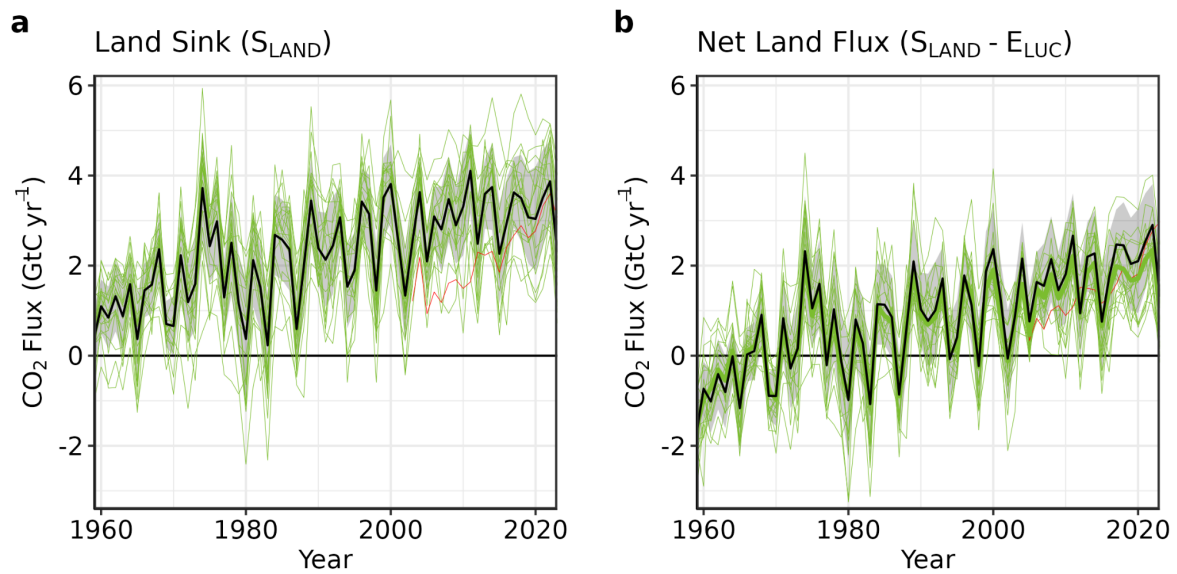


**Figure 9.** (a) The land CO<sub>2</sub> sink ( $S_{\text{LAND}}$ ) estimated by individual DGVMs (green), and CARDAMOM (red), as well as the budget estimate (black with  $\pm 1\sigma$  uncertainty), which is the average of all DGVMs. (b) Net atmosphere-land CO<sub>2</sub> fluxes ( $S_{\text{LAND}} - E_{\text{LUC}}$ ). The budget estimate of the net land flux (black with  $\pm 1\sigma$  uncertainty) combines the DGVM estimate of  $S_{\text{LAND}}$  from panel (a) with the bookkeeping estimate of  $E_{\text{LUC}}$  from Figure 7a. Uncertainties are similarly propagated in quadrature. DGVMs also provide estimates of  $E_{\text{LUC}}$  (see Figure 7a), which can be combined with their own estimates of the land sink. Hence panel (b) also includes an estimate for the net land flux for individual DGVMs (thin green lines) and their multi-model mean (thick green line).

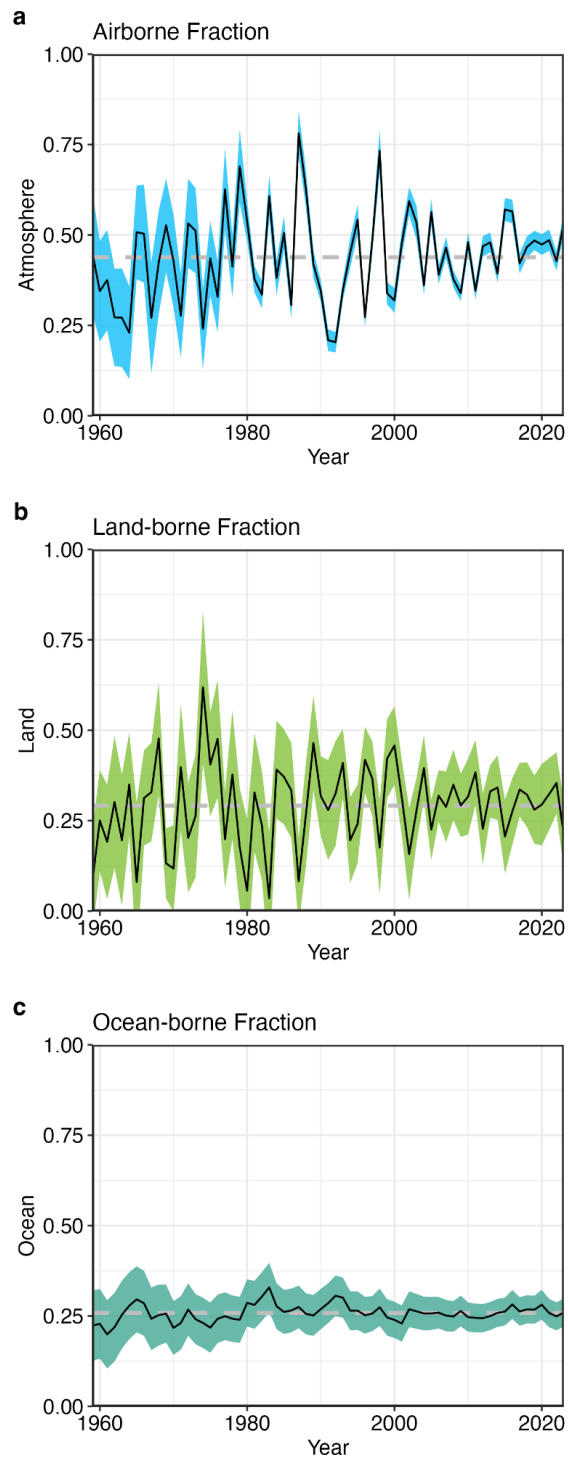


**Figure 10.** The partitioning of total anthropogenic CO<sub>2</sub> emissions ( $E_{\text{FOS}} + E_{\text{LUC}}$ ) across (a) the atmosphere (airborne fraction), (b) land (land-borne fraction), and (c) ocean (ocean-borne fraction). Black lines represent the central estimate, and the coloured shading represents the uncertainty. The grey dashed lines represent the long-term average of the airborne (44%), land-borne (30%) and ocean-borne (25%) fractions during 1960-2023 (with a  $B_{\text{IM}}$  of 1%).

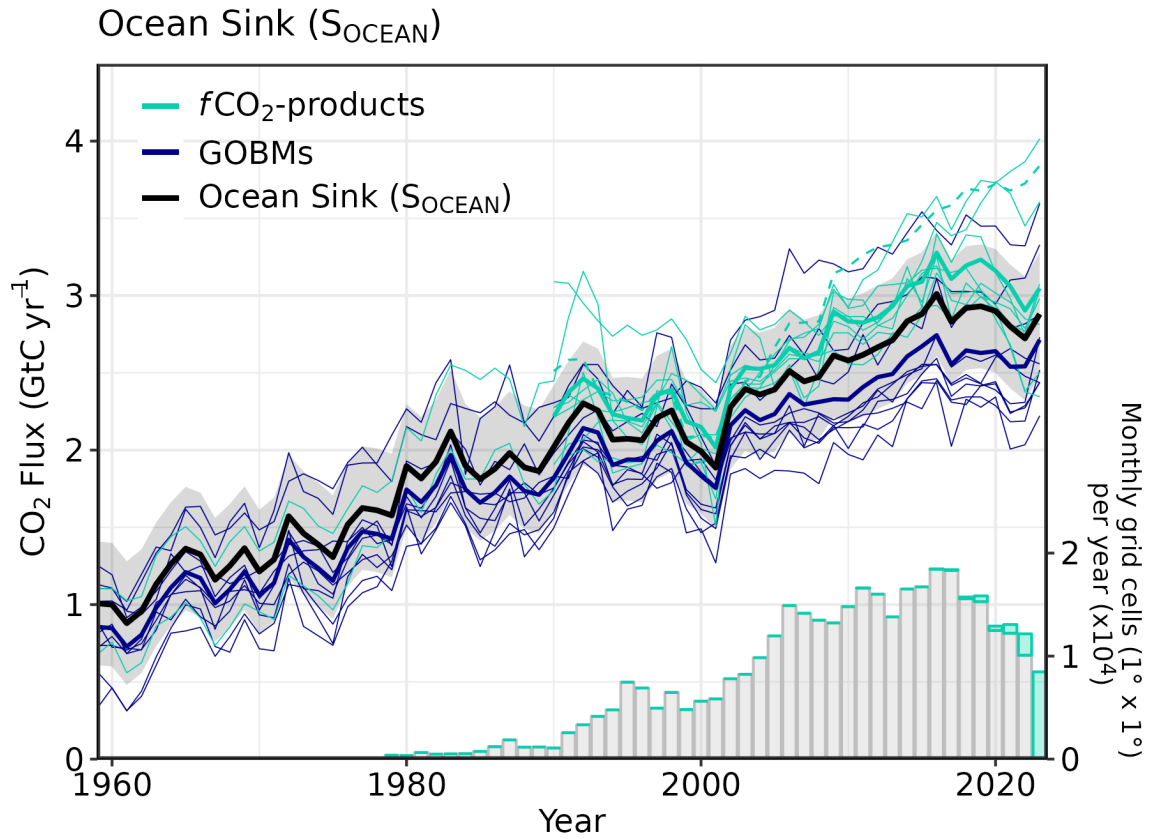


**Figure 11.** Comparison of the anthropogenic atmosphere-ocean CO<sub>2</sub> flux showing the budget values of  $S_{OCEAN}$  (black; with the uncertainty in grey shading), individual ocean models (royal blue), and the ocean  $fCO_2$ -products (cyan; with UExP-FFN-U, previously Watson et al. (2020), in dashed line as not used for ensemble mean). Two  $fCO_2$ -products (Jena-MLS, LDEO-HPD) extend back to 1959. The  $fCO_2$ -products were adjusted for the pre-industrial ocean source of CO<sub>2</sub> from river input to the ocean, by subtracting a source of 0.65 GtC yr<sup>-1</sup> to make them comparable to  $S_{OCEAN}$  (see Section 2.5). Bar-plot in the lower right illustrates the number of monthly gridded values in the SOCAT v2024 database (Bakker et al., 2024). Grey bars indicate the number of grid cells in SOCAT v2023, and coloured bars indicate the newly added grid cells in v2024.

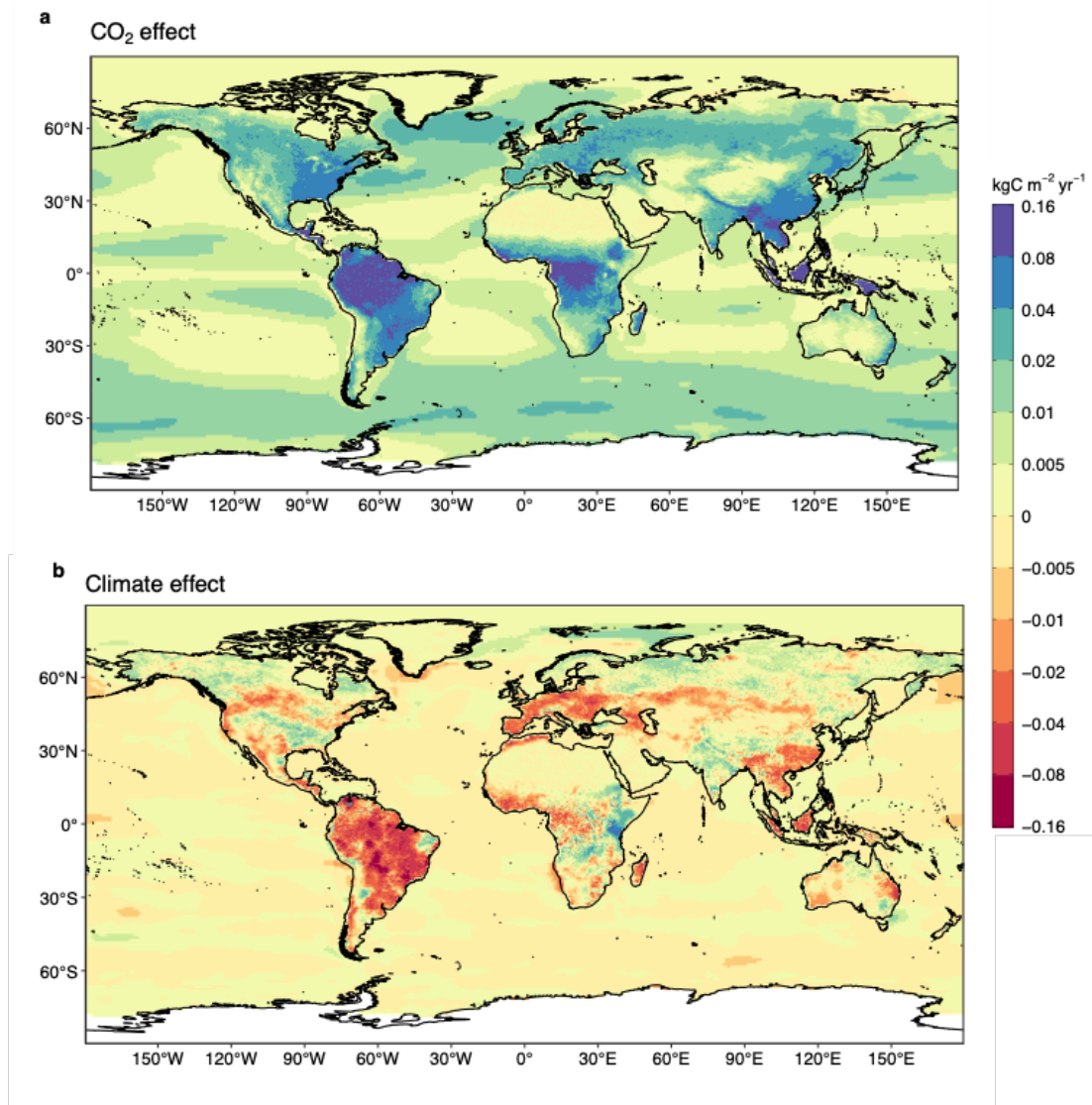


**Figure 12.** Attribution of the atmosphere-ocean ( $S_{\text{OCEAN}}$ ) and atmosphere-land ( $S_{\text{LAND}}$ ) CO<sub>2</sub> fluxes to (a) increasing atmospheric CO<sub>2</sub> concentrations and (b) changes in climate, averaged over the previous decade 2014-2023. All data shown is from the processed-based GOBMs and DGVMs. Note that the sum of ocean CO<sub>2</sub> and climate effects shown here will not equal the ocean sink shown in Figure 6, which includes the  $f\text{CO}_2$ -products. See Supplement S.3.2 and S.4.1 for attribution methodology. Units are in kgC m<sup>-2</sup> yr<sup>-1</sup> (note the non-linear colour scale). Positive values (blue) are CO<sub>2</sub> sinks, negative values (red) are CO<sub>2</sub> sources.

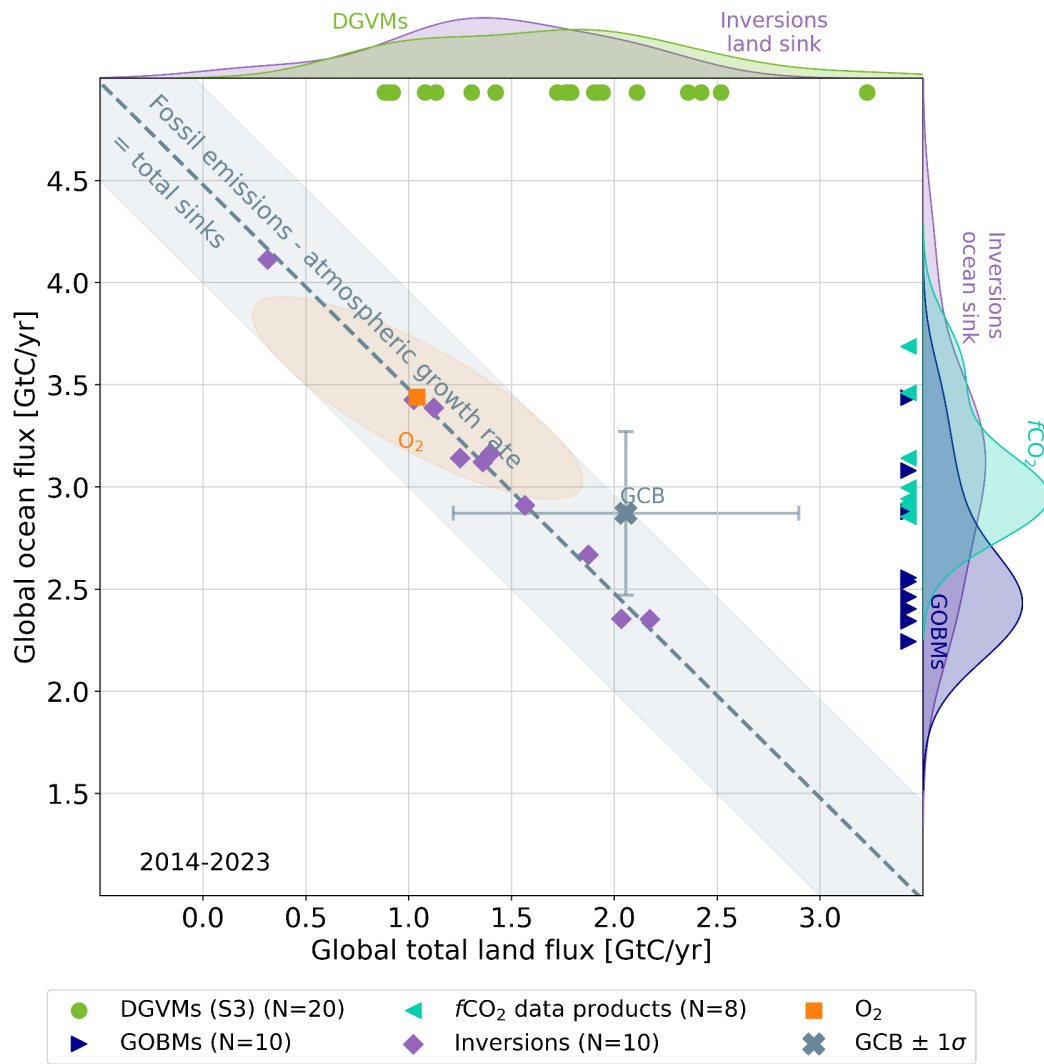


**Figure 13.** The 2014-2023 decadal mean global net atmosphere-ocean and atmosphere-land fluxes derived from the ocean models and  $f\text{CO}_2$  products (y-axis, right and left pointing blue triangles respectively), and from the DGVMs (x-axis, green symbols), and the same fluxes estimated from the atmospheric inversions (purple symbols). The shaded distributions show the densities of the ensembles of individual estimates. The grey central cross is the mean ( $\pm 1\sigma$ ) of  $S_{\text{OCEAN}}$  and  $(S_{\text{LAND}} - E_{\text{LUC}})$  as assessed in this budget. The grey diagonal line represents the constraint on the global land + ocean net flux, i.e. global fossil fuel emissions minus the atmospheric growth rate from this budget ( $E_{\text{FOS}} - G_{\text{ATM}}$ ). The orange square represents the same global net atmosphere-ocean and atmosphere-land fluxes as estimated from the atmospheric  $\text{O}_2$  constraint (the ellipse drawn around the central atmospheric  $\text{O}_2$  estimate is a contour representing the  $1\sigma$  uncertainty of the land and ocean fluxes as a joint probability distribution). Positive values are  $\text{CO}_2$  sinks. Note that the inverse estimates have been scaled for a minor difference between  $E_{\text{FOS}}$  and GridFEDv2024.0 (Jones et al., 2024a).

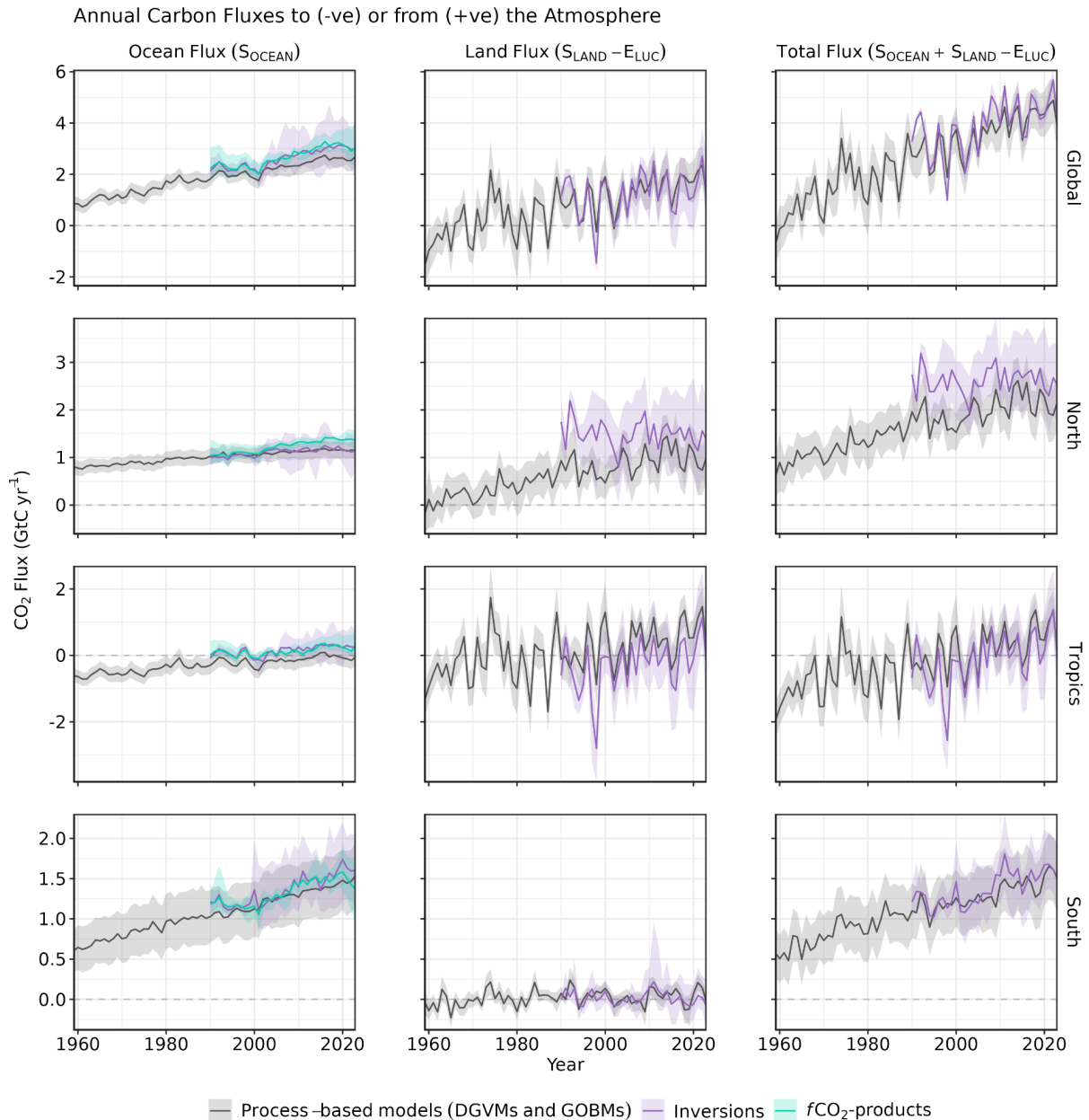


**Figure 14.** CO<sub>2</sub> fluxes between the atmosphere and the Earth's surface separated between land and oceans, globally and in three latitude bands. The ocean flux is  $S_{\text{OCEAN}}$  and the land flux is the net atmosphere-land fluxes from the DGVMs. The latitude bands are (top row) global, (2<sup>nd</sup> row) north (>30°N), (3<sup>rd</sup> row) tropics (30°S-30°N), and (bottom row) south (<30°S), and over ocean (left column), land (middle column), and total (right column). Estimates are shown for: process-based models (DGVMs for land, GOBMs for oceans); inversion systems (land and ocean); and  $f\text{CO}_2$ -products (ocean only). Positive values are CO<sub>2</sub> sinks. Mean estimates from the combination of the process models for the land and oceans are shown (black line) with  $\pm 1 \sigma$  of the model ensemble (grey shading). For the total uncertainty in the process-based estimate of the total sink, uncertainties are summed in quadrature. Mean estimates from the atmospheric inversions are shown (purple lines) with their full spread (purple shading). Mean estimates from the  $f\text{CO}_2$ -products are shown for the ocean domain (light blue

lines) with full model spread (light blue shading). The global  $S_{OCEAN}$  (upper left) and the sum of  $S_{OCEAN}$  in all three regions represents the anthropogenic atmosphere-to-ocean flux based on the assumption that the preindustrial ocean sink was  $0 \text{ GtC yr}^{-1}$  when riverine fluxes are not considered. This assumption does not hold at the regional level, where preindustrial fluxes can be significantly different from zero. Hence, the regional panels for  $S_{OCEAN}$  represent a combination of natural and anthropogenic fluxes. Bias-correction and area-weighting were only applied to global  $S_{OCEAN}$ ; hence the sum of the regions is slightly different from the global estimate ( $<0.07 \text{ GtC yr}^{-1}$ ).

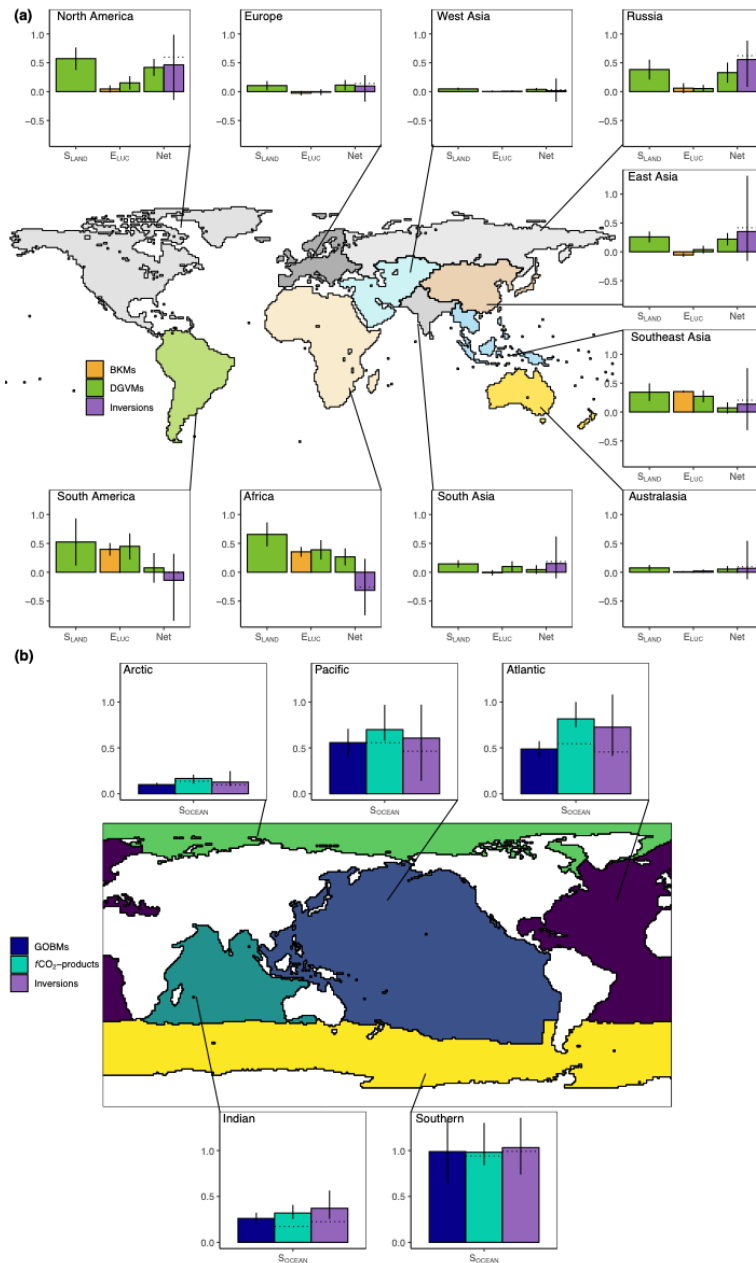


**Figure 15.** Decadal mean (a) land and (b) ocean fluxes for RECCAP-2 regions over 2014-2023. For land fluxes,  $S_{LAND}$  is estimated by the DGVMs (green bars), with the error bar as  $\pm 1\sigma$  spread among models. A positive  $S_{LAND}$  is a net transfer of carbon from the atmosphere to the land.  $E_{LUC}$  fluxes are shown for both DGVMs (green) and bookkeeping models (orange), again with the uncertainty calculated as the  $\pm 1\sigma$  spread. Note, a positive  $E_{LUC}$  flux indicates a loss of carbon from the land. The net land flux is shown for both DGVMs (green) and atmospheric inversions (purple), including the full model spread for inversions. The net ocean sink ( $S_{OCEAN}$ ) is estimated by GOBMs (royal blue),  $fCO_2$ -products (cyan), and atmospheric inversions (purple). Uncertainty is estimated as the  $\pm 1\sigma$  spread for GOBMs, and the full model spread for the other two datasets. The dotted lines show the  $fCO_2$ -products and inversion results without river flux adjustment. Positive values are  $CO_2$  sinks.



# Anthropogenic carbon flows

(a) Cumulative changes 1850-2023 GtC

(b) Mean fluxes 2014-2023 GtC per year



**Figure 16.** Cumulative changes over the 1850-2023 period (left) and average fluxes over the 2014-2023 period (right) for the anthropogenic perturbation of the global carbon cycle. See the caption of Figure 3 for key information and the methods in text for full details.



**Figure 17.** Kaya decomposition of the main drivers of fossil CO<sub>2</sub> emissions, considering population, GDP per person, Energy per GDP, and CO<sub>2</sub> emissions per energy, for China (top left), USA (top right), EU27 (middle left), India (middle right), Rest of the World (bottom left), and World (bottom right). Black dots are the annual fossil CO<sub>2</sub> emissions growth rate, coloured bars are the contributions from the different drivers to this growth rate. A general trend is that population and GDP growth put upward pressure on emissions (positive values), while energy per GDP and, more recently, CO<sub>2</sub> emissions per energy put downward pressure on emissions (negative values). Both the COVID-19 induced drop during 2020 and the recovery in 2021 led to a stark contrast to previous years, with different drivers in each region.